



# NBS SPECIAL PUBLICATION 400-43

U.S. DEPARTMENT OF COMMERCE / National Bureau of Standards

*Semiconductor Measurement Technology:*

## Accurate Linewidth Measurements on Integrated-Circuit Photomasks

OC  
00  
157  
No. 400-43  
980  
2

## NATIONAL BUREAU OF STANDARDS

The National Bureau of Standards<sup>1</sup> was established by an act of Congress on March 3, 1901. The Bureau's overall goal is to strengthen and advance the Nation's science and technology and facilitate their effective application for public benefit. To this end, the Bureau conducts research and provides: (1) a basis for the Nation's physical measurement system, (2) scientific and technological services for industry and government, (3) a technical basis for equity in trade, and (4) technical services to promote public safety. The Bureau's technical work is performed by the National Measurement Laboratory, the National Engineering Laboratory, and the Institute for Computer Sciences and Technology.

**THE NATIONAL MEASUREMENT LABORATORY** provides the national system of physical and chemical and materials measurement; coordinates the system with measurement systems of other nations and furnishes essential services leading to accurate and uniform physical and chemical measurement throughout the Nation's scientific community, industry, and commerce; conducts materials research leading to improved methods of measurement, standards, and data on the properties of materials needed by industry, commerce, educational institutions, and Government; provides advisory and research services to other Government agencies; develops, produces, and distributes Standard Reference Materials; and provides calibration services. The Laboratory consists of the following centers:

Absolute Physical Quantities<sup>2</sup> — Radiation Research — Thermodynamics and Molecular Science — Analytical Chemistry — Materials Science.

**THE NATIONAL ENGINEERING LABORATORY** provides technology and technical services to the public and private sectors to address national needs and to solve national problems; conducts research in engineering and applied science in support of these efforts; builds and maintains competence in the necessary disciplines required to carry out this research and technical service; develops engineering data and measurement capabilities; provides engineering measurement traceability services; develops test methods and proposes engineering standards and code changes; develops and proposes new engineering practices; and develops and improves mechanisms to transfer results of its research to the ultimate user. The Laboratory consists of the following centers:

Applied Mathematics — Electronics and Electrical Engineering<sup>2</sup> — Mechanical Engineering and Process Technology<sup>2</sup> — Building Technology — Fire Research — Consumer Product Technology — Field Methods.

**THE INSTITUTE FOR COMPUTER SCIENCES AND TECHNOLOGY** conducts research and provides scientific and technical services to aid Federal agencies in the selection, acquisition, application, and use of computer technology to improve effectiveness and economy in Government operations in accordance with Public Law 89-306 (40 U.S.C. 759), relevant Executive Orders, and other directives; carries out this mission by managing the Federal Information Processing Standards Program, developing Federal ADP standards guidelines, and managing Federal participation in ADP voluntary standardization activities; provides scientific and technological advisory services and assistance to Federal agencies; and provides the technical foundation for computer-related policies of the Federal Government. The Institute consists of the following centers:

Programming Science and Technology — Computer Systems Engineering.

<sup>1</sup>Headquarters and Laboratories at Gaithersburg, MD, unless otherwise noted; mailing address Washington, DC 20234.

<sup>2</sup>Some divisions within the center are located at Boulder, CO 80303.

JUL 20 1981

*Semiconductor Measurement Technology:*

# **Accurate Linewidth Measurements on Integrated-Circuit Photomasks**

---

John M. Jerke, Editor

Electron Devices Division  
Center for Electronics and Electrical Engineering  
National Engineering Laboratory  
National Bureau of Standards  
Washington, D.C. 20234

This activity was supported by

The Defense Advanced Research Projects Agency  
1400 Wilson Boulevard  
Arlington, Virginia 22203

and

The National Bureau of Standards  
Washington, D.C. 20234



---

U.S. DEPARTMENT OF COMMERCE, Philip M. Klutznick, Secretary

Luther H. Hodges, Jr., Deputy Secretary  
Jordan J. Baruch, Assistant Secretary for Science and Technology

NATIONAL BUREAU OF STANDARDS, Ernest Ambler, Director

Issued February 1980

Library of Congress Catalog Card Number: 79-600191

National Bureau of Standards Special Publication 400-43

Nat. Bur. Stand. (U.S.), Spec. Publ. 400-43, 166 pages (Feb. 1980)

CODEN: XNBSAV

U.S. GOVERNMENT PRINTING OFFICE

WASHINGTON: 1980

---

For sale by the Superintendent of Documents, U.S. Government Printing Office, Washington, D.C. 20402

Stock No. 003-003-02151-2

Price \$5.00

(Add 25 percent for other than U.S. mailing).

TABLE OF CONTENTS

	Page
Abstract . . . . .	1
1. Introduction and Highlights . . . . .	3
2. Background . . . . .	7
2.1 Line-Scale Measurements . . . . .	7
2.2 Linewidth Measurements . . . . .	10
2.3 Reduction of Measurement Offsets in Linewidth Calibration	13
3. Theoretical Analysis of Optical Microscope . . . . .	16
3.1 Optical Imaging of Lines . . . . .	16
3.2 Calculation of Image Profiles for Real Systems . . . . .	25
3.3 Filar and Image-Shearing Eyepieces . . . . .	35
3.4 A New Method for Measurement of Small Linewidths . . . . .	42
4. Linewidth-Measurement Artifacts . . . . .	43
4.1 Design and Materials . . . . .	43
4.2 Quality . . . . .	50
5. SEM/Interferometer System . . . . .	51
5.1 Requirements for the SEM . . . . .	51
5.2 Modeling of Electron Interaction with Material Line . . . . .	53
5.3 Apparatus . . . . .	59
5.3.1 Design . . . . .	59
5.3.2 Construction . . . . .	63
5.3.3 Operation and Performance . . . . .	66
5.4 Linewidth-Measurement Procedures . . . . .	68
5.5 Sample Data . . . . .	69
6. Photometric Optical Microscope . . . . .	78
6.1 Apparatus . . . . .	78
6.2 Comparison of Theory and Experimental Data . . . . .	82
6.3 Optimum Operating Conditions . . . . .	92
7. Conventional Optical Microscopes . . . . .	95
7.1 Precision Characteristics of Microscopes . . . . .	95
7.2 Comparison of Linewidths Measured with Filar and Image-Shearing Eyepieces . . . . .	99
8. Linewidth Calibration . . . . .	105
8.1 Calibration Hierarchy . . . . .	105
8.2 Preliminary Comparison of Linewidths Measured on SEM/In- ferometer and Photometric Optical Microscope . . . . .	107
8.3 Transfer of NBS Measurements to Industry . . . . .	109
8.4 NBS/IC-Industry Collaborative Test . . . . .	110
9. Continuing Micrometrology Project . . . . .	112
9.1 Measurements on See-Through Masks and Silicon Wafers . . . . .	112
9.2 Submicrometer Linewidth Calibration . . . . .	113

	Page
10. References . . . . .	115
Appendix A . . . . .	119
Appendix B . . . . .	132
Appendix C . . . . .	140
Appendix D . . . . .	146

LIST OF FIGURES

2-1. Schematic of a line-scale measurement . . . . .	9
2-2. Schematic of a line-scale measurement with a filar eyepiece on an optical microscope . . . . .	11
2-3. Schematic of a linewidth measurement . . . . .	12
2-4. Schematic of a linewidth measurement with a filar eyepiece on an optical microscope . . . . .	14
3-1. Image intensity profiles of an opaque line on a clear background for incoherent and coherent illumination . . . . .	19
3-2. Image intensity profiles of a single line edge for an illumination wavelength of 500 nm . . . . .	22
3-3. Image intensity profiles of a single line edge for coherent illumination with varying defocus . . . . .	24
3-4. Image intensity profiles of a single line edge for coherent illumination with $1\lambda$ spherical aberration and varying defocus	26
3-5. Coordinates for one-dimensional description of imaging system	28
3-6. Calculated image profiles of one edge of a 5- $\mu$ m wide clear line for an optical microscope with various objective and condenser numerical apertures; illumination wavelength of 560 nm, effective scanning slit of 0.13 $\mu$ m, and diffraction-limited optics . . . . .	30
3-7. Calculated image profiles of 1-, 3-, and 5- $\mu$ m wide clear lines for an optical microscope with a 0.90 N.A. objective, 0.60 N.A. condenser, illumination wavelength of 560 nm, effective scanning slit width of 0.13 $\mu$ m, and diffraction-limited optics . . . . .	31
3-8. Calculated image profiles of one edge of 0.4-, 0.5-, 0.6-, 0.8-, and 1.0- $\mu$ m wide clear lines for an optical microscope	

	Page
with the same parameters as figure 3-7 . . . . .	32
3-9. Calculated image profiles of one edge of a 5- $\mu$ m wide clear line for an optical microscope with defocus in steps of $\lambda/4$ from 0 to $\pm 1\lambda$ ; $\lambda/4$ corresponds to $\pm 0.06 \mu\text{m}$ for a 0.90 N.A. objective and an illumination wavelength of 560 nm; other microscope parameters are the same as in figure 3-7 .	33
3-10. Calculated image profiles of one edge of a 10- $\mu$ m wide clear line for an optical microscope with $2\lambda$ of spherical aberration and defocus varying in steps of $\lambda/4$ from 0 to $-2\lambda$ ; $\lambda/4$ corresponds to $\pm 0.39 \mu\text{m}$ for a 0.65 N.A. objective and an illumination wavelength of 560 nm; other microscope parameters are 0.22 N.A. condenser, effective scanning slit of 0.13 $\mu\text{m}$ , and diffraction-limited optics . . . . .	34
3-11. Schematic of symmetric impulse response of an optical microscope centered on a line edge; $T_o$ is transmittance of the opaque line, and the transmittance of the clear area is 1.0 . . . . .	36
3-12. Comparison of the calculated image profiles of a 1- $\mu$ m wide clear line with 0- and 2.5-percent background transmittance $T_o$ ; other microscope parameters are the same as in figure 3-7 . . . . .	37
3-13. Line-edge location with a filar eyepiece . . . . .	38
3-14. Line-edge location with an image-shearing eyepiece . . . . .	40
4-1. Basic pattern of initial NBS linewidth-measurement artifact; linewidths are nominal values . . . . .	44
4-2. Photograph of an antireflective chromium artifact . . . . .	45
4-3. SEM photomicrographs of an antireflective chromium artifact . . . . .	46
4-4. Photomicrograph of four nominally 1- $\mu$ m wide opaque lines on an iron-oxide artifact observed in an optical microscope with bright-field transmitted light at 2900X . . . . .	49
5-1. Schematic of the SEM/interferometer system for measuring linewidths . . . . .	52
5-2. Schematic of the effective path for the scanning electron beam when the linear motion of the scanning stage is combined with the line sweep of the SEM . . . . .	54
5-3. SEM photomicrograph showing contamination from repeated	

	Page
scans across a nominally 3- $\mu$ m wide clear line on an AR-chromium artifact; SEM operating voltage of 10 keV and magnification of 1700X . . . . .	55
5-4. Model of the line edge and a comparison of an experimental SEM line-edge trace with the calculated trace based on the model; broken lines show correspondence between edge location in the model and the SEM traces . . . . .	57
5-5. The interferometer output as a function of the inchworm motion for a linear time base . . . . .	60
5-6. Photograph of a scanning stage which uses a flexure-pivot system; stage is fixed at points A, while other stage sections move . . . . .	61
5-7. Schematic of the double-pass polarization interferometer as viewed by looking downward on the scanning stage . . . . .	62
5-8. Schematic of the angular errors for misalignment of the specimen lines in the SEM/interferometer system . . . . .	64
5-9. Photograph of the SEM/interferometer stage system with the front plate removed . . . . .	65
5-10. Photograph of the assembly attached to the SEM cover plate in the SEM/interferometer system . . . . .	67
5-11. SEM photomicrographs of calibrated lines on an anti-reflective chromium artifact . . . . .	70
5-12. Direct output of the SEM and interferometer data channels for a nominally 2- $\mu$ m wide opaque line . . . . .	72
5-13. SEM image profile for a nominally 2- $\mu$ m wide opaque line . . . . .	73
5-14. Relationship between the SEM image profile and the model of an opaque line; the points defined as edge locations of the line correspond to a 25-percent intensity transmittance . . . . .	74
5-15. SEM photomicrographs of cross-sectional views of a nominally 10- m wide clear line on an AR-chromium artifact . . . . .	76
6-1. Photograph of the photometric optical-microscope system . . . . .	79
6-2. Comparison of experimental line-edge profiles in white light and filtered green light for the photometric optical microscope with a 0.90 N.A. objective, a 0.60 N.A. condenser, and an effective scanning slit of 0.13 $\mu$ m . . . . .	81

	Page
6-3. Comparison of calculated and experimental image profiles of a nominally 10- $\mu$ m wide clear line for an optical microscope with various combinations of objective and condenser N.A.'s, illumination wavelength of 560 nm, effective scanning slit of 0.13 $\mu$ m, and diffraction-limited optics; the experimental profiles are for an AR-chromium artifact . . . . .	83
6-4. Comparison of calculated and experimental image profiles of clear lines of varying width for an optical microscope with a 0.90 N.A. objective, 0.60 N.A. condenser, illumination wavelength of 560 nm, effective scanning slit of 0.13 $\mu$ m, and diffraction-limited optics; the experimental profiles are for AR-chromium artifacts . . . . .	86
6-5. Experimental image profiles of a nominally 3- $\mu$ m wide opaque line on an AR-chromium artifact for the photometric optical microscope with a 0.45 N.A. objective, varying condenser N.A., illumination wavelength of 560 nm, effective scanning slit of 0.13 $\mu$ m, and nearly diffraction-limited optics; the dashed lines indicate line-edge locations based on a 33.5-percent transmittance threshold . . . . .	89
6-6. Experimental image profiles of one edge of a nominally 10- $\mu$ m wide clear line on an AR-chromium artifact for the photometric optical microscope with an illumination wavelength of 560 nm, effective scanning slit of 0.13 $\mu$ m, and nearly diffraction-limited optics; profiles a through e are for different focus settings with submicrometer displacements between them . . . . .	90
8-1. Hierarchy of NBS linewidth calibrations . . . . .	106

LIST OF TABLES

	Page
2-1. Differences Between Apparent Linewidths of Nominally 1-, 3-, and 10- $\mu$ m Wide Clear and Opaque Lines Measured with Filar and Image-Shearing Eyepieces . . . . .	8
3-1. Object Linewidths and Corresponding RMS Differences Determined from the Curves of Figure 3-1 . . . . .	21
3-2. Linewidth Measurement Errors of a Clear Line on an Opaque Background for an Illumination Wavelength of 550 nm . . . . .	41
5-1. Linewidth Measurements Made with the SEM/Interferometer System on an AR-Chromium Artifact . . . . .	77
6-1. Comparison of Linewidth Measurement Made with the Photoelec- vii	

	Page
tric Optical Microscope on a Nominally 3- $\mu$ m Wide Opaque Line for Various Combinations of Objectives and Condensers	88
6-2. Summary of Linewidth Measurements Made with the Photoelectric Optical Microscope on a Nominally 1- $\mu$ m Wide Clear Line . . . . .	93
7-1. Apparent Widths of Clear Lines . . . . .	97
7-2. Typical Data for Linewidth Measurements Repeated on Same Line . . . . .	98
7-3. Expected Relationships of Apparent Linewidths Measured Under Various Viewing Conditions . . . . .	100
7-4. Apparent Linewidths of Opaque Lines and Clear Spaces Measured on AR-Chromium Artifact in Bright-Field Illumination	101
7-5. Apparent Linewidths Measured in Transmitted Light with Filar and Image-Shearing Eyepieces Calibrated with Line Spacings . . . . .	103
7-6. Apparent Linewidths Measured in Transmitted Light with Filar and Image-Shearing Eyepieces Calibrated with Linewidths . . . . .	103
7-7. Comparison of Linewidths Measured in Transmitted Light by Filar and Image-Shearing Eyepieces Calibrated with 3- and 10- $\mu$ m Linewidths as Measured on NBS Photometric Optical Microscope . . . . .	104
8-1. Comparison of Linewidth Measurements from SEM/Interferometer and Photometric Optical Microscope . . . . .	108

## PREFACE

This study was carried out in the Optics and Micrometrology Section, Mechanics Division, National Bureau of Standards (NBS), with support from the Optical Physics Division, NBS, as a part of the Semiconductor Technology Program in the Electronic Technology Division at the National Bureau of Standards.\* The Semiconductor Technology Program serves to focus NBS research to enhance the performance, interchangeability, and reliability of discrete semiconductor devices and integrated circuits through improvements in measurement technology for use in specifying materials and devices in national and international commerce and for use by industry in controlling device fabrication processes. The Program receives direct financial support from a number of sources: The Defense Advanced Research Projects Agency (DARPA), The Defense Nuclear Agency (DNA), and the National Bureau of Standards. The specific work reported herein was supported jointly by DARPA and NBS.†

Special acknowledgment is gratefully made to William J. Keery, Semiconductor Characterization Section, Electronic Technology Division, NBS, for operating the scanning electron microscope (SEM) during linewidth measurements. These measurements require his special effort to ensure that the microscope operates at optimal resolution for an unconventional scanning mode. He also assisted in the evaluation of the quality of linewidth-measurement artifacts by taking numerous SEM photomicrographs. Special thanks go to Dr. Donald B. Novotny, Electron Devices Section, Electronic Technology Division, NBS, for his continued assistance in maintaining a strong liaison between NBS and the integrated-circuit (IC) industry to ensure that the results of the NBS project are directly applied to the measurement needs of the IC industry. He has also provided helpful suggestions in the preparation of technical papers and presentations covering the results of this program. Special thanks to Dr. E. Clayton Teague and Frederic E. Scire, Optics and Micrometrology Section, Mechanics Division, NBS, who assisted in the development and testing of a special flexure-pivot stage that is essential to accurate linewidth measurements on the SEM/interferometer system and the photometric optical microscope. Throughout the project, persons from the IC industry have continued to show a strong interest by keeping in direct contact with NBS personnel, visiting NBS facilities, and offering equipment and linewidth-measurement artifacts. For these efforts, special thanks are also gratefully made.

---

\* Significant changes in assigned organizational units have occurred between the end of the reporting period and the issue date of this report. Organizational designations given are those in existence during the reporting period. At the present time, the entire project, except for the submicrometer work (sec. 9.2), is being carried out in the Electron Devices Division.

† Through ARPA Order 2397.

### Disclaimer

Certain commercially available materials or instruments are identified in this publication for the purpose of providing a complete description of the work performed. The experiments reported do not constitute an evaluation of the performance characteristics of the products so identified. In no case does such identification imply recommendation or endorsement by the National Bureau of Standards nor does it imply that the items identified are necessarily the best available for the purpose.

*Semiconductor Measurement Technology:*  
Accurate Linewidth Measurements on  
Integrated-Circuit Photomasks

John M. Jerke, Editor  
Electron Devices Division  
Center for Electronics and Electrical Engineering  
National Bureau of Standards  
Washington, DC 20234

ABSTRACT

The progress of the NBS project to develop improved theory for accurate linewidth measurements with optical microscopes, to develop primary linewidth calibration of 1- to 10- $\mu\text{m}$  wide lines on integrated-circuit (IC) photomasks, and to provide calibrated measurement artifacts and measurement procedures to the IC industry is discussed. This report covers the initial period from September 1974 through December 1976.

Using coherence theory, line-image profiles are calculated for real optical-microscope systems. The effects of defocus, spherical aberration, and finite transmission of opaque mask areas on the line-image profiles and the location of the line edges are discussed.

A primary linewidth-calibration system, consisting of an interferometer located in a scanning electron microscope (SEM), has been fabricated and used to make measurements of nominally 1-, 2-, and 3- $\mu\text{m}$  wide opaque and clear lines on antireflective chromium artifacts. The goal for the measurement uncertainty (systematic and random errors) of linewidth measurements with the SEM/interferometer system is  $\pm 0.05 \mu\text{m}$ . Preliminary measurements show a standard deviation of about  $0.02 \mu\text{m}$ . A secondary linewidth-calibration system, which is a modified photometric optical microscope, has been fabricated and provides line-image profiles that compare very well with optical theory. At the time of this effort, the measurement uncertainty for the optical system was estimated to be about  $\pm 0.01 \mu\text{m}$  and the standard deviation was better than  $0.025 \mu\text{m}$ . The difference between the mean values of the opaque lines as measured by the SEM/interferometer system and the photometric optical microscope is approximately  $0.05 \mu\text{m}$ .

Linewidth measurements on optical microscopes equipped with filar and image-shearing eyepieces are presented. A preliminary effort shows that differences between linewidth measurements with these two eyepieces are significantly reduced when a linewidth artifact measured on the photometric optical microscope is used to calibrate the eyepieces.

Collaborative tests between NBS and the IC industry to evaluate procedures for accurate linewidth measurements with calibrated

artifacts are discussed. Some of the methods for transferring NBS-measured values to the industry are summarized. The plans for the continuing micrometrology project include accurate linewidth measurements on opaque wafers with reflected light and on see-through masks with transmitted light and submicrometer linewidth calibration.

Key words: Filar eyepiece; image-shearing eyepiece; integrated circuits; linewidth measurements; microelectronics; micrometrology; optical microscope; photomask; photoelectric microscope; scanning electron microscope; semiconductor technology.

## 1. INTRODUCTION AND HIGHLIGHTS

In the production of integrated-circuit (IC) devices, a photomask is the basic pattern for transferring the design circuit geometry to the semiconductor wafer [1]. The photomask is a repeated array of microphotographs of the circuit patterns on a glass substrate. Several masks are generally used to form successive patterns on a single wafer. Photoemulsion and hard-surface masks, such as chromium and iron oxide, are currently used to mass produce microelectronic devices having pattern elements with dimensions as small as 2 micrometers ( $\mu\text{m}$ ). A small number of special devices with submicrometer geometry are also being fabricated with masks produced by x-ray and electron-beam techniques.

The performance of the finished IC device depends strongly on the fidelity with which design dimensions of critical circuit elements, such as small linewidths, are transferred from the mask to the semiconductor wafer. Thus, the routine inspection of masks includes these linewidth measurements. The design rules generally used by the IC industry currently specify critical dimensions of  $5 \pm 0.5 \mu\text{m}$  for high-volume device production and  $2 \pm 0.25 \mu\text{m}$  for low-volume production. For the increasing number of devices with micrometer and submicrometer geometry, it is desirable to reduce the dimensional tolerances well below  $\pm 0.25 \mu\text{m}$ .

Many linewidth measurements are made with an optical microscope equipped with a filar or image-shearing eyepiece. Another measurement tool is a TV-microscope system in which the visual eyepiece is replaced with a TV camera and the eyepiece reticle is replaced with an electronically generated reticle displayed on the TV monitor [2]. Two other dimensional-measurement systems known to be under development include an automatic microdensitometer [3] and a Fourier-transform optical system [4]. The microdensitometer scans the line, and based on an edge-detection scheme, the scan data are reduced to give the linewidth. The Fourier-transform optical system, which is being investigated in a companion program, produces a diffraction pattern of the line, and the linewidth can be calculated from the measured positions of the maxima and minima of this pattern.

An earlier National Bureau of Standards (NBS) study identified the dimensional-measurement problems related to the fabrication and the use of IC photomasks [5]. These problems include the absence of calibrated measurement artifacts for determining the accuracy of linewidth measurements. Accurate linewidth measurements are needed to improve commerce between mask suppliers and customers by determining how closely mask geometries meet design specifications. In addition, these accurate measurements are needed to help resolve measurement differences among various equipment and procedures used in the IC industry.

In response to the need for accurate linewidth measurements and as part of the responsibility of NBS to provide industry with calibrated length standards referred to the defined unit of length, NBS initiated a metrology project with the following basic goals: (1) to develop im-

proved theory and experimental verification for accurate linewidth measurements with an optical microscope in transmitted light; (2) to make primary linewidth calibration of 1- to 10- $\mu\text{m}$  wide lines with uncertainty limits of  $\pm 0.05 \mu\text{m}$  (these error bounds include systematic and random errors); (3) to provide calibrated measurement artifacts and measurement procedures for optical microscopes; and (4) to disseminate the project results to the IC industry. The present report discusses the results of the initial effort from September 1974 through December 1976.

The format of this report is separate sections which discuss significant accomplishments or highlights. The sections were written by the staff members who were primarily responsible for these efforts.\* The sections include some overlapping material since the different tasks are all a part of the larger micrometrology project. Section 2 provides background material for the other sections, and section 9 discusses the continuing efforts in the project. Other technical publications based on the present micrometrology project have also been included as appendices in order to provide a more detailed discussion. Several papers which summarize the progress of the program at various stages during the initial two-year effort are listed as references [6] through [11].

Significant technical accomplishments during the two-year reporting period included:

1. A theoretical model based on physical optics and partial coherence has been developed for an optical microscope operating in transmitted, monochromatic, bright-field illumination. The model shows that under certain illumination conditions an analytic expression for the transmittance threshold corresponding to line-edge location may be derived for determining linewidths accurately. This threshold  $T_c$  is given by  $T_c = 0.25 (1 + \sqrt{T_o})^2$ , where  $T_o$  is the transmittance in the opaque area and the transmittance is 1.0 in the clear area. (See secs. 3.1 and 3.2.)

2. Theoretical models were developed for the filar and image-shearing eyepieces which are used widely throughout the industry for linewidth measurements. The modeling shows that these eyepieces use significantly different transmittance thresholds for locating the line edge. Calculated measurement errors for a 20- $\mu\text{m}$  wide line are as large as 0.6  $\mu\text{m}$  in each eyepiece under differing amounts of defocus. (See sec. 3.3.)

3. A linewidth-measurement technique based on coherent illumination and spatial filtering has been developed. This technique produces an optical transformation in which the locations of the line edges are marked by two narrow, dark lines within a bright surround. This changes a difficult, asymmetric linewidth measurement into an easier, symmetric spacing measurement between the two dark lines. Available microscope objectives, however, are not suitable for this system; the objective must be redesigned to implement the system. (See sec. 3.4.)

---

\* Authors of sections not prepared by the editor are indicated.

4. Both antireflective chromium and iron-oxide measurement artifacts were designed and fabricated. The basic pattern consists of opaque and clear lines (spaces) with nominal widths of 1, 3, and 10  $\mu\text{m}$ . The quality (steepness of line-edge slope and line raggedness) of the artifacts appears to be a major limitation in reducing measurement uncertainties on the NBS linewidth-measurement systems. (See sec. 4.)

5. A theoretical model was developed for determining the line-edge location in a measurement system that uses a scanning electron microscope (SEM) to measure linewidths. This model treats the electron interaction with the material line, and the parameters include physical properties of the line as well as operating adjustments of the SEM. (See sec. 5.2.)

6. A polarization interferometer operating in a scanning electron microscope was developed as a primary linewidth-measurement system that relates the length measurement to the defined unit of length. A special flexure-pivot stage was developed and fabricated for moving the line from one edge to the other edge during a measurement with this system. This stage uses piezo-elements whose length changes are amplified by a 20X mechanical flexure-pivot system, and the stage exhibits a smoothness of better than 0.001  $\mu\text{m}$  over a few micrometers. Comparison of experimental line profiles with line profiles calculated from the model shows relatively good agreement. (See secs. 5.3, 5.4, and 5.5.)

7. A photometric optical microscope was developed as a linewidth-measurement system. This system operates in bright-field, transmitted light (530 nm) with a piezoelectric focus adjustment, a ratio of condenser-to-objective numerical aperture of 2/3, and an effective scanning aperture (0.13  $\mu\text{m}$  by 1.3  $\mu\text{m}$ ) smaller than the impulse response of the objective. Comparison of experimental data with the theoretically calculated line-image profiles shows good agreement down to 0.5- $\mu\text{m}$  linewidths. This agreement demonstrates that this optical-microscope system can be used with the correct line-edge threshold to make accurate linewidth measurements. (See sec. 6.)

8. An experimental comparison of linewidth measurements was made using optical microscopes and operating conditions representative of those employed by the IC industry. Results from 90 different linewidth measurements on each of three different microscope systems suggest that the reproducibility is about  $\pm 0.3 \mu\text{m}$  for the filar eyepiece and about  $\pm 0.1 \mu\text{m}$  for both the image-shearing eyepiece and the TV-microscope system. Several trends between the apparent size of lines measured with the filar and image-shearing eyepieces were observed. These trends depend on the mode of illumination (transmitted or reflected light) and the polarity of the line (opaque line on a clear background or clear line on an opaque background). A comparison of linewidth measurements made after a line-spacing calibration with measurements made after a linewidth calibration shows that the measurement differences between the two eyepieces can, for the most part, be reduced to less than 0.05  $\mu\text{m}$  if a linewidth calibration is used. (See sec. 7.)

9. A preliminary comparison of linewidth measurements made on the same lines with the SEM/interferometer system and the photometric optical microscope shows that agreement is very good (difference of 0.05  $\mu\text{m}$ ) for two opaque lines. For a clear line, the difference is 0.24  $\mu\text{m}$  which is currently under investigation. (See sec. 8.2.)

## 2. BACKGROUND

In commonly used approaches for measuring linewidths on an optical microscope equipped with a filar or image-shearing eyepiece, the drum readings of the eyepiece are adjusted to agree with known center-to-center line spacings on a calibrated length scale. Assuming that the response of the measurement system to these scale measurements is linear, the scale error in the system can be corrected. However, this line-scale calibration can neither reveal the presence of, nor compensate for, any broadening or narrowing of the line image due to such effects as object size, lens aberrations, and degree of illumination coherence. To detect and correct for these changes in the measured line image, a calibrated linewidth artifact is needed.

An example of the differences in apparent linewidths of nominally 1-, 3-, and 10- $\mu\text{m}$  wide clear and opaque lines measured with filar and image-shearing eyepieces is given in table 2-1. For these linewidth measurements, the drum readings on the eyepieces were first made to agree with known values of line spacings. These differences typify those encountered in the IC industry when linewidth measurements are made with different eyepieces and on different object polarities (clear or opaque).

### 2.1 Line-Scale Measurements

In order to understand the relative difficulty of making a linewidth calibration as compared with a line-scale calibration, it is instructive to review the basic metrology of these measurements. A line-scale measurement is a relatively simple displacement measurement. As shown in figure 2-1a, a detector is initially centered on one line of a scale, and the measured or apparent position of the detector in units of length is given by

$$y_1 = \alpha(x_1 + C_1) , \quad (2-1)$$

where  $x_1$  is the actual location of the detector in the arbitrary units of the measurement-system axis,  $\alpha$  is the calibration scale factor which relates the divisions on the measurement-system axis to the defined unit of length, and  $C_1$  is a systematic offset, or bias, in locating the center of the line. This offset is distinct from the reproducibility of locating the line center in repeated settings of the detector. The detector is then moved to the center of an adjacent line, and the measured position  $y_2$  is given by

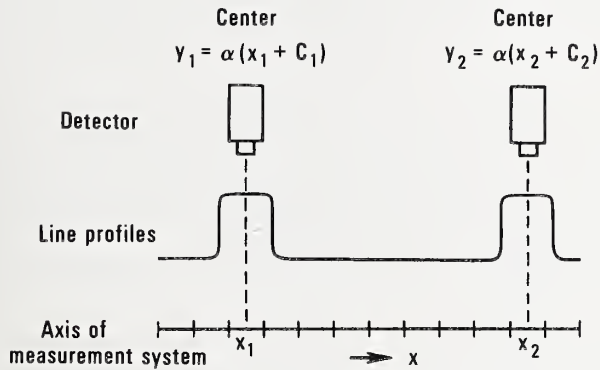
$$y_2 = \alpha(x_2 + C_2) . \quad (2-2)$$

The measured displacement of the detector between  $x_1$  and  $x_2$  is given by

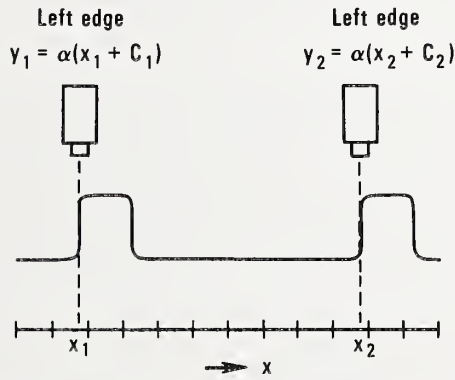
$$y_2 - y_1 = \alpha(x_2 - x_1) + \alpha(C_2 - C_1) . \quad (2-3)$$

Table 2-1 - Differences Between Apparent Linewidths of Nominally 1-, 3-, and 10- $\mu\text{m}$  Wide Clear and Opaque Lines Measured with Filar and Image-Shearing Eyepieces.

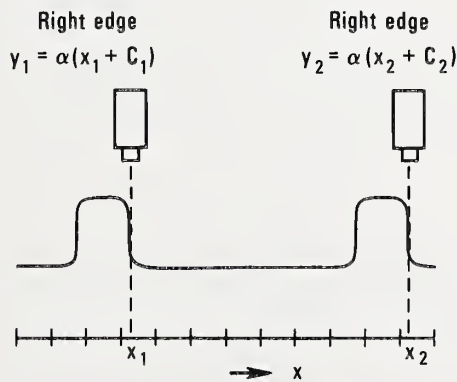
Nominal Linewidth ( $\mu\text{m}$ )	Difference between Linewidths Measured on Filar and Image-Shearing Eyepieces ( $\mu\text{m}$ )	
	Clear	Opaque
1	+0.26	-0.28
3	+0.26	-0.24
10	+0.19	-0.26



(a) Center-to-center measurement.



(b) Left-edge to left-edge measurement.



(c) Right-edge to right-edge measurement.

Figure 2-1. Schematic of a line-scale measurement.

If the cross-sectional profiles of adjacent lines are identical, the offsets  $C_1$  and  $C_2$  are equal, and the displacement measurement is written as

$$y_2 - y_1 = \alpha(x_2 - x_1) . \quad (2-4)$$

Thus, the offsets subtract out of a line-scale measurement, and offset values do not have to be known to perform accurate line-scale measurements. In practice, measurement systems may detect differences in line profiles for scales which exhibit line-edge raggedness. In this case, the differences in the offset may result in a larger systematic error associated with the measurement.

The line-scale measurement can also be made from left edge to left edge, or right edge to right edge, as shown in figures 2-1b and 2-1c, respectively. As in the center-to-center measurements, it is desirable that the line profiles of adjacent lines be very similar and show no edge raggedness. However, it is not necessary that the profiles of the left and right edges of a single line be identical.

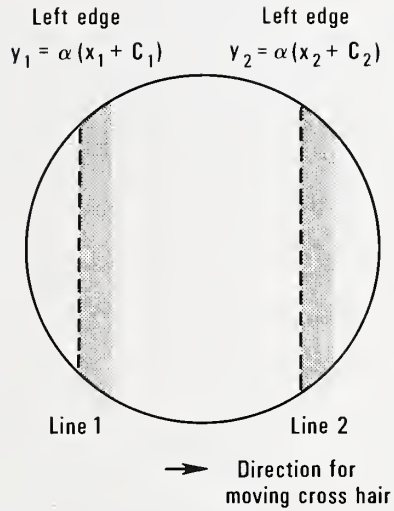
The line-scale measurement is considered a symmetrical measurement since the detector can approach the lines from either direction along the measurement axis to give the same displacement value between line centers, left edges, or right edges. As an example, consider the displacement measurement of two lines with a filar eyepiece on an optical microscope. As shown schematically in figure 2-2a for the first measurement case, the dashed cross hair is moved to the right across the field of view and set at the left edge of line 1 for the measurement  $y_1$ . The cross hair is then moved to the left edge of line 2 for the measurement  $y_2$ . In these measurements, the cross hair is going from a clear background to an opaque line; thus, the microscope operator should be able to set the cross hair so that the offsets in each measurement are nearly equal. In the second measurement case shown in figure 2-2b, the cross hair is moved to the left across the field of view. The cross hair is first set on the left edge of line 2 to measure  $y_2'$  and subsequently on the left edge of line 1 to measure  $y_1'$ . The offsets  $C_1'$  and  $C_2'$  for these measurements may be different from  $C_1$  and  $C_2$  in the first case since the cross hair in the second case is going from an opaque line to a clear background. However,  $C_1 = C_2$ , and  $C_1' = C_2'$  and the offsets again subtract out in each measurement case to give the same displacement measurement in both cases.

## 2.2 Linewidth Measurements

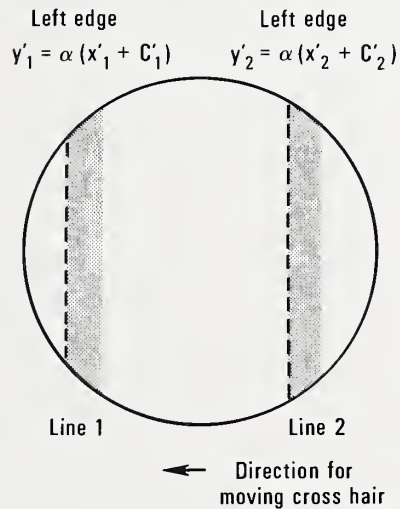
In contrast to a line-scale measurement, a linewidth measurement is a difficult separation measurement. As shown in figure 2-3, a detector is initially located at the left edge of a line, and the measured position  $y_L$  is given by

$$y_L = \alpha(x_L + C_L) , \quad (2-5)$$

where  $\alpha$  and  $x_L$  have the same meaning as the parameters  $\alpha$  and  $x_1$  described in eq (2-1), and  $C_L$  is the systematic offset, or bias, in



(a) Cross hair is moved from left to right across field of view.



(b) Cross hair is moved from right to left across field of view.

Figure 2-2. Schematic of a line-scale measurement with a filar eyepiece on an optical microscope.

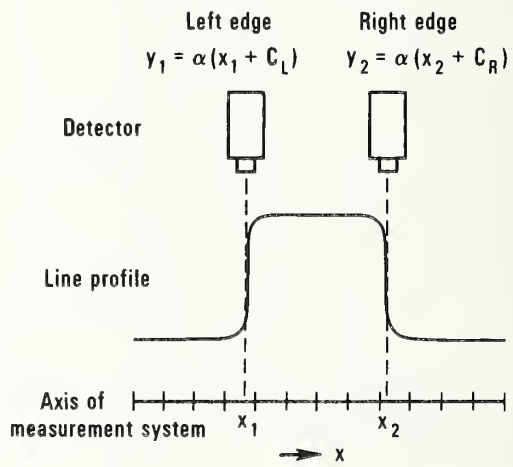


Figure 2-3. Schematic of a linewidth measurement.

locating the left edge of the line. The detector is then moved to the right edge, and the measured position  $y_2$  is given by

$$y_R = \alpha(x_R - C_R) , \quad (2-6)$$

where  $C_R$  is the systematic offset in locating the right edge. The offsets  $C_L$  and  $C_R$  are in opposite directions since the line appears either wider or narrower as a result of viewing the line with measurement-system detector. Thus,  $C_R$  is assigned a negative sign. The separation measurement between the left and right edges of the line is given by

$$y_R - y_L = \alpha(x_R - x_L) - \alpha(C_R + C_L) . \quad (2-7)$$

Therefore, in a linewidth measurement, the offsets add and, consequently, are part of the measured linewidth. This is a fundamental difference between a linewidth and a line-scale measurement.

The linewidth measurement is considered an asymmetrical measurement since the detector does not approach both edges of the line from the same direction and the offsets add. Consider the measurement of a linewidth with a filar eyepiece as shown schematically in figure 2-4. The dashed cross hair is moved to the right across the field of view and set on the left edge of the line for the measurement  $y_L$ . For this setting, the cross hair has gone from a clear background to an opaque line. The cross hair is then moved to the right edge of the same line for the measurement  $y_R$ . For this setting, the cross hair has gone from an opaque line to a clear background. The offset for the left-edge measurement is in the opposite direction of the offset for right-edge measurement, and these offsets will add in the linewidth measurement. It should be further noted that even if the profiles of the left and right edges are identical, the offsets still add. For this case, the offsets  $C_L$  and  $C_R$  are equal and the total offset is  $2C_L$  or  $2C_R$ .

### 2.3 Reduction of Measurement Offsets in Linewidth Calibration

Although the previous discussion of the differences between symmetrical and asymmetrical measurements treats line scales and linewidths, these differences apply to two larger classes of measurements. These measurement classes are: (1) a symmetrical length-interval measurement and (2) an asymmetrical measurement of the length of a physical object. A line-scale measurement is a length-interval measurement and is different in kind from a linewidth measurement which involves the width of a physical object. Length-interval measurements are typically 10 to 100 times more accurate than the measurement of the length of an object. Any attempt to make a direct measurement of object length, such as a linewidth measurement, involves an asymmetrical measurement and offsets which are part of the measurement uncertainties. As noted earlier, these offsets are not part of the measurement uncertainties in symmetrical measurements; therefore, these measurements are generally more accurate. The minimization of the measurement offsets in the current approach to measuring linewidths with inherently asymmetrical systems is the basis for making accurate linewidth calibrations.

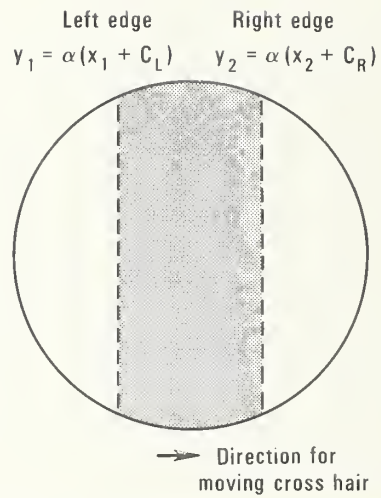


Figure 2-4. Schematic of a linewidth measurement with a filar eyepiece on an optical microscope.

An optical probe, consisting of a microscope with a filar eyepiece, was used in the previous examples to illustrate the behavior of offsets in locating line centers, or edges, in line-scale and linewidth measurement. An electron probe, such as a scanning electron microscope (SEM), which offers better resolving power than an optical probe, also gives a measurement offset; this offset subtracts in a symmetrical measurement and adds in an asymmetrical measurement. The important difference is that the SEM measurement offset is generally much smaller than the optical-microscope measurement offset, and thus, the uncertainties associated with the SEM measurement are potentially smaller.

In the present program, the primary method for linewidth calibration uses the electron probe of an SEM to locate the line edges. This system gives an asymmetrical measurement, but a major effort is being made to minimize the offsets in the calibrated linewidth. The residual offsets should be sufficiently small to permit the calibrated linewidths to be used for determining the resulting offsets when these linewidths are measured with optical microscopes in the IC industry. As discussed earlier, these offsets vary between measurement systems and measurement objects, but with a calibrated linewidth artifact, these offsets can be determined for each set of measurement conditions.

### 3. THEORETICAL ANALYSIS OF OPTICAL MICROSCOPE

Diana Nyssonen  
Electron Devices Division  
Center for Electronics and Electrical Engineering  
National Bureau of Standards  
Washington, DC 20234

and

Richard E. Swing\*  
Frederick, MD 21701

Linewidths in the micrometer range are commonly measured with an optical microscope equipped with a micrometer eyepiece. In this measurement, it is not the physical object or geometrical linewidth which is measured, but instead a magnified optical image of the line. Therefore, the accuracy of these measurements is strongly dependent on the quality of the line image and its relationship to the physical profile of the line. This quality depends, among other things, upon the aberrations of the imaging lens, the amount of defocus present, the spatial coherence of the illumination [12], and the physical properties of the line object.

#### 3.1 Optical Imaging of Lines

The variation in measurements on the same photomask linewidth with different optical-microscope systems, especially for linewidths below 10  $\mu\text{m}$ , has prompted the present investigation of the imaging properties of the optical microscope in transmitted light and a study of possible sources of the measurement error. The effects of diffraction and partial coherence on the mensuration of small objects has been discussed previously in the literature [13-22]. The degree of coherence is a function of the illumination source and the numerical apertures of both the condenser and objective. Light produced by a large incandescent source and focused by a lens is completely incoherent only when the source-to-lens distance is very small and the angle from the source subtended by the lens diameter is very large. As the source-to-lens distance increases, the coherence of the illumination increases. The degree of coherence affects the shape of the edge-image intensity profile and its displacement from the step-function edge position that would be predicted by geometric optical considerations only. The application of the theory of partial coherence to describe image formation in the optical microscope is well developed [20,23]; but the complexity of the numerical calculations involved in treating even simple line objects has prevented a systematic study of the errors introduced under different operating conditions. For diffraction-limited optical systems, the images of edges [18,24], circular discs [13,17], and lines [19,21] are computed for specific ratios of condenser-to-objective numerical apertures. The combinations of defocus and coma with partial coherence are treated by Barakat [19]. Rowe [22] calculates

---

\* Consultant.

the images of defocused edges at the coherent limit. There are difficulties in applying these earlier results to practical microscope systems for the case of circular objects [25]. These difficulties are attributed to the breakdown of scalar optical theory at high numerical apertures [20,26].

A theoretical investigation was begun early in the project to determine quantitatively the effects of coherence on the image of two parallel, opaque lines on a transparent background and its inverse. This is the simplest statement of the problem that must be solved to determine the effects of coherence on linewidth measurements. The first part of this investigation considers a single line and a diffraction-limited lens system. It addresses two questions: (1) what is the minimum size of a single opaque line on a transparent background that can be recognizably imaged as a line at any given quality level? and (2) how can this quality level be specified?

The first of these questions is approached by calculating the relative intensity profile of the image of an ideal line for both spatially incoherent light and spatially coherent light. An ideal opaque line is defined as having zero-percent transmittance across its width and a 100-percent transmittance elsewhere. The image intensity profile of an object [27] is written for the incoherent case as

$$I = \iint \tilde{h}(x,y) \tilde{h}^*(x,y) U_g(x,y) U_g^*(x,y) dx dy \quad (3-1)$$

and for the coherent case as

$$I = \left| \iint \tilde{h}(x,y) U_g(x,y) dx dy \right|^2 \quad (3-2)$$

where  $U_g(x,y)$  is the complex amplitude of radiation from the object, and  $\tilde{h}(x,y)$  is the complex response of the optical system.

Expressions for these functions are derived with the assumption that the lens is diffraction-limited with an impulse response of  $(\sin x)/x$  for the one-dimensional case. The characteristic width of this function, taken to be the distance between the first node points on each side of the line  $x = 0$ , is a measure of the smallest dimension that can be resolved by the lens. The expressions for the intensity profiles for both illumination cases are derived in terms of the ratio  $A$  of object linewidth  $2b$  to the width of the impulse response, the numerical aperture  $N.A.$ , the illumination wavelength  $\lambda$ , the magnification of the lens  $m$ , and the image coordinate  $\beta$ .

The expression for the image intensity profile for the coherent case is

$$I(\xi) = \left| 1 - \frac{1}{\pi} \left\{ \text{Si} \left[ 2\pi \left( \xi + \frac{A}{2} \right) \right] - \text{Si} \left[ 2\pi \left( \xi - \frac{A}{2} \right) \right] \right\} \right|^2, \quad (3-3)$$

and for the incoherent case is

$$I(\xi) = 1 - \frac{1}{\pi} \left\{ \text{Si} \left[ 4\pi \left( \xi + \frac{A}{2} \right) \right] - \text{Si} \left[ 4\pi \left( \xi - \frac{A}{2} \right) \right] \right. \\ \left. - \frac{1 - \cos \left[ 4\pi \left( \xi + \frac{A}{2} \right) \right]}{4\pi \left( \xi + \frac{A}{2} \right)} + \frac{1 - \cos \left[ 4\pi \left( \xi - \frac{A}{2} \right) \right]}{4\pi \left( \xi - \frac{A}{2} \right)} \right\} \quad (3-4)$$

where  $\xi = \beta(\text{N.A.})/\lambda m$  and  $\text{Si}[x] = \int_0^x [(\sin v)/v] dv$ . These functions are plotted in figure 3-1 as a function of the parameter  $\xi$  for the indicated values of A. In all calculations  $\lambda = 500 \text{ nm}$ . For illustrative purposes, this figure is divided vertically through the center with the edges of the ideal image intensity profile (the image profile that is an exact magnification of the object profile) located at  $\xi = \pm 1.0$ . The relative intensity profiles for incoherent illumination are plotted on the left side of the figure and the profiles for coherent illumination on the right side. Since the profiles are symmetrical about the center of the figure, the complete line profile may be visualized by mirroring any particular profile through the figure center. The profiles I-1 and C-1 in the figure show a badly degraded image and are indicative of the images that result when a line whose width is somewhat smaller than the resolution limit of the lens is imaged. The other curves in this figure represent relative intensity profiles for wider lines and illustrate that the edge image profiles become sharper as the linewidths become appreciably larger than the impulse response of the lens.

With the exception of the curves I-1 and C-1 in figure 3-1, all of the image intensity profiles cross the ideal edge image at nearly the same point for each illumination case. For the incoherent case, this point is at approximately 0.5 relative intensity (50-percent transmittance). This is a relatively easy intensity level to distinguish visually. However, the image intensity profiles for the coherent case cross the ideal edge image at 0.25 relative intensity (25-percent transmittance), and this cannot be consistently detected visually.

It is not uncommon to observe ringing near the edge of a line image in a microscope, that is, bright and dark bands near the edge image. Such ringing is shown for the case of coherent illumination by the oscillations of the image intensity profiles about 1.0 relative intensity (100-percent transmittance), while this phenomenon is absent for the incoherent case. Thus, it may be concluded that an appreciable amount of illumination coherence is present under normal microscope operating conditions.

To establish a quantitative measure of the image quality, the root-mean-square (RMS) difference between the spectra of the image intensity profiles and the ideal intensity profiles were evaluated. This RMS difference is arbitrarily defined as

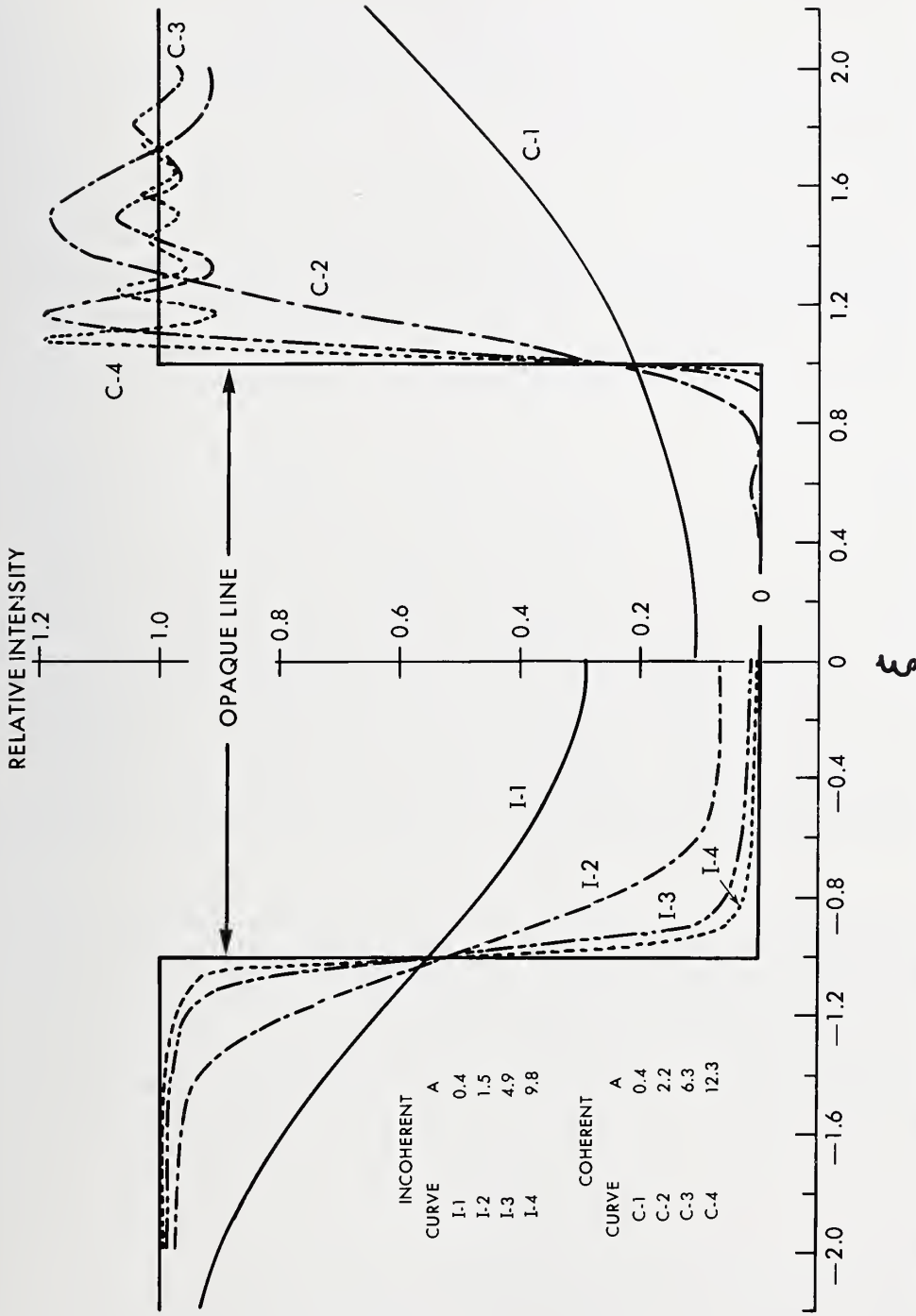


Figure 3-1. Image intensity profiles of an opaque line on a clear background for incoherent and coherent illumination.

$$D = \left[ \frac{1}{P} \int_0^P \left\{ F[I_1(\xi)] - F[I_a(\xi)] \right\}^2 d\xi \right]^{1/2} \quad (3-5)$$

where  $F[I_1(\xi)]$  is the spectrum of the ideal image intensity profile,  $F[I_a(\xi)]$  is the spectrum of the calculated or actual image profile, and  $P$  is the interval of integration.

The spectrum of the image profile is a function in the spatial-frequency domain (line cycles per unit length). Since a lens forms an image by transmitting information of different spatial frequencies, a comparison of the spectrum of the image with that of the object should provide a quantitative measure of the image quality. Values of the RMS differences are listed in table 3-1 as a function of the parameter  $A$ . For each of several numerical apertures commonly found in microscope objectives, table 3-1 also lists the approximate width of the impulse response and the corresponding object linewidths.

The previous analysis shows a wide disparity in the type of imagery for the limiting cases of coherent and incoherent illumination. The normal operation of a microscope employs neither of these limiting forms of illumination; instead the illumination is partially coherent. Very little information is available in the literature about the partially coherent imaging of lines. One such calculation shown in figure 3-2 (after Welford [28]) compares several theoretically calculated edge-image intensity profiles. Curve A represents the edge-image intensity profile for a large incandescent source and uniformly filled, matched condenser and objective lenses with numerical apertures of 0.65. Curve B represents the profile for incoherent illumination corresponding to an infinitely large condenser aperture. Curve C represents the profile for coherent illumination corresponding to an infinitely small condenser aperture. The ideal edge is shown by curve D. These curves are all normalized to converge to the 1.0 relative intensity level at large distances from the edge.

Several phenomena are illustrated in figure 3-2. The edge-image intensity profile for incoherent illumination (curve B) has zero displacement from the ideal edge position at the 0.5 relative intensity. This is the intensity level at which the edge is usually located by visual observations. On the other hand, a displacement of  $0.08 \mu\text{m}$  is observed at the 0.5 relative intensity for the edge profile obtained for matched numerical apertures (curve A). For a pair of matched numerical apertures, the displacement distance  $x$  from the ideal edge may be found from the relation

$$x = \left( \frac{0.65}{\text{N.A.}} \right) \cdot x_f \quad (3-6)$$

where  $x_f$  is the  $x$ -coordinate for curve A in figure 3-2.

Ringling is shown in curve A by the oscillations between the 0.9 and 1.0 relative intensities. This appears in the microscope image as alter-

Table 3-1 - Object Linewidths and Corresponding RMS Differences Determined from the Curves of Figure 3-1.

Curve	A	% RMS	Object Linewidth for N.A. of			
			0.25	0.5	0.65	0.85
<b>Coherent Illumination:</b>						
C-1	0.4	10	0.7 $\mu\text{m}$	0.4 $\mu\text{m}$	0.3 $\mu\text{m}$	0.2 $\mu\text{m}$
C-2	2.2	5	4.4	2.2	1.7	1.3
C-3	6.3	2	12.5	6.3	4.8	3.7
C-4	12.3	1	24.7	12.3	9.5	7.2
<b>Incoherent Illumination:</b>						
I-1	0.4	10	0.9 $\mu\text{m}$	0.4 $\mu\text{m}$	0.3 $\mu\text{m}$	0.2 $\mu\text{m}$
I-2	1.5	5	2.9	1.5	1.1	0.9
I-3	4.9	2	9.7	4.9	3.7	2.9
I-4	9.8	1	19.5	9.8	6.3	5.7
<b>Impulse-Response Width:</b>						
			2.0 $\mu\text{m}$	1.0 $\mu\text{m}$	0.76 $\mu\text{m}$	0.59 $\mu\text{m}$

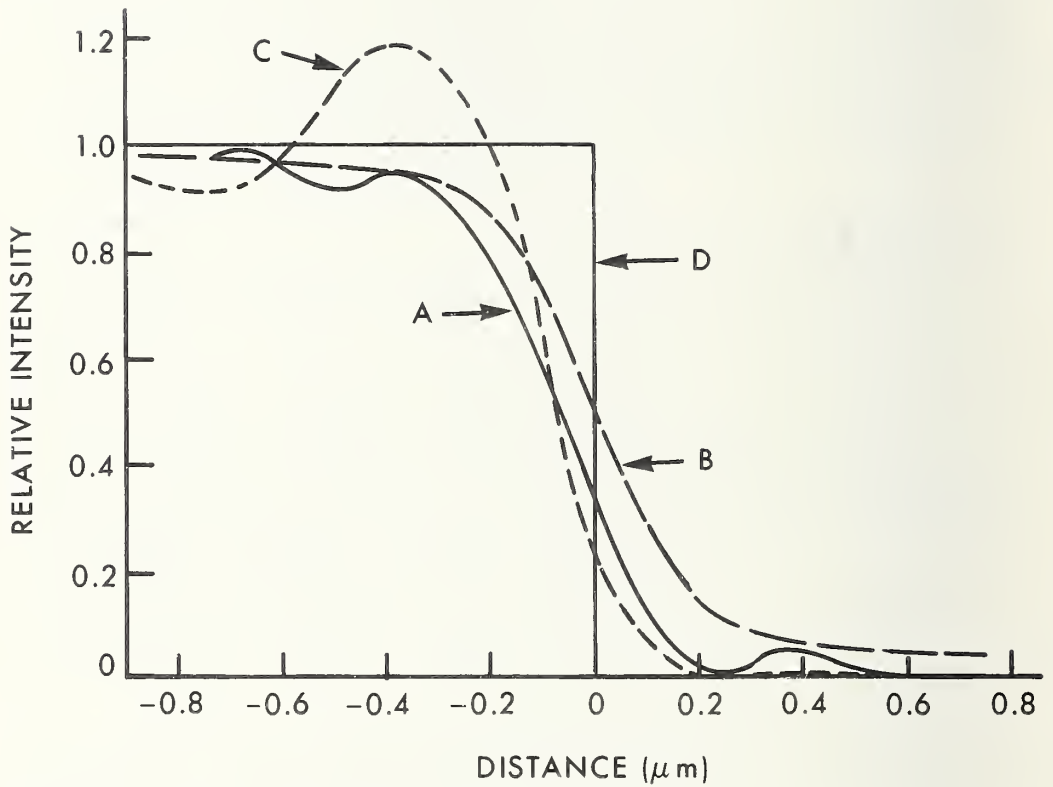


Figure 3-2. Image intensity profiles of a single line edge for an illumination wavelength of 500 nm; A - matched numerical apertures of 0.65, B - incoherent illumination, C - coherent illumination, D - ideal edge.

nate light and dark bands parallel to the edge image. This observed ringing indicates that the illumination has a high degree of coherence. Also, the edge intensity profile produced with matched numerical apertures is closer to the intensity profile for coherent illumination than it is to the intensity profile for incoherent illumination.

It is also known that focus affects the shape of the edge intensity profile and is subjectively determined by selecting the object-to-lens distance which produces the sharpest image. Theoretical calculations of the effect of defocusing on relative intensity profiles were made for coherent illumination. The amount of defocus  $\Delta$  is the longitudinal displacement of the actual object plane from the object plane predicted by geometric optics (the geometric focus). In making these calculations, it is more convenient to consider the maximum deviation of the actual wave front from the ideal spherical wave front. This deviation  $n\lambda$ , in multiples of wavelength, is related to  $\Delta$  by

$$n\lambda = \Delta(\text{N.A.})^2/2, \quad (3-7)$$

where  $\text{N.A.} = \sin \theta$  for a dry microscope objective.

Figure 3-3 shows image intensity profiles for various amounts of defocus. It may be seen from this figure that, due to the ringing, the contrast between the edge and the first dark band is greater for a small amount of defocus than for the proper focus. Consequently, an observer may easily choose a defocused microscope setting as the correct focus because of the increased sharpness produced by a small amount of defocusing. If this should occur, the location of the edge would be chosen from a degraded image intensity profile and would be displaced significantly from the geometric image. The tendency for an observer to choose an incorrect focus and degraded edge profile can be further appreciated by noting that  $1\lambda$  defocus for  $\lambda = 500 \text{ nm}$  and an objective lens with  $\text{N.A.} = 0.65$  corresponds to a defocus displacement of only about  $2.4 \mu\text{m}$ . It should be noted that for an objective with a higher numerical aperture, the term  $\tan \theta$ , where  $\tan \theta$  is the ratio of the radius of the lens aperture to the focal distance of the lens, cannot be approximated by  $\sin \theta$  as in eq (3-7). For this case, the wave-front deviation is

$$n\lambda = \Delta \tan^2 \theta / 2. \quad (3-8)$$

For an objective with  $\text{N.A.} = 0.90$ ,  $\lambda/4$  defocus for  $\lambda = 500 \text{ nm}$  corresponds to a defocus displacement of  $0.06 \mu\text{m}$ .

The image quality is also degraded by spherical aberration of the objective lens. This aberration causes light rays passing through the outer portions of the lens to be focused at a different distance from the lens than rays passing through the central portion of the lens and is present, to some degree, in all optical systems. Spherical aberration is greater when microscope objectives are used at the wrong tube length or when objectives and eyepieces of different types or manufacture are used together. The effects of this aberration may be partially compensated by introducing an equivalent amount of defocus; this results in a sharper image. Spherical aberration is also described in terms of  $n\lambda$  where  $n\lambda$

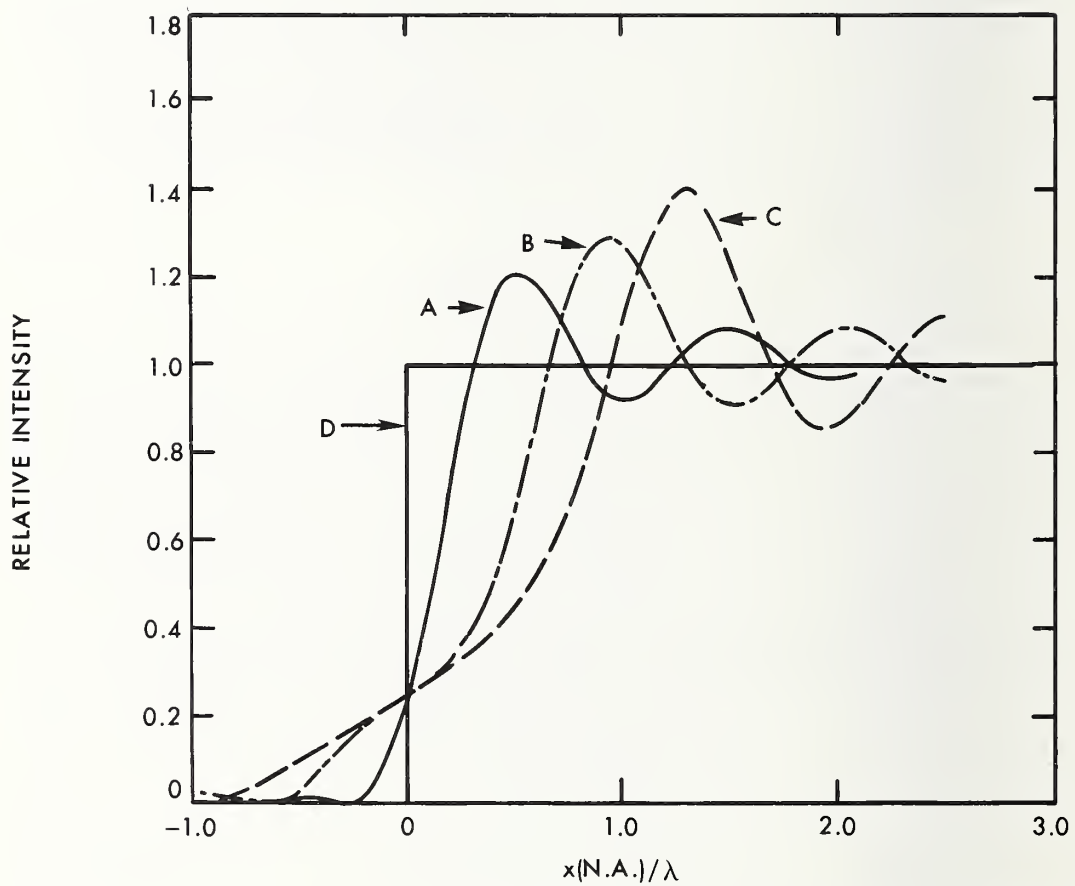


Figure 3-3. Image intensity profiles of a single line edge for coherent illumination with varying defocus; A - no defocus, B -  $\lambda/2$  defocus, C -  $\lambda$  defocus, D - ideal edge.

now refers to the maximum difference, in multiples of wavelength, between the aberrated wave front and the ideal spherical wave front produced by a diffraction-limited lens. Figure 3-4 shows calculated edge-image intensity profiles in coherent illumination for an objective lens with  $1\lambda$  spherical aberration and varying defocus. This figure shows that a sharp image intensity profile is produced when the amount of defocus suitably compensates the spherical aberration: this focus is usually called the best focus. This figure also shows that the contrast between the edge image and the bands produced by ringing increases as the defocus is increased. This illustrates the difficulty of visually choosing the correct focus because of the temptation to adjust the microscope for the highest contrast.

The previous analysis gives a quantitative idea of the effects of coherence and aberrations on microscope imagery. For a quantitative evaluation of linewidth-measurement errors with real microscope systems, a more accurate theoretical description of partially coherent imaging is necessary. In addition, experimental verification of the description for realistic microscope parameters is necessary. Therefore, a more detailed analysis was undertaken. This work includes numerical computation of line images for actual conditions of microscope operation. The computation is based on a mathematical model which incorporates partial coherence, optical aberrations including defocus, amplitude transmittance of the sample allowing for degraded edges, and the effect of the scanning aperture. In section 6, these theoretical profiles are compared with experimentally measured data for varying numerical apertures.

### 3.2 Calculation of Image Profiles for Real Systems

Starting with the scalar mutual coherence function  $\Gamma$  at the sample plane and propagating to the scanning aperture, the flux  $I$  at the detector as a function of the sample displacement  $\xi_0$  may be described in one dimension for quasi-monochromatic illumination by

$$I(\xi_0) = \int \Gamma_0(x_1, x_2) t(x_2 - \xi_0) t^*(x_2 - \xi_0) \exp \left\{ \frac{ik}{z_1} (\mu_2 x_2 - \mu_1 x_1) \right\} \cdot F(\mu_1) F^*(\mu_2) \exp \left\{ \frac{iky}{x_2} (\mu_2 - \mu_1) \right\} S(y) dx_1 dx_2 d\mu_1 d\mu_2 dy \quad (3-9)$$

where:

$\xi_0$  is the scanning variable corresponding to the displacement of the line from the optical axis,

$z_1$  and  $z_2$  are the object and image conjugates, respectively,

$t$  is the amplitude transmittance of the sample,

$F$  is the pupil function of the imaging objective and relay optics combined,

\* denotes the complex conjugate,

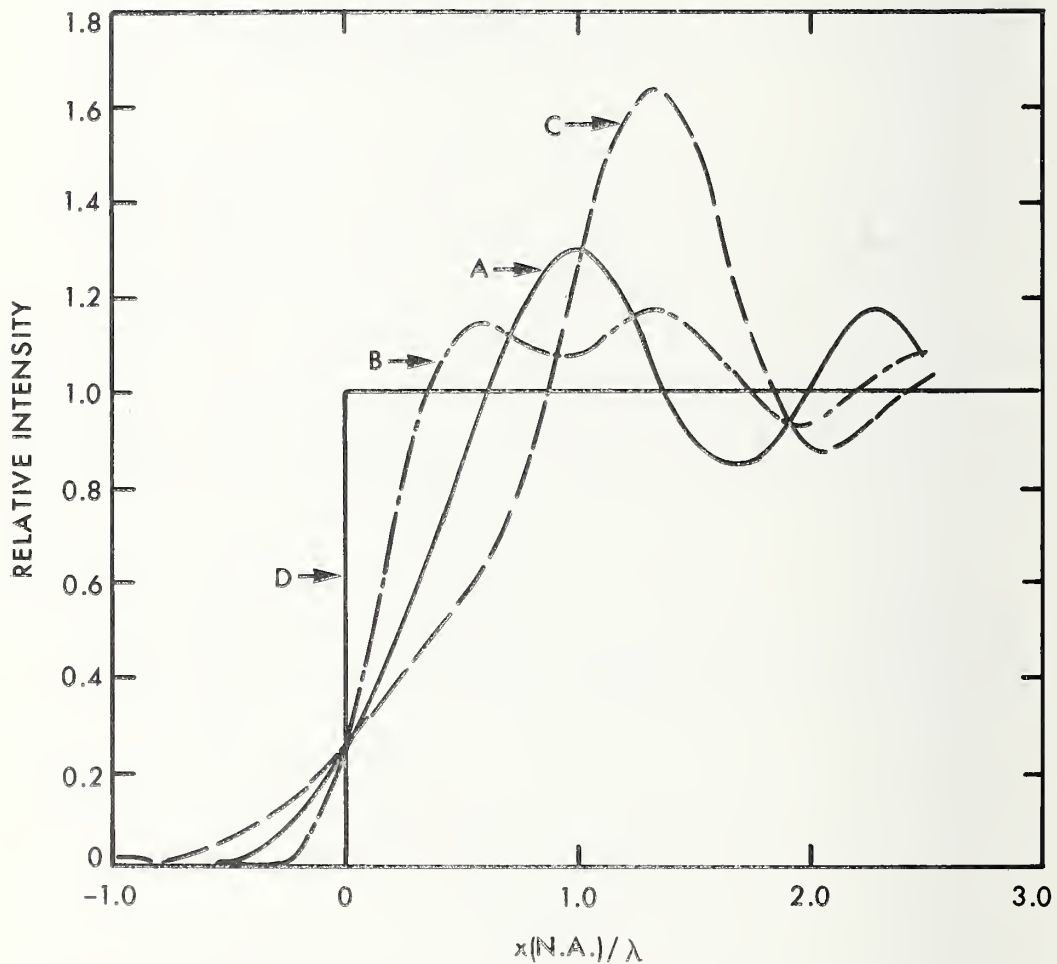


Figure 3-4. Image intensity profiles of a single line edge for coherent illumination with  $1\lambda$  spherical aberration and varying defocus; A - no defocus, B -  $-1\lambda$  defocus, C -  $-2\lambda$  defocus, D - ideal edge.

S is the intensity transmittance function of the scanning aperture, and the rectangular coordinates  $x$ ,  $y$ , and  $\mu$  are shown in figure 3-5. This equation simplifies to a form more convenient for computer calculations; namely,

$$I(\xi_0) = C \iiint \tilde{T}(\alpha) \tilde{t}(\alpha - \mu_2) \tilde{t}^*(\alpha - \mu_1) \exp[-ik\xi_0(\mu_1 - \mu_2)/z_1] \\ \cdot F(\mu_1) F^*(\mu_2) \tilde{S}\left(\frac{\mu_2 - \mu_1}{\lambda z_2}\right) d\alpha d\mu_1 d\mu_2 \quad (3-10)$$

where  $\tilde{\nu}$  denotes the spatial Fourier transform.

This one-dimensional description is accurate for one-dimensionally varying objects in a circular lens systems only at the coherent limit. The equivalent description for a partially coherent, two-dimensional lens system is

$$I(\xi_0) = C \iiint \tilde{T}(\alpha, \eta) \tilde{t}(\alpha - \mu_2) \tilde{t}^*(\alpha - \mu_1) \exp[-ik\xi_0(\mu_1 - \mu_2)/z_1] \\ \cdot F(\mu_1, \eta) F^*(\mu_2, \eta) \tilde{S}\left(\frac{\mu_2 - \mu_1}{\lambda z_2}\right) d\alpha d\mu_1 d\mu_2 d\eta \quad (3-11)$$

The computation time required for this two-dimensional case is prohibitive. Therefore, the one-dimensional description given in eq (3-9) was studied closely to determine if it adequately describes the measurement conditions. In photomask-linewidth measurements, the glass substrate requires the use of condensers with a numerical aperture less than the numerical aperture of the commonly used, high-resolution objective. This requirement results from the unavailability of long working-distance, high numerical-aperture condensers. From a comparison of theoretical and experimental results, it appears that for ratios  $R$  of condenser-to-objective numerical apertures less than 1.0, the system is closer to the coherent limit, and the imagery may be approximated by the one-dimensional solution given by eq (3-9). Therefore, the following calculations for image profiles are based on this equation.

When the condenser aperture is uniformly illuminated so that it is the limiting aperture in the illumination system and the illuminated area of the sample is large compared to the dimensions of the impulse response of the condenser,  $\tilde{T}$  is the flux distribution in the condenser aperture [23, 29]. When the area of illumination becomes very small, the system must be treated theoretically as a microdensitometer for which a different description applies [30]. Wide-field illumination is assumed in the following calculations.

The optical-transmittance function  $t$  of the sample is usually related to the physical profile of the chromium or other photomask material by the function  $\exp(-k\kappa d)$  where  $k$  is the wave number,  $\kappa$  is the imaginary part of the complex index of refraction of the photomask material, and  $d$  is the thickness of the material. If perfect edges are assumed, the

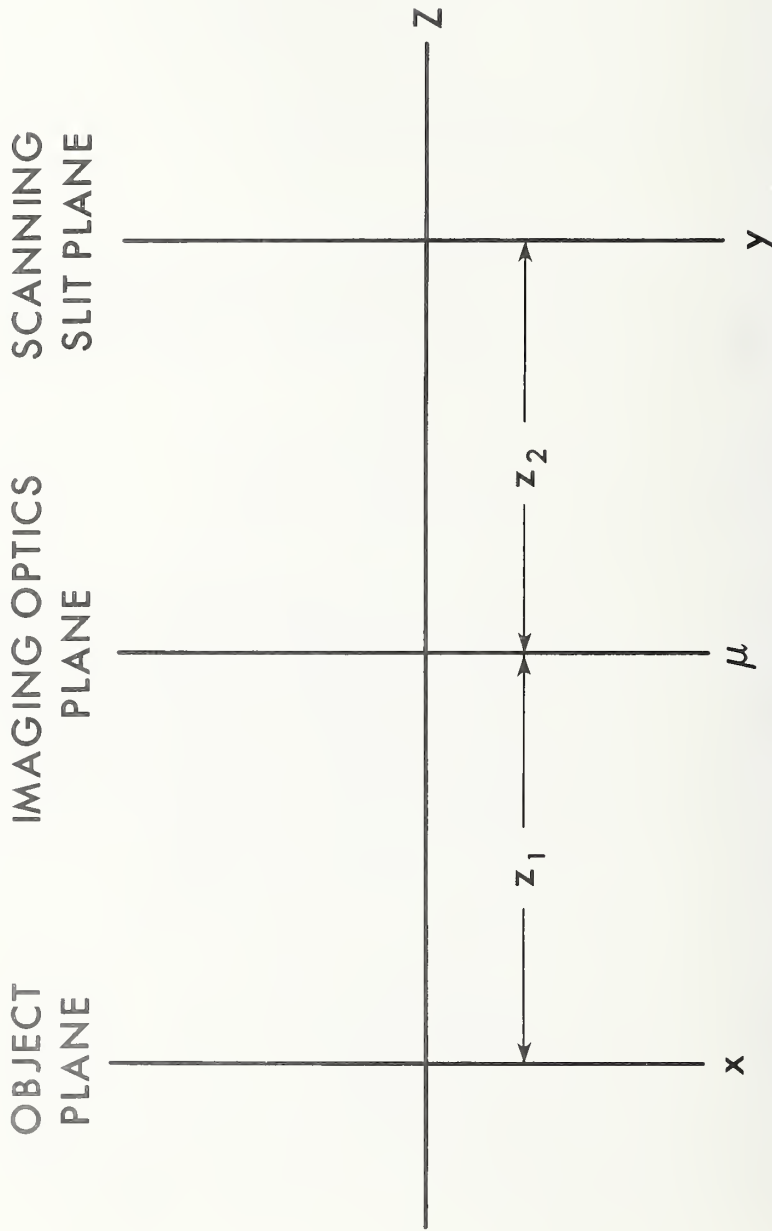


Figure 3-5. Coordinates for one-dimensional description of imaging system. [See eq (3-9).]

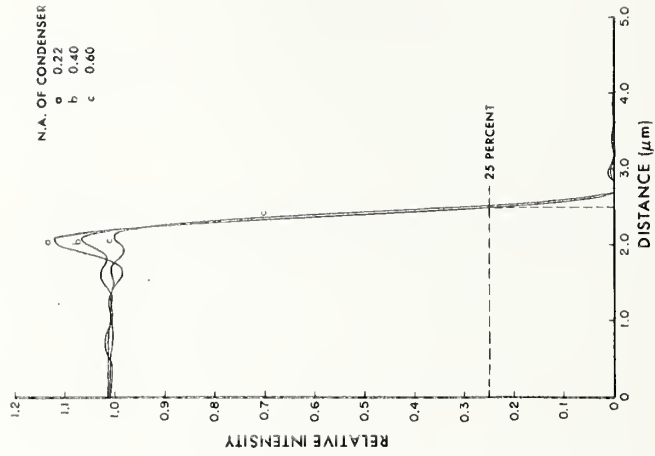
transmittances of the opaque and clear areas may be determined optically.

The pupil function of a microscope objective includes defocus and spherical aberration [31]. The calculation of image profiles in the present discussion assumes quasi-monochromatic illumination and, therefore, does not take into account the variation of the aberration terms with illumination wavelength. The present study indicates that chromatic aberrations in the microscope cause image degradation in white light and thereby contribute to linewidth-measurement errors. (See sec. 6.1.)

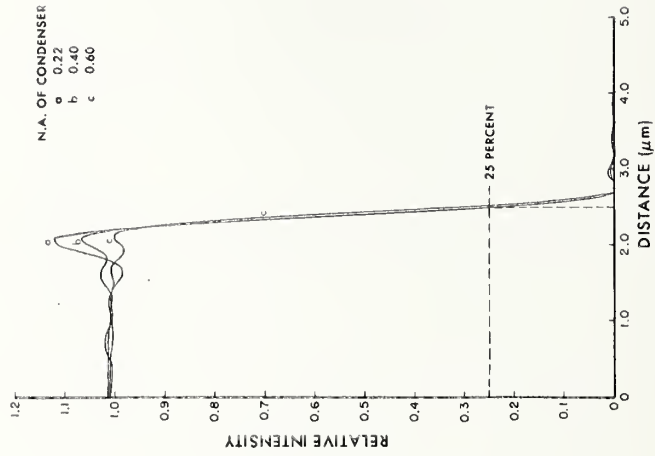
Using numerical-integration techniques, image profiles of a clear line were computed based on eq (3-9). The particular parameters of the system were chosen in order to explore the imaging behavior of the photometric optical microscope used for measuring linewidths in the present program. (See sec. 6.2.) Figure 3-6 shows the image profiles of a 5- $\mu\text{m}$  wide clear line for different combinations of condenser and objective numerical apertures. These profiles are similar to edge-image profiles found in the literature [19,21] and exhibit the suppression of the coherent edge ringing as the numerical aperture of the condenser increases. They also indicate that the true edge location corresponds to the 25-percent threshold with only a slight deviation beginning to show as the ratio of condenser-to-objective numerical apertures  $R$  approaches 1.0.

Figures 3-7 and 3-8 show image profiles of progressively smaller linewidths for the numerical-aperture ratio of 0.60/0.90 ( $R = 0.66$ ). This ratio appears to be a reasonable choice for linewidth measurement. As shown in figure 3-7, the detail in the vicinity of the edge of a line is significantly wider than the impulse response of the optics scales with N.A. and illumination wavelength. These two figures indicate that the 25-percent threshold corresponds to the true edge location for linewidths down to 0.5  $\mu\text{m}$ , despite the influence of the neighboring edge on the image profile.

In order to explore the effects of defocus and spherical aberration on the 25-percent threshold, the image profiles shown in figures 3-9 and 3-10 were calculated. These profiles correspond to stepping through focus in steps of  $\lambda/4$  without (fig. 3-9) and with (fig. 3-10) spherical aberration. The choice of  $2\lambda$  spherical aberration corresponds to using an incorrect tube length between the objective and eyepiece (i.e., 160 mm instead of 220 mm) or using a sample cover glass whose thickness does not match the thickness for which the objective was designed (i.e., 0.12 mm instead of 0.17 mm). The condition of steepest edge slope occurs at  $0\lambda$  defocus without spherical aberration and at  $-1.0\lambda$  with spherical aberration. This indicates that the usual aberration balancing of spherical and defocus used in incoherent illumination is not applicable to partially coherent images. Also, with no spherical aberration, maximum slope and maximum intensity overshoot at the edge coincide; whereas, with 2 spherical aberration present, maximum contrast in the ringing structure occurs at  $-0.5\lambda$  defocus. With no spherical aberration, the 25-percent threshold yields the true edge location only within the Rayleigh focus tolerance of  $\lambda/4$  corresponding to  $\pm 0.35\text{-}\mu\text{m}$  displacement at an N.A. of



(a) 0.90 N.A. objective.



(b) 0.65 N.A. objective.

Figure 3-6. Calculated image profiles of one edge of a 5- $\mu\text{m}$  wide clear line for an optical microscope with various objective and condenser numerical apertures; illumination wavelength of 560 nm, effective scanning slit of 0.13  $\mu\text{m}$ , and diffraction-limited optics.

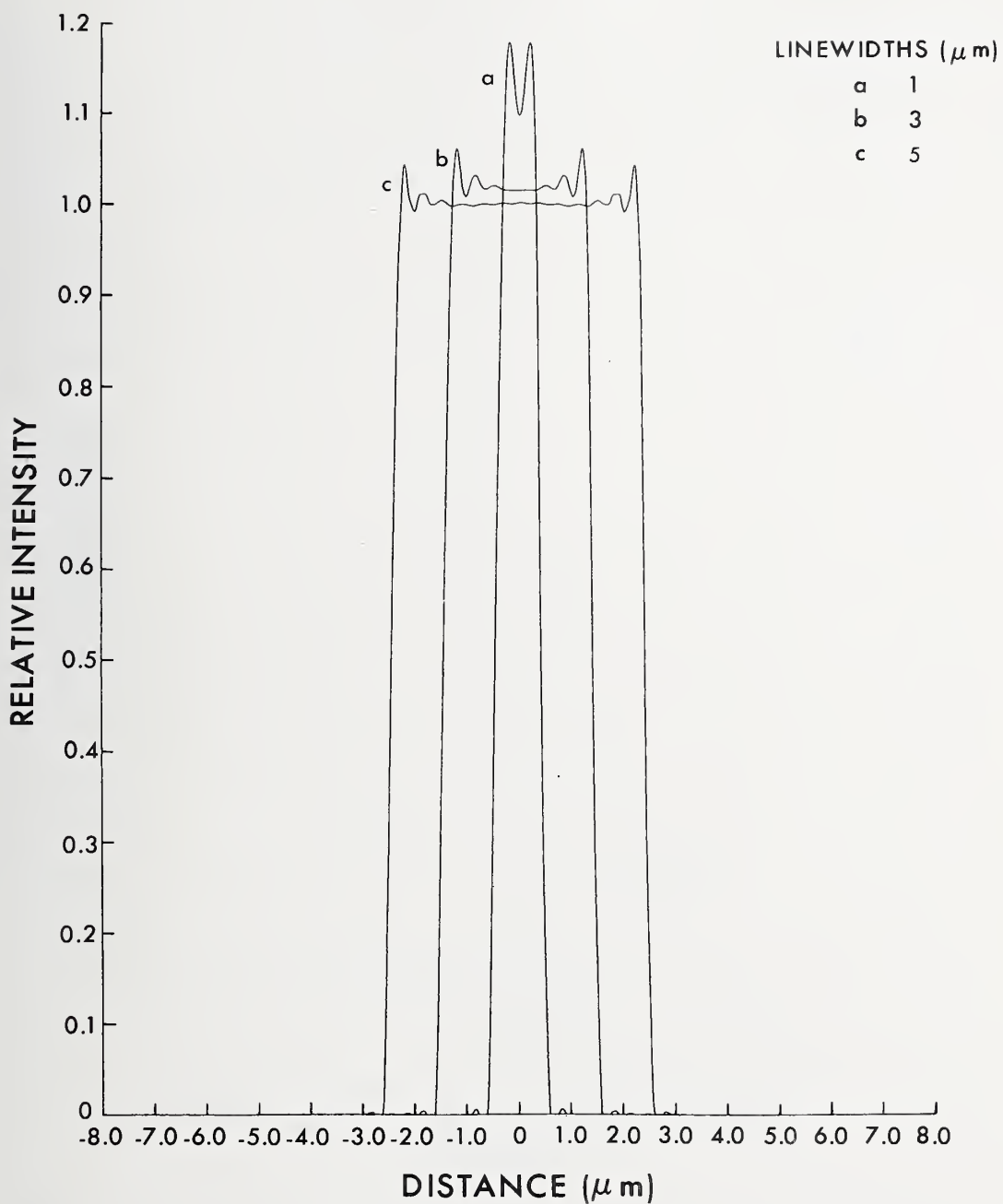


Figure 3-7. Calculated image profiles of 1-, 3-, and 5- $\mu\text{m}$  wide clear lines for an optical microscope with a 0.90 N.A. objective, 0.60 N.A. condenser, illumination wavelength of 560 nm, effective scanning slit width of 0.13  $\mu\text{m}$ , and diffraction-limited optics.

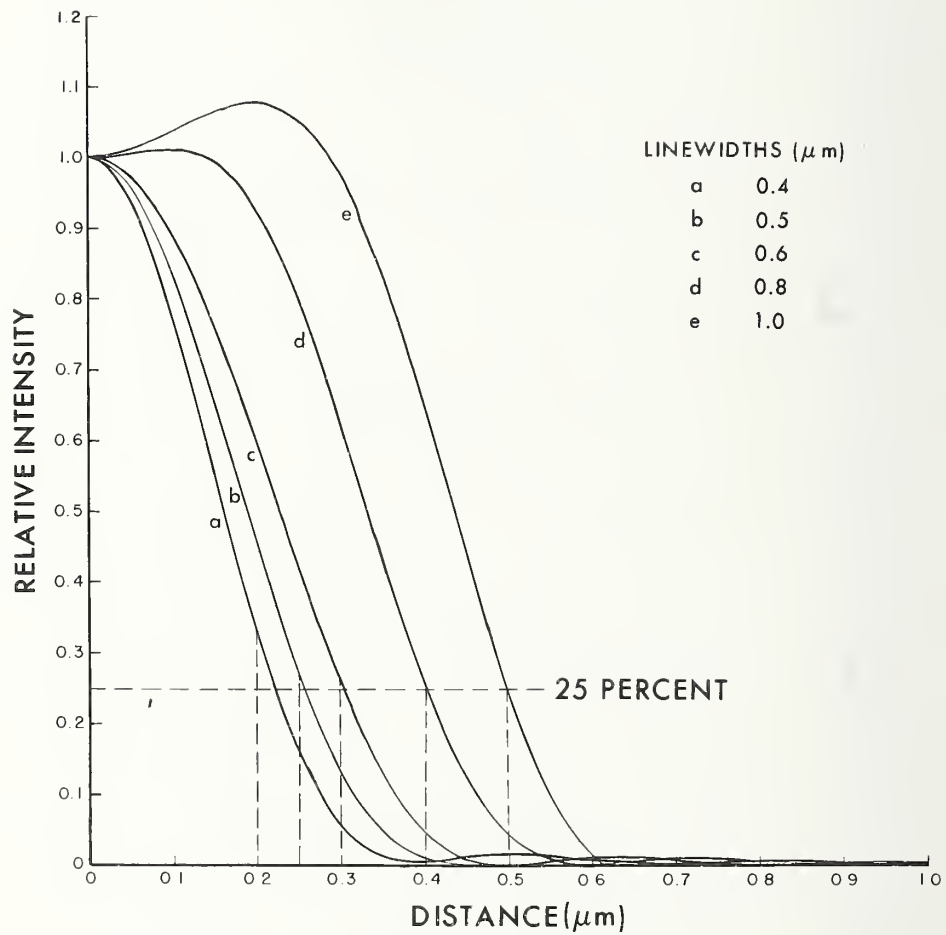


Figure 3-8. Calculated image profiles of one edge of 0.4-, 0.5-, 0.6-, 0.8-, and 1.0- $\mu\text{m}$  wide clear lines for an optical microscope with the same parameters as figure 3-7.

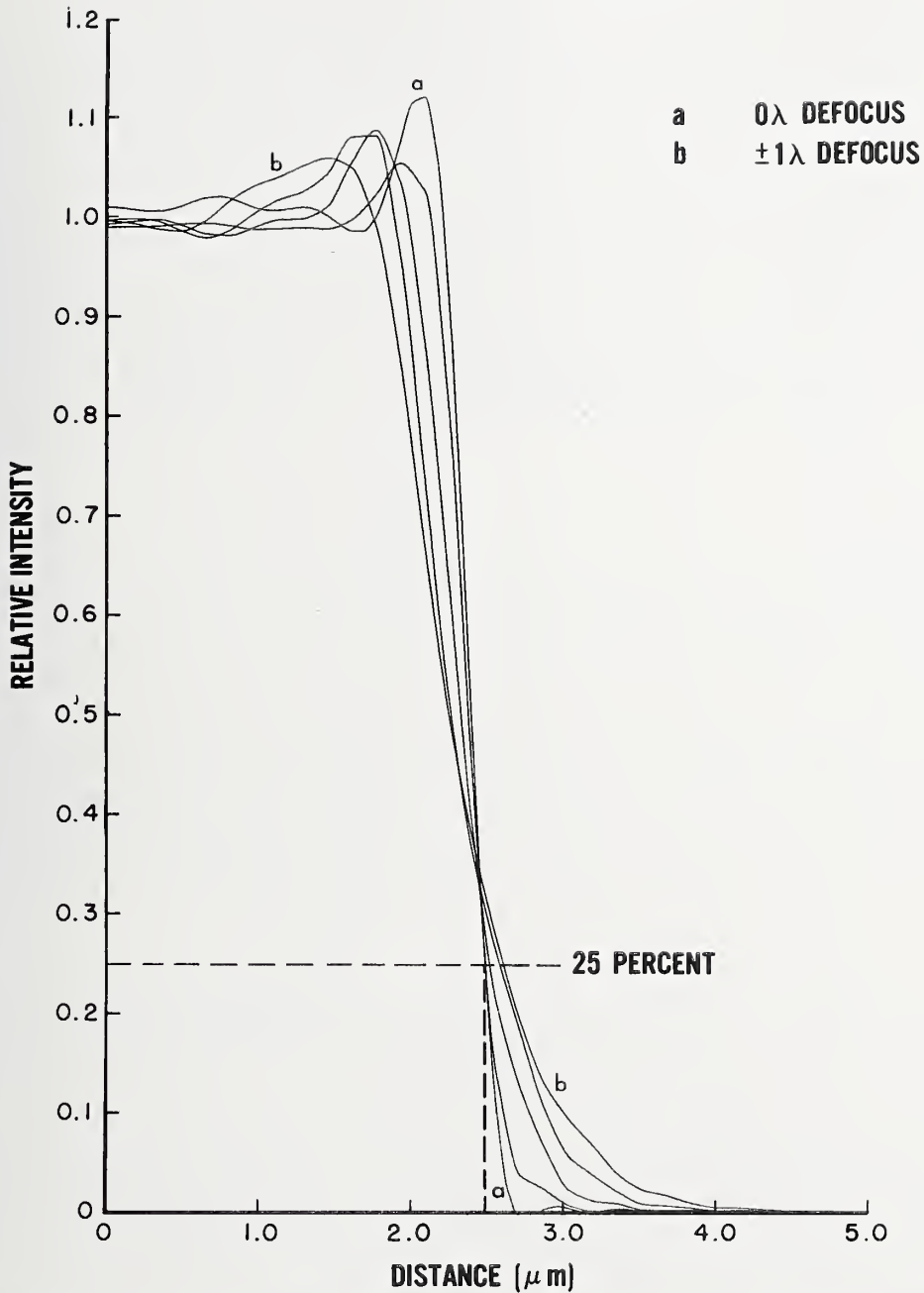


Figure 3-9. Calculated image profiles of one edge of a 5- $\mu\text{m}$  wide clear line for an optical microscope with defocus in steps of  $\lambda/4$  from 0 to  $+1\lambda$ ;  $\lambda/4$  corresponds to  $+0.06 \mu\text{m}$  for a 0.90 N.A. objective and an illumination wavelength of 560 nm; other microscope parameters are the same as in figure 3-7.

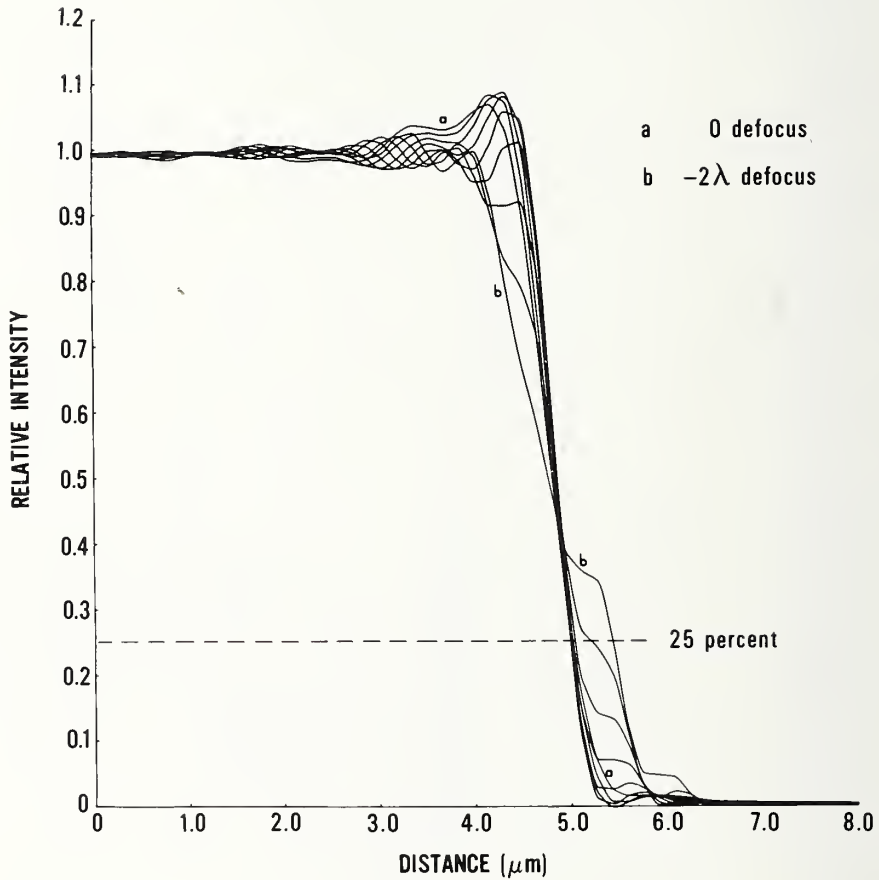


Figure 3-10. Calculated image profiles of one edge of a 10- $\mu\text{m}$  wide clear line for an optical microscope with  $2\lambda$  of spherical aberration and defocus varying in steps of  $\lambda/4$  from 0 to  $-2\lambda$ ;  $\lambda/4$  corresponds to  $\pm 0.39$   $\mu\text{m}$  for a 0.65 N.A. objective and an illumination wavelength of 560 nm; other microscope parameters are 0.22 N.A. condenser, effective scanning slit of 0.13  $\mu\text{m}$ , and diffraction-limited optics.

0.90; whereas, with  $2\lambda$  spherical aberration, any focus position between  $-1.0\lambda$  and  $-0.5\lambda$  (steepest slope and maximum ringing contrast) would yield the true edge location at the 25-percent threshold. The 25-percent threshold, therefore, appears to be the best criterion to use for linewidth measurement even when spherical aberration is present.

The 25-percent threshold must be corrected for finite transmission of the opaque area of the photomask. The correction is easily derived from the limiting case of coherent illuminations. Figure 3-11 shows the condition corresponding to the true edge location, that is, when a symmetric impulse response is centered at the edge. For an opaque area of the photomask, the amplitude transmittance can have a maximum value of 50 percent. Squaring this transmittance to get intensity yields a 25-percent threshold. If the transmittance is 1.0 in the clear area and  $T_0$  in the opaque area, the threshold corresponding to the true edge location is given by

$$T_c = 0.25(1 + \sqrt{T_0})^2. \quad (3-12)$$

For example, with a transmittance  $T_0$  of 0.04, the threshold increases to 0.36. The resulting change in the edge location for 0.90 N.A. objective is  $0.04 \mu\text{m}$ ; thus, using the uncorrected threshold gives a linewidth error of  $0.08 \mu\text{m}$ . This error increases with defocus or spherical aberration present.

A calculation of the effect of finite background transmittance was performed in order to check the validity of eq (3-12) for determining the threshold corresponding to edge location. Figure 3-12 shows a comparison of the calculated images of a  $1\text{-}\mu\text{m}$  wide clear line for zero-percent and 2.5-percent transmittance in the opaque area. For the latter transmittance, the proper threshold given by eq (3-12) is 0.335.

### 3.3 Filar and Image-Shearing Eyepieces

Some preliminary modeling of the interaction of the filar and image-shearing eyepieces with the microscope imagery described in the previous section was undertaken in order to assess the possible sources of linewidth-measurement error. The image intensity profiles for an ideal edge with incoherent illumination and for a filar eyepiece with the cross hair located in the image plane are illustrated in figure 3-13a. The cross hair is traversed from the dark region to the bright region. The edge position is taken as the center of the cross-hair image when the edge of the cross hair nearer to the bright region just begins to cover the bright region, as illustrated in figure 3-13b. The threshold visibility point is arbitrarily taken at the 10-percent intensity level. Thus, the edge is located by the filar eyepiece at the value of the coordinate corresponding to the 10-percent intensity level minus one-half the cross-hair width. When the cross hair is traversed from the bright region to the dark region, a bright line begins to appear on the dark side of the cross-hair image as shown in figure 3-13c. The edge position is taken as the position of the center of the cross-hair image when this bright line is just no longer visible. In this case, the edge is also

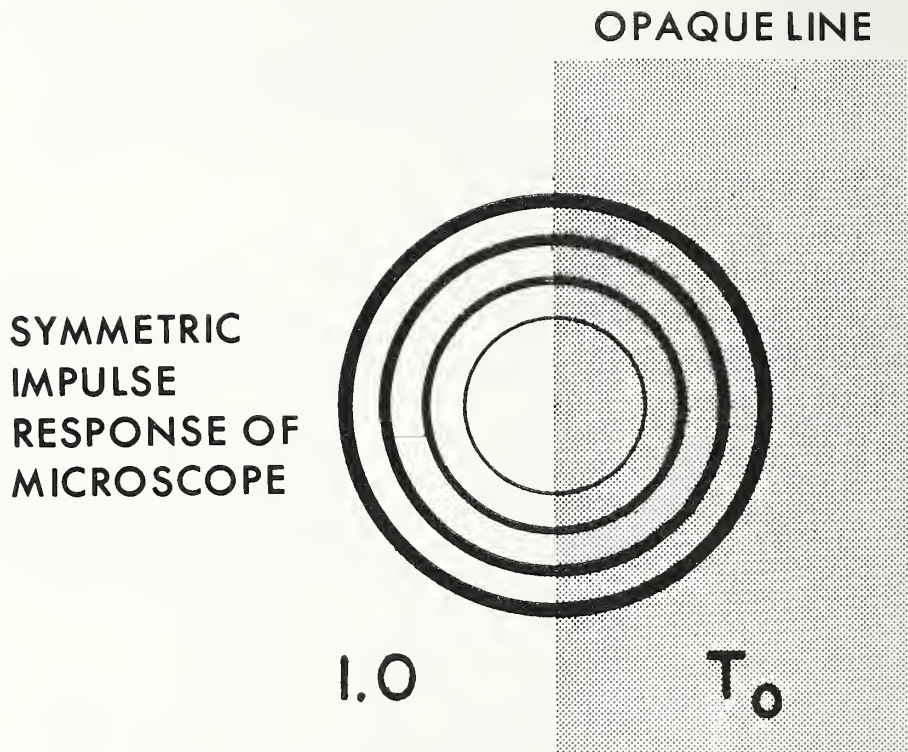


Figure 3-11. Schematic of symmetric impulse response of an optical microscope centered on a line edge;  $T_0$  is transmittance of the opaque line, and the transmittance of the clear area is 1.0.

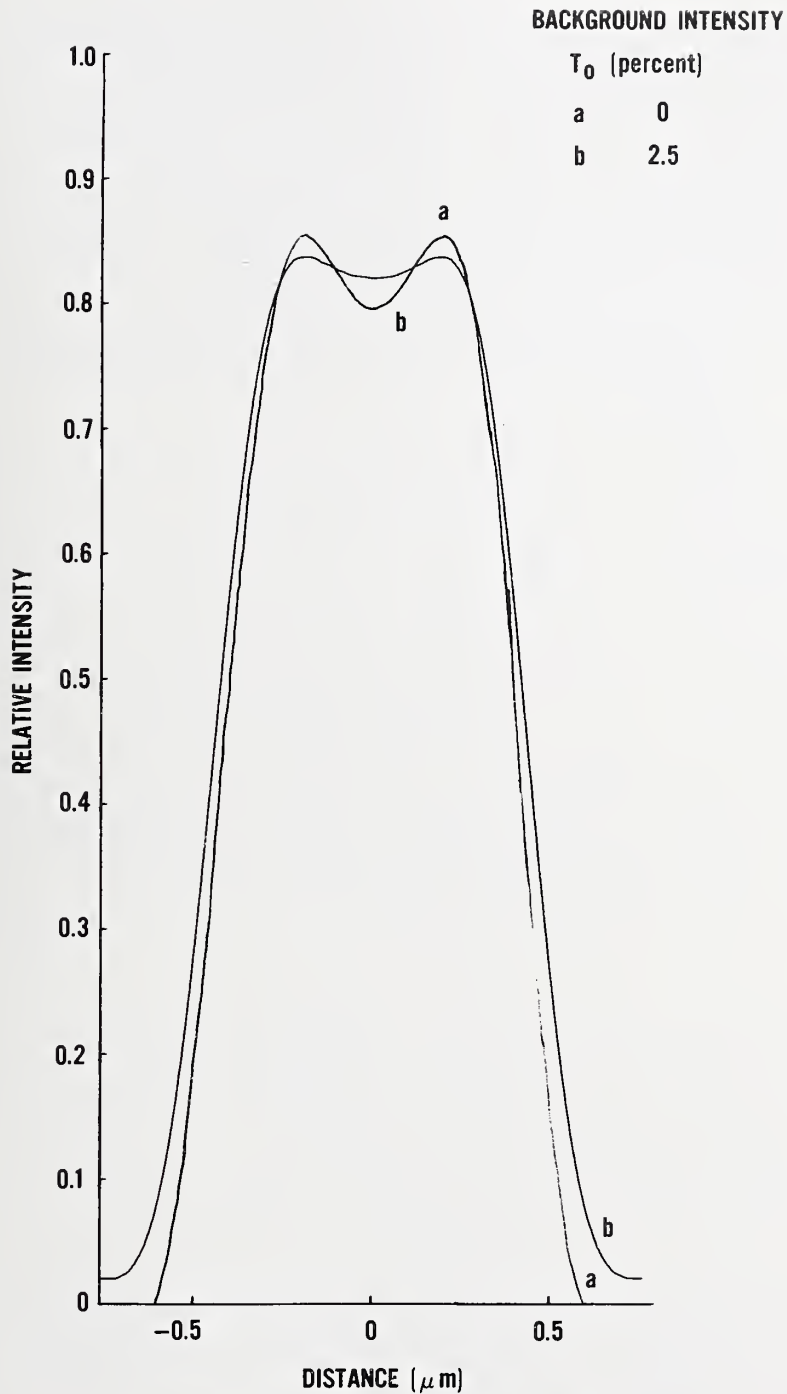
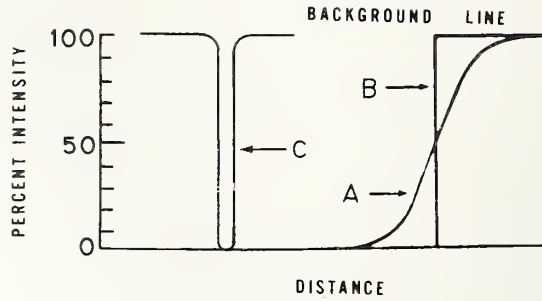
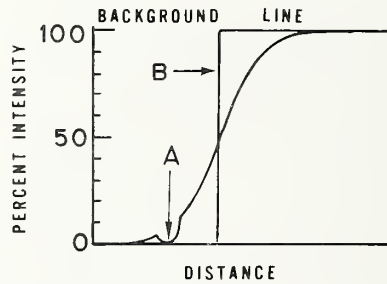


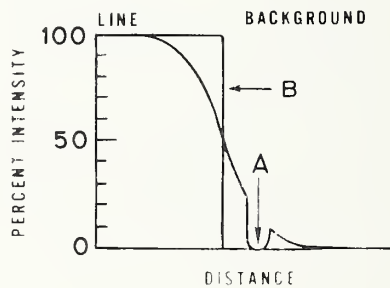
Figure 3-12. Comparison of the calculated image profiles of a 1- $\mu\text{m}$  wide clear line with 0- and 2.5-percent background transmittance  $T_0$ ; other microscope parameters are the same as in figure 3-7.



(a) Image intensity profiles; A - single edge as viewed by incoherent illumination, B - ideal edge, and C - filar-eyepiece cross hair.



(b) Superposition of the edge and filar-eyepiece cross-hair image intensity profiles; the apparent location of the edge (A) and the ideal edge (B) are shown as the cross hair moves from a dark region to a bright region.



(c) Superposition of the edge and filar-eyepiece cross-hair image intensity profiles; the apparent location of the edge (A) and the ideal edge (B) are shown as the cross hair moves from a bright region to a dark region.

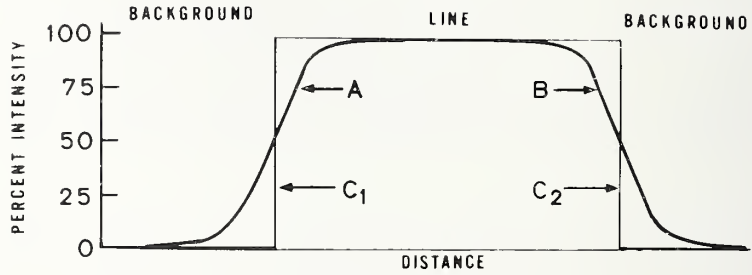
Figure 3-13. Line-edge location with a filar eyepiece.

located by the filar eyepiece at the value of the coordinate at the 10-percent intensity level minus one-half the cross-hair width. If the image of the cross hair is traversed across the line in one direction (as is usually the case), the measured linewidth is equal to the difference of the coordinates of the two 10-percent intensity levels plus or minus the width of the cross hair, depending upon whether the line is clear or opaque. Alternatively, for constant edge profiles, the filar may be viewed as measuring a threshold slightly higher than 10 percent. Although it appears that this threshold is most probably on the low side of 50 percent, its exact value will depend on the width of the cross hair and remains to be determined experimentally. Also, for the case where the filar employs a dashed rather than a solid cross hair, the measured threshold is apt to differ.

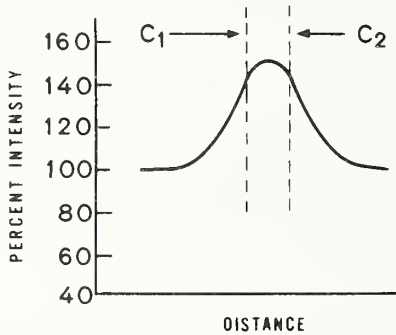
An image-shearing eyepiece positions the images of the two edges of the line side by side so that one of the edge images can be traversed across the other. The image intensity profiles of a line with symmetric left and right edges and the ideal edge located at the 50-percent intensity level are shown in figure 3-14a. As these two images are superimposed by the image-shearing eyepiece, the intensity profiles add. As the images cross, the bright region between them: (1) narrows to a bright line as shown in figure 3-14c when the two edge profiles cross at the 75-percent intensity level, (2) disappears when the two edge profiles cross at the 50-percent intensity level, and (3) changes to a narrow dark line as shown in figure 3-14b when the two edge profiles cross at the 25-percent intensity level. The line-edge location is generally picked when the two edge images touch with neither a bright line nor a dark line existing between the two images. For symmetric edges, this criterion results in locating the edge at the 50-percent intensity level, and no measurement error occurs if the illumination is incoherent. If the ideal edge location corresponds to some other intensity level, as would be the case for coherent or partially coherent illumination, there is some error in locating the edge.

Very explicit criteria may be applied consistently to determine the edge location with electronic processing and analysis of the image intensity profile. One of the commonly used criteria is to locate the edge at the 50-percent image intensity level which results in locating the edge at the same position as the image-shearing eyepiece in the incoherent case. Another of these criteria is to locate the edge at the position of maximum slope of the image intensity profile. This criterion results in locating the edge position at the 50-percent intensity level only for the case of incoherent illumination and diffraction-limited optics.

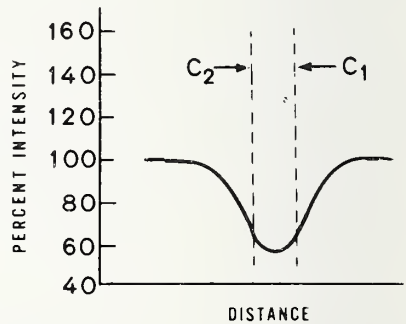
Calculated measurement errors, based on the above criteria, are listed in table 3-2. The apparent width is greater than the actual width when the error is negative. If the illumination is reflected rather than transmitted or if the line is opaque on a transparent background, the sign of the error is reversed. It should be noted that these results assume well-resolved line images where the two edges may be treated independently.



(a) Image intensity profiles of opposite line edges viewed with incoherent illumination illustrating the images prior to superpositioning them over each other with the image-shearing eyepiece: A, left edge; B, right edge;  $C_1$ , left ideal edge;  $C_2$ , right ideal edge.



(b) Overlap of image intensity profiles A and B with a bright band between the two light images corresponding to locating the line edge at the 75-percent intensity level.



(c) Overlap of image intensity profiles A and B with a dark band between the two light images corresponding to locating the line edge at the 25-percent intensity level.

Figure 3-14. Line-edge location with an image-shearing eyepiece.

Table 3-2 - Linewidth Measurement Errors<sup>a</sup> of a Clear Line (20  $\mu\text{m}$  or Wider) on an Opaque Background for an Illumination Wavelength of 550 nm.

Illumination Condition	Filar Eyepiece	Image-Shearing Eyepiece or 50-percent Intensity Level	Maximum Slope
Incoherent Illumination - Geometric Focus	+0.56 $\mu\text{m}$	0.0 $\mu\text{m}$	0.0 $\mu\text{m}$
Matched Numerical Apertures - Geometric Focus	+0.27	-0.17	-0.23
Coherent Illumination - Geometric Focus	+0.16	-0.19	-0.25
- $\pm 0.65 \mu\text{m}$ from Geometric Focus ( $\pm \lambda/4$ Defocus)	+0.25	-0.34	-0.46
- $\pm 1.3 \mu\text{m}$ from Geometric Focus ( $\pm \lambda/2$ Defocus)	+0.59	-0.66	-1.00
- $+\lambda/4$ Spherical Aberration	+0.17	-0.14	-0.28
- $+\lambda/4$ Spherical Aberration, $-\lambda/4$ Defocus	+0.14	-0.17	-0.30
- $+\lambda/4$ Spherical Aberration, $-\lambda/2$ Defocus	+0.20	-0.09	-0.30
- $+\lambda/2$ Spherical Aberration	+0.16	-0.19	-0.25
- $+\lambda/2$ Spherical Aberration, $-\lambda/2$ Defocus	+0.30	+0.02	-0.68
- $+\lambda/2$ Spherical Aberration, $-\lambda$ Defocus	+0.41	+0.14	-0.97

<sup>a</sup>Based on calculated image profiles.

### 3.4 A New Method for Measurement of Small Linewidths [32]

Since the current linewidth-measurement techniques are all inherently asymmetrical, we must either attempt to reduce the associated errors or to seek a new technique that removes the asymmetry. The magnified image in an optical microscope is identically equivalent to the object, and the measurement of width with either a filar or image-shearing eyepiece remains asymmetrical. Thus, there is no clear way of removing the asymmetry in linewidth measurements with conventional optical microscopes. However, since there is such a large industry-wide investment in the microscope and because there is a universal confidence in its use, an investigation aimed at altering the measurement techniques with optical microscopes was carried out.

A linewidth-measurement technique based on coherent illumination and spatial filtering has been developed. In this technique, the spectrum, or spatial-frequency content, of the object is imaged at one focal distance behind the objective lens. By occluding portions of the spectrum prior to passage of the light through the system to form the image, we are able to control certain aspects of the image. This operation is called spatial filtering, and through its application, the image no longer looks like the object. For a specific set of filter conditions, the image manifests the edges of the original object by two dark, narrow lines in a bright surround. These lines are easily observed with the eyepiece in the microscope, and the measurement is symmetric. The technique thus transforms the object rather than alters the measurement method; but the object no longer requires an asymmetric measurement of its width.

The technique appears feasible on all counts but one. Current microscope objectives of the high numerical apertures required for the observations of small lines are designed and fabricated so that the object spectrum, located a one focal distance from the rear of the lens, lies inside of the lens and is, therefore, inaccessible. Since spatial filtering requires insertion of the occluding filter in the plane of the object spectrum, it is necessary to redesign objectives to locate this plane outside of the last glass surface in the objective. No other aspect of the technique appears to be beyond the capability of current fabrication and alignment technology. The article [32] given in Appendix A discusses this technique.

#### 4. LINEWIDTH-MEASUREMENT ARTIFACTS

An artifact standard for length measurements is often described in terms of its use, namely, to transfer the defined unit of length (wavelength of radiation from krypton 86 [33] from a recognized standards laboratory to a user. The artifact gives the user practical access to this unit of length. The physical characteristics of a length artifact, such as shape and material, depend to a large extent on the specific needs of the users. For example, length artifacts currently available from NBS include end standards, such as gage blocks, and line standards, such as linear scales. The linear-scale artifact has assigned values that relate length intervals on the scale to the defined unit of length. These assigned values are obtained from displacement-measurement equipment at NBS and have associated measurement uncertainties. In the present study, the length artifact of interest is a linewidth-measurement artifact which relates the separation of the left and right edges of a line to the unit of length. The design and material selected for this artifact are based largely on the measurement needs of semiconductor manufacturers and others who routinely make linewidth measurements on IC photomasks.

##### 4.1 Design and Materials

The basic pattern used for the initial linewidth-measurement artifacts is shown in figure 4-1.\* This pattern consists of opaque lines on a clear background and clear lines (spaces) on an opaque background. The nominal widths of these lines are 1, 3, and 10  $\mu\text{m}$ . This pattern is repeated on the artifact with groupings of up to four lines. Serrations on one side of the opaque background are used as reference marks to locate the measurement area on a line. A pair of 2- $\mu\text{m}$  wide lines parallel to the measured lines are used for a line-spacing measurement.

The basic pattern shown in figure 4-1 is repeated at four locations on the artifact. A photograph of an artifact is shown in figure 4-2. Clear lines on the artifact help to locate the four basic patterns in the center of the artifact. These four patterns are barely visible in figure 4-2.

The artifacts are either antireflective (AR) chromium on glass or iron oxide on glass. The soda-lime glass substrates are square, approximately 36 mm on a side, and 6-mm thick. The AR-chromium used in the current artifacts is a layer of chromium oxide on chromium and has a lower specular reflectance than chromium without the chromium oxide. The thickness of the AR-chromium as measured on a Talystep stylus instrument at NBS is approximately 150 nm. Figure 4-3a is an SEM photomicrograph of part of a AR-chromium artifact observed at a magnification of about 600X. Figures 4-3b and 4-3c are SEM photomicrographs of four nominally 3- $\mu\text{m}$  wide opaque and clear lines, respectively, on the same AR-chromium artifact viewed at 2400X.

---

\* Subsequent to this initial artifact pattern, an improved version has been developed at NBS. (See ref. [34].)

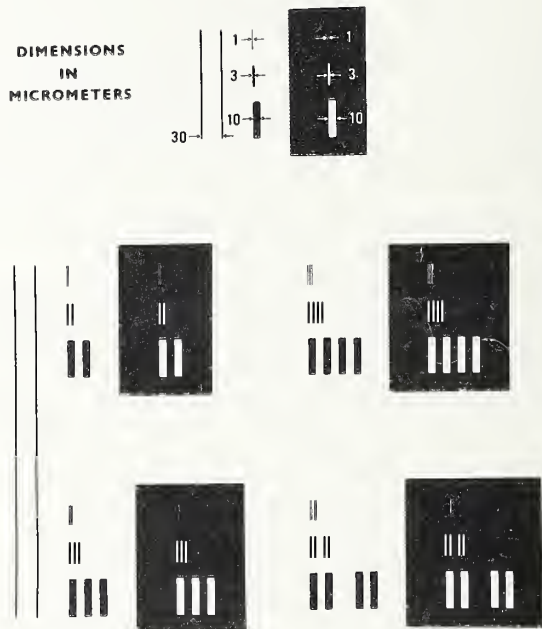


Figure 4-1. Basic pattern of initial NBS linewidth-measurement artifact; linewidths are nominal values.

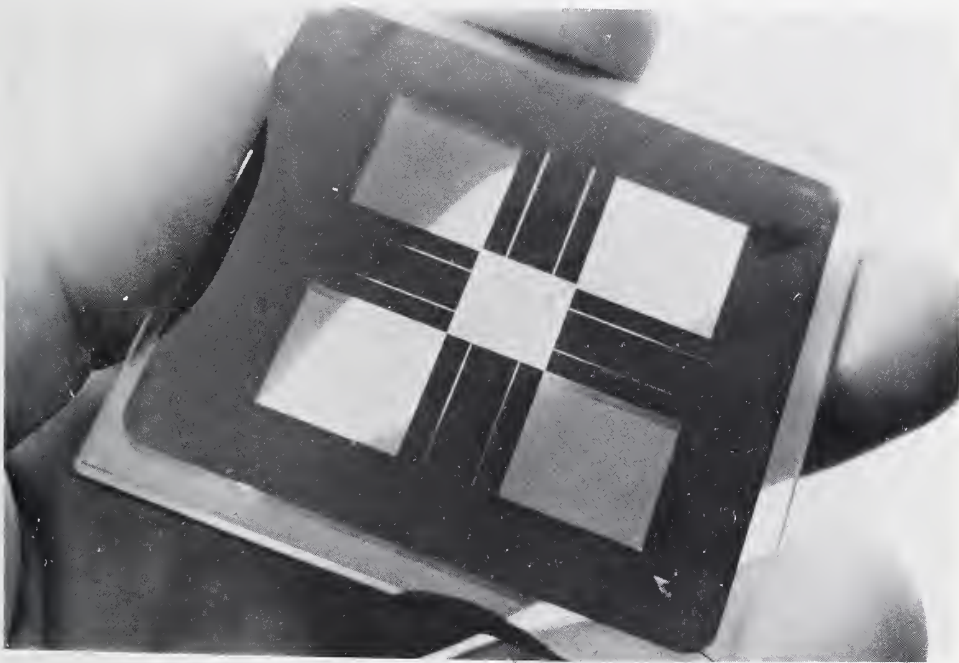
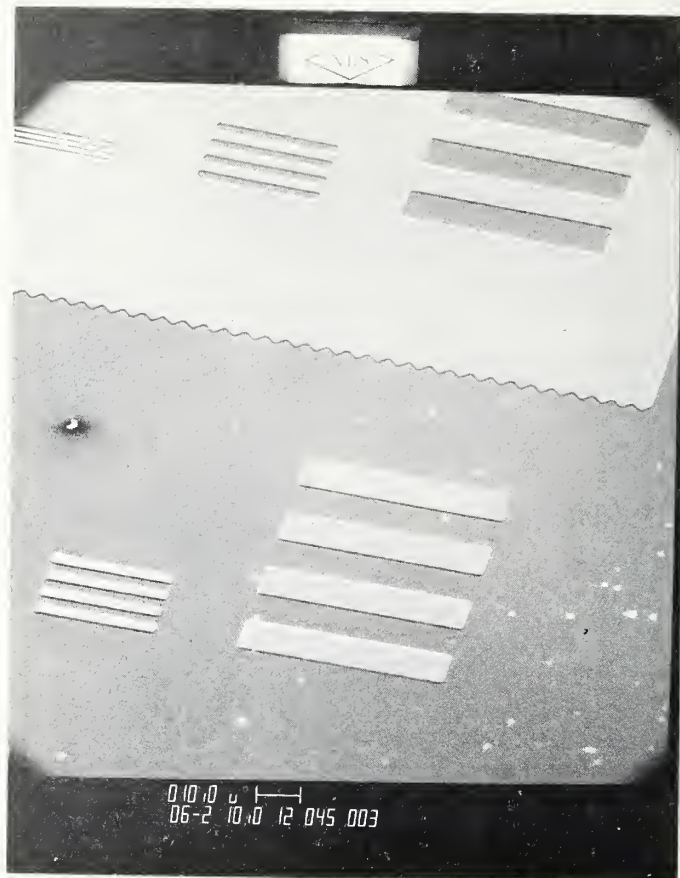
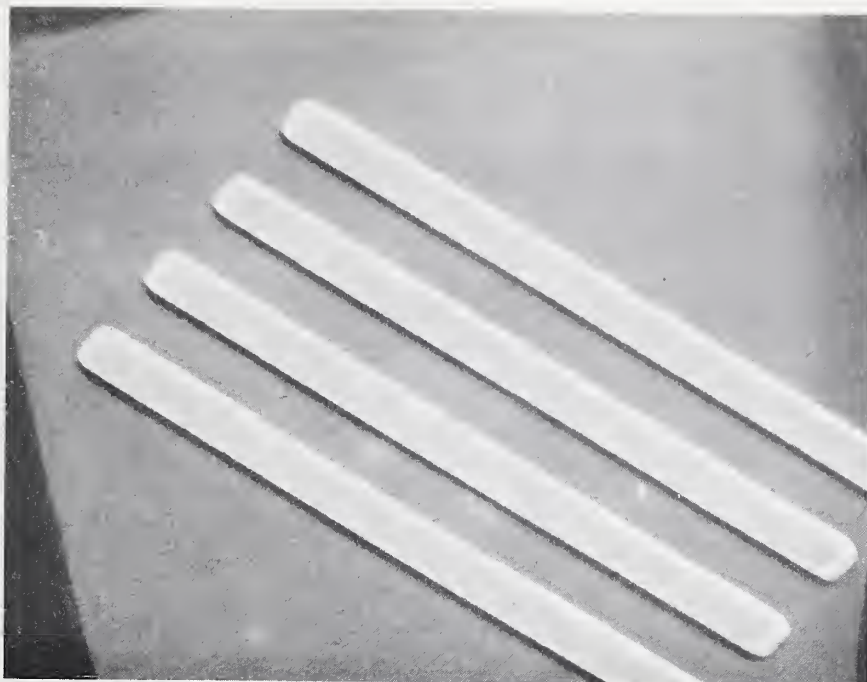


Figure 4-2. Photograph of an antireflective chromium artifact.

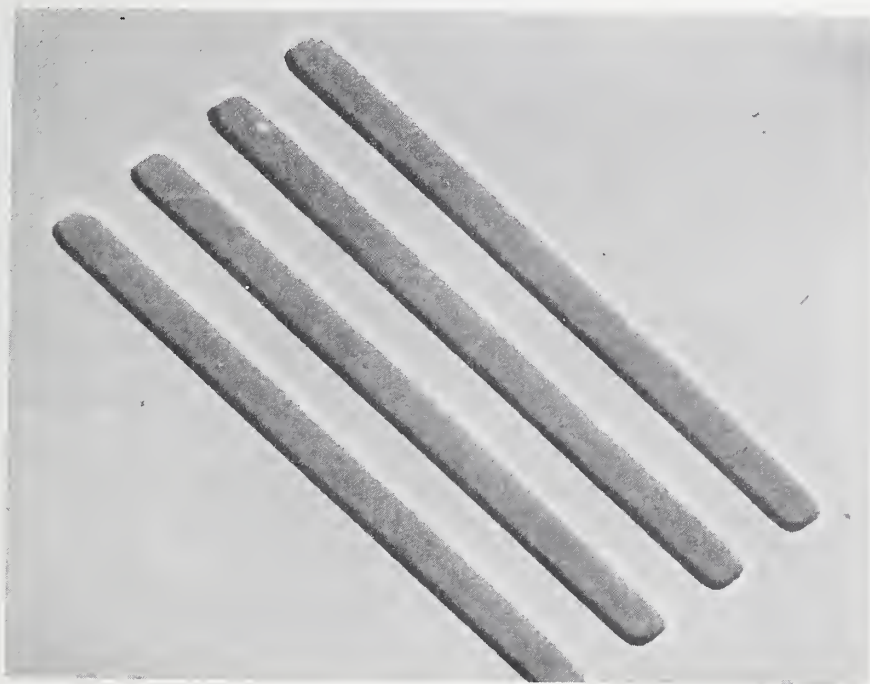


(a) Clear and opaque lines at 600X.

Figure 4-3. SEM photomicrographs of an antireflective chromium artifact.



(b) Four nominally 3- $\mu$ m wide opaque lines at 2400X.



(c) Four nominally 3- $\mu$ m wide clear lines at 2400X.

Figure 4-3. Concluded.

The iron oxide is partially transmitting and equivalent to coatings used on some see-through IC photomasks. The thickness of the iron oxide is reported by the supplier to be about 180 nm. Figure 4-4 is a photomicrograph of four nominally 1- $\mu$ m wide clear lines on an iron-oxide artifact observed in an optical microscope with bright-field transmitted light at about 2900X. The description of these lines as opaque is only relative to the surrounding area since the transmittance of these lines is about 50 percent. Viewing these specimens under transmitted light in an optical microscope shows a dark border at the edge of the iron oxide as shown in this figure. The cause of this optical effect has not been identified,\* but it results in a large uncertainty in setting the filar and image-shearing eyepieces for linewidth measurements. Since the iron-oxide artifacts show the dark border under the optical microscope, initial studies for linewidth calibration have been carried out only with AR-chromium artifacts. The optical effect with the iron-oxide artifacts is under study.

Although linewidth measurements are sometimes made with reflected light in an optical microscope, the theory and measurements developed in the present project were initially restricted to the transmitted-light case. Optical linewidth measurements are made with a scanning photometric microscope which is described in section 6. The primary means for transferring the length standard is an SEM/interferometer system which is described in section 5. In order to measure linewidths in the SEM and transfer these measured values to the optical microscope, it is necessary that the artifacts be electrically conductive in addition to being transparent to visible radiation in the clear part of the pattern. The first requirement is imposed because electrons incident on the artifact in the SEM must be conducted away from the measurement area to avoid a buildup of electrical charges and the resulting image distortion.

An initial attempt to meet both of these requirements involved overcoating the glass substrates with about 100 nm of indium-doped tin oxide prior to the chromium deposition. However, during the subsequent chemical etching of the pattern, it was discovered that the chromium appeared to have diffused into the tin-oxide coating. As a result, not all of the chromium could be removed from the pattern area designated as clear. Other available coatings that are electrically conductive and optically transparent were not desirable since they are not resistant to the chemical etchants used for processing chromium photomasks. The current approach is to overcoat the patterned artifact with approximately 50 nm of carbon. This carbon layer provides the necessary conduction for electrons in the SEM and does not affect the transparency of the artifact as viewed in an optical microscope in transmitted light.

---

\* Subsequent to the present report, work conducted at NBS has shown that this dark border arises from the combination of low contrast and optical path difference introduced by the iron oxide in conjunction with the partial coherence of the illumination. (See ref. [35].)

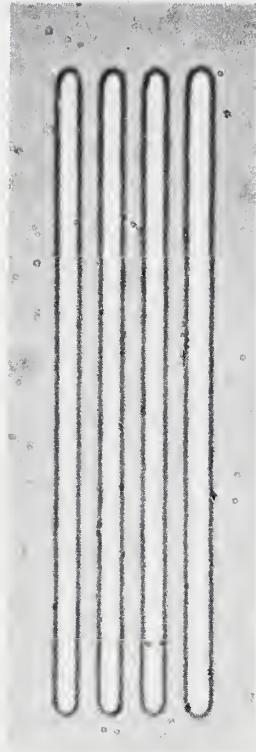


Figure 4-4. Photomicrograph of four nominally 1- $\mu\text{m}$  wide opaque lines on an iron-oxide artifact observed in an optical microscope with bright-field transmitted light at 2900X.

## 4.2 Quality

The geometry of the line profiles is an important factor in both line-scale and linewidth measurements. In particular, the edge profiles of the lines must be sharp and clean with no raggedness along the line. An ideal cross-sectional line profile might be rectangular as discussed in the theory of image formation of lines in section 3.1. In practice, the processing of lines and spaces on photomasks can give line profiles which exhibit a wide range of geometrical irregularities. The artifacts selected for linewidth measurements in the present study have lines and spaces with very good edge quality as shown in figures 4-3b and 4-3c. Some artifacts were cut and examined in the SEM to show the cross-sectional line profiles. These results are discussed in section 5.5.

In making linewidth measurements with the SEM/interferometer system and the photometric optical microscope, the electron and light probes cover a finite area of the line along its length. In the SEM/interferometer system, the electron beam has a diameter of  $0.1\ \mu\text{m}$  or larger and sweeps over  $1\ \mu\text{m}$  along the length of the line being measured. In the photometric optical microscope, the effective scanning slit is  $0.3\ \mu\text{m}$  across the width of the line and  $1.3\ \mu\text{m}$  along the length of the line. If the line raggedness along the length of the line is significant, linewidth measurements at various locations along the line could be statistically different. Furthermore, since the scan areas of the SEM and optical probes are slightly different, line raggedness could increase any difference in linewidth measurements between these systems.

The line-edge profiles directly affect the magnitude of the offsets in locating edges for linewidth measurements. It is desirable to have relatively steep edges to help minimize these offset values and the offset differences among various measurement systems. It is also desirable to know the line-edge profile in order to correlate the modeling of the interaction between the electrons and the physical line with the measured edge profile in the SEM/interferometer system.

The quality of the artifact appears to be the major limitation in reducing the uncertainty for the linewidth measurements on both the SEM/interferometer system and photometric optical microscope. Even with the use of improved systems and techniques for linewidth measurements in the IC industry, the quality of the measured photomasks will also be a primary limitation in reducing the associated measurement uncertainties. For the calibration of these measurement systems, the artifacts to transfer the measured linewidth values from NBS to industry are selected on the basis of quality to minimize the measurement uncertainties.

## 5. SEM/INTERFEROMETER SYSTEM

Arie W. Hartman  
Mechanical Processes Division  
Center for Mechanical Engineering and Process Technology  
National Bureau of Standards  
Washington, DC 20234

Diana Nyyssonen  
Electron Devices Division  
Center for Electronics and Electrical Engineering  
Washington, DC 20234

and

Richard E. Swing\*  
Frederick, MD 21701

The SEM/interferometer system relates the basic length measurement of a linewidth to the defined unit of length through the interferometric measurement of the line-specimen displacement. A schematic of the SEM/interferometer system is shown in figure 5-1. As the specimen is moved during the measurement process, the electron beam of the SEM is used as a very fine fiducial mark or cross hair. In an overly simple view of the measurement process, a very small beam of electrons, nominally a few tens of nanometers in diameter, is focused at normal incidence on the line specimen and remains relatively stationary as the specimen is moved. The interferometer records the motion of the specimen, and the location of the line edges is determined by the change in the electron-scattering coefficient. The SEM, therefore, acts as a high-resolution electron-beam probe.

Conventional SEMs are not designed to operate as metrological instruments. As a result, a number of changes were made in the operation of the Etec Autoscan Research Model SEM used for the initial linewidth measurements. The major modification was the replacement of the normally used stage with a prototype system incorporating a specially designed flexure-pivot stage [36] with extremely smooth motion during scanning. This flexure-pivot stage has limited one-dimensional motion of about 60  $\mu\text{m}$ ; therefore, another positioning mechanism is required to place the line to be scanned within the field of view. This positioning device uses two piezoelectric inchworms with orthogonal motions. This novel stage system and positioning devices are described in detail in section 5.3.

### 5.1 Requirements for the SEM

For linewidth measurements, the SEM is required to operate in an unconventional manner. The SEM used for these linewidth measurements does not have the electrical circuitry necessary to hold the electron beam sta-

---

\* Consultant.

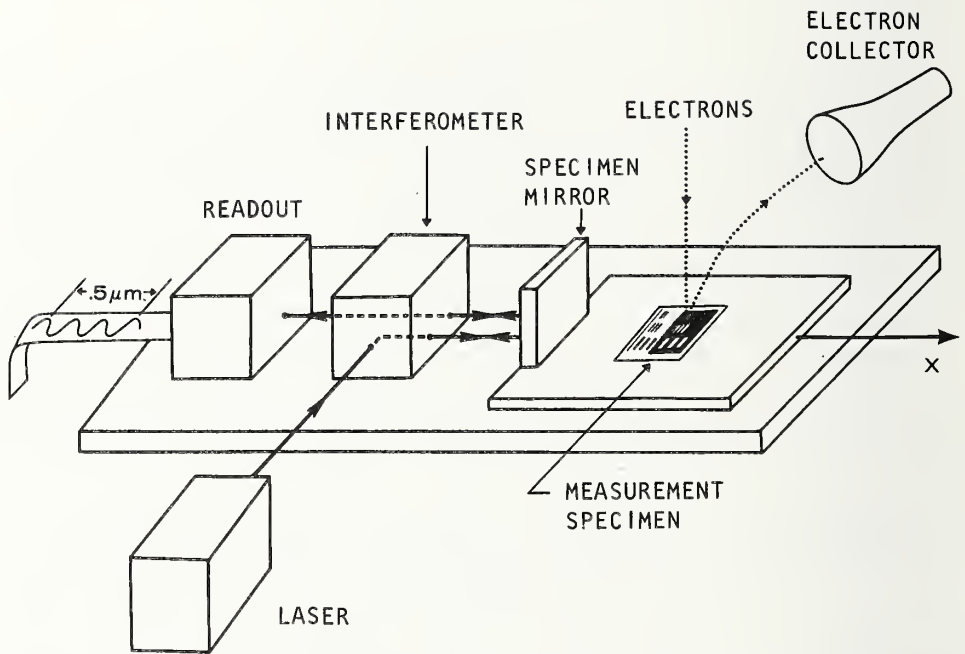


Figure 5-1. Schematic of the SEM/interferometer system for measuring linewidths.

tionary during scanning with the stage. Therefore, the SEM is operated in a line-sweep mode with approximately 1- $\mu\text{m}$  sweep length on the specimen. This mode of operation is shown schematically in figure 5-2. Hence, the beam averages the imperfections in the line over this sweep length which is comparable to the effective scanning-slit length in the photometric optical measurements discussed in section 6.

Many of the operating characteristics of the SEM and interferometer stage affect the ultimate precision and systematic error of the measurements. One obvious characteristic is the electron-beam spot size. Although beam diameters on the order of 20 nm are theoretically achievable with the present SEM, several compromises were made which produced larger effective beam diameters. At operating voltages of 20 keV, where the smallest beam diameter is found, there is an unacceptable level of contamination buildup on the specimen. The contamination level is typical of conventional SEMs and is not peculiar to this instrument. The contamination was reduced by use of a nitrogen cold trap and lower voltage during the measurements.

Fortunately, most of the contamination occurs during focusing or waiting time. By moving to a new area of the line just before making a measurement, minimal contamination results in the area where the measurements are made. The beam is also blanked whenever possible while other adjustments are made. Repeated scans of the same area of the line eventually show profile changes due to contamination. Figure 5-3 shows the contamination buildup for repeated scans of a nominally 3- $\mu\text{m}$  wide clear line.

Another characteristic of the instrument which affects the measurement is electron-beam stability. Rotational stability of the beam is particularly important for maintaining alignment between the line sweep and the line edge during measurement. Vibration and positional stability of the beam also affect the accuracy of the measurement. However, in the present mode of operation, it is difficult to separate these factors from the averaging of the imperfections in the line edges. All of these factors contribute to smearing of the edge profiles which in the present system produce effective beam diameters of 100 nm or more.

## 5.2 Modeling of Electron Interaction with Material Line\*

In the SEM, the line whose width is to be measured is moved through an electron beam as the movement is monitored interferometrically. The signal from the SEM is used to determine the line-edge locations so that the linewidth, or the measured distance between the edges, can be based on the wavelength of light. Thus, the SEM beam serves as an extremely accurate cross hair in the calibration procedure.

The signal received from the SEM must be modeled so that the line-edge locations can be specified with a minimum of systematic errors. Among the many factors in this model are the secondary-electron emission coef-

---

\* This model will be discussed in a subsequent NBS publication.

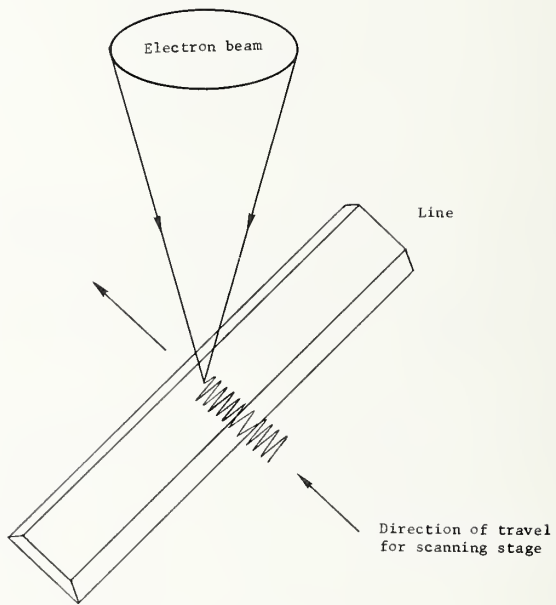


Figure 5-2. Schematic of the effective path for the scanning electron beam when the linear motion of the scanning stage is combined with the line sweep of the SEM.



Figure 5-3. SEM photomicrograph showing contamination from repeated scans across a nominally 3- $\mu\text{m}$  wide clear line on an AR-chromium artifact; SEM operating voltage of 10 keV and magnification of 1700X.

ficients [37] for the glass substrate, chromium and chromium-oxide overcoating, the radius of the electron beam, the material thickness, and the various operating adjustments of the SEM. Furthermore, since the SEM system operates at high magnification (30,000X) for the linewidth measurements, the nominally vertical line edge has a finite slope which is also included in the model.

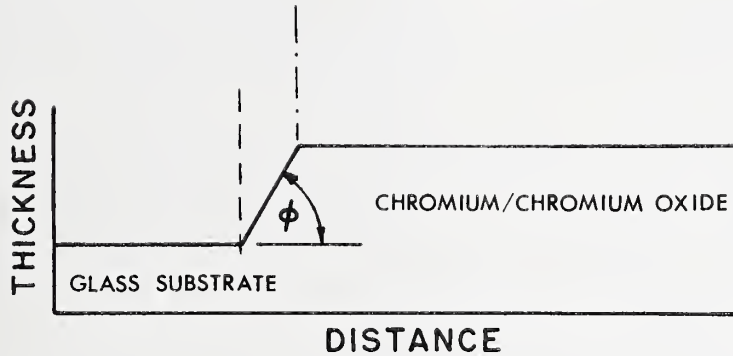
It was felt that the best approach to modeling the SEM output was to prepare a simplified model that can subsequently be made more complex in any or all of its components. In this way, effects can be isolated and anomalies can be interpreted at the least level of complexity. Furthermore, such an approach allows the analyst to modify one consideration at a time, thereby making only enough changes to bring the model into line with the experimental observations.

From SEM photomicrographs, it appears that the edges at the glass substrate/chromium interface are faired in smoothly, rise monotonically, and terminate abruptly at the chromium/chromium-oxide interface. The initial model for the SEM edge trace is simplified in that it ignores the fairing process and takes the edge as a linear ramp rising at an angle  $\phi$  from the substrate to the top of the chromium-oxide layer. This model is represented schematically in figure 5-4a. The fabrication process for the artifact dictates that the material along the sloped portion of the edge is chromium, while the bulk of the edge (at least at the surface) is chromium oxide. This requires three secondary-electron emission coefficients to characterize the glass substrate, chromium, and chromium oxide.

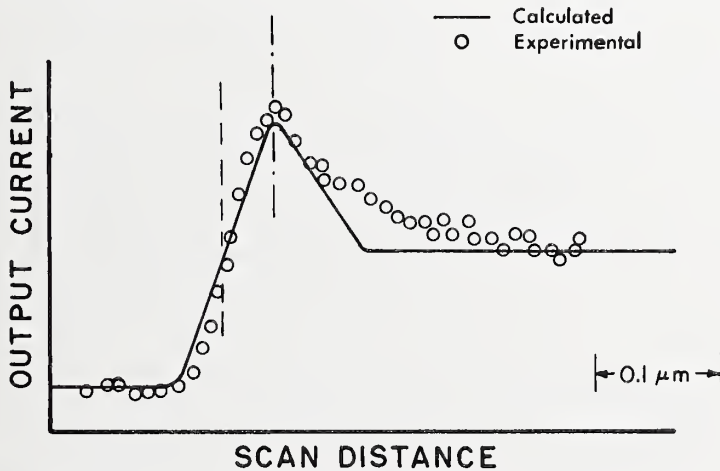
It is also known that the distribution of intensity in the electron beam is Gaussian, at least in normal operation of the SEM. The initial model ignores this and assumes the beam to have a uniform intensity within a well-defined circular area. This simplification is made primarily to reduce the complexity of the analysis and to enable a more precise definition of beam width. A subsequent modification to the analysis is currently in progress to include the Gaussian-beam characteristics.

Because of the three secondary-electron emission coefficients and the mathematical discontinuities associated with the edge model, the output from the SEM cannot be calculated in closed form. Computer programs have been written to carry out these calculations, and a companion program prepared to plot the resultant output. In these calculations, it is necessary to specify the chromium/chromium-oxide thickness, the angle of the edge slope  $\phi$ , the three secondary-electron emission coefficients, and the diameter of the electron beam.

By referring the chromium and chromium-oxide secondary-electron emission coefficients to the substrate coefficient (so that the latter value is unity), only two coefficients must be determined. Measurements from SEM photomicrographs show the edge slope to be about 55 deg. Interferometric measurements of the chromium/chromium-oxide layer show a thickness of approximately 110 nm, while measurements on the Talystep stylus instrument indicate a thickness of 150 nm. Although this difference in measured thickness is presently unresolved, the measurements do provide a nominal



(a) Model of the line edge;  $\phi$  is the angle of the line-edge slope.



(b) Comparison of an experimental SEM line-edge trace with the calculated trace; for the calculated trace, the electron-beam diameter is 80 nm, the chromium/chromium-oxide thickness is 114.3 nm,  $\phi$  is 55 deg, and the secondary-electron emission coefficients for the glass substrate, chromium, and chromium oxide are 1.0, 0.887, and 1.265, respectively.

Figure 5-4. Model of the line edge and a comparison of an experimental SEM line-edge trace with the calculated trace based on the model; broken lines show correspondence between edge location in the model and the SEM traces.

value of thickness with which to begin the calculations. Information from line-edge traces with the SEM has established the range of beam diameters as 40 to 120 nm at an operating voltage of 10 keV. In addition, from an analysis of the SEM edge traces, the number used for the secondary-electron emission coefficient for the chromium oxide is 1.265.

The remainder of the model parameters is determined from comparison of actual SEM line-edge traces with calculations from the model. The simple model fits the data well in the area of importance, namely, the region associated with the edge. In the region past the edge (on the chromium-oxide side), the SEM output does not fall off as rapidly as the model predicts. This may be evidence of electrical charging of the specimen or blooming phenomena [38] not included in the simple model. An example of experimental SEM data to which the model has been fitted is shown in figure 5-4b. For these data, the SEM was operated at 20 keV with an approximate beam diameter of 80 nm as determined from the curve-fitting. The secondary-electron emission coefficient for the chromium at the edge was calculated to be 0.877; however, on purely physical grounds, this coefficient probably should be equal to, or greater than, unity.

One of the interesting aspects of the modeling of the edge-traces is observed in the operating adjustments of the SEM. Focus adjustment appears optimum when the output distribution has a marked peak at the edge, and the electron microscopist adjusts the instrument to maximize both the slope of the output at the edge and this peak value. In the model, the maximum peak is obtained when the beam diameter is exactly equal to the width of the edge. For an assumed nominal 80-nm beam diameter and an edge-slope angle of 55 deg, the thickness is calculated from this model to be 114.3 nm; this thickness is extremely close to the interferometric thickness measurement of 110 nm. When the instrument is adjusted to produce a maximum peak such as shown in figure 5-4b, it is then possible to determine the edge location from the trace: it is the point halfway between the lowest portion of the curve and the peak value. Because of the physical basis for this interpretation, it ought to be independent of the analytic form of the beam as long as the beam is symmetrical about its center; that is, if a Gaussian cross section is assumed for the beam, the edge location should still be the same.

It is clear, however, that the abrupt transitions implied in the edge model are not physically realizable. Subsequent modifications of the model might soften the transition regions through use of a continuous function. However, specification of such a function must await more experimental data.

The present simple model gives a reasonable estimate of edge location and is useful for interpreting the results of current experiments. The next planned step in the SEM modeling is the characterization of the scanning-beam distribution by use of a Gaussian function. Should these results be inadequate to describe the SEM output, a reassessment of the edge and line profiles is clearly in order.

### 5.3 Apparatus

The *in situ* stage and interferometer developed in the present program convert an existing SEM into a one-dimensional length-measuring device with a range of 50  $\mu\text{m}$  and a resolution of 1 nm. The SEM stage system provides a specimen-mounting platform which can be moved around in two modes: (1) a search mode to bring selected specimen areas into the microscope field of view and (2) a scan mode in which the specimen is moved in a programmed linear fashion under the relatively stationary SEM electron beam. The search mode covers a 10- by 10-mm area in x and y with submicrometer resolution while the scan mode provides a maximum x-axis travel of about 50  $\mu\text{m}$  with subnanometer resolution. The combined stage travel in the x-direction is measured optically with an *in situ* interferometer with 1-nm resolution. The specimen is mounted with the lines parallel to the surface of the movable interferometer mirror. The specimen and mirror are moved as a unit by the SEM stage.

#### 5.3.1 Design

The design approach for the SEM/interferometer has been threefold: (1) use of movement actuators that work by remote control and produce a minimum of stray magnetic fields, heat, and mechanical vibrations; (2) adoption of an interferometer featuring minimum light losses at the beam-splitting and combining surfaces and multipass-beam characteristics to increase interferometer sensitivity; and (3) construction of the stage, light source, interferometer, and optical readout as a unit which can be quickly mounted on the unmodified SEM, thus facilitating the setup and maintenance of optical alignment.

The mechanical motions of the stage are carried out by piezoelectric means. For the search mode, the actuators are inchworm drivers. These are a set of three connected, tubular piezoelectric elements around a movable shaft. When energized, the outer elements change internal diameter and the center element changes length. They can, therefore, be made to clamp, loosen, and stretch sequentially, resulting in a worm-like motion along the shaft. The actual devices have the shaft slide in and out of a stationary housing containing the piezo-elements. The interferometer output as a function of the inchworm motion for a linear time base is shown in figure 5-5.

For the scan mode, the actuator is a stack of tubular piezo-elements whose length changes are amplified by a 20X mechanical flexure-pivot system [36]. A photograph of a flexure-pivot system like the one used for the scan stage is shown in figure 5-6. This system is machined out of a monolithic steel block and exhibits a smoothness of better than 1 nm over a few micrometers.

The interferometer is a double-pass polarization one of the Michelson-Bennett type [39]. A schematic of the interferometer is given in figure 5-7. The output is a rotational value of the polarization plane and is proportional to the travel of the SEM stage in the x-direction. The scale factor is 180 deg per  $\lambda/4$  travel where  $\lambda$  is the wavelength of the

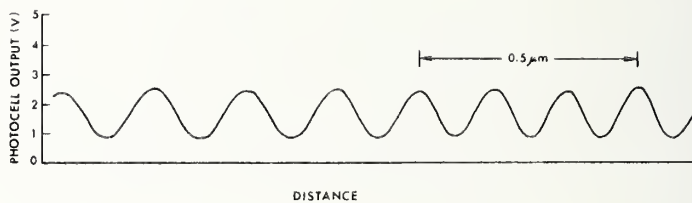


Figure 5-5. The interferometer output as a function of the inchworm motion for a linear time base.

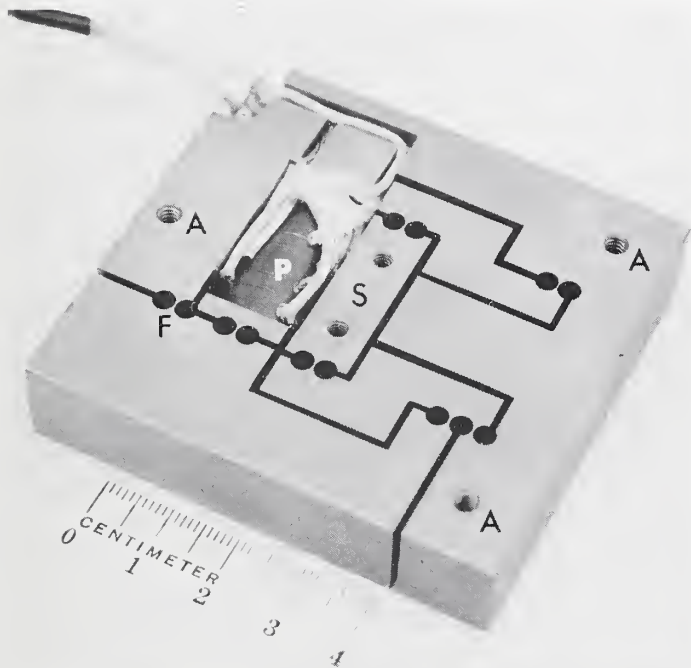


Figure 5-6. Photograph of a scanning stage which uses a flexure-pivot system; stage is fixed at points A, while other stage sections move; F - a flexure pivot, P - stack of piezoelectric elements, and S - specimen-mounting area.

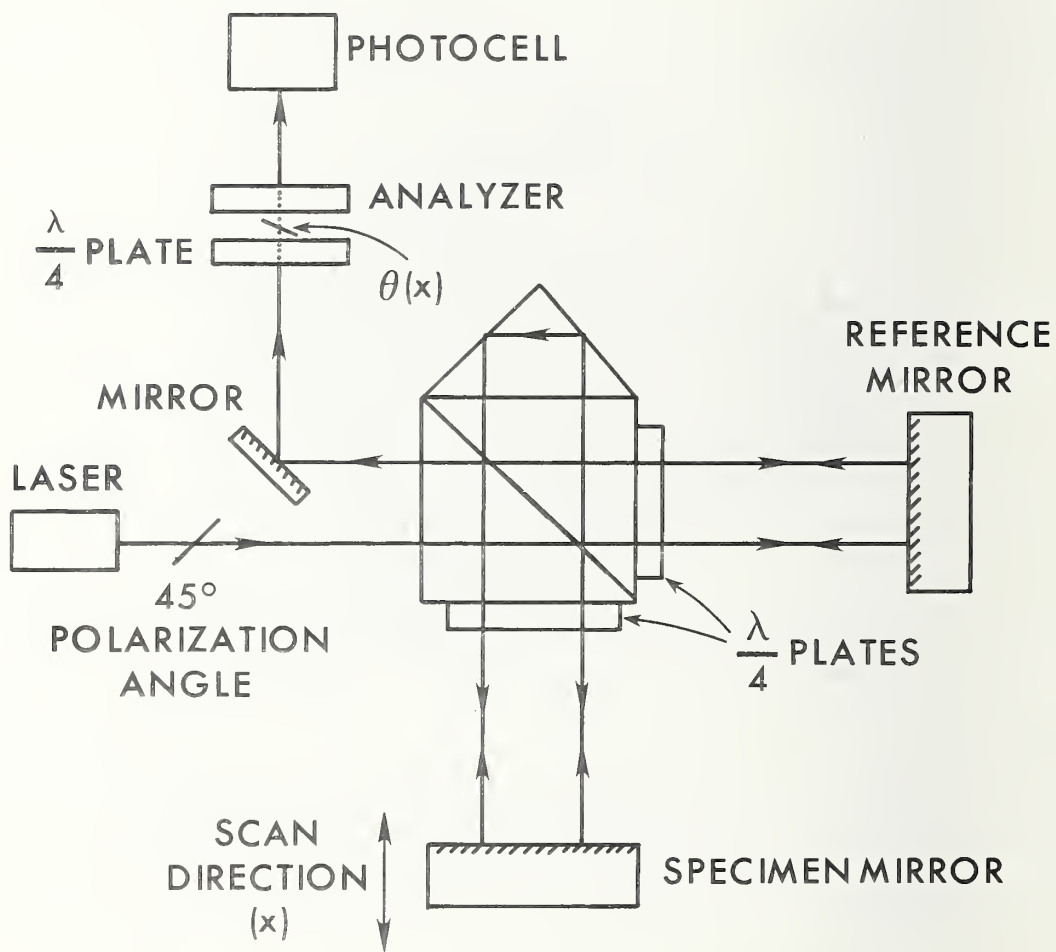


Figure 5-7. Schematic of the double-pass polarization interferometer as viewed by looking downward on the scanning stage.

He-Ne laser radiation (632.8 nm). The reflections and transmissions of the light beams at the beam-splitting plane occur virtually without losses because the interfering beams are first polarized by an  $\lambda/4$  retardation plate which they traverse twice. The specimen mirror reflects the beam twice at neighboring locations, and the interferometer senses the travel along the line of sight halfway between these two locations.

The interferometer is provided with an externally mounted, rotatable analyser and a beam-power sensor system utilizing a silicon photocell. For automated readout, the analyser is stationary and the linearly moving scanning stage produces sinusoidal variations in the output beam; these variations are digitized and recorded. For manual readout, the analyser is rotated for minimum beam intensity and its angle is read.

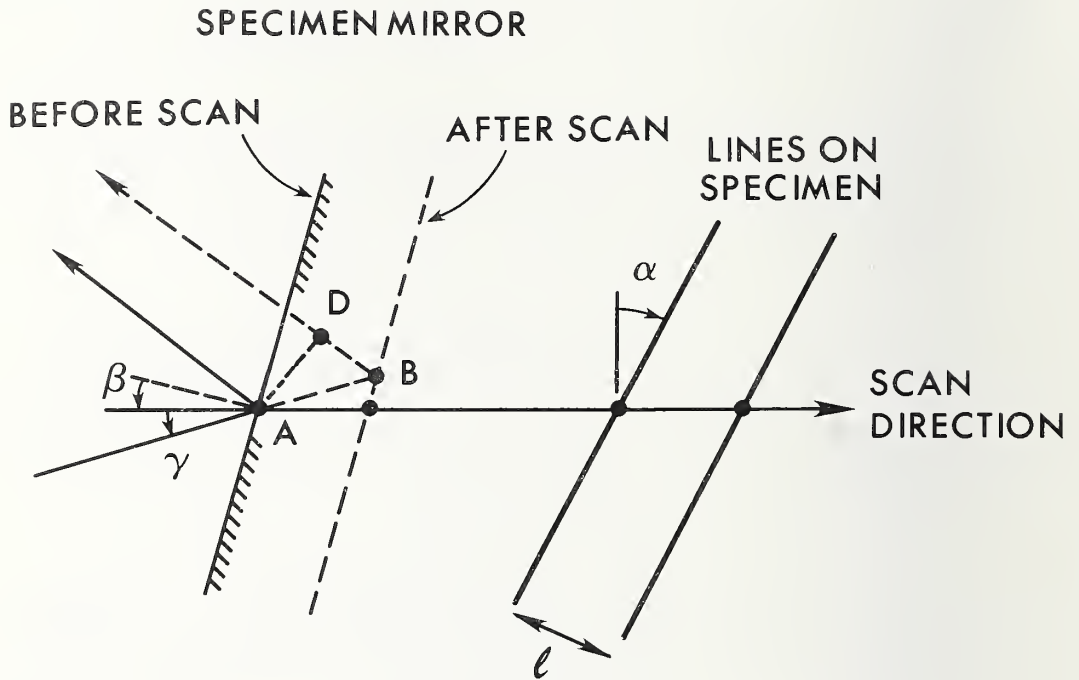
The stage system is constructed as a unit comprised of the stage with a built-in interferometer, the light source, and the interferometer readout - all mounted on a cover plate which seals off the specimen chamber of the SEM during operation. The SEM door is simply swung to the side to accommodate the new chamber cover plate. The laser is mounted in an adjustable fashion to provide proper routing of the beams and normally incident illumination of the target mirror. All other components are securely mounted to the SEM cover plate.

Proper angular and linear dimensions have to be maintained between the elements of the stage system, or linewidth-measurement errors can occur. Figure 5-8 defines angular errors for the specimen line ( $\alpha$ ), the mirror orientations ( $\beta$ ), and the beam alignment ( $\gamma$ ). All of these angular errors are measured relative to the direction of the scanning stage, and all are assumed to be in a common horizontal plane. These angular errors produce a measurement error given by the factor  $1 + \alpha^2 + \alpha\beta - \beta^2 - 2\beta\gamma - \gamma^2$ . Considering an example in which all angles are positive and equal to a relatively large value of 1 deg, the error factor is 1.0012, that is, an error of 1.2 nanometers per micrometer of measured length. The errors introduced by incorrect rotational tilt and leveling of the specimen are found in the same way.

If during a measurement  $\alpha$ ,  $\beta$ , or  $\gamma$  changes from its original value, cosine errors are introduced. For  $\gamma$ , the error is proportional to the measured length (about 1 to 30  $\mu\text{m}$ ). For  $\alpha$  and  $\beta$ , however, the error is proportional to the distance (about 30 mm) from the mirror to a point inside the corner-cube prism. An angular error of 1 mrad results in a linewidth error of 15 nm which is independent of the measured length. Therefore, if a maximum error of 15 nm is allowed, the interferometer system has to remain angularly stable to better than 1 mrad.

### 5.3.2 Construction

A convenient way to describe the construction of the stage system is based on tracing the components from the outside inwards. Referring to figure 5-9, we have a stage enclosure with a stiffened front plate (not shown), a bottom plate, and an open top. The front plate has three protruding lugs to provide fixed mounting of the complete stage structure to



ERROR ANGLES REFERENCED TO SCAN DIRECTION

LASER BEAM:  $\gamma$   
 TARGET MIRROR:  $\beta$   
 SPECIMEN LINES:  $\alpha$

OPTICAL PATH DIFFERENCE =  $ABD$

$$= 2\ell (1 + \alpha^2 + \alpha\beta - \beta^2 - 2\beta\gamma - \gamma^2) \text{ FOR THIS CASE}$$

ERROR FACTOR

Figure 5-8. Schematic of the angular errors for misalignment of the specimen lines in the SEM/interferometer system.

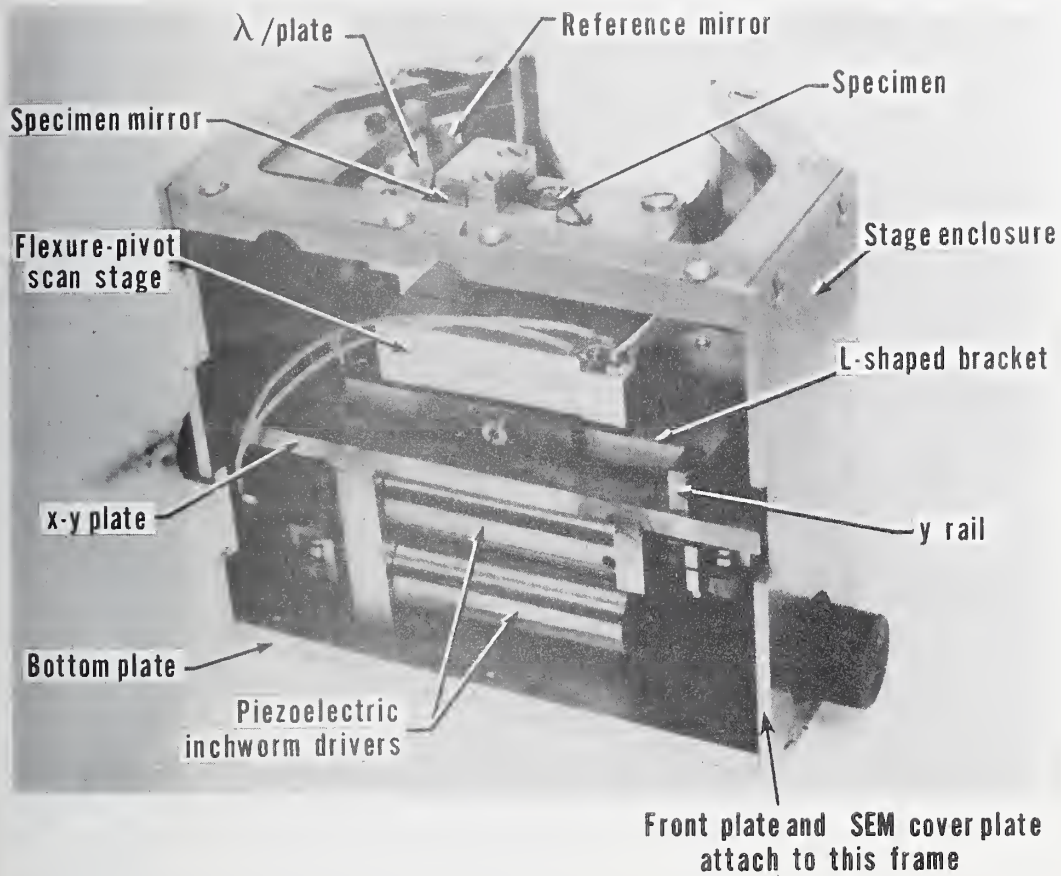


Figure 5-9. Photograph of the SEM/interferometer stage system with the front plate removed.

the SEM cover plate. The bottom plate carries three columns on which is mounted a horizontal plate. This plate defines the x-y plane over which the scan stage and specimen carrier slide during the search phase. The three columns can be replaced by three piezoelectric drivers to level the x-y plate so that during any long scans, no loss of focus will occur in the SEM imagery. Underneath the x-y plate are mounted two inchworm drivers which provide x- and y-motion by means of two lever systems. The y-drive causes one arm of a L-shaped bracket to slide over the x-y plate and along a fixed rail (y-axis). The x-drive causes the scan stage, which is mounted on an adapter plate, to slide along the other arm of the L-shaped bracket.

The scan stage carries a bracket on which is mounted the specimen mirror. This mirror serves to measure the location of the specimen. The specimen is easily mounted on the mirror bracket by pressing the specimen against a mechanical reference edge while bolting the specimen down.

The interferometer (beam-splitter assembly and reference mirror) is rigidly mounted on a horizontal shelf which, in turn, is welded to a main member of the stage enclosure. This construction is not visible in the figure.

A trough-like structure carrying the laser, relay mirrors, and interferometer readout is attached externally to the SEM cover plate as shown in figure 5-10. The laser can be aligned manually with the help of markers defining the entrance and exit of the light beam. The interferometer readout, which consists of a beam-sensing photocell and associated electronics, is also mounted on the cover plate. In this way, all alignments can be done on a laboratory bench prior to installation of the entire assembly in the SEM. The vacuum in the SEM assures a rigid mechanical coupling between the assembly and the SEM.

### 5.3.3 Operation and Performance

The preparation for measurement of linewidths consists of three basic steps. First, the alignment of the interferometer is checked to ensure that the two interfering beams are coincident. If they are not coincident, a slight rotation of the specimen mirror in the horizontal plane is sufficient to correct the misalignment; however, this correction has rarely been necessary.

Secondly, the specimen carrier is mounted on the specimen-mirror holder and is pressed against a reference edge. The specimen is mounted on its carrier such that the line is nearly parallel to the front surface of the specimen mirror. After mounting, the deviation from parallelism is measured to within 2 min of arc; its value is usually between 2 and 10 min of arc. After assembly, the specimen surface is perpendicular to the specimen mirror surface to within 10 min of arc. This arrangement avoids cosine errors and also helps to assure that the SEM focus is maintained during scanning.

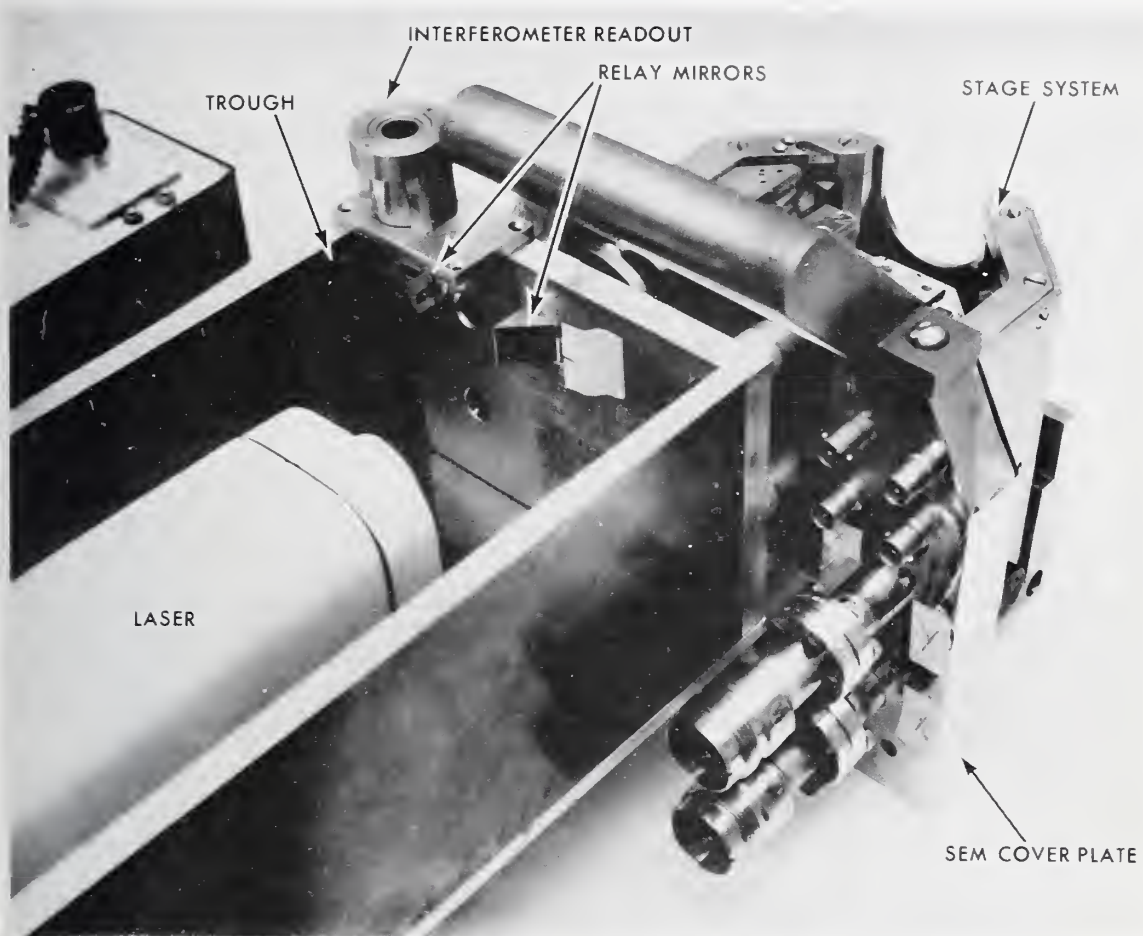


Figure 5-10. Photograph of the assembly attached to the SEM cover plate in the SEM/interferometer system.

Thirdly, the laser is adjusted such that its beam is perpendicular to the specimen-mirror surface. This adjustment is checked by manually inserting a  $\lambda/4$  retardation plate in the specimen beam. The insertion of the  $\lambda/4$  plate adds  $\lambda/2$  retardation to the reflected beam which already has  $\lambda/2$  retardation, thus sending the return beam back to the laser. In this way, perpendicularity of the imaging laser beam can be observed to 8 min of arc, and changes in this condition can be monitored to 2 min of arc.

Principal indicators of performance of the SEM/interferometer system include: (1) the level of distortion in the recorded sinusoidal fringes and (2) the linearity of the scan. Fringe distortion can be caused by stage vibrations, laser-beam power changes, and spurious beam reflections entering the interferometer readout system. Scan linearity is controlled by linearity of the ramp voltage and by response of the scan stage to a linear ramp. At present, stage vibration is less than 10 nm peak-to-peak, and efforts are under way to reduce this to 1 and 2 nm. An evaluation of the SEM stage system for measurement errors caused by both short-term and long-term angular instabilities is also underway.

#### 5.4 Linewidth-Measurement Procedures

For the initial linewidth measurements, the SEM was modified by replacing the conventional stage and door with the interferometer described in section 5.3. During data taking, the system is minicomputer controlled. Two data channels are provided: (1) interferometer output consisting of the sinusoidal voltage signal containing the position data and (2) the SEM voltage signal proportional to the beam current at the detector. The minicomputer is a 16-bit Interdata Model 716 with floppy-disc data storage, a keyboard for entering instructions, a cathode-ray tube (CRT) display, and additional electronics to provide interfacing to the interferometer and stage. The minicomputer is programmed so that upon command from keyboard, a trigger signal is generated which activates a linear voltage ramp to drive the piezoelectric scanning stage.

After a given time delay, which is entered from the keyboard, data are taken from both channels for 2 s at millisecond intervals to yield a total of 2000 data points from each of the two channels. Before initiating this relatively short sequence, a long series of adjustments of all the system components is required. These adjustments are as follows: the interferometer adjustments described in section 5.3.3, positioning the line specimen in the center of the SEM field of view by means of the inchworms, focus and adjustment of the SEM as described in section 5.1, alignment of the SEM line sweep with the line specimen to be scanned, check of signal levels, and a lengthy set of computer instructions for setting up a data file. In addition, the slope and amplitude of the voltage ramp, which drives the scanning stage, must be checked initially; and the appropriate time delay before data taking must be determined in order to allow damping of the initial stage vibrations.

## 5.5 Sample Data

The linewidth-measurement data given in this section are for three lines on an AR-chromium artifact. These lines are a nominally 2- $\mu\text{m}$  wide opaque line, a nominally 3- $\mu\text{m}$  wide opaque line, and a nominally 3- $\mu\text{m}$  wide clear line. A total of 34 measurements resulted from data taken on three different occasions; these data gave a minimum of ten measurements per line. No more than four measurements were taken in exactly the same place due to contamination buildup. All of the data were taken at an SEM operating voltage of 10 keV and a magnification of 30,000X.

The edge quality of these lines represents the best seen on AR-chromium artifacts during the present project. No imperfections were visible in the SEM in the scanned regions; if there are any imperfections, their sizes are below the vibration level of approximately 10 nm. Some deviations of the line edges from straightness are visible as shown in the SEM photomicrographs in figure 5-11. Figure 5-11d, which is a low-magnification photograph taken after scanning, shows the contamination that accrued during data taking.

A sample plot of the direct output of the two data channels (SEM and interferometer) is shown in figure 5-12. The two channels are shown with respect to the same linear time base, and the interval between data points is 1 ms. For determining linewidth from such a data scan, the interferometer data are first converted to length where one cycle of the sine wave is equal to  $\lambda/4$  ( $\lambda = 632.8$  nm). In this conversion, a nonlinear time base was first fitted to the full length of the scan to remove any small drifts in the interferometer. Values of the constant,  $c$ , and modulation term,  $m$ , over approximately one period of the data are then found by curve-fitting; these values allow inversion of the equation

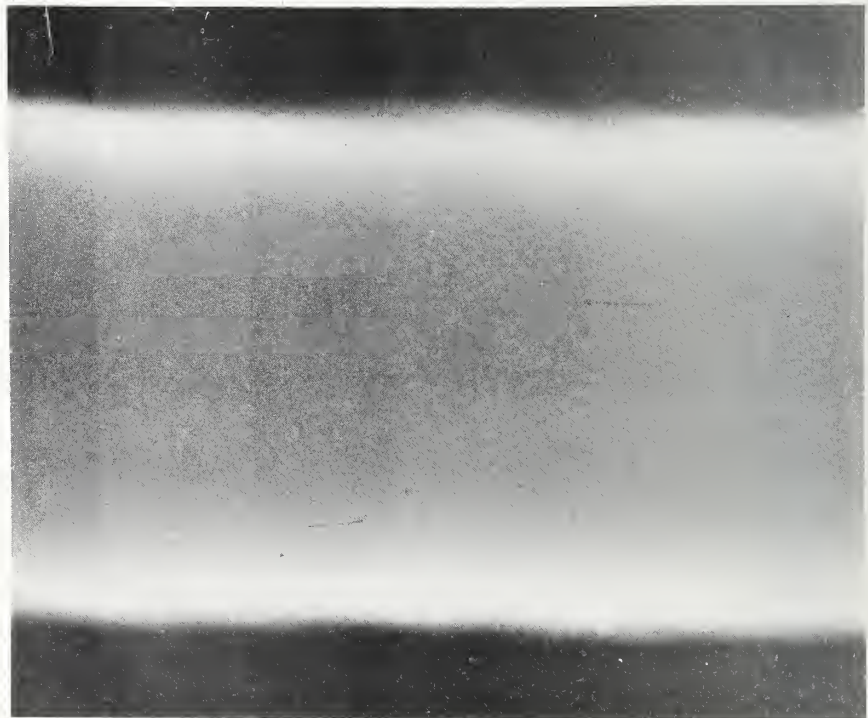
$$y = m \cos(2x/P) + c , \quad (5-1)$$

where  $x$  is the distance to be determined in multiples of  $\lambda/4$ ,  $P$  is the spatial period equal to  $\lambda/4$ ,  $m$  is an integer, and  $y$  is the interferometer data. Figure 5-13 shows a plot of the converted SEM signal as a function of distance. With the data in this form, the remaining analysis requires determination of the edge location from the SEM image profile as discussed in section 5.2.

From a simple model of the material line, which assumes a linearly increasing thickness from zero to the maximum thickness of the combined chromium and chromium-oxide layers, the edge location is determined as illustrated in figure 5-14. The midpoint of the sloped portion of the SEM image profile corresponding to the start of the physical slope is determined and a correction term is added, or subtracted (depending upon whether the line is clear or opaque), so that the edge is located at the physical thickness corresponding to the 25-percent intensity transmittance of the chromium. This correction is based on a slope angle of 55 deg and an optical absorption coefficient for chromium of 1.8. The correction corresponding to these values is  $\pm 0.023$   $\mu\text{m}$  for one edge or  $\pm 0.046$   $\mu\text{m}$  for a linewidth measurement. The slope angle of 55 deg was determined

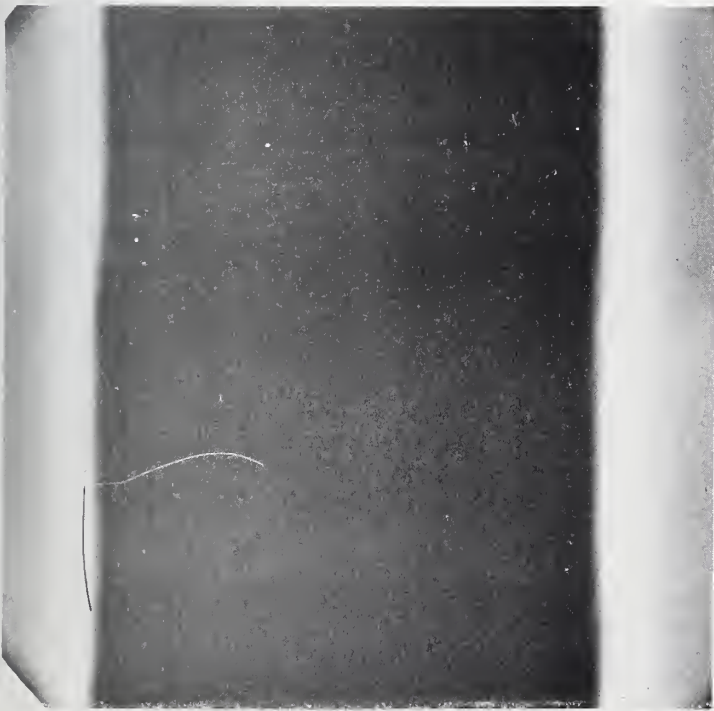


(a) A nominally 3- $\mu\text{m}$  wide opaque line; 30,000X.

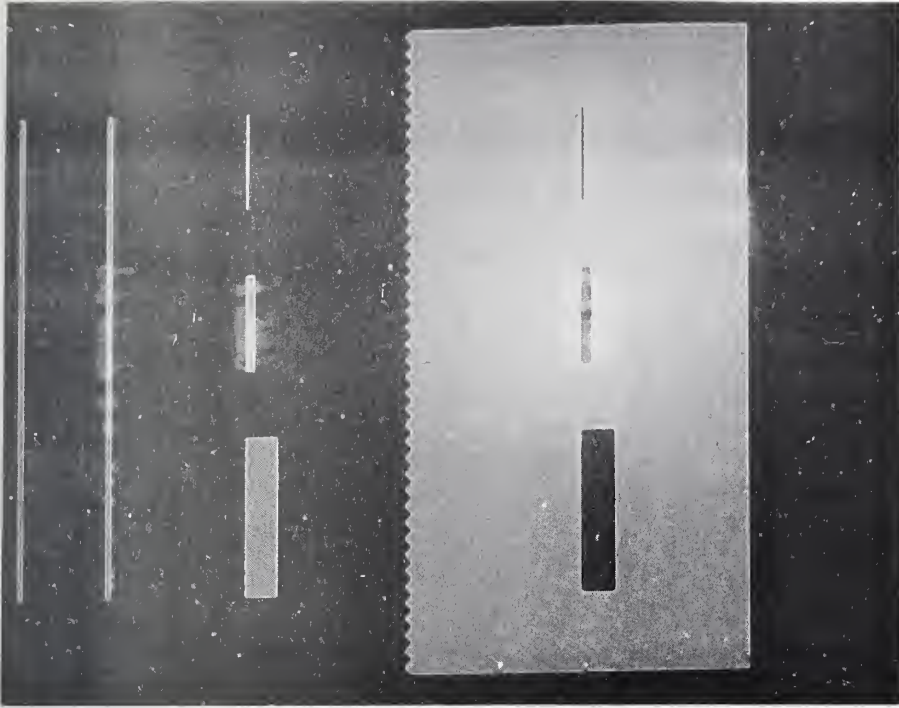


(b) A nominally 2- $\mu\text{m}$  wide opaque line; 30,000X.

Figure 5-11. SEM photomicrographs of calibrated lines on an anti-reflective chromium artifact.



(c) A nominally 3- $\mu$ m wide clear line; 22,000X.



(d) An overview of the scanned areas showing the contamination; 300X.

Figure 5-11. Concluded.

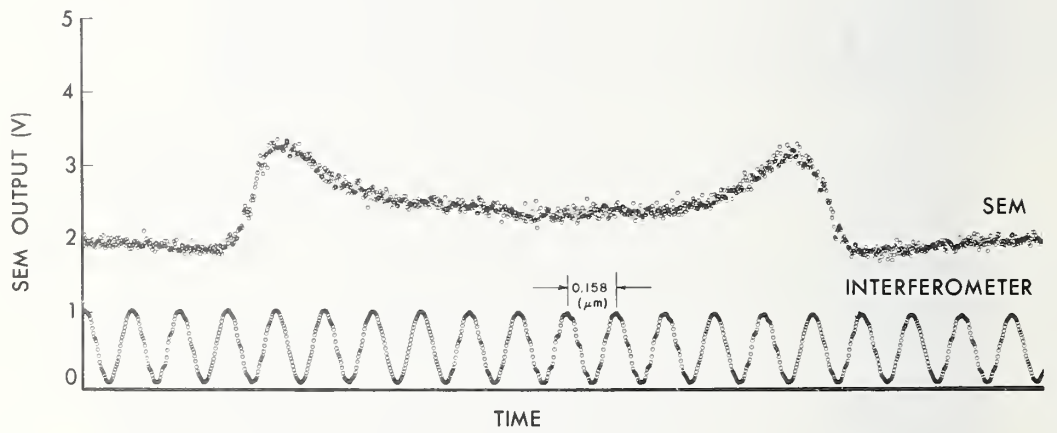


Figure 5-12. Direct output of the SEM and interferometer data channels for a nominally 2- $\mu\text{m}$  wide opaque line.

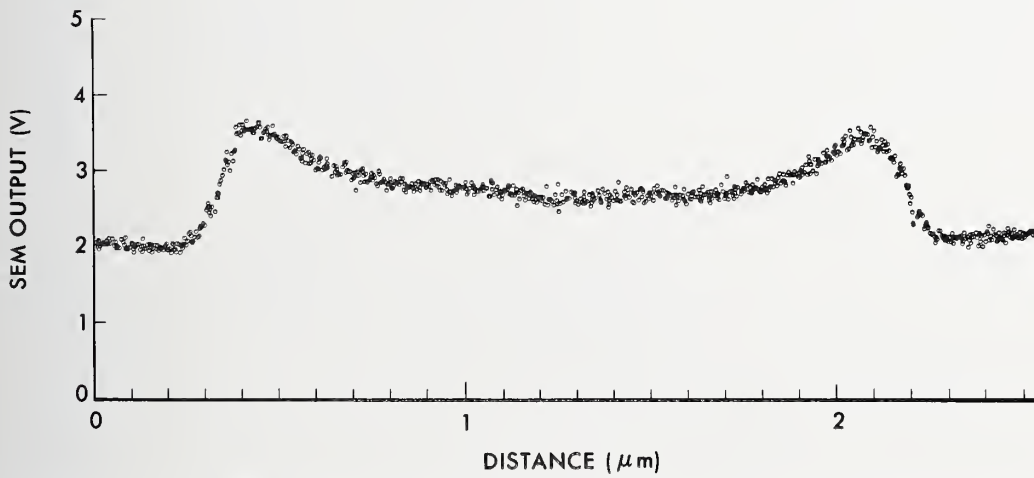
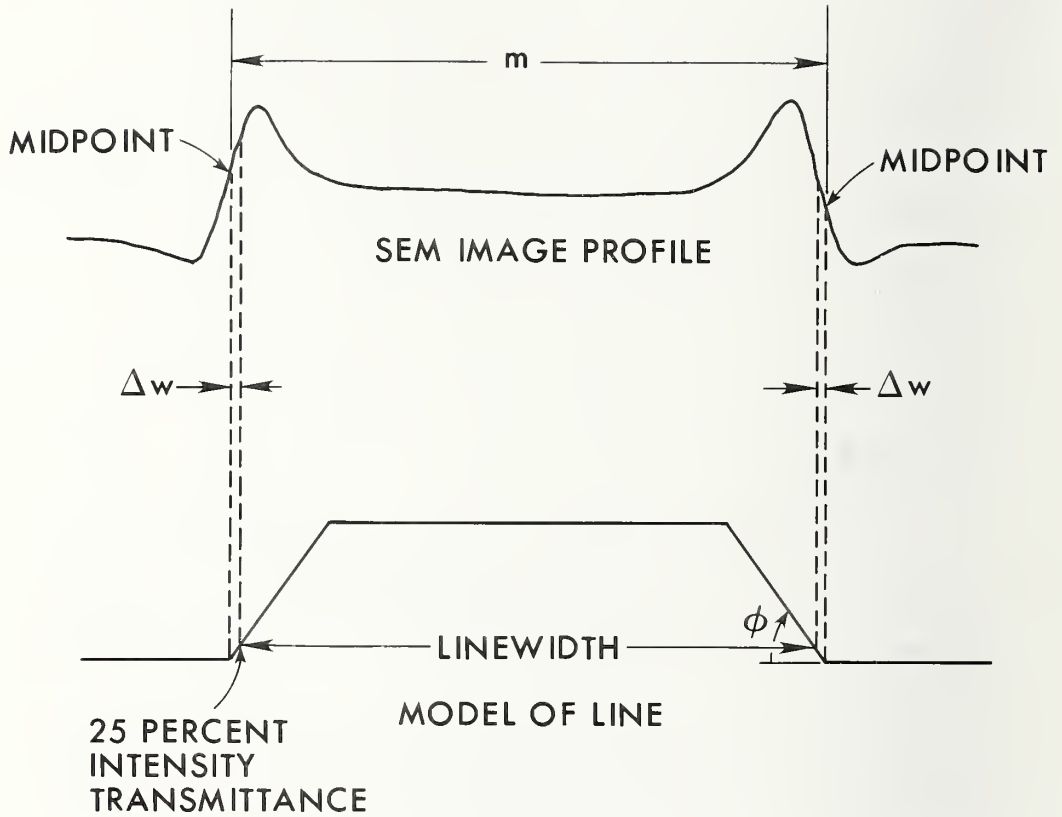


Figure 5-13. SEM image profile for a nominally 2- $\mu\text{m}$  wide opaque line.



$m$  is the distance between the midpoints of the sloped portion of the SEM image profiles which correspond to the left and right line edges

$\Delta w$  is a correction which is added to, or subtracted from, the distance  $m$  for opaque and clear lines, respectively;  $\Delta w = 0.023 \mu\text{m}$  for one edge of a chromium/chromium-oxide line with  $\phi = 55 \text{ deg}$  and an optical absorption coefficient of 1.8

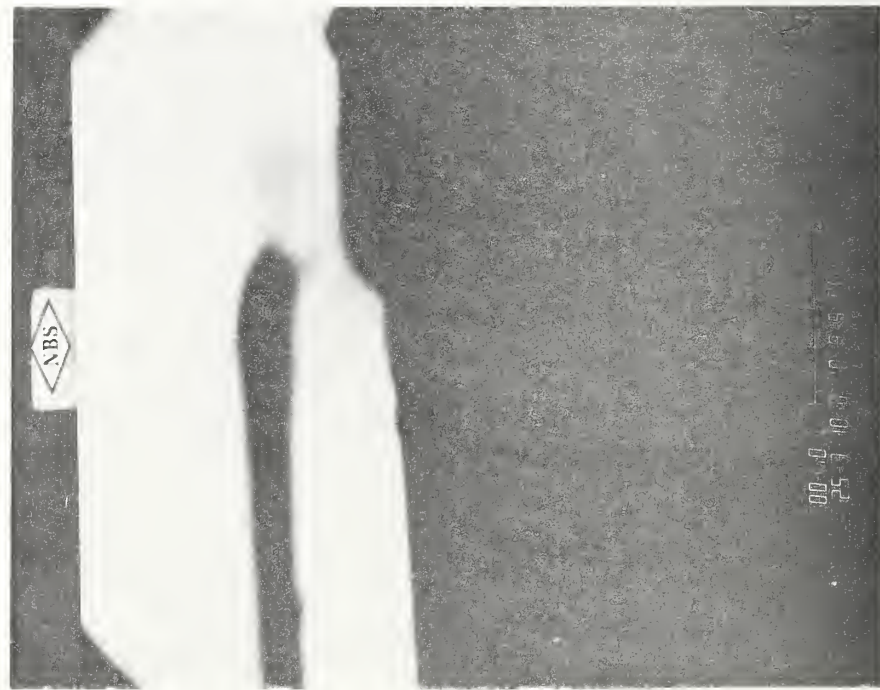
$$\text{linewidth} = m - 2(\Delta w) \quad \text{for an opaque line with symmetric left and right edges}$$

Figure 5-14. Relationship between the SEM image profile and the model of an opaque line; the points defined as edge locations of the line correspond to a 25-percent intensity transmittance (50-percent amplitude transmittance).

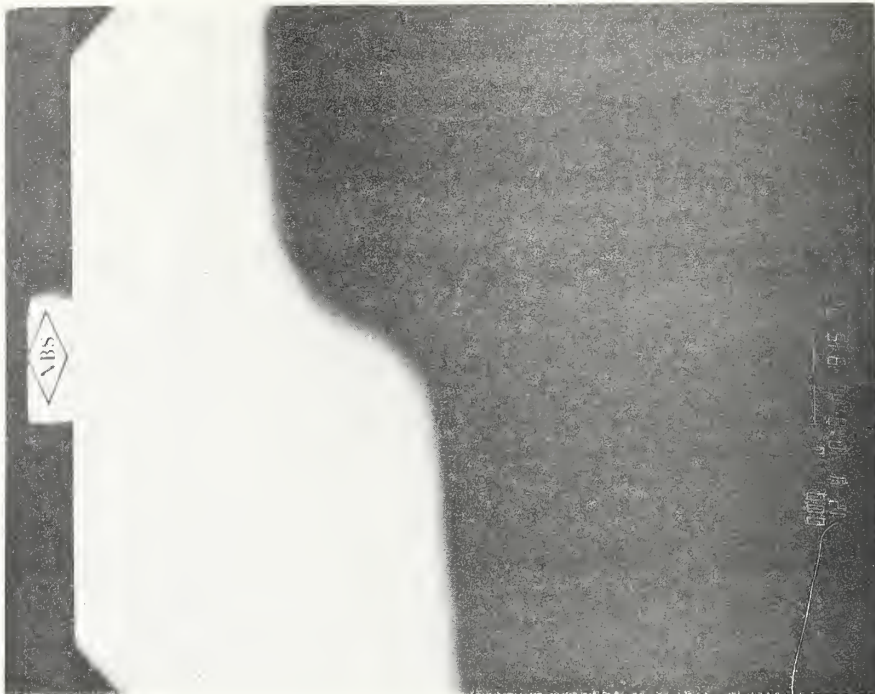
from an SEM photomicrograph shown in figure 5-15. This photomicrograph was taken at an angle of approximately 1 deg from the surface. At this low angle, the view shows the cross section of a line which has been cut perpendicular to its length.

The results of measurements on the three lines are shown in table 5-1. The brackets are used to group repeated measurements made on an identical area of the same line. If the mean of the multiple measurements is calculated, the standard deviation associated with this local mean is 0.015  $\mu\text{m}$ . This value is an estimate of the precision, or repeatability, of the measurement process. One may also look at the variation of the measurements made at different places along the length of the line. This analysis yields a sample standard deviation of 0.007  $\mu\text{m}$  for the linewidth variation which is less than the reproducibility of a single measurement. This means that the method of SEM scanning which averages over a sweep length of approximately 1  $\mu\text{m}$  is successfully averaging out the imperfections along the length of a line. When these data were taken, the principle limitation on the precision was vibration which appears in the interferometer data of figure 5-12 as high-frequency modulation. The noise in the SEM data represents the statistical nature of the electron-scattering process.

The limitation on the accuracy of the measurements is dependent on the physical profiles of the line edges. Although the method of averaging over a 1- $\mu\text{m}$  length of the line guarantees repeatability of the measurements, this method introduces considerable degradation in the steepness of the edge profile as compared with the edge profiles seen during normal SEM operation. Normally, a single sweep of the beam is perpendicular to the edge without the interferometer stage in operation. It should be noted that there also appears to be a difference in the edge profiles of clear and opaque lines; this difference could affect the measurement accuracy. The effect of differences in the physical edge profiles on the measurements is presently being studied.



(a) 25,000X.



(b) 120,000X.

Figure 5-15. SEM photomicrographs of cross-sectional views of a nominally 10- $\mu$ m wide clear line on an AR-chromium artifact.

Table 5-1 - Linewidth Measurements Made with the SEM/Interferometer System on an AR-Chromium Artifact.

Linewidth, $\mu\text{m}$	Local Mean, $\mu\text{m}$	Deviation from Local Mean, $\mu\text{m}$	Mean of all Measurements, $\mu\text{m}$
Nominally 2- $\mu\text{m}$ Opaque Line:			
1.811	1.800	-0.011	1.799
1.789		+0.011	
1.773	1.787	+0.014	
1.801		-0.014	
1.799	1.800	+0.001	
1.800		0.000	
1.804	1.808	+0.004	
1.823		-0.015	
1.797		+0.011	
1.797	-	-	
Nominally 3- $\mu\text{m}$ Opaque Lines:			
2.876	2.877	+0.002	2.863
2.877		+0.001	
2.879		-0.002	
2.863	-	-	
2.782	2.847	+0.065	
2.866		-0.019	
2.860		-0.013	
2.880		-0.033	
2.847	-	-	
2.852	2.873	+0.021	
2.889		-0.016	
2.878		-0.005	
2.870		-	
Nominally 3- $\mu\text{m}$ Clear Line:			
3.388	-	-	3.374
3.351	3.361	+0.010	
3.370		-0.009	
3.366	3.361	-0.005	
3.358		+0.003	
3.381		-0.020	
3.339		+0.042	
3.429	3.401	-0.030	
3.404		-0.003	
3.371		+0.030	
3.356	-	-	

## 6. PHOTOMETRIC OPTICAL MICROSCOPE

Diana Nyssonen  
Electron Devices Division  
Center for Electronics and Electrical Engineering  
National Bureau of Standards  
Washington, DC 20234

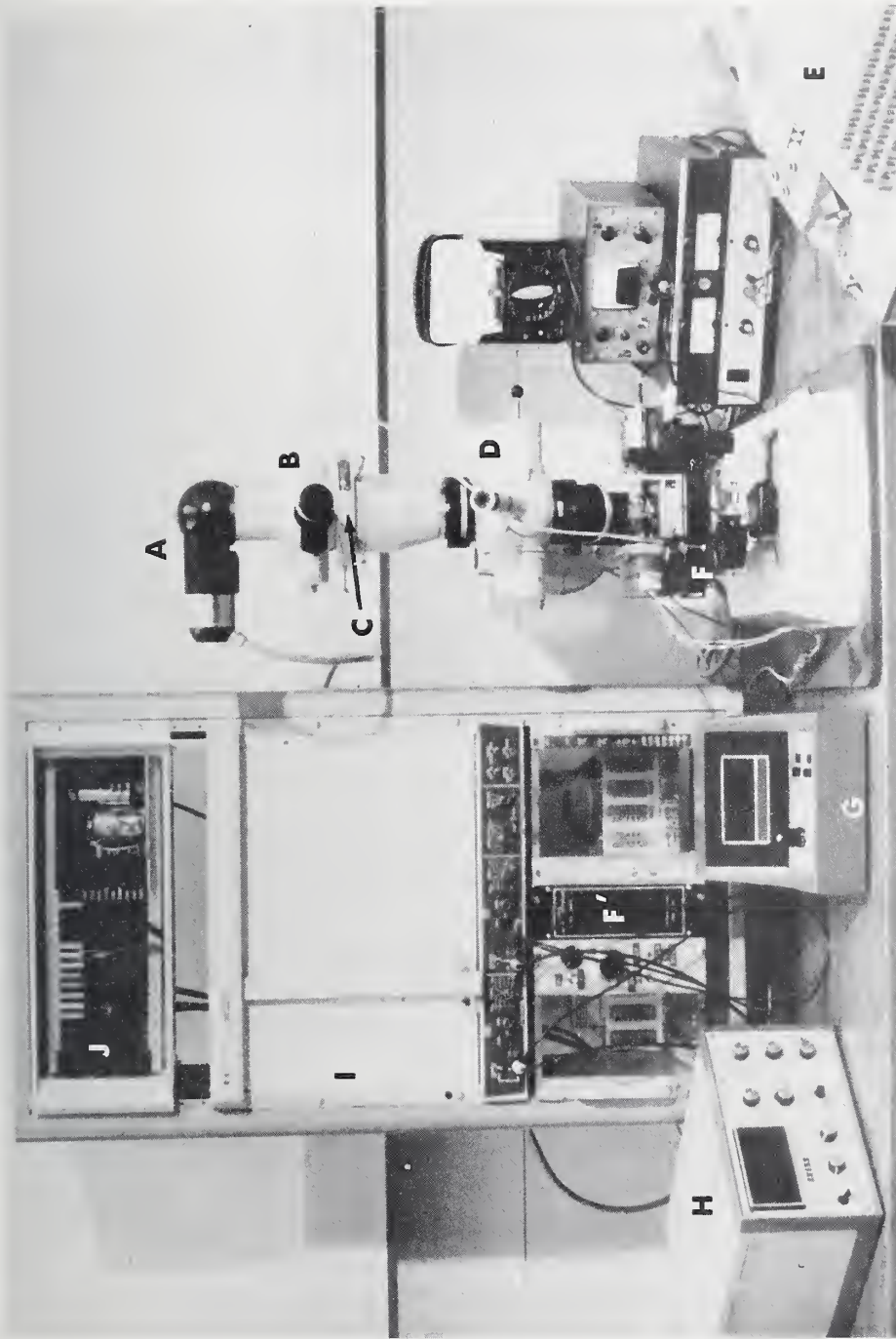
There is no standard photometric optical microscope for measuring line-widths on photomasks. The present approach is to determine under what operating conditions the image profiles from a photometric optical microscope can be made to agree with the theoretical profiles in order to make accurate measurements. This approach requires a system which can be used to examine detail in the image profiles smaller than the diameter of the Airy disc of the imaging optic [40]. For diffraction-limited optics and green light (530 nm), the Airy disk diameter is approximately  $1\ \mu\text{m}$  for an objective with an 0.65 numerical aperture and about  $0.7\ \mu\text{m}$  for an objective with an 0.90 numerical aperture.

Initially, a test system for determining the amounts of aberrations present in microscope optics was not available; thus, only diffraction-limited optical performance could be expected to agree well with theory. For this reason, scanning of the line was achieved by moving the sample with a translating stage instead of scanning the image, thereby avoiding possible off-axis aberrations. Moving the sample during the measurement places additional demands on the stage in terms of accurate positional information. Since the Airy disc diameter is about  $1\ \mu\text{m}$  or less for a high-resolution objective, the stage position must be known accurately at the submicrometer level. The measurement system based on these considerations is discussed in this section, and a detailed description is given in Appendix B [41].

### 6.1 Apparatus

A photograph of the photometric optical-microscope system is shown in figure 6-1. The basic microscope consists of a Zeiss Universal microscope with a photometer head. This microscope is modified to include the best available mechanical stage driven at a slow, constant speed by a stepping motor and function generator developed at NBS [42]. The positional readout is given by a linear-voltage transducer (LVT) gage so that the readout is independent of the mechanical wobble in the stage. The stage motion, therefore, does not have to be perfectly smooth provided that the gage can accurately track the scanning motion. The limitation on the positional accuracy is vibration which was successfully reduced to a level of  $0.01\ \mu\text{m}$ . At this level, the repeatability of focus settings becomes more significant in determining the overall repeatability of the measurement system.

Other modifications to the basic Zeiss microscope system are based on theoretical considerations and earlier experimental work in the present project. These experimental results indicate that diffraction-limited performance cannot be achieved with white-light illumination. Experiments



- A - photomultiplier tube
- B - viewing eyepiece
- C - scanning slit
- D - optical microscope
- E - printer
- F - scanning stage
- F' - scanning-stage controls
- G - linear voltage transducer gage
- H - photometer
- I - X-Y recorder
- J - microprocessor

Figure 6-1. Photograph of the photometric optical-microscope system.

tal edge profiles for white light and filtered green light (Wratten 60 filter and hot mirror) are shown in figure 6-2. (In this figure, the edge locations are arbitrary.) The filtered data are close to diffraction-limited performance. An examination of a large variety of available optics indicates that these differences between edge profiles for white light and filtered light are typical of most optics; in some cases, even further degradation is observed for white-light illumination.

As a result of filtering the illumination for peak response of the optical system and the use of smaller scanning apertures for submicrometer image resolution, the wattage of the tungsten-halogen lamp was boosted to 150 W. Initially, a 50- $\mu\text{m}$  diameter circular scanning aperture was used with a system magnification of 158X. This aperture was later changed to a 20- by 200- $\mu\text{m}$  slit yielding less noisy image profiles because of the higher flux density reaching the detector and the averaging effect over small imperfections in the edges of the scanned lines. The effective slit dimensions in the present system are 0.13 by 1.3  $\mu\text{m}$  which, according to theoretical calculations, have a negligible effect on the imagery. Contrary to conventional usage, this scanning slit is chosen smaller than the diameter of the impulse response of the imaging optics in order to preserve detail in the image. This image detail is related to the structure of the Airy disc and yields information about edge location.

The optics for linewidth measurements are chosen to give the best optical resolution as determined by the agreement of experimental and theoretical line-image profiles. A Zeiss planachromat (63X, 0.90 N.A., and designed for use without a cover glass) shows the best agreement and, consequently, is the only objective used for linewidth calibrations. The choice of condenser aperture is based on theoretical considerations. As shown previously in section 3.2, the choice of transmittance threshold for locating the edges is dependent upon the contrast of the object or, in this case, the background transmittance of the antireflective (AR) chromium. An analytic expression for the proper threshold is derivable only in the limiting cases of coherent or incoherent illumination. For wide-field illumination, the incoherent case would require a condenser numerical aperture much larger than the numerical aperture of the imaging optics (by a factor of two or more). The high numerical-aperture imaging optics required to achieve the best possible resolution makes that choice impossible. However, sufficiently coherent illumination can be achieved by selecting the numerical aperture of the condenser smaller than that of the objective. The calculated image profiles of figure 3-6a show that a condenser numerical aperture of 0.60 with an imaging objective of 0.90 is sufficiently coherent to use eq (3-12) for determining the proper threshold for edge location. (See sec. 3.2.)

Another modification to the microscope system is the incorporation of a piezoelectric focus-adjustment mechanism. This fine-focus device consists basically of a piezoelectric ring stack in between two plates. A hole in the center of the ring stack and corresponding holes in the plates allow the condenser to be brought up through the ring stack into focus at the object plane for transmitted light measurements. The lower plate is supported by the stage while the photomask to be measured rests

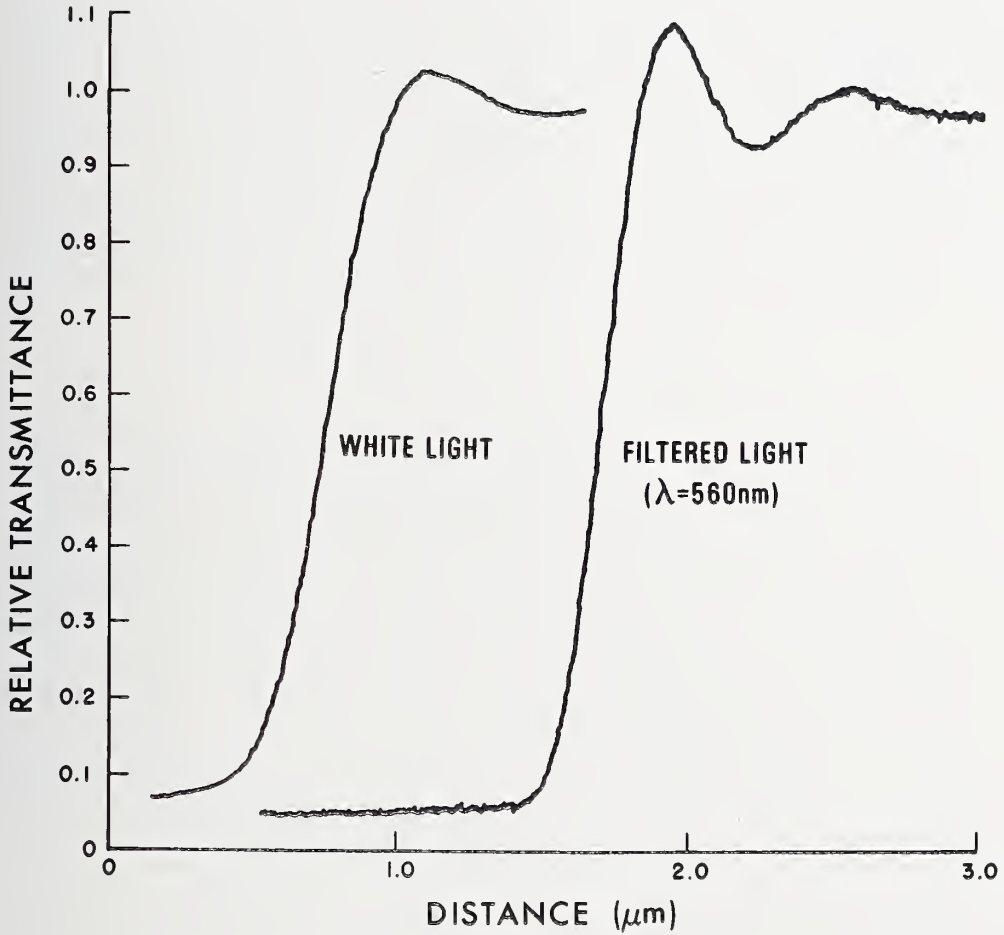


Figure 6-2. Comparison of experimental line-edge profiles in white light and filtered green light for the photometric optical microscope with a 0.90 N.A. objective, a 0.60 N.A. condenser, and an effective scanning slit of 0.13  $\mu\text{m}$ .

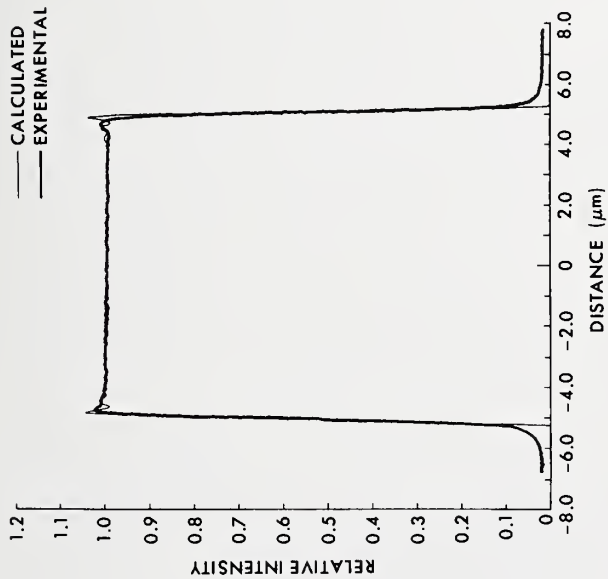
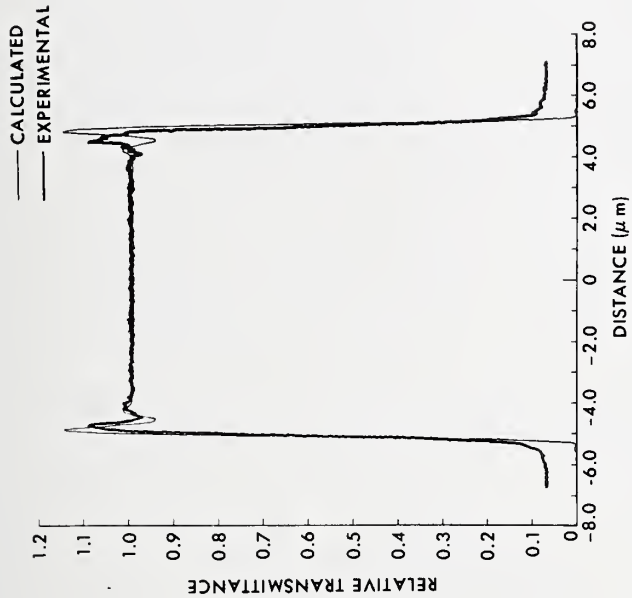
on the upper plate. Focusing accuracy to better than  $0.1 \mu\text{m}$  is achievable with this device. Because of hysteresis in the piezoelectric elements, one must go through focus in one direction only. This extremely smooth, fine motion allows an enormous improvement over conventional fine-focus adjustments.

Both the photometer and LVTD gage have dual analog and digital output. The analog output is used to drive an x-y recorder which is used primarily for monitoring the accuracy of focus. The digital output is fed to a microprocessor developed especially for this application. Its sole purpose is digital recording of the position and photometer data from which the linewidth is determined. The microprocessor is controlled from a printer which allows input of scan information such as run number, date, and number of data points desired. The data recording is initiated by a carriage return, and at the conclusion of the scan, there is an option to transfer the data to punched paper tape. As the linewidth-measurement procedure becomes more formalized, a higher degree of automation is possible by suitable changes in the microprocessor software.

## 6.2 Comparison of Theory and Experimental Data

Figures 6-3a through 6-3d show calculated and experimental image profiles of a nominally  $10\text{-}\mu\text{m}$  wide clear line for different combinations of condenser and objective numerical apertures. The calculated curves are obtained from eq (3-10) with the amplitude transmittance  $t$  of the sample, the pupil function  $F$  of the imaging objective and relay optics, the intensity transmittance function  $S$  of the scanning aperture, and the mutual coherence function  $\Gamma$  as the input parameters. (See sec. 3.2.) The optical model assumes that the amplitude transmittance profile is discontinuous at the line edge, corresponding to a material line profile with a 90-deg edge slope. Thus, the amplitude transmittance is 0 on one side of the edge for samples with no background transmittance and 1.0 on the other side of the edge. For edge slopes from 90 deg down to approximately 50 deg, the optical model adequately describes the line-image profile. For the calculated curves shown in figures 6-3a through 6-3d, the imaging objective and relay optics are assumed to be diffraction-limited, and therefore, the pupil function has a value of 1.0 at all points. The intensity transmittance function of the scanning aperture has a value of 1.0 over an effective slit width of  $0.13 \mu\text{m}$  and 0 elsewhere. The numerical aperture of the imaging objective determines the mutual coherence function.

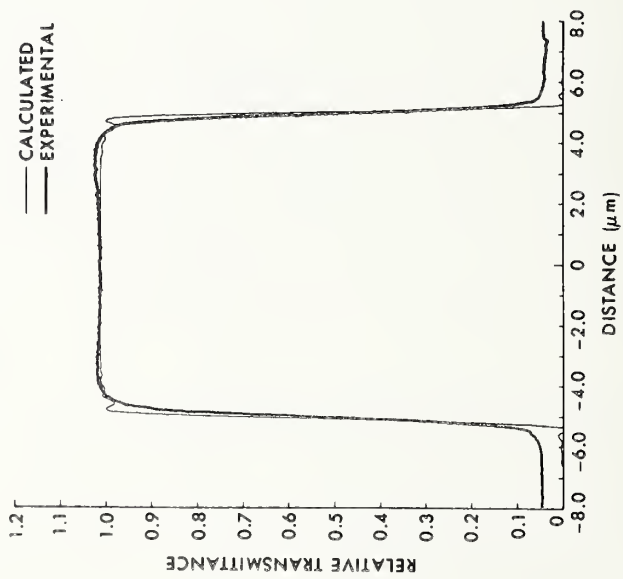
Differences between the calculated and experimental profiles in the low-transmittance region are readily attributable to the small but finite background transmittance of the AR-chromium. All of the calculated curves assume zero background transmittance; there is a substantial increase in computing time for the more general case of a finite background transmittance. As the numerical aperture is increased, the edge ringing in the shoulder of the experimental curves is reduced as compared with the edge ringing in the calculated curves. This difference is expected from using eq (3-9), instead of the two-dimensional solution given by eq (3-11), to calculate the image profiles and from the presence of a small



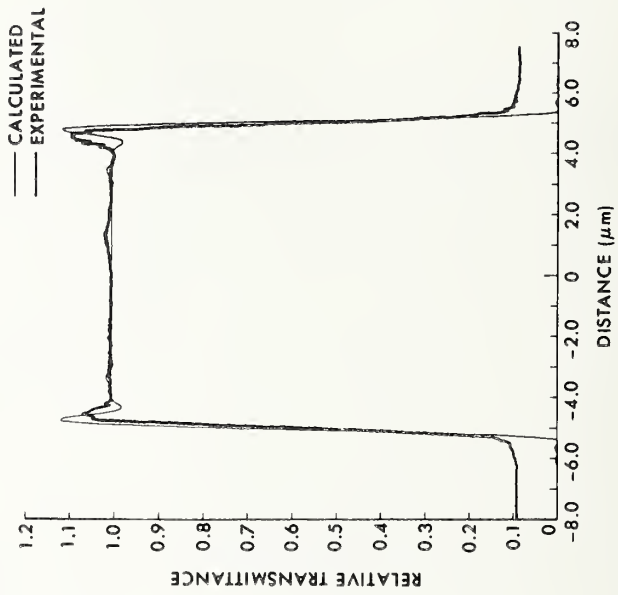
(a) 0.90 N.A. objective and 0.60 N.A. condenser.

(b) 0.90 N.A. objective and 0.22 N.A. condenser; most coherent case.

Figure 6-3. Comparison of calculated and experimental image profiles of a nominally 10- $\mu$ m wide clear line for an optical microscope with various combinations of objective and condenser N.A.'s, illumination wavelength of 560 nm, effective scanning slit of 0.13  $\mu$ m, and diffraction-limited optics; the experimental profiles are for an AR-chromium artifact.



(c) 0.65 N.A. objective and 0.60 N.A. condenser; least coherent case.



(d) 0.65 N.A. objective and 0.22 N.A. condenser.

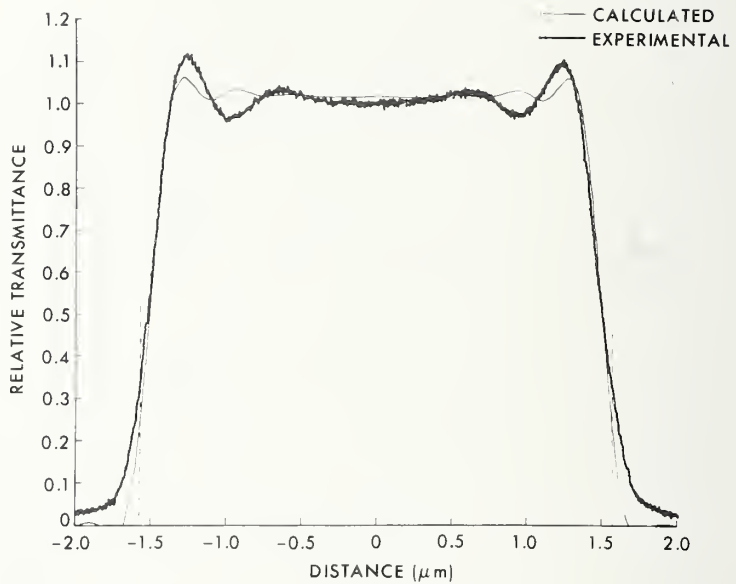
Figure 6-3. Concluded.

amount of spherical aberration in the objective. That this is indeed the case is more apparent from figures 6-4a, 6-4b, and 6-4c. As the linewidths are reduced so that the coherence interval is comparable to the linewidth and the illumination is effectively coherent, there is better agreement between the calculated and experimental profiles. In each of these figures, the calculated profile is computed for a linewidth corresponding to the width of the experimental profile at the appropriate threshold, namely, the 25-percent value corrected for the finite transmittance of the photomask. Figure 6-4b shows the only calculated curve computed for a finite background transmittance.

The remaining differences between calculated and experimental profiles appear to be related to the physical profiles of the lines. The samples scanned were chosen for best possible image quality. Raggedness along the line edges was barely visible, thereby indicating that the edge variations were  $0.1 \mu\text{m}$  or smaller. However, some variations in edge images were observed. An indication of these variations may be found in comparison of the right and left edges of the experimental profiles shown in figures 6-3a through 6-3d. Variations have also been observed between artifacts manufactured at different times. The effect of edge quality, including edge slope, on optical measurements is presently under study.

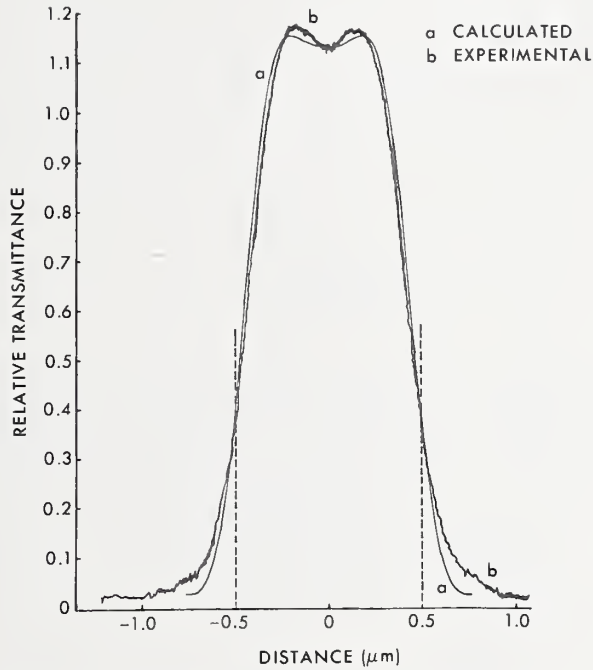
Theoretical calculations show that there is an error in a linewidth measurement if the proper threshold for edge location, as given by eq (3-12), is not used. This result is supported by table 6-1 which compares experimental measurements made on a nominally  $3\text{-}\mu\text{m}$  wide opaque line on an AR-chromium artifact for various combinations of microscope objectives and condensers. In all cases, the width was determined from the photometric image profile in green light. For one set of linewidth values, the proper threshold for line-edge location was determined from eq (3-12). The other linewidth values are based on the conventionally used 50-percent threshold. The nominally  $3\text{-}\mu\text{m}$  wide line was chosen so that it was well resolved for all of the combinations of optics and for some cases with obvious spherical aberration. The experimental results agree with theory even where aberrations are present; namely, as long as the line is well resolved, accurate measurements may be made within the precision of the measurement system ( $0.025 \mu\text{m}$ ) provided that the proper threshold is used. This table also illustrates the linewidth errors with the conventionally used threshold of 50 percent. The first three measurements in this table are made from the photometric image profiles reproduced in figure 6-5. The dashed lines in that figure indicate the line-edge locations determined from the proper threshold.

Figures 6-6a, 6-6b, and 6-6c illustrate experimental profiles with defocus and spherical aberration present. The curves show good agreement with the calculated profiles of figures 3-9 and 3-10, exact correspondence is impossible because of the difficulties of determining both absolute focus position and the amount of spherical aberration. One important finding was made in regard to focus: the theory of incoherent imaging indicates a focus tolerance corresponding to a quarter-wave aberration of  $\pm 0.30 \mu\text{m}$  for a 0.90 N.A. objective. Differences in image profiles and resulting linewidth measurements are observable unless focal

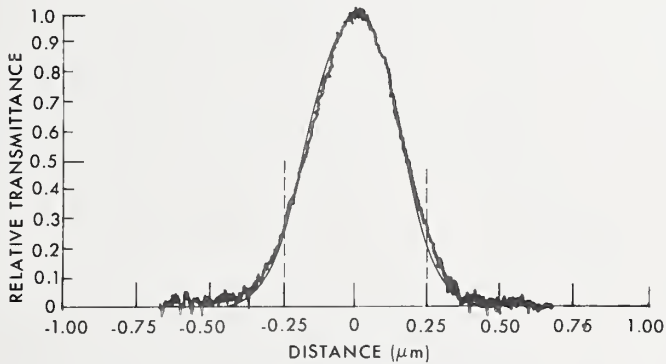


(a) Nominally 3- $\mu\text{m}$  wide line; the dashed lines indicate line-edge locations based on a 33.5-percent transmittance threshold for the experimental profile (background transmittance for the sample is 2.5 percent).

Figure 6-4. Comparison of calculated and experimental image profiles of clear lines of varying width for an optical microscope with a 0.90 N.A. objective, 0.60 N.A. condenser, illumination wavelength of 560 nm, effective scanning slit of 0.13  $\mu\text{m}$ , and diffraction-limited optics; the experimental profiles are for AR-chromium artifacts.



- (b) Nominally 1- $\mu\text{m}$  wide line; the dashed lines indicate line-edge locations based on a 33-5-percent transmittance threshold for the experimental profile (background transmittance for the sample is 2.5 percent); the background transmittance for the calculated profile is also 2.5 percent.



- (c) 0.50- $\mu\text{m}$  wide line; the dashed lines indicate line-edge locations based on a 25-percent transmittance threshold for the experimental profile (background transmittance for the sample is 0 percent).

Figure 6-4. Concluded.

Table 6-1 - Comparison of Linewidth Measurement Made with the Photoelectric Optical Microscope on a Nominally 3- $\mu\text{m}$  Wide Opaque Line for Various Combinations of Objectives and Condensers.

Objective N.A.	Condenser N.A.	Measured at Proper Threshold, <sup>a</sup> ( $\mu\text{m}$ )	Measured at 50-percent Threshold, ( $\mu\text{m}$ )
0.45 (Wild)	0.60	2.90	3.06
0.45 (Wild)	0.40	2.92	3.15
0.45 (Wild)	0.22	2.91	3.16
0.90 (Zeiss)	0.60	2.92	3.01
0.90 (Vickers)	0.60	2.95	3.01
0.65 (Vickers)	0.60	2.90	3.10

<sup>a</sup>Twenty-five percent threshold corrected for finite transmittance of opaque area.

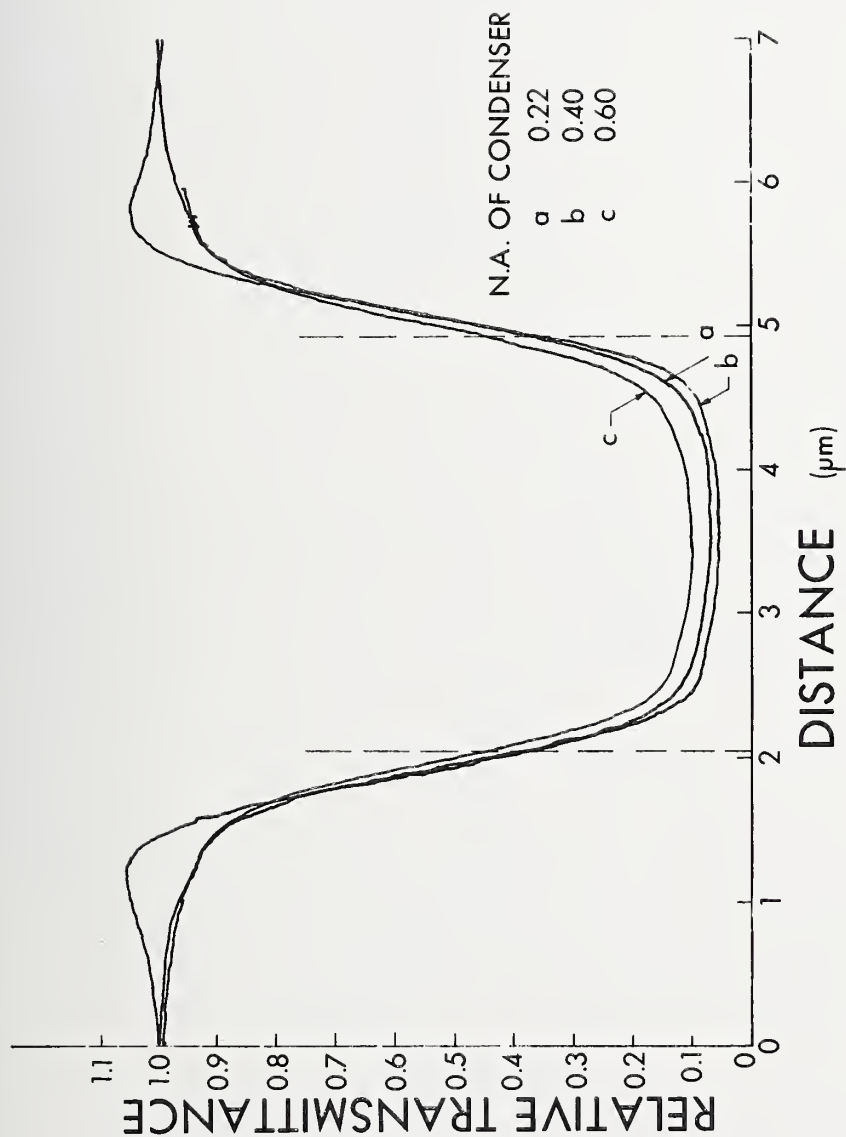
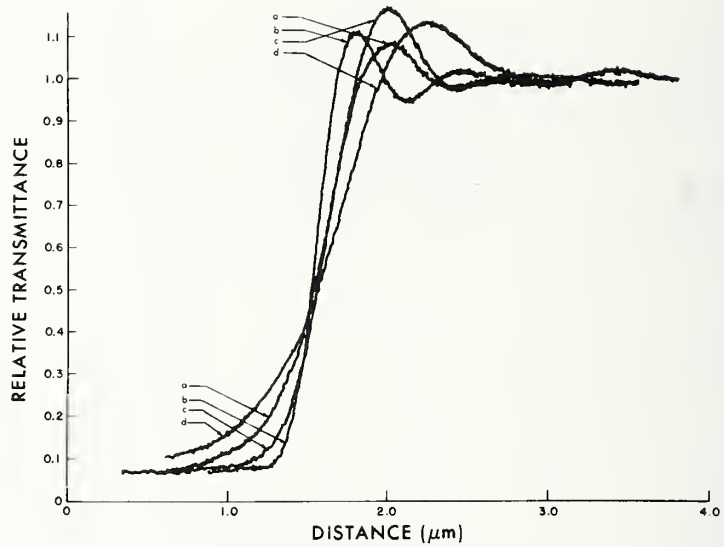
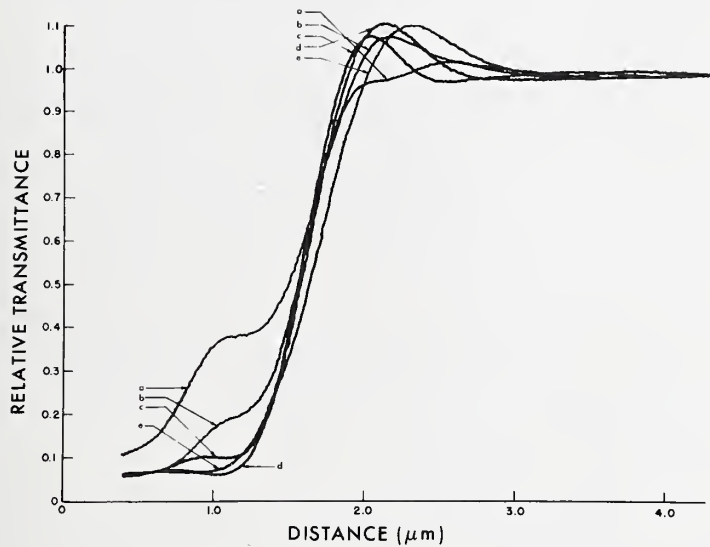


Figure 6-5. Experimental image profiles of a nominally 3- $\mu\text{m}$  wide opaque line on an AR-chromium artifact for the photometric optical microscope with a 0.45 N.A. objective, varying condenser N.A. (this variation corresponds to a variation in the degree of coherence of the illumination), illumination wavelength of 560 nm, effective scanning slit of 0.13  $\mu\text{m}$ , and nearly diffraction-limited optics; the dashed lines indicate line-edge locations based on a 33.5-percent transmittance threshold.

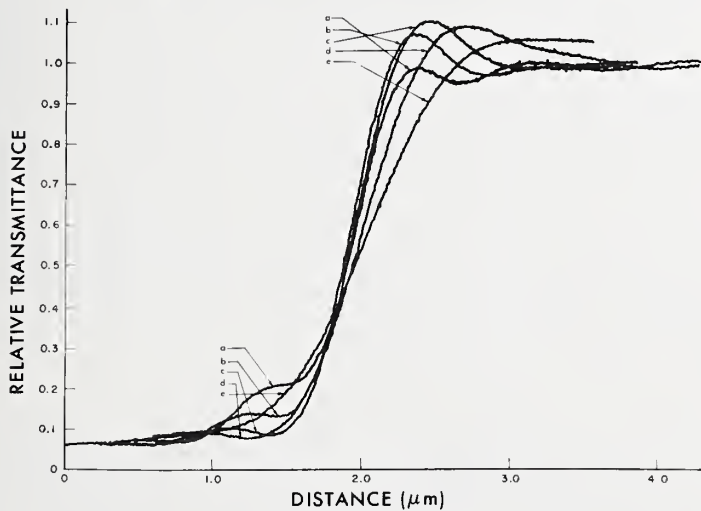


(a) 0.90 N.A. objective and 0.60 N.A. condenser.  
(Compare with fig. 3-9.)

Figure 6-6. Experimental image profiles of one edge of a nominally 10- $\mu\text{m}$  wide clear line on an AR-chromium artifact for the photometric optical microscope with an illumination wavelength of 560 nm, effective scanning slit of 0.13  $\mu\text{m}$ , and nearly diffraction-limited optics; profiles a through e are for different focus settings with submicrometer displacements between them. (Registration of all profiles at edge is not exact.)



(b) 0.65 N.A. objective, 0.22 N.A. condenser, and an improper cover-glass thickness (0.12 mm instead of 0.17 mm). (Compare with fig. 3-10.)



(c) 0.95 N.A. objective, 0.22 N.A. condenser, and an incorrect microscope tube length (160 mm instead of 215 mm). (Compare with fig. 3-10.)

Figure 6-6. Concluded.

displacements are less than  $0.10 \mu\text{m}$  ( $\pm 0.05 \mu\text{m}$ ). Within this tolerance, variations in linewidth measurements do not appear to be related to any single parameter.

Table 6-2 shows a summary of measurement data on a nominally  $1\text{-}\mu\text{m}$  wide clear line made under the following nonstandard operating conditions: (1) 0.90 N.A. objective (Zeiss planachromat 63X, designed for use without a cover glass) with 2X Optovar and 1.25X tube lens yielding a total magnification of 157.5X; (2) 0.60 N.A. condenser; (3) effective scanning aperture of 0.13 by  $1.3 \mu\text{m}$ ; (4) Wratten 60 filter and a heat reflecting mirror; and (5) scanning speed of approximately 0.03 micrometers per second. Best focus is determined from maximum transmittance overshoot at the line edge; for lines under  $1 \mu\text{m}$  in width, best focus is determined steepest slope. The threshold used for linewidth measurements is determined from eq (3-12). Although the daily precision is better than  $0.025 \mu\text{m}$  (standard deviation), the uncertainty in the measurement is dependent upon the physical-edge width, that is, the width of the sloped portion of the physical edge which is estimated to be about  $0.1 \mu\text{m}$ .

Better agreement between calculated and experimental image profiles can be achieved if the optical aberrations of the imaging system and the effects of the physical profile of the line on its image profile are known. Both of these problems are currently being studied. Several commonly used methods for measuring aberrations of optical systems involve interferometers [43]. Interferometer measurement of the optical aberrations of microscope objectives with 0.90 numerical aperture is, however, extremely difficult because of the need to generate a perfect spherical wave front to fill this high numerical aperture. Since the objective in the photometric optical microscope is used on axis, we are primarily interested in the symmetric aberrations, *viz*, spherical aberration. A wavefront-shearing interferometer developed at NBS [44] is currently being adapted to measure spherical aberration in microscope objectives.

Concurrently, an effort is underway to obtain more details about the physical line profile from high resolution SEM photomicrographs of the cross-sectional line profiles. (See sec. 5.5.) This additional information can be included in both the optical and SEM modeling to reduce further the uncertainty in the measurement processes.

### 6.3 Optimum Operating Conditions

It appears that scalar one-dimensional theory may be used to predict line image profiles in the optical microscope for ratios of condenser-to-objective numerical apertures less than 1.0 where the objective numerical aperture is equal to or less than 0.90. Good agreement between theoretical and experimental profiles exists for a microscope operating under the following conditions: (1) spectrally filtered illumination to eliminate chromatic aberrations, (2) on-axis scanning of the line to eliminate off-axis aberrations, and (3) an effective scanning aperture smaller than the impulse response of the objective to preserve detail in the line-edge image. Under these conditions, theory predicts that accurate linewidth measurement may be made using the 25-percent threshold (corrected for the

Table 6-2 - Summary of Linewidth Measurements Made with the Photoelectric Optical Microscope on a Nominally 1- $\mu\text{m}$  Wide Clear Line.

Number of Runs Per Day	Daily Mean ( $\mu\text{m}$ )	Daily Standard Deviation	Mean of All Measurements ( $\mu\text{m}$ ) and Standard Deviation
5	1.09	0.025	
5	1.06	0.024	
5	1.07	0.018	1.08 $\pm$ 0.01
5	1.09	0.020	
5	1.08	0.010	
5	1.08	0.015	

finite transmittance of the photomask material or film). For ratios of condenser-to-objective numerical apertures less than 1.0, this threshold is nearly invariant with condenser numerical aperture and spherical aberration provided that accurate focus position is used. Focus may be determined by either maximum slope or maximum overshoot at the edge.

Presently, the only known method of determining the 25-percent threshold is from a photometric image scan. Measurement eyepieces frequently used for linewidth measurements, such as filar or image-shearing eyepieces, measure different thresholds. Theory predicts that, depending on the transmittance of the photomask, measurement of the 50-percent threshold will yield linewidth-measurement errors up to  $0.15 \mu\text{m}$  with a 0.90 N.A. objective; the errors increase with lower N.A. The errors introduced by measurement of the wrong threshold are additive and constant for a given optical system. Attempting to correct for them by the usual calibration methods produces greater nonlinear errors at linewidths smaller and larger than the calibration linewidth. These errors also increase with defocus or spherical aberration.

In summary, the largest sources of variations in linewidth measurement with optical microscopes include: (1) nonrepeatability of focus at high numerical apertures with conventional fine-focus adjustments, (2) variation in edge quality which has a particularly noticeable effect for measurements on state-of-the-art photomasks, and (3) the effect of chromatic aberrations in the microscope with white light. These sources of error affect measurements made with filar and image-shearing eyepieces as well as photometric image scans; however, these effects may be masked by larger variations in the response of the human eye.

## 7. CONVENTIONAL OPTICAL MICROSCOPES

Fred W. Rosberry and Dennis A. Swyt  
Mechanical Processes Division  
Center for Mechanical Engineering and Process Technology  
National Bureau of Standards  
Washington, DC 20234

Measurements of linewidths on photomask-like artifacts have been made with filar and image-shearing eyepieces in order to: (1) define quantitatively the problem of discrepancies in similar measurements reported by the IC industry [5] and (2) establish an information base for the use of NBS-calibrated linewidth artifacts by the IC industry. In the first part of this section are presented results of an initial study of the filar/image-shearing problem. These measurements were made on the best artifact then available to NBS, namely, an artifact with nominally 2-, 5-, and 10  $\mu\text{m}$ -wide clear lines in bright chromium on a glass substrate and similar to a widely used commercial photomask standard. In the second part of this section are presented the results of a later study of the effects of line-scale *versus* linewidth calibrations of microscopes. These measurements were made on an NBS prototype artifact (see sec. 4.), namely, an AR-chromium artifact with opaque and clear lines of nominally 1-, 3-, and 10- $\mu\text{m}$  widths.

### 7.1 Precision Characteristics of Microscopes

An experimental comparison of linewidth measurements was made using optical microscopes and operating conditions representative of those employed by the IC industry for photomask inspection. At the outset of this study, photomask linewidth measurements in industry were being made with conventional optical microscopes fitted with visually measuring eyepieces of either the filar or image-shearing type; to a limited degree, automatic TV-microscope systems were in use.\*

The majority of measurements reported here were made with a monocular research-quality microscope with separate filar and image-shearing eyepieces. During the study, a binocular image-shearing microscope and an automatic TV-microscope system were available for short-term use.

The monocular microscope was equipped with an objective lens with a 0.95 N.A. and a magnification of 80X, and either bright-field or dark-field illumination; the image-shearing eyepiece had an intensity beamsplitter as the shearing element. The binocular microscope was equipped with an objective lens with a 0.90 N.A. and a magnification of 63X and bright-field illumination only; the image-shearing eyepiece had a polarization beamsplitter as the shearing element. The TV-microscope system was equipped with an objective lens with 0.95 N.A. and a magnification of

---

\* By the time of issuance of this report, automatic TV-microscope systems were in much wider use.

80X, and bright field illumination only. All three microscopes had capabilities for both reflected and transmitted light.

The three systems differed in their fundamental principles of operation and means of data output. The filar and image-shearing eyepieces required operator judgment for locating image edges in linewidth measurements; the TV system used automatic image scanning and electronic thresholding. The filar eyepiece had a vernier-scale readout which required the calculation of linewidths from arbitrary scale divisions. This filar eyepiece, which had a magnification 7X and a movable, full-field pair of cross hairs, had the best repeatability of three available filar eyepieces and was used throughout this study. The binocular image-shearing system had direct digital readout as did the TV-microscope system. Preliminary tests to determine the precision for each of the optical microscope-measurement systems resulted in variations from the mean of ten measurements of the width of a nominally 5- $\mu\text{m}$  wide clear line of 0.03 to 0.09  $\mu\text{m}$  (standard deviations). The linearity of each of the microscope systems was checked for gross misbehavior by measuring four line spacings which had been calibrated with the NBS line-standard interferometer [45]. Within the measurement precision and the calibration uncertainty, no significant deviations from linearity were observed.

A cosine error results when the axis of measurement is not perpendicular to the line whose width is to be measured. In a filar eyepiece, cosine error is minimized when the cross hair lies parallel to the line and travels perpendicular to it. In the image-shearing eyepiece, the direction of shear must also be perpendicular to the length of the line, similarly with a TV-microscope system. For filar and image-shearing eyepieces, the degree to which the line to be measured can be made to lie along the axis of measurement depends on: (1) the fraction of the field of view the line occupies and (2) the least detectable increment of field of view between some part of the line and a reference mark on the viewer. A series of experiments showed that, provided the line fills at least 5 to 10 percent of the field, misalignment need not be a significant source of measurement error.

Detailed linewidth measurements were made with each of the systems on clear lines of 2-, 5-, and 10- $\mu\text{m}$  nominal width on an opaque background. Each microscope was calibrated in magnification using a line spacing previously measured to be  $34.927 \pm 0.007 \mu\text{m}$  with the NBS line-standard interferometer. In addition, the TV-microscope system was adjusted to measure a line-to-space ratio of a value predetermined by the manufacturer-supplied artifact.

The results of the measurements appear in table 7-1. Each of the entries in the table represents the mean of ten sequential measurements. To determine how much significance can be attributed to each entry, measurements on each of three systems were repeated ten times successively on nine occasions for measurements of the nominally 5- $\mu\text{m}$  wide line in bright-field, transmitted illumination. Typical data for a series of ten measurements on a single occasion are summarized in table 7-2 which also

Table 7-1 - Apparent Widths of Clear Lines.

Microscope	Apparent Linewidth, $\mu\text{m}$		
<b>a. Bright-Field Transmitted Illumination:</b>			
Filar Eyepiece	2.25	5.25	10.05
Shearing Eyepiece (Intensity)	1.95	4.65	9.10
Shearing Eyepiece (Polarization)	2.00	4.85	9.40
TV Display	2.55	5.25	9.75
<b>b. Bright-Field Reflected Illumination:</b>			
Filar Eyepiece	2.15	5.00	9.80
Shearing Eyepiece (Intensity)	2.45	5.35	9.75
Shearing Eyepiece (Polarization)	2.50	5.40	9.90
TV Display	2.55	5.25	9.75
<b>c. Dark-Field Transmitted Illumination:</b>			
Filar Eyepiece	2.10	4.80	9.30
Shearing Eyepiece (Intensity)	2.15	5.15	9.65
<b>d. Dark-Field Reflected Illumination:</b>			
Filar Eyepiece	2.25	5.15	9.50
Shearing Eyepiece (Intensity)	2.25	5.20	9.55

Table 7-2 - Typical Data for Linewidth Measurements Repeated on Same Line.

Microscope		Filar Eyepiece	Image-Shearing Eyepiece (Intensity Type)	TV Display
Results of Ten Measurements on Same Occasion	Mean, $\mu\text{m}$	5.25	4.65	5.40
	Sample Std. Dev., $\mu\text{m}$	0.077	0.014	0.009
Average Sample Standard Deviation, $\mu\text{m}$		0.078	0.015	0.010
Mean of Means of Ten Measurements on Nine Occasions	Mean, $\mu\text{m}$	5.22	4.65	5.40
	Sample Std. Dev., $\mu\text{m}$	0.072	0.034	0.028
Reproducibility, $\mu\text{m}$		0.28	0.10	0.08

shows the arithmetic means for nine such series taken on different occasions.

The spread in the means of measurements taken on different occasions cannot be explained by the spread within measurements on one occasion. If the standard deviations associated with  $n$  repetitions of a measurement made on a single occasion is  $\sigma_w$ , the sample standard deviation of the means of these  $n$  repetitions taken on a number of occasions is a measure of the total standard deviation [46], namely,

$$\sigma_{\text{total}} = \sqrt{\sigma_B^2 + \frac{\sigma_w^2}{n}}, \quad (7-1)$$

where  $\sigma_B^2$  is the between-laboratory component of the variance. The reproducibility can be defined as the spread about the grand mean which includes 95 percent of all test results. Therefore, the reproducibility associated with test results based on a single measurement on each occasion [46] is

$$\text{Reproducibility} = \pm 2.77 \sqrt{\sigma_B^2 + \sigma_w^2}. \quad (7-2)$$

These results suggest that the reproducibility is about  $\pm 0.3 \mu\text{m}$  for the filar eyepiece and about  $\pm 0.1 \mu\text{m}$  for both the image-shearing eyepiece and the TV-microscope system.

## 7.2 Comparison of Linewidths Measured with Filar and Image-Shearing Eyepieces

The results of table 7-1 also show some general trends between the apparent sizes of lines measured with the two different types of eyepieces. For a clear line on an opaque background viewed in bright-field transmitted light,

$$w_F (\text{width measured by filar}) > w_S (\text{width measured by image shearing}); \quad (7-3)$$

and for the same clear line viewed in bright-field reflected light,

$$w_F (\text{width measured by filar}) < w_S (\text{width measured by image shearing}). \quad (7-4)$$

These observed trends, or relationships, are the basis of a phenomenological model to account for differences in linewidths as measured under various combinations of three viewing variables, namely, eyepiece (filar or image shearing), illumination (transmitted or reflected), and line polarity (clear or opaque). The model is discussed in Appendix C [47]. This model is consistent with the relationships (7-3) and (7-4) given earlier and implies a number of other relationships among apparent linewidths. For a clear line (space) and opaque line of equal width, table 7-3 gives twelve expected relationships of apparent linewidths for different combinations of the three viewing variables.

Table 7-4 gives experimentally measured values of clear and opaque lines on an NBS AR-chromium artifact. Each entry in the table is the mean of

Table 7-3 - Expected Relationships of Apparent Linewidths Measured Under Various Viewing Conditions ( $W$ , apparent width; F, filar eyepiece; S, image-shearing eyepiece; T, transmitted; R, reflected; C, clear line; O, opaque line).

	Clear Line	Opaque Line
Transmitted	$W_F > W_S$	$W_F < W_S$
Reflected	$W_F < W_S$	$W_F > W_S^*$
	Filar	Image Shearing
Clear Line	$W_T > W_R$	$W_T < W_R$
Opaque Line	$W_T > W_R$	$W_T > W_R$
	Transmitted	Reflected
Filar	$W_C > W_O$	$W_C < W_O$
Image Shearing	$W_C < W_O$	$W_C > W_O^*$

Table 7-4 - Apparent Linewidths of Opaque Lines and Clear Spaces Measured on AR-Chromium Artifact in Bright-Field Illumination.

Nominal Linewidth, $\mu\text{m}$	Measured Linewidth, $\mu\text{m}$	
	Filar	Image Shearing
Clear Space, Transmitted Light:		
1	1.12	0.86
3	3.17	2.91
10	10.16	9.97
Opaque Line, Transmitted Light:		
1	0.91	1.19
3	2.90	3.14
10	9.77	10.03
Clear Space, Reflected Light:		
1	0.78	1.00
3	2.86	2.99
10	9.91	10.03
Opaque Line, Reflected Light:		
1	1.04	1.08
3	3.07	3.08
10	9.98	9.99

measurements taken on ten occasions. Each eyepiece was calibrated using a line-scale calibration. Comparison of tables 7-3 and 7-4 shows that all but 2 of the 12 relationships in table 7-3 are present in the experimental results of table 7-4. Two relationships in table 7-3 (indicated by asterisks) are not entirely supported by the experimental data in table 7-4. These differences involve reflected-light measurements and may indicate that the model is not entirely satisfactory for describing linewidth measurements in reflected light with filar and image-shearing eyepieces.

The most consistent relationships are shown in table 7-5 where significant differences between filar and image-shearing results are shown for clear and opaque lines viewed in transmitted light (the usual means of photomask inspection). Both measurement eyepieces were first calibrated with a single line scale having a nominal spacing of 35  $\mu\text{m}$ .

Table 7-6 also shows differences between linewidths measured in transmitted light by filar and image-shearing eyepieces, but for these data the eyepieces were first calibrated with lines having nominally assigned linewidths of 3 and 10  $\mu\text{m}$ . Within the range of calibration, the differences are effectively zero since they are small fractions of the uncertainty in either the filar or image-shearing measurements. Comparison of tables 7-5 and 7-6 shows the efficacy of linewidth calibration compared with line-scale calibration.

Details of the calibration study are given in table 7-7. Filar and image-shearing eyepieces were first calibrated with respect to lines measured photometrically and then used to measure unknown linewidths which were also measured photometrically. The widths of eleven lines were measured on the photometric optical microscope discussed in section 6. With one pair of 3- and 10- $\mu\text{m}$  wide lines treated as calibration lines, each eyepiece was calibrated and the widths of the other lines of similar polarity (clear or opaque) were measured; then each pair of calibrated lines was remeasured to check the constancy of the eyepiece calibrations relative to the calibrated linewidths. (Each entry in table 7-7 is the mean of 9 measurements - 3 each on 3 occasions.) The results show that, with the exception of the combination of the image-shearing eyepiece and opaque line which shows a slight bias, the eyepieces can be made to read proper linewidth relative to a linewidth calibration.

Table 7-5 - Apparent Linewidths Measured in Transmitted Light with Filar and Image-Shearing Eyepieces Calibrated with Line Spacings.

Width of Clear Lines, $\mu\text{m}$			
Filar	1.12	3.17	10.16
Image Shearing	0.86	2.91	9.97
Difference	+0.26	+0.26	+0.19
Width of Opaque Lines, $\mu\text{m}$			
Filar	0.91	2.90	9.77
Image Shearing	1.19	3.14	10.03
Difference	-0.28	-0.24	-0.26

Table 7-6 - Apparent Linewidths Measured in Transmitted Light with Filar and Image-Shearing Eyepieces Calibrated with Linewidths.  
(Note: Results of tables 7-5 and 7-6 are for different artifacts.)

Width of Clear Lines, $\mu\text{m}$			
Filar	0.75	2.95	10.14
Image Shearing	0.77	2.97	10.16
Difference	-0.02	-0.02	-0.02
Width of Opaque Lines, $\mu\text{m}$			
Filar	0.90	3.00	9.97
Image Shearing	1.05	3.05	9.97
Difference	-0.15	-0.05	0.00

Table 7-7 - Comparison of Linewidths Measured in Transmitted Light by Filar and Image-Shearing Eyepieces Calibrated with 3- and 10- $\mu\text{m}$  Linewidths as Measured on NBS Photometric Optical Microscope.

Nominal	Photometric	Filar	Image Shearing
Width of Clear Lines, $\mu\text{m}$			
3	2.98	2.98*	2.98*
10	10.17	10.17*	10.17*
1	0.78	0.75	0.77
3	2.98	2.95	2.97
10	10.10	10.14	10.16
Width of Opaque Lines, $\mu\text{m}$			
3	3.00	3.00*	3.00*
10	9.95	9.95*	9.95*
1	0.96	0.90	1.05
2	1.86	1.87	2.02
3	2.96	3.00	3.05
10	10.03	9.97	9.97

\* Measurement eyepieces were first calibrated with respect to these linewidths which were previously measured with a photometric optical microscope.

## 8. LINEWIDTH CALIBRATION

A primary objective of the present project is to calibrate linewidth artifacts that can be used by the IC industry for the accurate measurement of linewidths on photomasks. The calibration of artifacts and instruments is basically a refined form of measurement. In particular, calibration is a comparison procedure in which an unknown, or test item, is compared with a known, or standard, and the value of the test item is determined from the accepted value of the standard.

### 8.1 Calibration Hierarchy

For length calibrations, several calibrations are successively linked in order to relate, by comparative measurements, the generally inaccessible defined unit of length to an accessible artifact for the user. At each stage of this calibration hierarchy, there are three items of interest: (1) a standard item with announced values and associated uncertainties (systematic and random errors), (2) an assembly of equipment and procedures required for comparing the items, and (3) the items to be measured or calibrated for some useful task.

The hierarchy of the linewidth calibration is shown in figure 8-1. The first stage in linewidth calibrations relates the physical standard for the defined unit of length (wavelength of radiation from krypton 86) to the width of a material line. The measurement system developed for this purpose is the SEM/interferometer described in section 5, and the item to be calibrated is a photomask-like artifact such as the one described in section 4. The wavelength of the laser in the interferometer is monitored by comparison with the radiation wavelength from a stabilized laser which, in turn, is compared with the krypton radiation. In any case, this interferometric approach obviates the need for an intermediate calibrated length artifact with its associated measurement uncertainties. For this reason, the SEM/interferometer is considered a primary measurement system.

The second stage for linewidth calibrations relates the linewidths calibrated by the SEM/interferometer on the first artifact to the user artifact. The measurement system used for this comparison is the photometric optical microscope discussed in section 6, and this system is considered to be the secondary measurement system. The artifact to be calibrated for the user is the same type of artifact calibrated in the primary measurement system.

The third stage relates the linewidths calibrated by the photometric optical microscope on the second artifact to the readout of a linewidth-measurement instrument used in the IC industry. The user then desires to make accurate measurement of unknown photomask linewidths with this calibrated instrument. In some cases, the user may even desire to calibrate other working artifacts by comparison with the NBS artifact and, subsequently, calibrate other instruments by means of these additional artifacts.

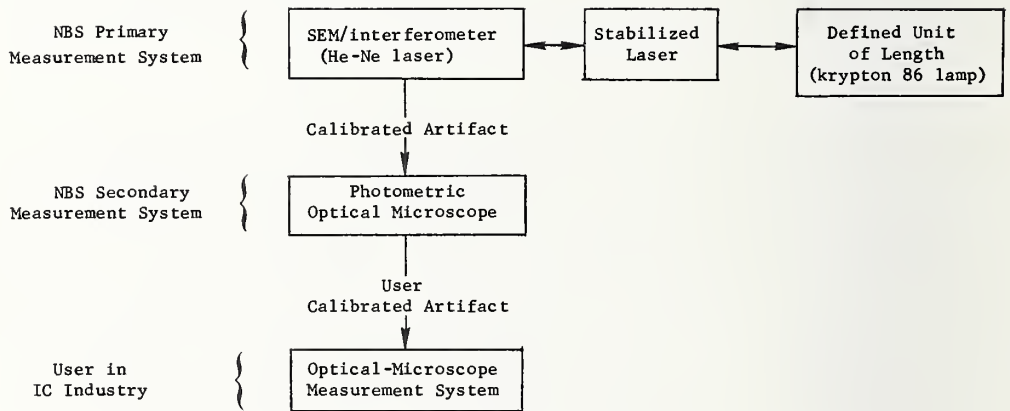


Figure 8-1. Hierarchy of NBS linewidth calibrations.

## 8.2 Preliminary Comparison of Linewidths Measured on SEM/Interferometer and Photometric Optical Microscope

The measurement uncertainties of the NBS linewidth-measurement systems (SEM/interferometer and photometric optical microscope) have not yet been fully evaluated. A preliminary comparison of linewidth measurements made on the same lines by these two systems has been made, and the results are presented in this section. A more detailed discussion is given in Appendix D [48].

Known sources of systematic error in the SEM/interferometer are currently being investigated. Based on preliminary measurements presented in section 5.5, a standard deviation associated with nine or more repetitions made on a single occasion is  $0.015 \mu\text{m}$  for the SEM/interferometer. This value is dependent, in part, on the random noise in the interferometer output. Some of this noise is being introduced from stage vibrations. An effort is currently underway to eliminate or reduce this vibration and, thereby, decrease the present value of the standard deviation.

The linewidth-measurement uncertainty (systematic and random errors) for the photometric optical microscope is currently estimated to be about  $\pm 0.1 \mu\text{m}$  and the standard deviation is better than  $0.025 \mu\text{m}$ . By comparison, the SEM/interferometer has the potential for a significantly lower uncertainty than the photometric optical microscope because of the better resolution of the SEM. The project goal for the measurement uncertainty of linewidth measurements in the 1- to  $10\text{-}\mu\text{m}$  regime with the SEM/interferometer is  $\pm 0.05 \mu\text{m}$ .

Table 8-1 shows the means of linewidth measurements made with both the SEM/interferometer and the photometric optical microscope for two opaque lines and a clear line on an AR-chromium artifact. After completion of the SEM/interferometer measurements, the artifact was placed in the photometric optical microscope and measurements were made in approximately the same area of the artifact. The contamination deposited on the surface of the artifact by the SEM/interferometer is not visible in transmitted illumination in the optical microscope; thus, this contamination appears not to have affected location of the edge profiles in the optical microscope. The contamination, however, is easily observed in reflected light. The measured linewidths in this table are the mean of nine or more measurements for each measurement system; the  $3\sigma$  standard deviations for these mean values are also given in the table. These values are preliminary data and, as such, only indicate trends in the comparative linewidth measurements of these two systems for a given line. The difference between the mean values of the opaque lines as measured by the SEM/interferometer and the photometric optical microscope is  $0.05 \mu\text{m}$ . The corresponding difference between the mean values of the clear line is  $0.24 \mu\text{m}$ ; this difference appears to be an anomaly and is currently being investigated. Considering that the estimated uncertainty is about  $\pm 0.10 \mu\text{m}$  for the photometric optical microscope and assuming that the uncertainty for the SEM/interferometer should be less than the uncertainty for the photometric optical microscope, the agreement of the measured linewidths for the opaque lines is very good.

Table 8-1 - Comparison of Linewidth Measurements from SEM/Interferometer and Photometric Optical Microscope.

	SEM/Interferometer <sup>a</sup>	Photometric Optical <sup>b</sup>
Opaque	1.80	1.85
Opaque	2.86	2.90
Clear	3.37	3.13

<sup>a</sup> 3 $\sigma$  standard deviation of 0.016  $\mu\text{m}$ .

<sup>b</sup> 3 $\sigma$  standard deviation of 0.025  $\mu\text{m}$ .

### 8.3 Transfer of NBS Measurements to Industry

Several methods are available for transferring the linewidth values measured at NBS to the user. These methods include the issuance of a Standard Reference Material (SRM) [49], a calibration service to measure artifacts submitted to NBS by the user [50], or a formal Measurement Assurance Program (MAP) [51,52]. At present, these methods are under consideration, and data are being collected in NBS/IC-industry collaborative tests to help select the means for transferring NBS measurements to industry.

The SRMs are typically samples of materials of well-known, thoroughly described properties or compositions which may be used to calibrate measurement systems, to check on-line quality control, or to evaluate device performance at the user's plant or laboratory. For linewidth measurements, the resulting SRM might be an AR-chromium-on-glass artifact which has been measured on the NBS photometric optical microscope. The measurement uncertainty assigned to the artifact would be based primarily on the NBS measurement process. The artifact would become available to users through the NBS Office of Standard Reference Materials.

The calibration, measurement, and testing services of NBS are aimed primarily at those user needs requiring accuracy or uncertainty that can be obtained only by direct comparison of the user's item with NBS standards. However, NBS also provides services for items requiring lesser accuracy, but suitable for working standards in the user's plant or laboratory. A service for linewidth measurements might become available whereby a user would submit a photomask to NBS, NBS would make measurements with the SEM/interferometer system or photometric optical microscope, and the photomask along with the measurement data would be returned to the user. It should be noted that the measurement uncertainty associated with these measurements would be very dependent on the quality (edge uniformity and steepness) of the photomask submitted by the user. Such measurement services are usually arranged through the NBS Office of Measurement Services.

A MAP is the approach to the development of a length-measurement process, such as a linewidth calibration, which assures the user that the measurements are suitably accurate for their intended use. This approach is carried out at NBS to support its own measurements as well as those participating users. Calibrated artifacts issued by NBS under a MAP are assigned measurement uncertainties which are realistic for the intended application regardless of the number of comparisons or transfers between the defined standard and the user.

For linewidth measurements under a MAP, the specified measurement process might include the following: measurement systems at NBS, such as the SEM/interferometer and photometric optical microscope; measurement systems in industry, such as the optical microscopes used for measurement of critical dimensions; the NBS-calibrated artifact, NBS-recommended measurement procedures, the photomask being routinely measured by industry; and conditions at NBS and in industry under which the measurements are

made. Linewidth-measurement data collected from this entire measurement process over an extended time would be analyzed to alert the users of a shift in their measurement process, to establish the limitations of this measurement method, and to define clearly the level at which various performance factors significantly affect the measurement uncertainty. Assuming that the appropriate realistic uncertainties are assigned to the linewidth artifacts and both the NBS and the user's measurement processes are in control, the linewidth measured at these different facilities would have overlapping uncertainty bands, i.e., closure between the measurement systems would exist.

This discussion is not meant to imply that the three methods mentioned here are independent of one another. The distinction is primarily one of the ways in which the measurement uncertainty is derived for the NBS-calibrated artifact or the NBS calibration service. For example, a MAP could also lead to the issuance of a linewidth SRM or to a linewidth-calibration service for a user-submitted photomask.

#### 8.4 NBS/IC-Industry Collaborative Test

For linewidth-measurements in the IC industry, many different procedures are used with several basic types of measurement systems. The possible combinations of these procedures, instruments, and in addition, operator conditions have given rise to a wide range of measurement uncertainties for linewidths. Based on the present study, certain procedures and instrument conditions have been developed that reduce the measurement uncertainties for linewidth measurements. Thus far, these results have been demonstrated only at NBS. (See sec. 7-2.)

A pilot collaborative test involving NBS and three participants from industry was undertaken to evaluate the linewidth-measurement procedures developed at NBS. In a full-scale collaborative test, there is a risk of wasting much effort if the test reveals differences among the results that can only be explained by shortcomings and ambiguities in the instructions for performing the measurements. Therefore, the initial effort was a relatively modest collaborative test.\* A larger test involving ten companies followed this pilot study.†

One AR-chromium artifact of the type described in section 4 was sent to each participant and was returned directly to NBS after the measurements by the participant. Prior to sending these artifacts to the participants, NBS measured certain linewidths by means of the photometric optical microscope described in section 6. In addition, NBS measured a line spacing on the artifact by means of the line-scale interferometer [45]. None of these measured values was supplied to the participant. Using instruments and procedures prescribed by NBS, each participant measured the

---

\* This test was completed prior to issuance of this report; results have been presented in several publications [53,54].

† This test was in progress at the time of issuance of this report.

same linewidths and line spacing that NBS measured. Some of these linewidths were labeled "control lines," and the participant made measurements on these lines before and after the measurements on the other specified lines.

The type of instruments, operating conditions, and data-acquisition procedures were defined in detail for the participants. Although these items are not described fully in the present report, it is worthwhile to mention some of their general characteristics. Equipment specifications included filtered illumination, specified range for numerical apertures of condenser and objective, and type of condenser illumination; operating conditions included alignment of artifact, criteria for best focus, same operator for all measurements, and only specified allowable changes in adjustment after initial setup; and data-acquisition procedures included following a prescribed measurement routine, entering data on forms supplied by NBS, and restarting the entire set of measurements if procedures were inadvertently not followed.

Participants furnished their data to NBS in the form of direct readings from their instruments. The participants were neither to modify their data in any way nor to try to make their data agree with any other measurements made previously on their instruments. These data were analyzed at NBS and the over-all results furnished to the participants. The results were not identified with a particular participant except to the extent that each participant was given his own results.

## 9. CONTINUING MICROMETROLOGY PROJECT

The results of the initial two-year effort in the NBS micrometrology project have been presented in this report. The micrometrology project is continuing, and in addition to the basic goals outlined in section 1, this project is addressing several other measurement needs of the IC community. The current effort includes: (1) developing theory and procedures for accurate linewidth measurements on see-through masks in transmitted light, (2) developing theory and procedures for accurate linewidth measurements on silicon wafers in reflected light, and (3) extending linewidth calibration into the submicrometer regime. In addition, project results are presented at technical meetings and in technical publications. Throughout the project, there continues a strong effort to interact directly with the IC community through visits to plant facilities, visits by industry personnel to NBS, and NBS participation in voluntary standards organizations.

### 9.1 Measurements on See-Through Masks and Silicon Wafers

The optical-microscope theory presented in this report is for the imaging of opaque lines on a clear background and clear lines on an opaque background in transmitted light. (See sec. 3.1.) In particular, this theory does not consider phase changes for light transmitted through objects or for light reflected from objects. For the AR-chromium artifacts measured in transmitted light, the opaque areas have, in fact, a finite transmittance of about two percent. However, the effects of a phase change in the transmitted light on the image profiles of lines have been considered to be relatively small for the artifacts measured. It is recognized that even though there is good agreement between the line-image profiles calculated from theory and those obtained experimentally from the artifact, the slight differences may be due to the phase changes in the light transmitted through the AR-chromium.

A type of photomask which has a relatively significant transmittance is a see-through iron-oxide photomask. An example of a mask-like, iron-oxide artifact with a visual transmittance of about 50 percent has been described in section 4.1. The visual transmittance of the coating varies depending on the type of material and the manufacturer, but these masks are all partially transparent. This transparency reduces the difficulty of registering multiple masks that are used to form successive patterns on a single wafer. The use of these see-through masks in the IC industry has increased significantly since the beginning of the current program. The IC industry has encountered large measurement uncertainties for linewidths measured on these masks and, therefore, has requested that NBS consider them in the linewidth-metrology program.

For viewing see-through masks in transmitted light, there is a significant change in the phase of light as it passes through the iron oxide. For viewing these masks in reflected light, there is a phase difference between the light reflected from the top and bottom surfaces of a step height on the iron oxide. The wavelength of the incident illumination

must be narrowly filtered for repeatable and accurate measurements with reflected light, as compared with transmitted-light measurements. This filtering of illumination leads to a relatively low signal-to-noise ratio for a photometric line-image profile, and therefore, linewidths on see-through masks should generally be measured in transmitted light.\*

Silicon wafers, on the other hand, must be viewed in reflected light. Measurements of linewidths and oxide windows on a wafer help to establish how well the circuit geometry has been transferred from the mask to the processed wafer. The surface of a processed wafer can be relatively complex in comparison with that of a mask; the materials on the wafer surface often have widely varying indices of refraction, and the surface topography exhibits step heights over a wide dimensional range. For reflected light on a wafer, there are phase changes from the reflection at the air/material interface and from the difference in heights of two adjacent surface areas.†

The optical theory is being modified to include phase changes for transmitted and reflected light. Based on the results of this more general theory, accurate estimates of the line-edge locations for see-through masks and wafers should be possible. Accurate measurements with an optical microscope may require modifications to the photometric optical microscope or alternative approaches. In the interim, an effort is underway to make some accurate linewidth measurements on these masks and wafers with the SEM/interferometer system. These measurements can eventually be compared with those from the optical microscope.

## 9.2 Submicrometer Linewidth Calibration

The IC industry continues to reduce the size of critical dimensions in order to increase both the circuit response time and the packing density. Currently, special devices with linewidths in the 0.5- to 1- $\mu\text{m}$  regime are being fabricated at the research level. Some IC manufacturers have produced a few circuits with geometries below 0.5  $\mu\text{m}$ .

One project objective is to calibrate linewidths in the 0.5- to 1- $\mu\text{m}$  regime with an uncertainty of  $\pm 0.01 \mu\text{m}$ . The measurement artifacts with submicrometer lines must meet tighter tolerances on geometry than the initial artifacts for the 1- to 10- $\mu\text{m}$  regime. Fabrication of the newer artifacts may require electron-beam or x-ray lithographic techniques and plasma etching or ion milling. The basic approach for the primary submicrometer-linewidth calibration is to use an interferometer in an electron-beam instrument which is manufactured with tighter tolerances than existing commercial SEMs. (See sec. 5-1.) With improvements, such as the use of an oil-immersion objective, a vibration-isolation table,

---

\* Additional information is given in reference [55] which was published prior to the issuance of this report.

† Additional information is given in reference [56] which was published prior to the issuance of this report.

and an improved translation stage, it should be possible to use the photometric optical microscope for the secondary calibration of these submicrometer linewidths.

## 10. REFERENCES

1. Horne, D. F., *Dividing, Ruling and Mask-Making*, Chapter 8 (Crane, Russak and Co., New York, N. Y., 1974).
2. Holyfield, S., Optical Comparators: A Look at Visual Inspection System, *Electron. Packag. Prod.* 16, No. 3, 54-61 (March 1976).
3. O'Callaghan, F. G., Automatic Mask Inspection System, *Technical News* 5, No. 1, 8-10 (Optical Group, Perkin-Elmer Corp., Wilton, Connecticut, July 1976).
4. Kasdan, H. L., and George, N., Linewidth Measurement by Diffraction Pattern Analysis, *Proc. Soc. Photo-Optical Instrumentation Engineers* 80, *Developments in Semiconductor Microlithography*, 54-63 (1976).
5. Jerke, J. M., *Semiconductor Measurement Technology: Optical and Dimensional-Measurement Problems with Photomasking in Microelectronics*, NBS Special Publication 400-20 (October 1975).
6. Swyt, D. A., NBS Program in Photomask Linewidth Measurements, *Solid State Technol.* 19, No. 4, 55-61 (April 1976).
7. Semiconductor Measurement Technology: Progress Report, October 1 to December 31, 1974, W. M. Bullis, Ed., NBS Special Publication 400-17, pp. 36-38 (November 1975).
8. Semiconductor Measurement Technology: Progress Report, January 1 to June 30, 1975, W. M. Bullis, Ed., NBS Special Publication 400-19, pp. 34-43 (April 1976).
9. Semiconductor Measurement Technology: Progress Report, January 1 to June 30, 1976, W. M. Bullis, Ed., NBS Special Publication 400-29, pp. 48-56 (March 1977).
10. Jerke, J. M., Hartman, A. W., Nyssonen, D., Rosberry, F. W., Swing, R. E., Swyt, D. A., and Young, R. D., Accurate Linewidth Measurements at the National Bureau of Standards, *Proc. Microelectronics Seminar INTERFACE '76*, Monterey, California, October 3-5, 1976, pp. 51-59 (Eastman Kodak Co., Rochester, New York), publication G-47.
11. Young, R. D., Length Calibrations in the Micrometer and Sub-Micrometer Range, *Annals of the CIRP* 25, 245-250 (1977).
12. Considine, P. S., Effects of Coherence on Imaging Systems, *J. Opt. Soc. Am.* 56, 1001-1009 (August 1966).
13. Weinstein, W., Images of Incoherently Illuminated Bright and Opaque Disks, *J. Opt. Soc. Am.* 45, 1006-1008 (December 1955).
14. Slater, P. N., Measurement of Submicron Circular Apertures by Scanning Microscopy, *J. Opt. Soc. Am.* 49, 562-567 (June 1959).

15. Osterberg, H., and Smith, L. W., Diffraction Theory for Images of Disk-Shaped Particles with Kohler Illumination, *J. Opt. Soc. Am.* 50, 362-369 (April 1960).
16. Smith, L. W., Diffraction Images of Disk-Shaped Particles Computed for Full Kohler Illumination, *J. Opt. Soc. Am.* 50, 369-374 (April 1960).
17. De, M., and Som, S. C., Diffraction Images of Circular Openings with Partially Coherent Illumination, *Opt. Acta* 9, 17-31 (January 1962).
18. Welford, W. T., Length Measurements at the Optical Resolution Limit by Scanning Microcopy, *Optics in Metrology*, P. Mollet, Ed., pp. 85-90 (Pergamon Press Inc., Elmsford, N.Y., 1960).
19. Barakat, R., Partially Coherent Imagery in the Presence of Aberrations, *Opt. Acta.* 17, 337-347 (May 1970).
20. Martin, L. C., *The Theory of the Microscope*, pp. 422-428 (Blackie and Son, Ltd., London, 1966).
21. Grimes, D. N., Imaging of Tri-Bar Targets and the Theoretical Resolution Limit in Partially Coherent Illumination, *J. Opt. Soc. Am.* 61, 870-876 (July 1971).
22. Rowe, S. H., Light Distribution in the Defocussed Image of a Coherently Illuminated Edge, *J. Opt. Soc. Am.* 59, 711-714 (June 1969).
23. Hopkins, H. H., Applications of Coherence Theory in Microscopy and Interferometry, *J. Opt. Soc. Am.* 47, 508-526 (June 1957).
24. Kinzly, R. E., Partially Coherent Imaging in Microdensitometer, *J. Opt. Soc. Am.* 62, 386-394 (March 1972).
25. Charman, W. N., Diffraction Images of Circular Objects in High-Resolution Microscopy, *J. Opt. Soc. Am.* 53, 415-419 (April 1963).
26. Richards, B., and Wolf, E., Electromagnetic Diffraction in Optical Systems II, Structure of the Image Field in an Aplanatic System, *Proc. Roy. Soc.* A253, 358-379 (December 1959).
27. Goodman, J. W., *Introduction to Fourier Optics*, p. 127 (McGraw-Hill Book Co., N.Y., 1968).
28. Reference [18], pp. 322-323.
29. Born, M., and Wolf, E., *Principles of Optics*, Fifth edition, pp. 522-526 (Pergamon Press Inc., Elmsford, N.Y., 1975).
30. Swing, R. E., Conditions for Microdensitometer Linearity, *J. Opt. Soc. Am.* 62, 199-207 (February 1972).

31. Swing, R. R., The Case for the Pupil Function, *Proc. Soc. Photo-Optical Instrumentation Engineers* 46, *Image Assessment and Specification*, 104-113 (1974).
32. Swing, R. E., The Theoretical Basis of a New Optical Method for the Accurate Measurement of Small Line-Widths, *Proc. Soc. Photo-Optical Instrumentation Engineers* 80, *Developments in Semiconductor Microlithography*, 65-77 (1976).
33. *The International System of Units (SI)*, C. H. Page and P. Vigoureux, Eds., NBS Special Publication 333, 1972 Edition, 45 pages (April 1972).
34. Swyt, D. A., Design of a Pattern on a Photomask-Like Physical Standard for Evaluation and Calibration of Linewidth-Measuring Systems, *Solid-State Technol.* 21, 35-42 (January 1978).
35. Nyssonen, D., Optical Linewidth Measurements on Silicon and Iron-Oxide Photomasks, *Proc. Soc. Photo-Optical Instrumentation Engineers* 100, *Developments in Semiconductor Microlithography II*, 127-134 (1977).
36. Scire, F. E., and Teague, E. C., Piezodriven 50- $\mu$ m Range Stage with Subnanometer Resolution, *Rev. Sci. Instrum.* 49, 1735-1740 (December 1978).
37. Oatley, C. W., *The Scanning Electron Microscope. Part 1 - The Instrument*, pp. 156-161 (Cambridge University Press, London, 1972).
38. Young, R. D., Surface Microtopography, *Phys. Today* 25, No. 11, 42-49 (November 1971).
39. Bennett, S. J., A Double-Passed Michelson Interferometer, *Opt. Commun.* 4, No. 6, 428-430 (February/March 1972).
40. Reference [29], pp. 395-398.
41. Nyssonen, D., Linewidth Measurement with an Optical Microscope: Effect of Operating Conditions on the Image Profile, *Appl. Opt.* 16, 2223-2230 (August 1977).
42. Layer, H. P., High-Resolution Stepping Motor Drive, *Rev. Sci. Instrum.* 47, No. 4, 480-483 (April 1976).
43. Briers, J. D., Interferometric Testing of Optical Systems and Components: A Review, *Opt. Laser Technol.* 4, 28-41 (February 1972).
44. Nyssonen, D., and Jerke, J. M., Lens Testing with a Simple Wavefront Shearing Interferometer, *Appl. Opt.* 12, No. 9, 2061-2070 (September 1973).

45. Cook, H. D., and Marzetta, L. A., An Automatic Fringe-Counting Interferometer for Use in the Calibration of Line Scales, *J. Res. Nat. Bur. Stand. (U.S.)* 65C, No. 2, 129-139 (1961).
46. Mandel, J., Repeatability and Reproducibility, *Mater. Res. Stand.* 11, No. 8, 8-15, 52 (August 1971).
47. Swyt, D. A., and Rosberry, F. W., A Comparison of Some Optical Microscope Measurements of Photomask Linewidths, *Solid State Technol.* 20, 70-75 (August 1977).
48. Jerke, J. M., Hartman, A. W., Nyyssonen, D., Swing, R. E., Young, R. D., and Keery, W. J., Comparison of Linewidth Measurements on an SEM/Interferometer System and an Optical Linewidth Measuring Microscope, *Proc. Soc. Photo-Optical Instrumentation Engineers* 100, *Developments in Semiconductor Microlithography*, 37-45 (1977).
49. *Catalog of NBS Standard Reference Materials*, R. W. Seward, Ed., NBS Special Publication 260, 1979-80 Edition, 102 pages (April 1979).
50. *Calibration and Related Measurement Services of the National Bureau of Standards*, NBS Special Publication 250, 1978 Edition (April 1978).
51. Cameron, J. M., Measurement Assurance, *J. Qual. Technol.* 8, No. 1, 53-55 (January 1976).
52. Pontius, P. E., *Measurement Assurance Program - A Case Study: Length Measurements. Part 1. Long Gage Blocks (5 in to 20 in)*, Nat. Bur. Stand. (U.S.), Monogr. 149, 75 pages (November 1975).
53. Swyt, D. A., Rosberry, F. W., and Nyyssonen, D., Calibration of Optical Microscopes for Photomask Linewidth Measurements, *Proc. Microelectronics Seminar INTERFACE '77*, pp. 131-144 (Eastman Kodak Co., Rochester, N.Y., 1978).
54. Swyt, D. A., Rosberry, F. W., and Nyyssonen, D., Photomask Linewidth Measurement, *Circuits Manufacturing* 18, 20-26 (September 1978).
55. Nyyssonen, D., Optical Linewidth Measurements on Silicon and Iron-Oxide Photomasks, *Proc. Soc. Photo-Optical Instrumentation Engineers* 100, *Developments in Semiconductor Microlithography II*, 127-134 (1977).
56. Nyyssonen, D., Optical Linewidth Measurements on Wafers, *Proc. Soc. Photo-Optical Instrumentation Engineers* 135, *Developments in Semiconductor Microlithography III*, 115-119 (1978).

THE THEORETICAL BASIS OF A NEW OPTICAL METHOD FOR  
THE ACCURATE MEASUREMENT OF SMALL LINE-WIDTHS\*

Richard E. Swing  
National Bureau of Standards  
Washington, D. C. 20234

Abstract

As part of the effort conducted at NBS to solve some of the fundamental problems associated with width measurement of very small ( $1\text{-}5\text{-}\mu\text{m}$ ) lines and spaces, the performance of an optical microscope with coherent illumination is investigated. From these studies, the theoretical basis for a new method of accurate width measurements is developed and explored. The new method, in effect, produces an optical transformation in which the image no longer resembles the original line but in which the location of the line-edges is marked by two narrow, dark lines within a bright surround. The correct line-width is then given by the distance between these two lines, a measurement that eliminates the orientation problems normally associated with filar eyepieces and sidesteps the coherence problem that affects shearing eyepieces. Suggestions are made about implementing the technique. Available microscope objectives are not suitable for such a system, and a re-design is recommended.

Introduction

Problem of Line-Width Measurement

An outstanding unsolved dimensional measurement problem is the accurate measurement of small ( $1\text{-}5\text{-}\mu\text{m}$ ) line and space widths. Current methods employ the optical microscope, generally at the limit of its resolution. Since the illumination of these lines cannot be

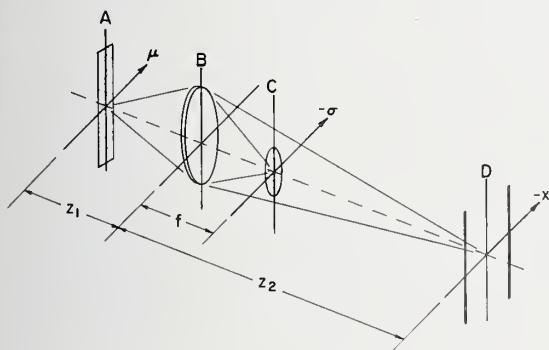


Fig. 1. Sketch of the single-lens coherent optical system, showing the locations of the planes and coordinate system. A: object plane, with an opaque line shown as the object; B: plane of lens; C: plane of object spectrum, located one focal length from the B-plane, showing an opaque obstacle inserted at the center of the field; D: image plane, with an idealized filtered image shown.

completely incoherent, the image formed by the microscope is not a true representation of the object; i.e., measurements on the image are rendered inaccurate because of the partial coherence in the illumination and the size limitations dictated by physical

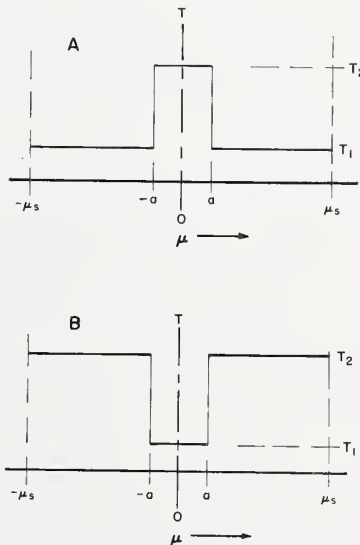


Fig. 2. Sketch of a line-object cross-section. A: clear line, dark background; B: dark line, clear background. The width of the object aperture is  $2\mu_s$ , the lines are  $2a$  units wide. The ordinate is transmittance.

\*Contribution of the National Bureau of Standards. Not subject to copyright. The program is part of a larger Program on the Advancement of Reliability, Processing, and Automation for Integrated Circuits sponsored by the Advance Research Projects Agency through the NBS Electronic Technology Division with funding provided jointly by NBS and ARPA (Order No. 2397).

optics (1,2,3).

The most commonly-used measurement apparatus utilized with the microscope are the filar and shearing eyepieces. The latter requires incoherent illumination for an accurate judgement of shear<sup>(4)</sup> whereas the former involves two judgments of hairline position, one of which is the inverse of the other; i.e., the measuring reticle moves from the left-hand to the right-hand edge (or *vice versa*) and does not "see" the same thing on both sides. Measurements of the same line with these two eyepieces are rarely in agreement<sup>(5)</sup> and it is common practice for an institution to accept the inherent inaccuracy of one to the exclusion of the other, in the interests of in-house reproducibility.

Line-edge location, even assuming a perfect rectangular cross-section imaged by a diffraction-limited system is difficult to specify without knowledge of the illumination partial coherence. For incoherent illumination with the object well-resolved by the optics, the half-power point corresponds to the edge-position; with coherent illumination and the same resolution conditions, the edges are found at the quarter-power point. For intermediate states of partial coherence and/or marginally-resolved lines the correct measurement locus falls somewhere between. Unless the state of partial coherence is correctly known, the line-edge locations cannot be stated without a large uncertainty<sup>(6,7)</sup>. Non-rectangularity and non-symmetry of the line cross-section compounds this problem.

In seeking a solution to this measurement problem, some needs predominate. We need to provide a means to image this line so that the edges are sufficiently defined (in the optical sense) for measurement of its width. Since the filar and shearing eyepieces are accurate measurement devices, we would like to retain their use, but must eliminate the problem of orientation of hairline placement with the former and the image ambiguity of the latter when used in partially coherent illumination.

At the same time, we would like to tamper as little as possible with the basic microscope system, since it is a familiar instrument, its operation is comparatively simple and it exists in large numbers in industry (and would be expensive to replace or extensively modify). Further, we would like to minimize or compensate systematic errors introduced by any new configuration, make the system independent of the partial coherence of the illumination and retain the real-time measurement aspects of present systems.

These goals severely restrict the domain of investigation, but serve to delineate the necessary approaches. A more detailed discussion of the line-width measurement problem as it applies to the microelectronics industry, as well as the program undertaken at NBS to solve it, is given by Swyt<sup>(5)</sup>.

#### An Approach Through Coherent Illumination

The employment of systems using coherent illumination is well-summarized in Ref. 7. Generally, they exhibit non-linear response because of the sharp frequency cutoff at the lens aperture; this is manifested by "ringing" at points in the image corresponding to sharp edges of the object, a fine example of which is shown in Ref. 6, Fig. 2. Such an image is a poor source for accurate measurements because of this. For measurements on an image that *resembles* the object, the illumination ought properly to be incoherent.

However, one of the properties of coherent optical systems is the capability for spatial filtering. This allows the user to modify the frequency content of the image so that certain aspects of the image can be enhanced, suppressed or even drastically changed. Thus, with suitable filtering, it might be possible to concentrate on the measurement aspects of lines and spaces while disregarding the linearity of their image formation.

Such techniques are certainly not new. Investigators in France in the 1950's and 1960's<sup>(8,9,10)</sup> applied the technique to a wide class of problems. O'Neill followed their work in this country and was especially successful in filtering periodic signals from noisy backgrounds<sup>(11)</sup>. The technique proposed in this paper is similar to one reported by O'Neill for raising the contrast of an image. In applying filtering methods to an optical system suggested by Suzuki, *et al*<sup>(12)</sup>, Mueller stored and retrieved multiple images on the same photographic plate<sup>(13)</sup>. Subsequently, he was able to recreate color imagery, with essentially the same optical system, from black-and-white, single-exposure photography<sup>(14)</sup>. Recently, Considine varied the partial coherence of the illumination to exploit the information inherent in the relief image of the photographic emulsion<sup>(15)</sup>. Thus, the use of spatial filtering with coherent illumination appears to be adaptable to a wide variety of problems, and the technique to be presented in this paper widens the field further.

#### The Proposed Measurement Technique

The detailed analysis of the technique will follow shortly, but will be summarized here to outline the major considerations. The microscope will employ a single-lens coherent system (discussed and analyzed in Appendix A). Fig. 1 illustrates this. An opaque line

in a clear background (for illustration) is the object (A). When it is illuminated coherently, its spectrum is imaged in a plane one focal length behind the lens (C). An opaque obstacle inserted in the plane prevents a selected portion of the spectrum from passing through the system to form the image at the conjugate distance,  $z_2$ , in the plane (D). When the obstacle is the correct size, the image that is produced consists (essentially) of two very thin, dark lines that correspond to the location of the two line-edges. Fig. 1 shows this pair, spaced to exhibit the system magnification. Measurement of the distance between these two lines by either filar or shearing eyepieces determines the line-width. This measurement eliminates the orientation problem associated with the filar eyepiece and sidesteps the coherence problem that affects the shearing eyepiece.

While this is essentially a theoretical investigation, the ideas developed will be applied to a suggested implementation of the ideas and conclusions. Some of the practical problems that will be encountered will be discussed, and some areas for further investigation will be outlined.

## Analysis

### General Considerations

In a microscope, the objective lens forms a real image at a fixed distance from its rear mounting shoulder. This distance is called the "tube length," and has been standardized at 160 mm (more or less). An ocular is added to form a virtual image at an apparent magnification given by the product of the separate magnifications of both elements. These two are designed to be used together, but in an elementary sense the ocular adds only magnification to the system; the significant imagery is carried out by the objective. We will therefore eliminate the ocular from subsequent consideration, and reduce the optical system under investigation to an objective lens working at finite conjugates.

The system will be analyzed as a single-lens coherent system (see Appendix A), employing coherent illumination at a wavelength  $\lambda$ . We will assume paraxial and sagittal approximations<sup>(16)</sup>, and the impulse response will be taken to be constant over the region of interest (assumption of stationarity<sup>(17)</sup>). The analysis will be scalar. While the performance of microscope objectives at high numerical apertures cannot be rigorously so characterized, the simplification it provides will permit a clear look at the underlying physics. The analysis will be one-dimensional, and unless otherwise noted, all integrals are to be evaluated between infinite limits.

The optical system to be studied is sketched in Fig. 1. The lens is assumed to be thin, diffraction-limited and in correct focus, with object and image distances related by the thin-lens equation<sup>(18)</sup>.  $z_1$  and  $z_2$  are object and image distances, respectively. We will calculate the effect on the image at  $z_2$  of the opaque obstacle placed in the system at a distance,  $f$ , from the lens, in image space.

In Appendix A, it is shown that the Fourier transform of the object field is located a distance,  $f$ , in the rear of the lens. This is the complex object spectrum and its calculation is the first step in the analysis of system performance. We will use a line in two manifestations as the object: 1) a clear line on a dark background, and 2) a dark line on a clear background. The cross-section will be rectangular, the width uniformly  $2a$ . It will be placed in a aperture  $2\mu_s$  units wide. Details of these objects are shown in Fig. 2.

The complex image spectrum,  $\tilde{f}_1(\sigma)$ , for the lines of Fig. 2 is given by the Fourier transform of the object field. After integration, application of limits and normalization, we will have

$$\tilde{f}_1(\sigma) = \sqrt{T_1} \operatorname{sinc}(2\pi\sigma\mu_s) + (\sqrt{T_2} - \sqrt{T_1}) \operatorname{sinc}(2\pi\sigma a), \quad (1)$$

for the clear line, dark background, and

$$\tilde{f}_2(\sigma) = \sqrt{T_2} \operatorname{sinc}(2\pi\sigma\mu_s) - (\sqrt{T_2} - \sqrt{T_1}) \operatorname{sinc}(2\pi\sigma a), \quad (2)$$

for the dark line, clear background, where  $\sin(x)/(x)$  is defined as  $\operatorname{sinc}(x)$ , and the remaining symbols are defined in Fig. 2.

### The Spatial Filter

The physical makeup of the microscope in the  $\sigma$ -plane determines the frequency content of the image. The outer aperture of the system determines the spatial frequency limit of this plane; the origin of the  $\sigma$ -plane is equivalent to optical "dc" and spatial frequency increases outward to the aperture limit, linearly. A clear aperture therefore acts as a low-pass filter, passing without attenuation all frequencies below its upper cutoff, but truncating all those above.

Let us specify a filter known as "band-pass." This has the normal lens cutoff at the upper limit, but will also have a lower cutoff centered about the origin. It is accomplished by inserting an opaque obstacle of width  $2\sigma_1$  in the center of the  $\sigma$ -plane. A

sketch of the transmittance of such a filter is shown in Fig. 3. For the present, we assume this filter is centered perfectly in the  $\sigma$ -coordinate system.

### The Filtered Image

The filtered image field is given by the Fourier transform of the product of the image spectrum (either Eq. (1) or (2)) and the spatial filter of Fig. 3. We will first treat the clear line on a dark background, so that

$$f(x) = \int_{-\sigma_2}^{\sigma_2} \tilde{f}_1(\sigma) \exp(-2\pi i \sigma x/m) d\sigma$$

$$- \int_{-\sigma_1}^{\sigma_1} \tilde{f}_1(\sigma) \exp(-2\pi i \sigma x/m) d\sigma$$

$$= \sqrt{T_1} \int_{-\sigma_2}^{\sigma_2} \text{sinc}(2\pi \sigma \mu_s) \exp(-2\pi i \sigma x/m) d\sigma$$

$$+ (\sqrt{T_2} - \sqrt{T_1}) \int_{-\sigma_2}^{\sigma_2} \text{sinc}(2\pi \sigma a) \exp(-2\pi i \sigma x/m) d\sigma$$

$$- \sqrt{T_1} \int_{-\sigma_1}^{\sigma_1} \text{sinc}(2\pi \sigma \mu_s) \exp(-2\pi i \sigma x/m) d\sigma$$

$$- (\sqrt{T_2} - \sqrt{T_1}) \int_{-\sigma_1}^{\sigma_1} \text{sinc}(2\pi \sigma a) \exp(-2\pi i \sigma x/m) d\sigma,$$

(3)

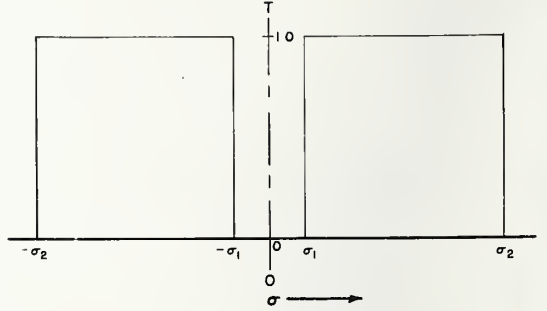


Fig. 3. Sketch of the transmittance of the spatial filter to be located in the plane one focal length to the rear of the lens, in image space. Upper and lower cutoff frequencies are  $\sigma_2$  and  $\sigma_1$ , respectively; units are cycles/mm.

where the transform kernels are specified in Appendix A, and  $m$  is the magnification. After a lengthy evaluation and normalization, it can be shown that the observable image luminance (given by the squared modulus of Eq. (3)) is<sup>(19)</sup>

$$I(x) = |f(x)|^2$$

$$= (1/\pi^2) \left[ \sqrt{T_1} \left\{ S_i [2\pi \mu_s \sigma_2 (1 + x/m\mu_s)] + S_i [2\pi \mu_s \sigma_2 (1 - x/m\mu_s)] \right\} \right.$$

$$+ (\sqrt{T_2} - \sqrt{T_1}) \left\{ S_i [2\pi a \sigma_2 (1 + x/ma)] + S_i [2\pi a \sigma_2 (1 - x/ma)] \right\}$$

$$- \sqrt{T_1} \left\{ S_i [2\pi \mu_s \sigma_1 (1 + x/m\mu_s)] + S_i [2\pi \mu_s \sigma_1 (1 - x/m\mu_s)] \right\}$$

$$\left. - (\sqrt{T_2} - \sqrt{T_1}) \left\{ S_i [2\pi a \sigma_1 (1 + x/ma)] + S_i [2\pi a \sigma_1 (1 - x/ma)] \right\} \right]^2. \quad (4)$$

If we normalize the distribution to the object-edge, so that

$$\xi = x/ma, \quad (5)$$

and restrict the domain of the equation to the vicinity of the line-image (by eliminating terms that describe the imaging of the object aperture), we will have the observable, filtered line image

$$I(\xi) = (1/\pi^2) (\sqrt{T_2} - \sqrt{T_1})^2 \left\{ S_i [2\pi a \sigma_2 (\xi + 1)] - S_i [2\pi a \sigma_2 (\xi - 1)] \right.$$

$$\left. - S_i [2\pi a \sigma_1 (\xi + 1)] + S_i [2\pi a \sigma_1 (\xi - 1)] + \left[ \sqrt{T_1} / (\sqrt{T_2} - \sqrt{T_1}) \right] \left[ \pi - 2S_i (2\pi \mu_s \sigma_1) \right] \right\}^2. \quad (6)$$

When we consider a clear line in an opaque background,  $T_1 = 0$  and  $T_2 = 1$ . The filtered image for those transmittance conditions, and the one we will subsequently study in this analysis, is then given by Eq. (7) for the cited transmittances:

$$I(\xi) = (1/\pi^2) \left\{ S_i [2\pi a \sigma_2 (\xi + 1)] - S_i [2\pi a \sigma_2 (\xi - 1)] - S_i [2\pi a \sigma_1 (\xi + 1)] + S_i [2\pi a \sigma_1 (\xi - 1)] \right\}^2. \quad (7)$$

If we follow the same form of analysis for the second line-type, we can show that for the image of the dark line on the clear background,

$$I(\xi) = (1/\pi^2) \left( \sqrt{T_2} - \sqrt{T_1} \right)^2 \left\{ \left[ \sqrt{T_2} / \left( \sqrt{T_2} - \sqrt{T_1} \right) \right] \left[ \pi - 2S_i(2\pi \mu_s \sigma_1) \right] - S_i [2\pi a \sigma_2 (\xi + 1)] + S_i [2\pi a \sigma_2 (\xi - 1)] + S_i [2\pi a \sigma_1 (\xi + 1)] - S_i [2\pi a \sigma_1 (\xi - 1)] \right\}^2, \quad (8)$$

and when we let  $T_1 = 0$  and  $T_2 = 1$ , as before, and require the object aperture to be large enough so that  $S_i(2\pi \mu_s \sigma_1)$  passes to its limiting value of  $\pi/2$ , Eq. (8) will reduce to Eq. (7), exactly. We thus have the important result that *when we use an occluding band-pass filter, the images of clear and opaque small lines are identical*. This result is very useful since we need only consider one filtered line-image for both cases, and engineering applications of this technique need not differentiate between the two.

#### Line-Edge Location: The Optimum Filter

Let us now investigate one of the properties of the image in Eq. (7). Since we have normalized the image in terms of the line-edges, the value of image luminance there will be given by  $I(\xi)$  for  $\xi = \pm 1$ . Thus, at the right-hand line-edge (where  $\xi$  is positive),

$$I(1) = (1/\pi^2) \left[ S_i(4\pi a \sigma_2) - S_i(4\pi a \sigma_1) \right]^2. \quad (9)$$

If we now demand that the luminance drop to a value of zero at the exact location of the line-edge, it is clearly necessary that

$$S_i(4\pi a \sigma_2) = S_i(4\pi a \sigma_1). \quad (10)$$

The obvious approach of taking the inverse of both sides of the equation and solving for  $\sigma_1$  leads to an invalid result (upper and lower cutoffs are equal). Since the Inverse Sine Integral is multiple-valued, we must specify the region of tabulation that must be used so that the solution of Eq. (10) gives a meaningful result. From physical considerations, the less energy occluded, the more there will be available for observation in the image. Thus, to obtain the smallest  $\sigma_1$  we will stipulate that the *lowest possible value* of the Inverse Sine Integral must be taken (i.e., values between 0 and  $\pi$ ), and denote this by a small superscripted zero on the inverse symbol. Thus,

$$\sigma_1 = \left\{ 1 / [(2\pi)(2a)] \right\}^0 S_i^{-1} \left\{ S_i [ (2\pi)(2a \sigma_2) ] \right\}. \quad (11)$$

and we have defined the lower cutoff value in terms of the line-width ( $2a$ ) and upper cutoff frequency ( $\sigma_2$ ). This pairing of upper and lower cutoffs is the *optimum filter*, since it relates  $\sigma_1$  and  $\sigma_2$  for a specific line width,  $2a$ .

To examine imagery with this system and illustrate the filtering effects, we can calculate representative examples. Table I lists three microscope objectives and their parameters and equivalent frequency values. Table II lists the optimum filters for several lenses and line-widths of interest. The lower cutoff is determined from Eq. (11), while the upper cutoff value is determined from

$$\sigma_2 = (NA)/\lambda, \quad (12)$$

which is the diffraction-limit as defined by the numerical aperture (NA). Figures 4, 5 and 6 contain plots of images calculated for 5, 2 and 1- $\mu$ m lines, respectively, with different numerical apertures. These figures show A) the line object, B) the line imaged with coherent illumination at full aperture and C) the line-image after optimum-filtering. Comparison of the plots in each figure clearly shows that while the coherent image is an extremely poor representation of the original line, the filtered version converts the essential width information into two dark lines in a bright surround; measurement of the distance between them is essentially identical to the measurement of periodicity, and this

TABLE I: Some Microscope Objective Parameters  
( $\lambda = 500 \text{ nm.}$ )

Numerical Aperture	Typical Focal Length (mm)	$\sigma_2$ (cycles/mm)
.50	8	1000
.65	4	1300
.95	4	1900

TABLE II: Optimum Filter Parameters ( $\lambda = 500 \text{ nm.}$ )

Numerical Aperture	$\sigma_2$ (cycles/mm)	Values of $\sigma_1$ (cycles/mm)		
		Line-Widths ( $\mu\text{m}$ )		
		1	2	5
.50	1000	262.2	141.2	59.3
.65	1300	314.5	162.1	63.0
.95	1900	287.1	151.5	62.4

is an established art. The orientation problem of filar eyepieces no longer is present.

The sequence of Figures 6, 7 and 8 show three lines (1, 2 and 5- $\mu\text{m}$ ) with the same numerical aperture, for the appropriate optimum filters. The improvement in measurement with use of the filtered image is clear for all three cases.

#### Measurement with Non-Optimum Filters

Since line-width and cutoff frequencies always occur as multiples, the optimum filter is always determined by the line-width it is desired to measure. Since, in a real situation, we will not know the exact line-width, *a priori*, we will generally be observing an image modified by a non-optimum filter. We therefore must devise a means for compensating errors produced in measuring such images.

We can show (by calculation of the distribution of Eq. (7)) that when a line is imaged with a filter optimum for a different width, two zeroes do, in fact, occur. If the measurement is made between two zero positions, the result will be in error by a small amount, since the zeroes have shifted from their nominal positions at  $\pm I(1)$ .

When we hold everything else fixed and allow the line-width to change by an amount  $2\delta$ , we will have for the image luminance

$$I(\xi) = (1/\pi^2) \left\{ S_i \left[ \pi\sigma_2(2a + 2\delta)(\xi + 1) \right] - S_i \left[ \pi\sigma_2(2a + 2\delta)(\xi - 1) \right] - S_i \left[ \pi\sigma_1(2a + 2\delta)(\xi + 1) \right] + S_i \left[ \pi\sigma_1(2a + 2\delta)(\xi - 1) \right] \right\}^2 \quad (13)$$

When we now observe the distribution, we will find that the line-edge zeroes occur at  $\pm \xi_0$ . Thus when the new zero locations are determined for a given set of upper and lower cutoff values (optimum for  $2a$ ), we can ask for the value of  $(2a + 2\delta)$  that makes  $I(\xi_0)$  go to zero, and then solve the equation

$$S_i \left[ \pi\sigma_2(2a + 2\delta)(\xi_0 + 1) \right] - S_i \left[ \pi\sigma_2(2a + 2\delta)(\xi_0 - 1) \right] - S_i \left[ \pi\sigma_1(2a + 2\delta)(\xi_0 + 1) \right] + S_i \left[ \pi\sigma_1(2a + 2\delta)(\xi_0 - 1) \right] = 0 \quad (14)$$

for  $2\delta$ . Thus we can determine the correction to the nominal line-width,  $2a$ , since  $\xi_0$ ,  $\sigma_1$  and  $\sigma_2$  are experimentally measured. Since we know this equation describes the variation of the image field about the zeroes, it should undergo a sign change in the region of interest, and the solution can easily be implemented through digital computation.

#### Analytical Experiments

##### Non-Optimum Filters

To assess the ability to correct routine measurements with non-optimum filters, we will carry out "measurements" on two sets of lines. One will be in the 5- $\mu\text{m}$  width range (and is therefore well-resolved by the optics), while the other will center about 2- $\mu\text{m}$  (and therefore be marginally resolved). If we consider a set of filters that deviate from the nominal value by -20%, -5%, +10% and +20%, we will require four filters optimum for 4.0, 4.75, 5.5 and 6.0- $\mu\text{m}$  for the 5- $\mu\text{m}$  range, and 1.6, 1.8, 2.1 and 2.4- $\mu\text{m}$  for the 2- $\mu\text{m}$  range. The two sets of optimum filters are listed in Tables III and IV for the optics of Table I. The lower cutoff frequencies are specified to three decimal places. This is well beyond any normal fabrication capability, but will enable us to eliminate errors due to computational roundoffs. No other errors are assumed in the "measurement" process.

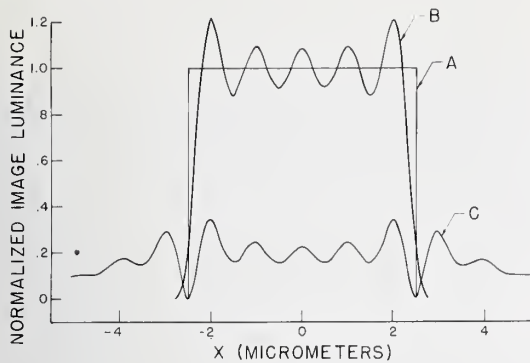


Fig. 4. Calculated images of a 5- $\mu$ m clear line in an opaque background for coherent illumination at 500 nm, using a 0.50 numerical aperture lens; A: object line; B: image without filtering; C: (optimum) filtered image (See Table II).

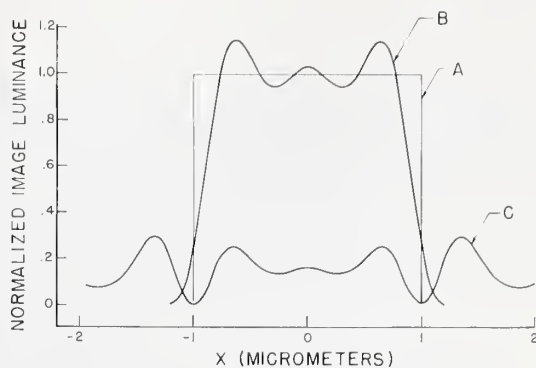


Fig. 5. Calculated images of a 2- $\mu$ m clear line in an opaque background for coherent illumination at 500 nm, using a 0.65 numerical aperture lens; A: object line; B: image without filtering; C: (optimum) filtered image (See Table II).

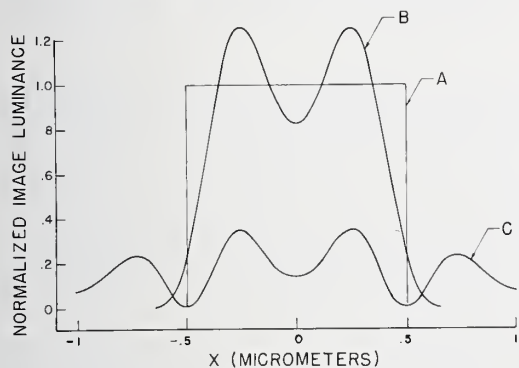


Fig. 6. Calculated images of a 1- $\mu$ m clear line in an opaque background for coherent illumination at 500 nm, using a 0.95 numerical aperture lens; A: object line; B: image without filtering; C: (optimum) filtered image (See Table II).

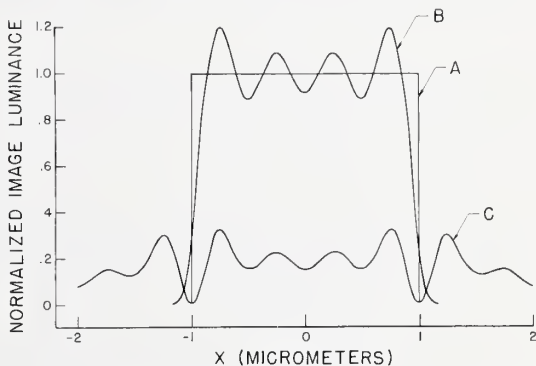


Fig. 7. Calculated images of a 2- $\mu$ m clear line in an opaque background for coherent illumination at 500 nm, using a 0.95 numerical aperture lens; A: object line; B: image without filtering; C: (optimum) filtered image (See Table II).

For each of these filter ranges we will choose three line-widths, none of them paired with the filters already selected: 4.6, 5.0 and 5.75- $\mu$ m for use with Table III and 1.7, 2.0, and 2.3- $\mu$ m for use with Table IV. Because we know these dimensions in advance, we will be able to calculate relative errors.

The general technique for the experiment is as follows:

- 1) Determine the image distribution in the vicinity of the line-edge zero for each filter, with each line (within the two sets);
- 2) Determine the position of the line-edge zero; calculate the relative error of the uncorrected line-width based on the measurement;
- 3) Determine the corrected line-width (by solving Eq. (14)) and calculate

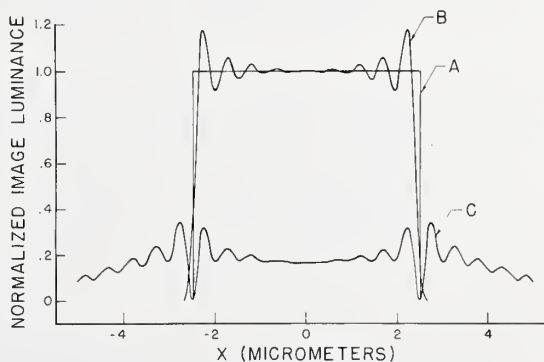


Fig. 8. Calculated images of a 5- $\mu$ m clear line in an opaque background for coherent illumination at 500 nm, using a 0.95 numerical aperture lens; A: object line; B: image without filtering; C: (optimum) filtered image (See Table II).

the relative error of the result.

For the tests, we will also vary numerical aperture, using 0.50, 0.65 and 0.95, three of the most commonly-employed microscope objectives. 72 separate sets of calculations are required and are best presented in tabular form. Tables V and VI are two such summaries, and show values of "measured" width accompanied by the relative error (in percent) in parentheses. Rather than exhibit the remainder of the tables, we will summarize the essential results briefly.

TABLE III: Optimum Filters for Four Line-Widths ( $\lambda = 500 \text{ nm.}$ )

Numerical Aperture	$\sigma_2$ (cycles/mm)	Values of $\sigma_1$ (cycles/mm)			
		Line-Widths ( $\mu\text{m}$ )			
		4.00	4.75	5.50	6.00
.50	1000	73.518	64.626	57.513	49.690
.65	1300	75.815	63.712	54.955	50.781
.95	1900	78.079	63.365	56.614	51.716

TABLE IV: Optimum Filters for Four Line-Widths ( $\lambda = 500 \text{ nm.}$ )

Numerical Aperture	$\sigma_2$ (cycles/mm)	Values of $\sigma_1$ (cycles/mm)			
		Line-Widths ( $\mu\text{m}$ )			
		1.60	1.80	2.10	2.40
.50	1000	210.517	166.802	136.567	135.014
.65	1300	178.304	176.395	147.665	122.646
.95	1900	181.627	177.809	140.046	132.369

1) For all lines and filters, the zeroes can be quickly established and the widths measured. The largest errors are found when the test line-widths are smallest and the optimum filter widths are largest; e.g., the 4.6- $\mu\text{m}$  line with the 6.0- $\mu\text{m}$  optimum filter. The opposite case, when the test lines are largest and the filter-widths the smallest, does not produce nearly as large an error. The size of these relative errors is generally a function of numerical aperture, and tends to diminish with increasing numerical aperture. The magnitudes of these errors vary, being smallest (less than 1%) when within 10% of the nominal value for the range, and growing to about 6%, in some instances, when calculated at the +20% limit. It is clear that the closer the filter-width is to the test line-width the less the relative error, considering those "measurements" that are not corrected by application of Eq. (14).

2) The corrected measurements appear to be independent of numerical aperture. The ability to apply corrections through Eq. (14) is generally very good, and the error for those "measurements" that could be corrected is vanishingly small (0.01% or less). In a few instances, no sign change in the domain of calculation is observed for Eq. (14). This seems to stem from a disparity in the arguments in the region of the zero-crossing, so that the point of interest has either not been reached or has been passed by, or because the function is tangent to the axis. In other instances, unreasonable *a priori* knowledge of the test line-width is necessary to make the judgment of the correct zero from several in the region of calculation. These difficulties most often arise for the smallest line-widths and the lower numerical apertures, and it may result from the marginal resolution of the lines in question. In a practical microscope system, the microscopist would change his filter and try to remove the ambiguity.

3) In all cases where the optimum filter is paired with its corresponding line, an unambiguous determination of line-width is always possible. But this is impossible to implement with fixed filter sets in a real system. However, if continuously-adjustable filters were used, we could approximate the optimum filter for each test line. It should be noted that the calculated images of Figs. 4 through 8 show nearly equal luminance peaks on either side of the zeroes with the optimum filter. If the microscopist were to adjust  $\sigma_1$  to produce approximate equality in those peaks (which he would estimate visually), his subsequent measurements would be very near the proper value; they could be further refined by application of the correction algorithm.

#### Filter Misalignment

We assumed throughout the preceding developments that the filters were accurately made and perfectly located. We will continue to specify the fabrication accuracy but will now look quickly at misalignment. Appendix B develops the necessary relation, calculating the image for a displacement of upper and lower cutoff frequencies by  $\Delta$  and  $\epsilon$ , respectively. Because the shift in the cutoff values results in unequal portions of negative and positive sides of the spectrum passing through to the image, the zero at the line-edge location now becomes a minimum; i.e., there is a constant (non-zero) illuminance in the image that lowers contrast. The line-edge location remains unchanged; its determination and correction become more difficult.

TABLE V: (Analytically) Measured Line-Widths for a 0.65 NA Objective ( $\lambda = 500 \text{ nm}$ )

		Measured Line-Widths ( $\mu\text{m}$ ) and % Relative Error			
Test Line Width ( $\mu\text{m}$ )	†	Optimum Filter Line-Widths ( $\mu\text{m}$ )			
		1.60	1.80	2.10	2.40
1.70	C	‡	‡	1,700 (-0.01)	1,700 (-0.01)
	U	1.697 (-0.20)	1.700 (-0.03)	1.748 (+2.82)	1.798 (+5.74)
2.00	C	2,000 (+0.00)	2,000 (+0.00)	2,000 (+0.00)	2,000 (+0.00)
	U	1.979 (-1.04)	1.982 (-0.92)	2.022 (+1.08)	2.066 (+3.30)
2.30	C	‡	‡	* 2,300 (-0.00)	2,300 (+0.00)
	U	2.224 (-3.29)	2.226 (-3.21)	2.262 (-1.64)	2.307 (+0.30)

‡ Because of rapid variation of sign, broad regions of tangency along the axis or general ambiguity of locus, it is not possible to determine the corrected value without absolute prior knowledge of the true line-width.

\* Determination of correction required interpretation of calculation by the observer that implies fore-knowledge of a rough estimate of line-width.

† Type of measurement: C - Corrected; U - Uncorrected.

TABLE VI: (Analytically) Measured Line-Widths for a 0.50 NA Objective ( $\lambda = 500 \text{ nm}$ )

		Measured Line-Widths ( $\mu\text{m}$ ) and % Relative Error			
Test Line Width ( $\mu\text{m}$ )	†	Optimum Filter Line-Widths ( $\mu\text{m}$ )			
		4.00	4.75	5.50	6.00
4.60	C	4,600 (-0.00)	4,600 (-0.00)	4,600 (+0.00)	4,600 (-0.00)
	U	4,581 (-0.42)	4,619 (+0.40)	4,655 (+1.19)	4,701 (+2.19)
5.00	C	* 5,000 (+0.01)	5,000 (-0.01)	5,000 (+0.00)	5,000 (-0.01)
	U	4,938 (-1.25)	4,974 (-0.53)	5,010 (+0.19)	5,057 (+1.14)
5.75	C	5,750 (+0.00)	5,750 (+0.00)	5,750 (-0.00)	5,750 (-0.00)
	U	5,671 (-1.37)	5,698 (-0.91)	5,728 (-0.38)	5,772 (+0.38)

\* Determination of correction required interpretation of calculation by the observer that implies fore-knowledge of a rough estimate of line-width.

† Type of measurement: C - Corrected; U - Uncorrected.

As in the preceding experiment, a large number of calculations are carried out, the results of which will be summarized here.

1) It is felt that when ordinary alignment tolerances are met in adjusting such a system, the error produced will be virtually negligible. When a test line is imaged with its optimum filter, a misalignment of the lower cutoff by 20% of the value of  $\sigma_1$  results in a relative error in line-width of 0.5%. A 5% misalignment results in errors typically 0.03% or less.

2) The misalignment of the lower cutoff has larger effect on the image (an order of magnitude) than does misalignment of the upper cutoff. The errors due to each add algebraically, so that it is possible to eliminate small errors by stopping the system down (the procedure is not recommended).

### Discussion

During the course of this study, a number of microscope objectives were examined to see if the technique of this paper could be demonstrated. It was found that for numerical apertures above approximately 0.3, the plane of the object spectrum fell inside the last glass surface, and was therefore inaccessible for filtering. The design of such systems is not so rigid that the repositioning of this plane cannot be accommodated. However, until such lenses are made available, the present technique cannot be implemented. Use of reflecting objectives<sup>(20)</sup> or catadioptric systems might also be feasible, but none were studied in this program.

Line shapes for this analysis had a rectangular profile, and possessed symmetry about the centerline. Not very many lines in practice have such a perfect profile, and the modeling of lines to accommodate these variations in their description is necessary before we can extend the results of this paper to the prediction of measurement accuracy on real lines and spaces. It is an area for further study and can best be carried out by analyzing profiles of current lines and edges in terms of the physical processes that formed them. Hopefully (and preferably through first principles) we can obtain a line-model that will not only serve our analytical purposes but also assist in understanding the physics of the problem.

The analysis indicates that fixed spatial filters are not desirable, not only because of the larger number required, but also because their alignment becomes a problem. Of the various possibilities, one configuration that appears to have a good chance for success is the diversion of the light path in image space by a front-surface mirror split in the center to form a slit whose width is adjustable. Thus, the lower cutoff is the edge of the slit that allows the light to pass out of the system instead of occluding it. A sketch of such a system is shown in Fig. 9. It would work as follows: the system would be focused on the line with the slit closed. The slit would then be slowly opened, until a pattern such as those typified in Figs. 4 through 8 was obtained. Final adjustments to the width would be made with a piezo-electric micrometer. Calibration of the slit adjustments would provide a precise and accurate determination of filter width ( $2\sigma_1$ ). The pattern width (dark-line to dark-line) would then be measured with a shearing or filar eyepiece, to which the correction algorithm of Eq. (14) would then be applied. This approach appears to be feasible; many microscope systems use reflecting surfaces to bend the light path for viewing convenience, so the configuration is not unusual. Since non-uniformly opening slit jaws can be compensated through calibration, imperfect jaw motions need not be a bar to application.

The large number of reflecting surfaces in microscope systems precludes the use of illumination with a large temporal coherence. The resulting interference patterns would seriously affect image clarity. Further, because the size of the intended objects is so

small, lateral coherence intervals need not be extremely large. Both of these considerations appear to rule out the laser as a source. The mercury arc, filtered for the 5461 Å line will provide sufficient lateral coherence and virtually no temporal coherence, and would seem to be ideal because the green wavelength is near the peak of the eye response and would be reasonably comfortable for viewing. On the other hand, since radiance falls-off as the square of the magnification, and because the central portion of the spectrum where most of the image energy is located is occluded in the filtering process, high illumination power is required. Some testing to choose among the available light sources is clearly indicated.

A great many simplifications have been introduced in the analysis. The simple scalar theory employed is sufficient to illustrate the technique and develop the basic concepts, but at the high numerical apertures that must eventually be used in a practical system, a more rigorous analysis is recommended. In addition the assumption of diffraction-limited optics ignored the spherical aberration, flare light and the difficulty of focusing in coherent illumination that are commonly present with such systems. Flare light alone is sufficient to significantly reduce the contrast of the imagery of the zero-crossings at the line-edges. Those interested in extending and developing this technique will have to take these practical aspects of the microscope into account.

### Conclusions

The study of measurement of small line and space widths by spatial filtering in a microscope system employing coherent illumination shows that such a method is feasible in principle, although experimental verification is not immediately possible. The major constraint at present is that suitable microscope objectives of high enough numerical aperture are not available. Development of the technique must await the design and fabrication of such objectives.

### Acknowledgements

The author wishes to thank Mr. H. Zoranski for his patience and painstaking care in the preparation of the Figures.

### References

1. D. N. Grimes, *J. Opt. Soc. Am.* 61, 870 (1971).
2. R. Becherrer and G. B. Parrent, Jr., *J. Opt. Soc. Am.* 57, 1479 (1967).
3. R. Swing and J. Clay, *J. Opt. Soc. Am.* 57, 1180 (1967).
4. J. Dyson, *J. Opt. Soc. Am.* 50, 754 (1960).
5. D. Swyt, *Solid State Technology* 19, 51 (1976).
6. P. S. Consideine, *J. Opt. Soc. Am.* 56, 1001 (1966).
7. B. J. Thompson, *Proc. SPIE, Image Assessment & Specification*, 46, 27 (1974).
8. A. Marechal and P. Croce, *Compte. Rend.* 237, 607 (1953).
9. A. Marechal, P. Croce and K. Dietzel, *Opt. Act.* 5, 256 (1958).
10. a) J. Tsujiuchi, *Opt. Act.* 7, 243 (1960); 385 (1960)  
b) J. Tsujiuchi, *Opt.* 8, 161 (1961).
11. E. L. O'Neill, *I. R. E. Trans. (P.G.I.T.)* 2, 56 (1956).
12. T. Suzuki, M. Mino and G. Shinoda, *Appl. Opt.* 3, 825 (1964).
13. P. F. Mueller, *Appl. Opt.* 8, 267 (1969).
14. P. F. Mueller, *Appl. Opt.* 8, 2051 (1969).
15. P. S. Consideine, *Opt. Eng.* 12, 36 (1973).
16. G. B. Parrent, J. and B. J. Thompson, *Physical Optics Notebook* (Society of Photo-Optical Instrumentation Engineers, Redondo Beach, Calif., 1969), p. 3.
17. Ref. 16, p. 11.
18. Ref. 16, p. 13.
19. The image is given in terms of the Sine and Cosine Integrals. These are defined by:

$$S_i(z) = \int_0^z \text{sinc}(x) dx$$

and

$$C_i(z) = - \int_z^\infty (1/x) \cos(x) dx .$$

20. A. Bouwers, *Achievements in Optics* (Elsevier Publishing Co., Inc., New York, New York, 1946), pp. 46-52.
21. J. W. Goodman, *Introduction to Fourier Optics* (McGraw-Hill Book Co., New York, New York, 1968), p. 166.
22. Ref. 21, p. 169.
23. Ref. 6, Eq. (1).

## Appendix A: Single-Lens Coherent Optical System

The single-lens coherent system discussed by Goodman<sup>(21)</sup> will form the basis for analysis, since it can be incorporated into a microscope system. A general single-lens system is sketched in Fig. (A-1), where the distances  $z_1$  and  $z_2$  are arbitrary. The lens is thin, has a focal length,  $f$ , and the object has complex transmittance characteristics (the object field),  $\psi_0(\mu)$ .

The object will be illuminated by a plane wave of wavelength  $\lambda$ , and we will assume paraxial optics<sup>(16)</sup>. In characterizing the lens, we will employ the sagittal approximation<sup>(16)</sup>; the pupil function is given by  $F(\alpha)$ . The system impulse response will be considered invariant over the region of interest (stationarity). Then, the field in  $x$  is given by the expression

$$\psi_1(x) = \iint \psi_0(\mu) F(\alpha) \exp\left[ik(\alpha - \mu)^2/2z_1\right] \exp\left[-ik\alpha^2/2f\right] \exp\left[ik(x - \alpha)^2/2z_2\right] d\mu d\alpha. \quad (\text{A-1})$$

When we expand the exponentials, recombine them and focus the lens so that the thin lens equation holds (i.e.,  $1/z_1 + 1/z_2 = 1/f$ ), the field becomes

$$\psi_1(x) = \int \psi_0(\mu) \exp\left\{i(k/2)(\mu^2/z_1 + x^2/z_2)\right\} \left\{ \int F(\alpha) \exp(ik\alpha)(\mu/z_1 + x/z_2) d\alpha \right\} d\mu. \quad (\text{A-2})$$

The expression in braces is a Fourier transform. The transform of the pupil function is the complex impulse response, and is the image of a geometrical point, the smallest image obtainable with a given lens. Since the lens now obeys the thin lens equation, we will have, for the lens magnification,  $m$ ,

$$z_1 = (1 + 1/m)f; \quad z_2 = (1 + m)f. \quad (\text{A-3})$$

When we carry out the transform indicated in Eq. (A-2) and employ the relations of Eq. (A-3), we obtain

$$\psi_1(x) = \exp(ikx^2/2z_2) \int \psi_0(\mu) \tilde{F}\left[\frac{x + m\mu}{(1+m)\lambda f}\right] \exp(ik\mu^2/2z_1) d\mu. \quad (\text{A-4})$$

The quadratic phase terms exemplify the imaging of a spherical field onto a sphere<sup>(22)</sup> but since we are imaging lines of extremely small width (compared to  $z_1$  and  $z_2$ ) the exponential arguments are also very small. Under these circumstances, we drop further consideration of the exponentials, and the observable luminance in the  $x$ -plane is

$$\left| \psi_1(x) \right|^2 = \left| \int \psi_0(\mu) \tilde{F}\left[\frac{x + m\mu}{(1+m)\lambda f}\right] d\mu \right|^2. \quad (\text{A-5})$$

This is a known result<sup>(23)</sup> and represents the convolution of the complex impulse response with the object amplitude. It also shows that the system is linear in complex amplitude, but non-linear in luminance. When the Convolution theorem is applied to the field in Eq. (A-5), we will have

$$\psi_1(x) = \int \tilde{\psi}_0(\sigma) F\left[-\sigma\left(\frac{1+m}{m}\right)\lambda f\right] \exp(-2\pi i x \sigma/m) d\sigma. \quad (\text{A-6})$$

and it is clear that the image is the Fourier transform of the product of the complex spectrum and the pupil function. It is important because it implies that if we can image the spectrum somewhere in the system, we could physically modify it before the image is formed, and thereby control the frequency content of the image.

It is known that when object and image are each located a distance of one focal length from the lens, the image is the Fourier transform of the object field: the object spectrum<sup>(24)</sup>. It can also be shown that when the lens obeys the thin-lens equation, the spectrum is also formed at  $f$  (in the image space) for all finite values of object distance<sup>(12,13)</sup>. The field there is given by

$$\psi_1(x) = \exp\left[ikx^2/2f^2\right](f - z_1) \int \psi_0(\mu) F(x + \mu) \exp(-ik\mu x/f) d\mu. \quad (\text{A-7})$$

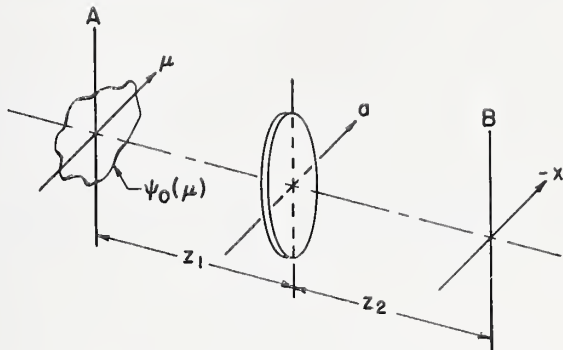


Fig. A-1. Sketch of general optical system, showing planes of interest, object and image distances and coordinate systems.  $\psi_0(\mu)$  is the complex field representation of a generalized object.

In this equation, for a diffraction-limited lens, the pupil function  $F(x + \mu)$  has the value of unity over the region of interest, and hence makes no contribution to the integrand. The remainder of the integral is a Fourier transform. When we employ the relation of Eq. (A-3) and carry out the indicated transformation, we obtain

$$\begin{aligned}\psi_1(x) &= \exp[-(ikx^2)/(2mf)] \tilde{\psi}_0(x/\lambda f) \\ &= \exp(-2\pi i \sigma^2 \lambda f / 2m) \tilde{\psi}_0(\sigma)\end{aligned}\quad (A-8)$$

since  $\sigma = x/\lambda f$ , (A-9)

which shows the existence of the object spectrum (independent of the system magnification) in the plane at  $f$ , but imaged onto a spherical surface whose radius is given by the exponential argument. We therefore have the spectrum available for modification by a filter. If we insert such a filter,  $g(\sigma)$ , in the plane at  $f$ , the image field will be given by

$$\psi_1(x) = \int \tilde{\psi}_0(\sigma) g(\sigma) F \left[ -\sigma \left( \frac{1+m}{m} \right) \lambda f \right] \exp(-2\pi i x \sigma / m) d\sigma. \quad (A-10)$$

and what will be observed there will be the squared modulus of this expression.

The analysis of such a system follows a simple procedure, and this will be done in the main text: calculate the spectrum of the complex object, multiply it by the function that describes the spatial filter, Fourier transform that product and then (complex) square the result. This produces the filtered image in the image plane of the microscope objective.

#### Appendix B: Effect of Filter Misalignment

We need to determine the effects caused by a misalignment of upper and lower filter cutoff frequencies. We will restrict the analysis to the vicinity of the line so that we neglect the object aperture boundary terms. We achieve this by eliminating the "dc" portion of the image spectrum. Thus, both line types will have the same spectrum,

$$\tilde{F}(\sigma) = \text{sinc}(2\pi\sigma a), \quad (B-1)$$

and if the system is low-pass, the image will be that of a clear line in a dark background. This occurs because we have taken out the image polarity in Eq. (B-1).

We will consider a band-pass filter with the lower and upper cutoff frequencies shifted laterally by  $\epsilon$  and  $\Delta$  (cycles/mm), respectively. The geometry is sketched in Fig. (B-1). For the spectrum of Eq. (B-1), the image field is given by

$$f(x) = \int_{-\sigma_2 + \Delta}^{\sigma_2 + \Delta} \tilde{f}(\sigma) \exp(-2\pi i \sigma x / m) d\sigma - \int_{-\sigma_1 + \epsilon}^{\sigma_1 + \epsilon} \tilde{f}(\sigma) \exp(-2\pi i \sigma x / m) d\sigma. \quad (B-2)$$

This can be written in functional form so that

$$f(x) = f_1(x, \sigma_2, \Delta) - f_2(x, \sigma_1, \epsilon), \quad (B-3)$$

and the integrals can be evaluated through use of the Sine and Cosine Integrals (19). Because the limits are not symmetric, and because these integrals are odd and even functions, respectively, we will have

$$\int_{-a_2}^{a_1} (1/x) \cos(x) dx = C_i(a_1) - C_i(a_2); \quad (B-4)$$

$$\int_{-a_2}^{a_1} (1/x) \sin(x) dx = S_i(a_1) + S_i(a_2). \quad (B-5)$$

When these are applied to the evaluation of Eqs. (B-2) and (B-3), and the image coordinate is normalized to the object-edge by

$$\xi = x/ma, \quad (B-6)$$

we will obtain

$$\begin{aligned}f_1(\xi, \sigma_2, \Delta) &= (1/2) \left\{ S_i \left[ 2\pi a (\sigma_2 + \Delta) (\xi + 1) \right] + S_i \left[ 2\pi a (\sigma_2 - \Delta) (\xi + 1) \right] \right. \\ &\quad \left. - S_i \left[ 2\pi a (\sigma_2 + \Delta) (\xi - 1) \right] - S_i \left[ 2\pi a (\sigma_2 - \Delta) (\xi - 1) \right] \right\} \\ &+ (i/2) \left\{ C_i \left[ 2\pi a (\sigma_2 + \Delta) (\xi + 1) \right] - C_i \left[ 2\pi a (\sigma_2 - \Delta) (\xi + 1) \right] \right. \\ &\quad \left. - C_i \left[ 2\pi a (\sigma_2 + \Delta) (\xi - 1) \right] - C_i \left[ 2\pi a (\sigma_2 - \Delta) (\xi - 1) \right] \right\}\end{aligned}\quad (B-7)$$

and

$$\begin{aligned}
 f_2(\xi, \sigma_1, \epsilon) = (1/2) & \left\{ S_1 \left[ 2\pi a(\sigma_1 + \epsilon)(\xi + 1) \right] + S_1 \left[ 2\pi a(\sigma_1 - \epsilon)(\xi + 1) \right] \right. \\
 & - S_1 \left[ 2\pi a(\sigma_1 + \epsilon)(\xi - 1) \right] - S_1 \left[ 2\pi a(\sigma_1 - \epsilon)(\xi - 1) \right] \left. \right\} \\
 & - (1/2) \left\{ C_1 \left[ 2\pi a(\sigma_1 + \epsilon)(\xi + 1) \right] - C_1 \left[ 2\pi a(\sigma_1 - \epsilon)(\xi + 1) \right] \right. \\
 & \left. - C_1 \left[ 2\pi a(\sigma_1 + \epsilon)(\xi - 1) \right] - C_1 \left[ 2\pi a(\sigma_1 - \epsilon)(\xi - 1) \right] \right\}. \tag{B-8}
 \end{aligned}$$

Finally, when we calculate the observable image, we must form the squared modulus of Eq. (B-3). Thus, the image luminance is given by

$$\begin{aligned}
 I(\xi) = (1/4\pi^2) & \left[ \left\{ \text{Re} \left[ f_1(\xi, \sigma_2, \Delta) - f_2(\xi, \sigma_1, \epsilon) \right] \right\}^2 \right. \\
 & \left. + \left\{ \text{Im} \left[ f_1(\xi, \sigma_2, \Delta) - f_2(\xi, \sigma_1, \epsilon) \right] \right\}^2 \right], \tag{B-9}
 \end{aligned}$$

where we have inserted the factor  $(1/4\pi^2)$  for normalization, and where the real and imaginary parts of the arguments in Eqs. (B-7) and (B-8) are denoted by Re and Im, respectively.

It is clear that when there is a filter misalignment ( $\epsilon$  and/or  $\Delta$  are non-zero), the zero normally expected at the line-edge location will be raised to a finite value by the luminance contributed by the second term of Eq. (B-9). This is a slowly varying factor, and serves mainly to add a constant to the image luminance.

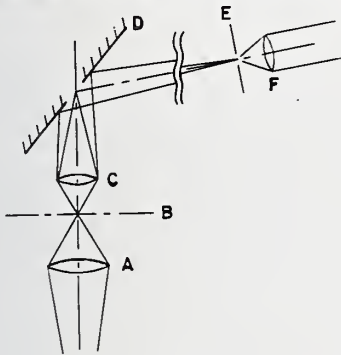


Fig. 9. Sketch of one possible configuration for a microscope system employing the spatial filtering system suggested in the text. A: substage condenser; B: sample (object) plane; C: objective lens; D: front-surface mirror located so that its center lies one focal length from the objective, and the opening of which can be varied as the jaws of a slit; E: plane of intermediate image (system is shown collapsed to save space), located at a tube-length's distance from C; F: microscope eyepiece. The portion of the image spectrum that is eliminated passes through the center of the reflecting surface and does not pass to the image plane.

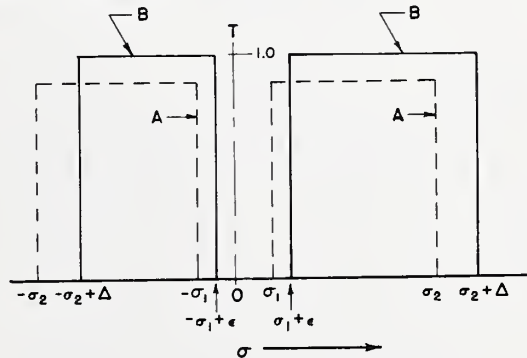


Fig. (B-1). Sketch of the misaligned spatial filter, showing the shifts of upper and lower passband cutoff frequencies; A: original, aligned filter; B: misaligned filter.

Note Added In Acknowledgement

During the investigation and subsequent preparation and submission of this paper, the author was unaware of a prior study by K. G. Birch (*Optica Acta* 15, 113 (1968)) that considered essentially the same problem in a more general context. However, the methods of approach and some of the conclusions of the two papers differ; the idea of optimum filter, correction of measurements for non-optimum filters and the application of the technique to micrometer-size lines and spaces in the optical microscope are the basic contributions of this present paper. This work was a resumption of earlier spatial-filtering studies reported by the author (*J. Opt. Soc. Am.* 51, 478A (1961)).

# Linewidth measurement with an optical microscope: the effect of operating conditions on the image profile

D. Nyssonen

A theoretical model of the optical microscope based on the theory of partial coherence is used to predict the image profiles of lines on IC photomasks and assess factors contributing to measurement errors for different conditions of microscope operation. A comparison of experimental and theoretical image profiles is given, showing good agreement with theory for a 0.9 N.A. and linewidths as small as 0.5  $\mu\text{m}$ . The primary sources of differences appear to be edge quality and accuracy of focus. The theory indicates that for well-corrected microscope optical systems, spectrally filtered to eliminate longitudinal chromatic aberration and chromatic difference of magnification, accurate determinations of linewidth may be made from the image profile using a threshold of 25% of maximum intensity (corrected for finite background transmittance in the opaque region). The correspondence between the edge location and the 25% threshold appears to be nearly invariant with small amounts of defocus and spherical aberration as well as variation in the numerical aperture of the condenser.

## Introduction

The variation in linewidth measurements on IC photomasks made with different optical microscope systems, especially for linewidths below 10  $\mu\text{m}$ , has prompted a more thorough investigation of the imaging properties of the optical microscope and a study of possible sources of measurement error. The effects of diffraction and partial coherence on the mensuration of small objects have been discussed in the literature.<sup>1-10</sup> The application of the theory of partial coherence to describe image formation in the optical microscope is well developed,<sup>11,8</sup> but the complexity of the numerical calculations involved in treating even simple line objects has prevented a systematic study of the errors introduced under different conditions of operation. For diffraction-limited optical systems, the images of edges,<sup>6,12</sup> circular disks,<sup>1-5</sup> and lines<sup>7,9</sup> have been computed for specific ratios of condenser to objective numerical apertures. The combinations of defocus and coma with partial coherence were treated by Barakat.<sup>7</sup> Rowe<sup>10</sup> calculated the images of defocused edges at the coherent limit. Difficulties in applying these results to practical microscope systems have been encountered for the case of circular objects<sup>13</sup> and have been attributed to the breakdown of scalar theory at high numerical apertures.<sup>8,14</sup> However, calculations by Lin<sup>15</sup> based on Sommerfeld's exact solution to the problem of dif-

fraction at an edge indicate that the far-field diffraction patterns of very small slits, down to widths of half a wavelength, may be described by scalar theory.

Deviations begin to appear only at high angles of incidence of the illuminating field. One would therefore expect that in an optical system with high magnification such as a microscope, scalar theory would apply once the diffracting field reaches the lens aperture assuming that the lens response is characterized by the appropriate pupil function. The results described here support this view for numerical apertures up to 0.9 and slit widths as small as 0.5  $\mu\text{m}$ . The work described here includes numerical computation of line images for actual conditions of microscope operation using a mathematical model which incorporates partial coherence, optical aberrations including defocus, amplitude transmittance of the sample allowing for degraded edges, and the effect of the scanning aperture. These theoretical profiles are compared with experimentally measured data for varying numerical apertures. The effects of defocus, spherical aberration, chromatic aberrations, and edge quality are discussed.

## Calculation of Image Profiles

Starting with the scalar mutual coherence function  $\Gamma$  at the sample plane and propagating to the scanning aperture, the flux  $I$  at the detector as a function of the sample displacement  $\xi_0$  may be described in 1-D for quasi-monochromatic illumination by

$$I(\xi_0) = C \int \int \int \bar{F}(\alpha) \bar{t}(\alpha - \mu_2) \bar{t}^*(\alpha - \mu_1) \exp[-ik\xi_0(\mu_1 - \mu_2)/z_1] \cdot F(\mu_1) F^*(\mu_2) \bar{S} \left( \frac{\mu_2 - \mu_1}{\lambda z_2} \right) d\alpha d\mu_1 d\mu_2 \quad (1)$$

The author is with U.S. National Bureau of Standards, Washington, D.C. 20234.

Received 4 November 1976.

where  $z_1$  are the object and image conjugates, respectively;  
 $t$  is the amplitude transmittance of the sample;  
 $F$  is the pupil function of the imaging objective and relay optics combined;  
 $S$  is the intensity transmittance function of the scanning aperture, and  
 $\sim$  denotes the spatial Fourier transform.

This 1-D description is accurate for one-dimensionally varying objects in circular lens systems only at the coherent limit.<sup>8</sup> The equivalent description for partially coherent 2-D lens systems is

$$I(\xi_0) = C \int \int \int \bar{\Gamma}(\alpha, \eta) \bar{t}(\alpha - \mu_2) \bar{t}^*(\alpha - \mu_1) \exp[-ik\xi_0(\mu_1 - \mu_2)/z_1] \\ \cdot F(\mu_1, \eta) F^*(\mu_2, \eta) \bar{S}\left(\frac{\mu_2 - \mu_1}{\lambda z_2}\right) d\alpha d\mu_1 d\mu_2 d\eta. \quad (2)$$

The calculations shown here are based on Eq. (1). In photomask linewidth measurements, the glass plate dictates use of condenser apertures less than that of the high resolution objective commonly employed because of unavailability of long working distance high numerical aperture condensers. It appears from the comparison of theoretical and experimental results that for ratios of condenser to objective numerical apertures  $R$  less than 1.0, the system is closer to the coherent limit, and the imagery may be approximated by the 1-D solution given by Eq. (1).

When the condenser aperture is uniformly illuminated so that it is the limiting aperture in the illumination system and the illuminated area of the sample is large compared to the dimensions of the impulse response of the condenser,  $\bar{\Gamma}$  is the flux distribution in the condenser aperture.<sup>11,16</sup> When the area of illumination becomes very small, the system must be treated theoretically as a microdensitometer for which a different description applies.<sup>17</sup> Wide field illumination is assumed in the following calculations.

The amplitude transmittance function of the sample  $t$  is usually related to optical density by the function  $\exp(-k\kappa d)$ , where  $k$  is the wavenumber,  $\kappa$  is the imaginary part of the complex index of refraction, and  $d$  is the thickness of the absorbing layer. For chromium and other metallic photomasks, accurate determination of  $\kappa$  may be difficult. It is known that the physical properties of thin films of these metals are different from the bulk properties.<sup>18</sup> However, if perfect edges are assumed, the transmittances of the semiopaque and clear areas may be determined optically. When the edge slope begins to affect the image profile, however, a more detailed description of the nonideal transmittance function is required.

The pupil function of the imaging objective includes the optical aberration function, thus defocus and spherical aberration are included. This formulation has assumed quasi-monochromatic illumination and does not take into account the variation of the aberration terms with wavelength. Results of this study indicate that chromatic aberrations in the microscope cause deviations in white light imagery which contribute to linewidth measurement errors.

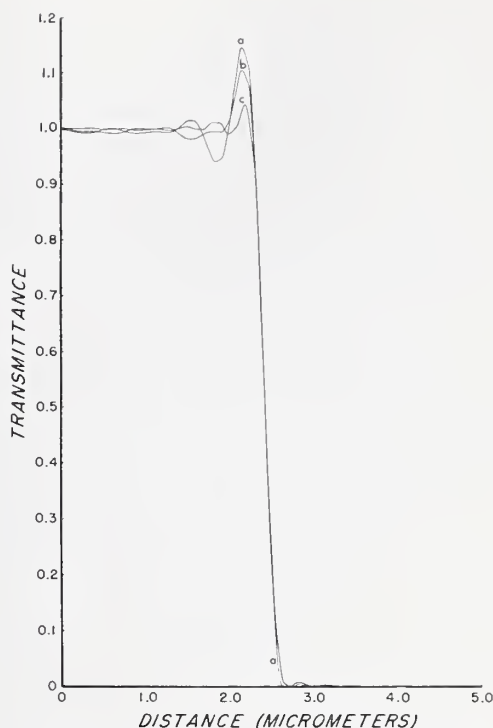


Fig. 1. Theoretical image profiles of a 5- $\mu$ m clear line with microscope parameters as follows: 0.9 objective N.A., condenser N.A. (a) 0.22, (b) 0.40, and (c) 0.60, wavelength 560 nm, effective scanning slit 0.13  $\mu$ m, and diffraction-limited optics.

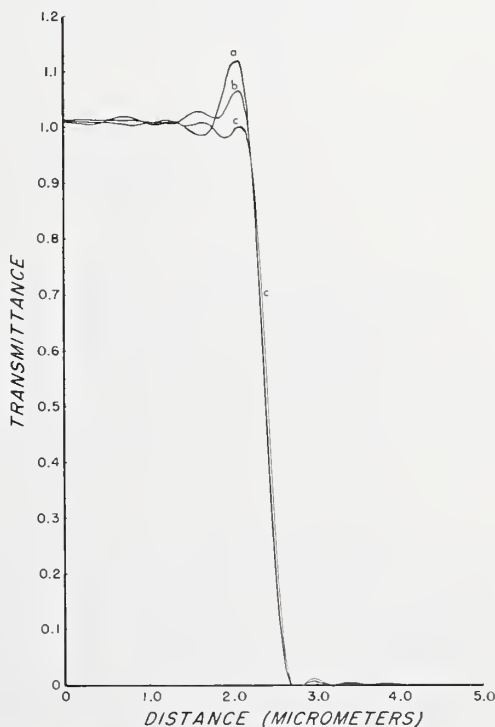


Fig. 2. Same as Fig. 1 except the objective N.A. is 0.65.

Using Eq. (1), image profiles of a clear line were computed using straightforward numerical integration techniques. The particular parameters of the system were chosen in order to explore the imaging behavior of the microscope to be used for optical linewidth measurements. Figures 1 and 2 show the image profiles of a 5- $\mu\text{m}$  line for different combinations of condenser and objective numerical apertures. These are similar to edge image profiles found in the literature<sup>7,9</sup> and exhibit the suppression of the coherent edge ringing as the numerical aperture of the condenser is increased. They also indicate that the true edge location corresponds to the 25% threshold with only a slight deviation beginning to show as the ratio of condenser to objective numerical apertures  $R$  approaches one (curve c of Fig. 2). Figures 3 and 4 show image profiles of progressively smaller linewidths for the numerical aperture combination 0.60/0.90 ( $R = 0.66$ ) which appears to be a reasonable choice for linewidth measurement. As shown in Fig. 3 the detail in the vicinity of the edge of a line significantly wider than the impulse response scales with N.A. and wavelength. These two figures indicate that the 25% threshold corresponds to the true edge location for linewidths down to 0.5  $\mu\text{m}$ , despite the influence of the neighboring edge on the image profile. In order to explore the effects of defocus and spherical aberration on the 25% threshold, Figs. 5 and 6 were calculated. The profiles correspond to stepping through focus in steps of  $\lambda/4$  without (Fig. 5) and with (Fig. 6) spherical aberration. The particular choice of  $2\lambda$  spherical aberration corresponds to the amount that would be introduced at a numerical aperture of 0.65 by use of the incorrect cover glass thickness (i.e., a 0.05-mm error resulting from use of 0.12 mm instead of 0.17) or use of an objective at the wrong tube length (160 mm instead of 220 mm). The condition of steepest edge slope occurs at  $0\lambda$  defocus without spherical aberration and at  $-1.0\lambda$  with spherical. This indicates that the usual aberration balancing of spherical and defocus used in incoherent illumination is not applicable to partially coherent images. Also, with no spherical aberration, maximum slope and maximum intensity overshoot at the edge coincide while with  $2\lambda$  spherical aberration present, maximum contrast in the ring structure occurs at  $-0.5\lambda$  of defocus. With no spherical aberration, the 25% threshold yields the true edge location only within the Rayleigh focus tolerance of  $\lambda/4$  corresponding to  $\pm 0.35\text{-}\mu\text{m}$  displacement at an N.A. of 0.9 (see Ref. 19), whereas with  $2\lambda$  spherical aberration, any focus position between  $-1.0$  and  $-0.5\lambda$  (steepest slope and maximum ring contrast) would yield the true edge location at the 25% threshold. The 25% threshold therefore appears to be the best criteria to use for linewidth measurement even when spherical aberration is present. This threshold, however, must be corrected for finite transmission of the opaque area of the photomask. The correction is easily derived from consideration of the coherent limit case. Figure 7 shows the condition corresponding to the true edge location, that is, when a symmetric impulse response is centered at the edge. When the photomask is opaque, the amplitude transmittance is 50% of maximum. Squaring to get intensity yields the 25% threshold in this case. If

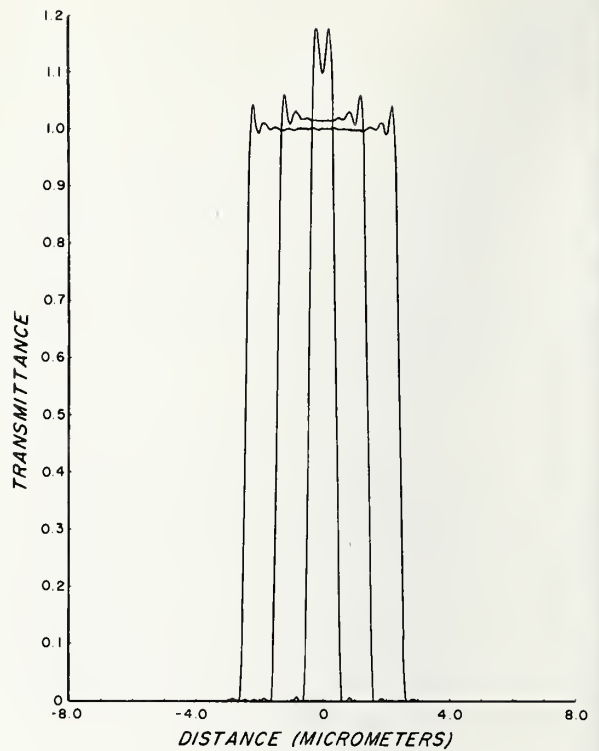


Fig. 3. Theoretical image profiles of 5- $\mu\text{m}$ , 3- $\mu\text{m}$  and 1- $\mu\text{m}$  clear lines with microscope parameters: 0.9 objective N.A., 0.60 condenser N.A., wavelength 560 nm, effective scanning slit 0.13  $\mu\text{m}$ , and diffraction-limited optics.

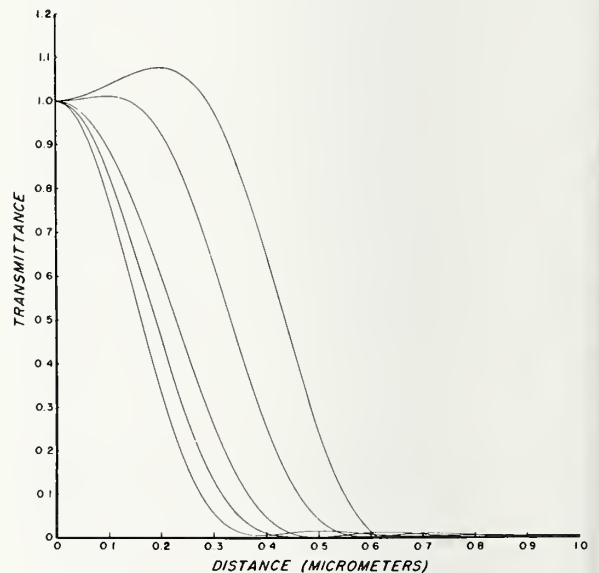


Fig. 4. Same as Fig. 3 except linewidths are 1.0  $\mu\text{m}$ , 0.8  $\mu\text{m}$ , 0.6  $\mu\text{m}$ , 0.5  $\mu\text{m}$ , and 0.4  $\mu\text{m}$ .

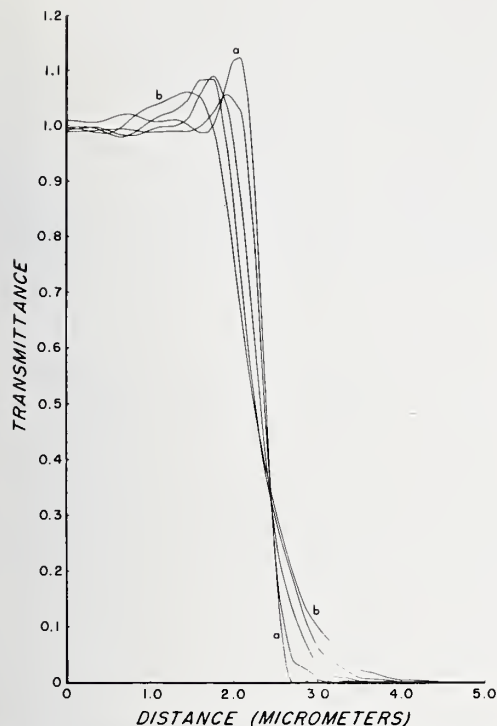


Fig. 5. Theoretical image profiles of a 5- $\mu\text{m}$  clear line with defocus in steps of  $\lambda/4$  or  $\pm 0.35\text{-}\mu\text{m}$  displacement from (a)  $0.0\lambda$  to (b)  $\pm 1.0\lambda$ . Remaining microscope parameters are the same as Fig. 3.

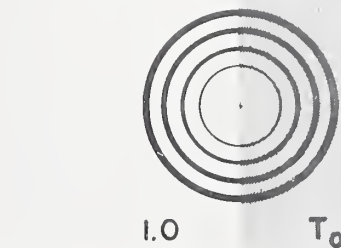


Fig. 7. Method of determining the proper threshold for locating true edge position.

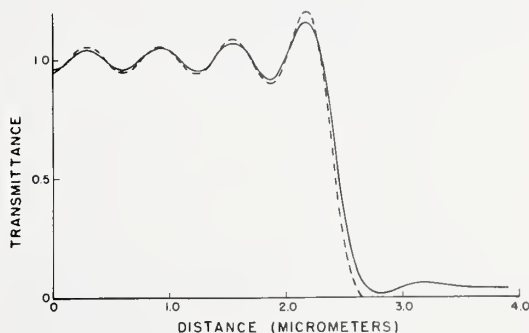


Fig. 8. Comparison of theoretical image profiles at the coherent limit (very small condenser aperture) for 0.9 objective N.A. and 0.60 condenser N.A. for 0% and 4% background transmittance.

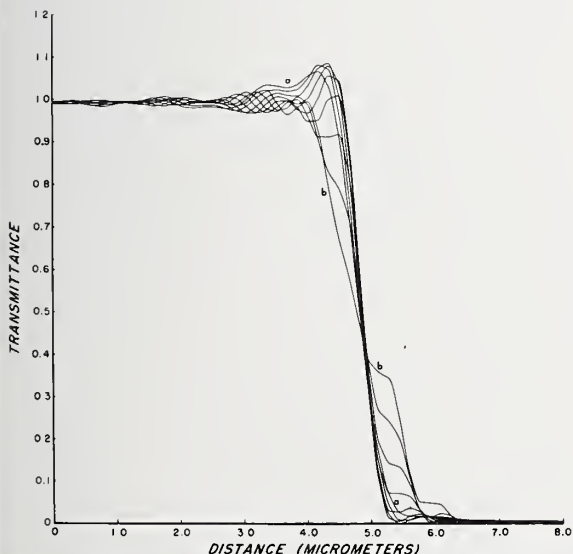


Fig. 6. Theoretical image profiles of a 10- $\mu\text{m}$  clear line with defocus and  $2\lambda$  spherical aberration. Defocus runs from (a)  $0.0\lambda$  to (b)  $-2.0\lambda$  in steps of  $\lambda/4$ . Microscope parameters are 0.65 objective N.A. and 0.22 condenser N.A.

the transmittance is taken as 1.00 in the clear area and  $T_0$  in the opaque area, the threshold corresponding to the true edge location is given by

$$T_c = 0.25(1 + \sqrt{T_0})^2 \quad (3)$$

For a transmittance  $T_0$  of 0.04, the threshold increases to 0.36, but the corresponding change in determination of the edge location for 0.9 N.A. is  $0.04\ \mu\text{m}$ , resulting in a linewidth error of  $0.08\ \mu\text{m}$  if the uncorrected threshold is used. This error increases with defocus or spherical aberration present. Figure 8 shows a comparison of image profiles for 4% and zero background transmittance at the coherent limit.

### Experimental Image Profiles

Since there is no standard microscope arrangement for measuring photomask linewidths, the approach taken here was to determine under what conditions of operation the image profiles could be made to agree with the theoretical profiles so that the edge location could be determined and accurate measurements made. A test system for determining the amounts of aberrations present in given microscope optics was not available at the time of this work so that only objectives exhibiting

near diffraction-limited performance were used. For the same reason, scanning was achieved by moving the sample instead of image scanning, so that the optical system is always used axially and is therefore devoid of off-axis aberrations such as coma, distortion, and curvature of field. This choice puts severe demands on the stage in terms of accurate positional information. However, extremely good performance was achieved by use of a mechanical stage driven at slow constant speed by a combination stepping motor and function generator.<sup>20</sup> The positional readout came from an LVDT gauge so that it was independent of the mechanical wobble in the stage. The stage therefore does not have to be perfect as long as the gauge can accurately track the motion. The limitation on the positional accuracy is vibration which was successfully reduced to a level of  $0.01\ \mu\text{m}$  by moving the whole system to a basement with solid foundation and isolating acoustical and mechanical sources of vibration. The microscope system was adapted to use a 150-W tungsten halogen lamp filtered in most cases for green light with a Wratten 60 filter and a hot mirror producing a bandwidth of approximately 60 nm. Initially a  $50\text{-}\mu\text{m}$  circular scanning aperture was used with a system magnification of 158 $\times$ . This was later changed to a  $20 \times 200\text{-}\mu\text{m}$  slit yielding less noisy image profiles because of the higher flux at the detector and the averaging effect over small imperfections in the edges of the objects scanned. The effective slit width in the latter case is  $0.13\ \mu\text{m}$  which theoretical calculations indicate has a negligible effect on the imagery. Contrary to conventional use, the scanning slit here is deliberately chosen smaller than the diameter of the impulse response of the imaging optics in order to preserve detail in the image that relates to the structure of the Airy disk and yields information about the edge

location. The samples used in the examples shown consisted of custom-made black chrome photomasks with nominal  $0.5\text{-}\mu\text{m}$ ,  $1.0\text{-}\mu\text{m}$ ,  $3.0\text{-}\mu\text{m}$  and  $10.0\text{-}\mu\text{m}$  clear and opaque lines. For the  $0.5\text{-}\mu\text{m}$  line, the background transmittance was less than 1%, while for the other lines it varied between 2% and 6%.

Figures 9–12 show comparisons of theoretical and experimental image profiles of a nominal  $10\text{-}\mu\text{m}$  clear line for different combinations of condenser and objective numerical apertures. Best focus was achieved by maximizing the intensity overshoot at the edge in

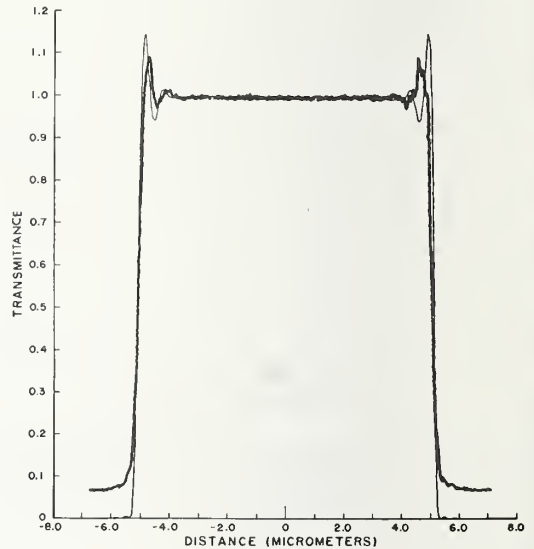


Fig. 10. Same as Fig. 9 except 0.9 objective N.A. and 0.22 condenser N.A. (most coherent case).

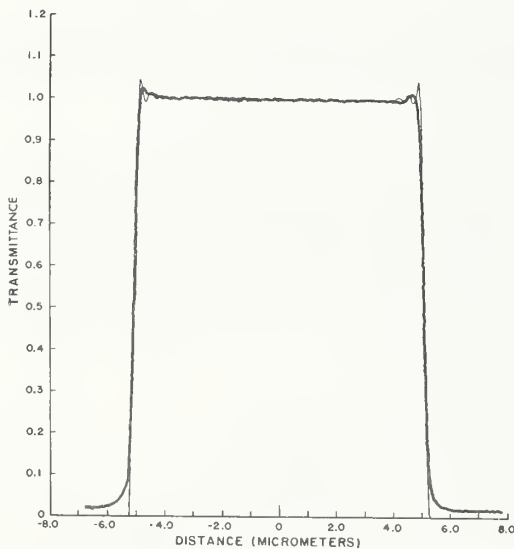


Fig. 9. Comparison of theoretical (—) and experimental (---) image profiles of a  $10.2\text{-}\mu\text{m}$  clear line and microscope parameters of Fig. 3 (0.9 objective N.A. and 0.60 condenser N.A.).

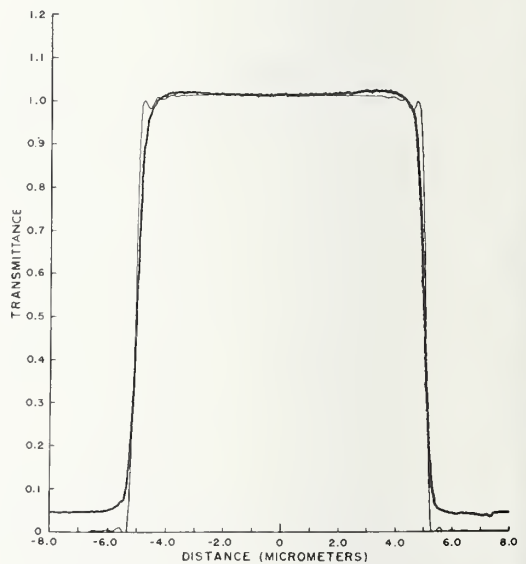


Fig. 11. Same as Fig. 9 except 0.65 objective N.A. and 0.60 condenser N.A. (least coherent case).

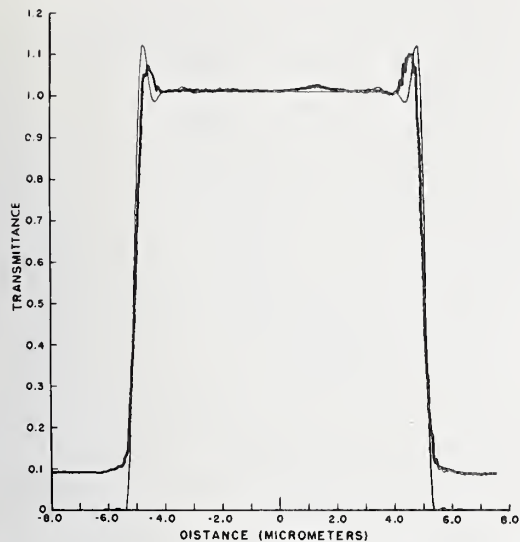


Fig. 12. Same as Fig. 9 except 0.65 objective N.A. and 0.22 condenser N.A.

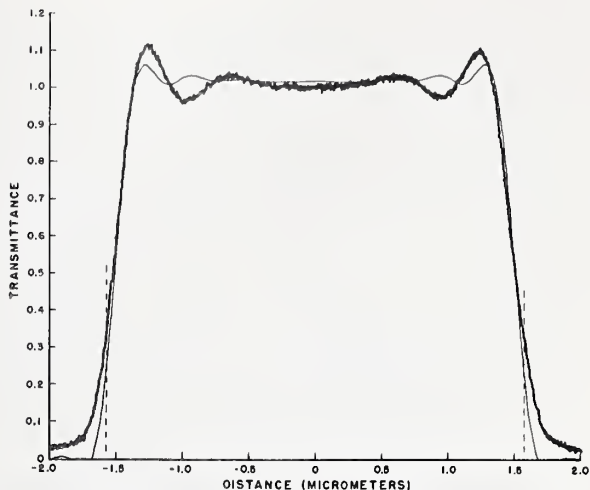


Fig. 13. Same as Fig. 9 except 3.15- $\mu\text{m}$  clear line (0.9 objective N.A. and 0.6 condenser N.A.).

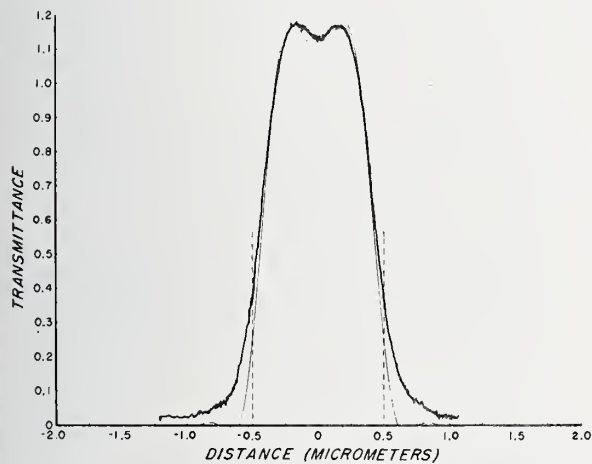


Fig. 14. Same as Fig. 13 except 1.0- $\mu\text{m}$  clear line.

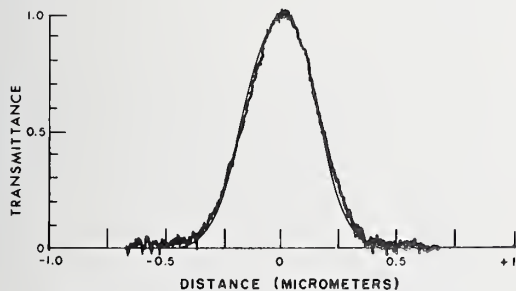


Fig. 15. Same as Fig. 13 except 0.5- $\mu\text{m}$  clear line.

accordance with theoretical results discussed previously. Differences in the low transmittance region of the curve are readily attributable to the finite background transmittance of the black chrome photomask. This region compares with the curve of Fig. 8. In the shoulder of the curves, the edge ringing is damped in the experimental curves as compared to the theoretical ones as the condenser numerical aperture is increased. This difference is what one would expect from use of Eq. (1) instead of the 2-D solution of Eq. (2) as well as the presence of a small amount of spherical aberration in the objective. That this is indeed the case is more apparent from Fig. 13, 14, and 15. As the linewidths are reduced so that the illumination is effectively coherent, there is better agreement between the theoretical and experimental profiles. In each case, the theoretical profile was computed for a linewidth corresponding to the width of the experimental profile at the appropriate threshold (25% corrected for the finite transmittance of the photomask).

Figures 16, 17, and 18 illustrate experimental profiles with defocus and spherical aberration present. The curves show good agreement with the calculations of Figs. 5 and 6 although exact correspondence is impossible because of the difficulties of determining both absolute focus position and the amount of spherical aberration present.

Several sources of differences with theory were immediately apparent in the course of this research. Ability to focus an objective with 0.9 N.A. within the Rayleigh tolerance is difficult with conventional fine focus adjustments found on microscope systems. The sample cannot be stepped through focus repeatedly in submicrometer increments to determine best focus

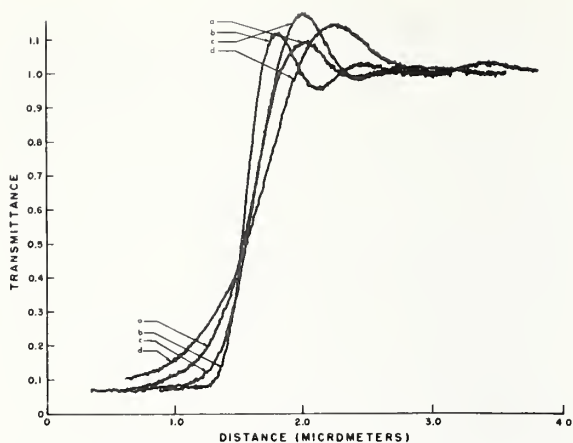


Fig. 16. Experimental image profiles at the edge of a nominal 10- $\mu$ m clear line as a function of focus displacement in submicrometer steps of approximately 0.1  $\mu$ m from a to d, 0.90 objective N.A., and 0.60 condenser N.A. Registration at edge may not be accurate. Compare with Fig. 5.

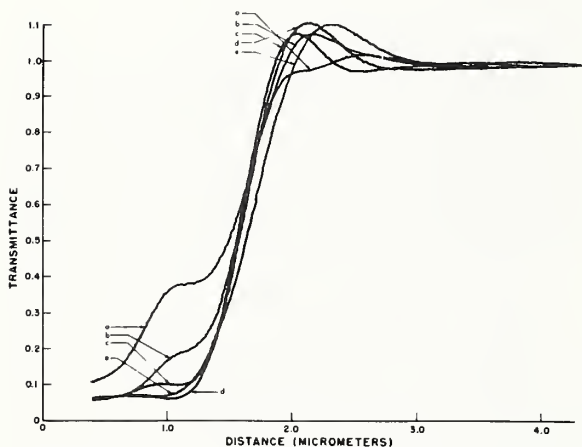


Fig. 17. Experimental image profiles at the edge of a nominal 10- $\mu$ m clear line as a function of focus displacement in submicrometer steps of approximately 0.3  $\mu$ m from a to e for a 0.65 objective N.A. and 0.22 condenser N.A. with improper cover glass correction (0.12 mm instead of 0.17 mm). Registration at edge may not be accurate. Note similarity to Fig. 6.

photometrically. One must therefore depend on a visual determination which varies increasingly with operator fatigue. To eliminate this problem, a piezoelectric fine focus adjustment is being incorporated into the system.

It is also apparent that the use of white light illumination introduces measurement errors. Diffraction-limited imagery at all wavelengths would not affect the correspondence between the 25% threshold and the true

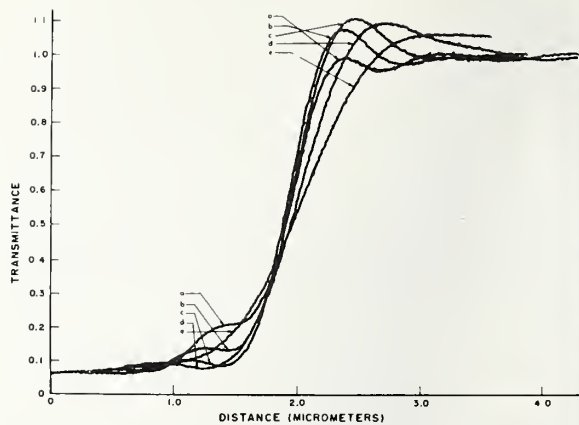


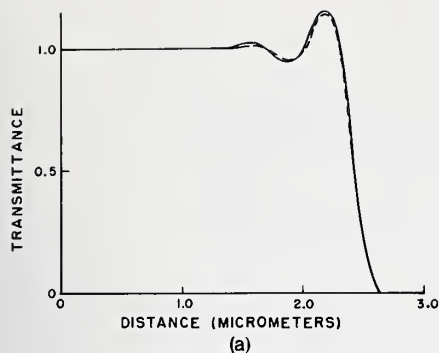
Fig. 18. Experimental image profiles at the edge of a nominal 10- $\mu$ m clear line as a function of focus displacement in submicrometer steps from a to e for a 0.90 objective N.A. and 0.22 condenser N.A. with the objective used at the incorrect tube length (160 mm instead of 215 mm). Registration at edge may not be accurate. Note similarity to Fig. 6.

edge location as shown in Fig. 19(a). The white light image was computed by integrating the responses at different wavelengths assuming a Gaussian spectral response (illumination and photomultiplier combined) peaked at 530 nm with a halfwidth of 160 nm. The comparable differences in the experimental curves is much greater as shown in Fig. 19(b). All the microscope objectives examined exhibited this difference to a varying degree indicating the presence of varying amounts of longitudinal chromatic aberration and chromatic difference of magnification.

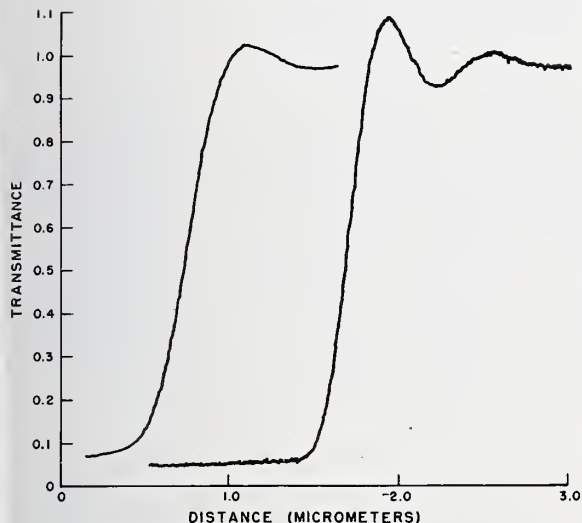
The remaining source of error is the edge quality of the photomask. The samples used were the best obtainable with less than 0.1- $\mu$ m variations barely observable optically at high magnification. However, variations in the edge response were observed. Some indication of the variation may be found in comparison of the right and left edges of the experimental profiles given in Figs. 9–15, although these profiles have been selected for edge sharpness in order to get the best possible correspondence with theory. It appears that the edge quality may be the limiting factor in the accuracy and repeatability of linewidth measurements below 10  $\mu$ m.

## Conclusions

It appears that scalar 1-D theory may be used to predict line image profiles in the optical microscope for ratios of condenser to objective numerical apertures less than 1.0 and objective numerical apertures equal to or less than 0.9. Correspondence between theoretical and experimental profiles was found for a microscope operated under the following conditions: (1) filtered spectrally to eliminate chromatic aberrations; (2) operated axially by moving the stage and keeping the scanning slit fixed to eliminate off-axis aberrations; and (3) using an effective scanning aperture smaller than the



(a)



(b)

Fig. 19. Comparison of (a) theoretical (---) white light and (—) filtered green light and (b) experimental white light (left) and filtered green light (right) edge profiles with microscope parameters same as Fig. 3. Theoretical curve is based on diffraction-limited performance at all transmitted wavelengths.

impulse response of the objective. Under these conditions, theory predicts that accurate linewidth measurements may be made using the 25% threshold (corrected for the finite transmittance of the photomask). For ratios of condenser to objective numerical apertures less than 1.0, this threshold is nearly invariant with condenser numerical aperture, and the presence of spherical aberration providing accurate focus position is used. Focus may be determined by either maximum slope or maximum overshoot at the edge.

At this time, the only known method of determining the 25% threshold is from a photometric image scan. Measurement eyepieces frequently used for linewidth measurements, such as filar or image shearing eyepieces, measure different thresholds. Theory predicts that measurement of the 50% threshold will yield linewidth

measurement errors up to  $0.15 \mu\text{m}$  with a 0.9 N.A. objective (increasing with lower N.A.) depending on the transmittance of the photomask. The errors introduced by measurement of the wrong threshold are additive and constant for a given optical system. Attempting to correct for them by the usual calibration methods will produce greater nonlinear errors at larger and smaller linewidths than the calibration linewidth. These errors increase with defocus or spherical aberration present.

The largest contributions to variations in measurement appear to be due to (1) nonrepeatability of focus at high numerical apertures with conventional fine focus adjustments found on microscopes, (2) variation in edge quality which has a noticeable effect for state-of-the-art photomasks, and (3) the effect of chromatic aberrations in the microscope when white light is employed. These sources of error will affect measurements made with filar and shearing eyepieces as well as photometric image scans although they may be masked because of larger variations contributed by visual factors.

This research was conducted as part of the NBS program on semiconductor measurement technology with partial funding from the Defense Advanced Research Projects Agency through ARPA order 2397.

## References

1. W. Weinstein, *J. Opt. Soc. Am.* **45**, 1006 (1955).
2. P. N. Slater, *J. Opt. Soc. Am.* **49**, 562 (1959).
3. H. Osterberber and L. W. Smith, *J. Opt. Soc. Am.* **50**, 363 (1960).
4. L. W. Smith, *J. Opt. Soc. Am.* **50**, 369 (1960).
5. M. De and S. C. Som, *Opt. Acta* **9**, 17 (1962).
6. W. T. Welford, in *Optics in Metrology*, P. Mollet, Ed. (Pergamon, New York, 1960), p. 85.
7. R. Barakat, *Opt. Acta* **17**, 337 (1970).
8. L. C. Martin, *The Theory of the Microscope* (Blackie, London, 1966), pp. 332, 422-428.
9. D. N. Grimes, *J. Opt. Soc. Am.* **61**, 870 (1971).
10. S. Rowe, *J. Opt. Soc. Am.* **59**, 711 (1969).
11. H. H. Hopkins, *J. Opt. Soc. Am.* **47**, 508 (1957).
12. R. E. Kinzly, *J. Opt. Soc.* **62**, 3861 (1972).
13. W. N. Charman, *J. Opt. Soc. Am.* **53**, 415 (1963).
14. B. Richards and E. Wolf, *Proc. R. Soc. London Ser. A*: **253**, 358 (195/9).
15. B. J. Lin, IBM Research Report RC3659 (21 December 1971).
16. M. Born and E. Wolf, *Principles of Optics* (Pergamon, New York, 1965), p. 522.
17. R. E. Swing, *J. Opt. Soc. Am.* **62**, 199 (1972).
18. G. Henderson and C. Weaver, *J. Opt. Soc. Am.* **56**, 1551 (1966).
19. The apparent discrepancy between the computed Rayleigh depth of focus ( $\pm 0.35 \mu\text{m}$ ) and the experimentally determined depth of focus ( $\pm 0.1 \mu\text{m}$ ) is currently being investigated.
20. H. Layer, *Rev. Sci. Instrum.* **47**, 480 (1976).

# A Comparison of Some Optical Microscope Measurements of Photomask Linewidths\*

Dennis A. Swyt and F. W. Rosberry

Optics and Micrometrology Section  
National Bureau of Standards  
Washington, D.C.

Results of photomask linewidth measurements which depend systematically on the type of linespacing-calibrated optical microscopes used for the measurements have been observed during National Bureau of Standards work on developing calibrated photomask linewidth standards. Depending on the combination of microscope, measuring device, illumination type and object polarity present, repeatably regular differences in the apparent width of the same line, most often in the range from  $+0.25 \mu\text{m}$  to  $-0.25 \mu\text{m}$ , were seen. Opaque lines and clear spaces from 1 to  $10 \mu\text{m}$  in width on chromium-on-glass photomask-like targets were measured. For the most part, a filar eyepiece microscope and an image-shearing eyepiece microscope were used. Some data for an automatic TV/microscope system and a second type of image-shearing microscope were obtained. Results support the contention that proper calibration of measuring instruments for photomask linewidth measurements requires true linewidth standards rather than line-spacing standards.

AS A RESULT of a National Bureau of Standards study of measurement needs within the microelectronics industry,<sup>1</sup> work is proceeding at NBS on the overall problem of how to make accurate dimensional measurements of photomask pattern linewidths in the important 1 to  $10 \mu\text{m}$  range.<sup>2,3</sup> The general program includes development of photomask-like targets bearing lines of calibrated widths, and development of recommended procedures for the calibration of the measuring instruments used by industry for mask measurements.

Currently, the usual instrument for measurement of pattern elements on production photomasks is the optical microscope. Most measurements are made visually, using either filar or image-shearing micrometer eyepieces; some are made using automatic scanning-type instruments.

The purpose of this paper is to present the results of an empirical study of the relationships between optical microscopes as used in the microelectronics industry and the linewidth measurement results they yield. The purpose of the study, in turn, was twofold: to determine the nature and magnitude of the "discrepancies" in line-

width measurements encountered in industry,<sup>1,2</sup> and to establish a basis for recommended procedures for instrument calibration and use.

## The Equipment

The majority of measurements were made on two systems: a monocular filar-eyepiece microscope and a binocular image-shearing microscope. Also reported are some measurements made with a monocular image-shearing microscope and an automatic TV microscope system.

All microscopes were of the general quality and type typically used for photomask inspection in industry. Each microscope was used with 0.95 N.A. objective lenses for bright-field transmission (substage) and bright-field reflection (surface) illumination. Each had electronic digital display of linewidth measurement readings.

The monocular filar-eyepiece microscope was equipped with an 80X objective, a 2X extender and a 16X eyepiece for an overall magnification of 2560X. The binocular image-shearing microscope was equipped with a maximum 63X objective, nominal 10X eyepiece, and an estimated 1.5X added magnification for a probable overall magnification of 1000X. The automatic TV microscope system had an 80X objective; the effective magnification on the TV viewing screen was not determined. The filar system's condenser had a 0.90 N.A. while the numerical apertures of the built-in condensers of the other two systems were not determined.

\*This effort was conducted as part of the Micrometrology Program and of the Semiconductor Technology Program at the National Bureau of Standards and was funded by the National Bureau of Standards and by the Defense Advanced Research Projects Agency Order 2397. Contribution of the National Bureau of Standards and not subject to copyright.

Each microscope was used in the unmodified form as supplied by the manufacturer and set up as described in the operating manuals. The TV-microscope system was adjusted according to instructions to read a prescribed "line-to-space ratio" (width of opaque line relative to width of clear space) using a standard supplied with the instrument.

### The Targets

The majority of measurements reported were made on NBS prototype line-width standards; hard-surface non-conformable masks commercially made to NBS specifications. One such target was of "black chrome", that is, chromium oxide-on-chromium-on-glass. A second such target was of "bright chrome," that is, chromium-on-glass. The overall pattern of 1, 3, and 10  $\mu\text{m}$ -wide opaque lines and clear spaces on the NBS target is shown in Fig. 1. Measurements were made on the single isolated lines and spaces.

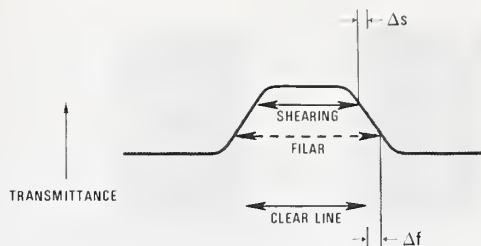
Some measurements briefly noted here for comparison were made earlier<sup>4</sup> on the best target then made available to NBS, a widely used commercial photomask standard of bright chrome-on-glass bearing nominally 2, 5, and 10  $\mu\text{m}$  wide clear spaces only.

### Procedure

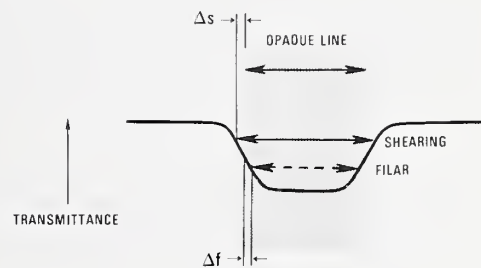
Measurements on each photomask line were made in groups of ten on ten separate occasions over periods from 5 to 10 days. For each of the ten separate occasions, the light source of each microscope was restarted and allowed to warm-up for 30 minutes at the same power setting, and the target restaged. For each of ten separate measurements on any one occasion, each microscope was refocused. One operator performed all of the visual measurements. The significance of the measurement repetition scheme and the implications of its results will be discussed below.

Each microscope had been calibrated at its working magnification using lines of known spacing. These line spacings had been determined to an accuracy of better than  $\pm 0.01 \mu\text{m}$  by direct and transfer calibrations from the NBS line standard interferometer.<sup>5</sup>

The calibration procedure followed was the conventional one in which the drum readings of the micrometer



(a) Clear



(b) Opaque

Fig. 1—Schematic of clear and opaque line image profiles in transmitted light for an optical microscope with filar and image-shearing measurement eyepieces;  $\Delta f$  is the measurement error for the filar eyepiece, and  $\Delta s$  is the measurement error for the image-shearing eyepiece.

screw of a visual eyepiece, or their analogues in electronic instruments, are calibrated in terms of known center-to-center spacings of line scale graduations.

This method has a deficiency with regard to accurate linewidth measurements and it is an object of this paper to point it out. Since linewidths are measured between a left edge and a right edge of a line, linespacing calibrations of a measuring instrument can neither reveal the presence of nor compensate for any broadening or narrowing of the image of a line due to optical effects of object size, lens aberrations, degree of illumination coherence, etc. The consequences of this deficiency in the use of line-scale calibration technique for linewidth measurements are demonstrated later in this paper.

Table I—Apparent Widths of Clear and Opaque Lines as Measured in Transmission and Reflection Illumination with Filar and Image-Shearing Eyepiece Microscopes; "Black Chrome" Target.

TRANSMISSION ILLUMINATION			
WIDTH OF OPAQUE LINE			
Nominal	Filar	Shear	
1 $\mu\text{m}$	0.91 $\mu\text{m}$	1.19 $\mu\text{m}$	
3	2.90	3.14	
10	9.77	10.03	
WIDTH OF CLEAR SPACE			
Nominal	Filar	Shear	
1 $\mu\text{m}$	1.12 $\mu\text{m}$	0.86 $\mu\text{m}$	
3	3.17	2.91	
10	10.16	9.96	

REFLECTION ILLUMINATION			
WIDTH OF OPAQUE LINE			
Nominal	Filar	Shear	
1 $\mu\text{m}$	1.04 $\mu\text{m}$	1.08 $\mu\text{m}$	
3	3.07	3.08	
10	9.98	9.99	
WIDTH OF CLEAR SPACE			
Nominal	Filar	Shear	
1 $\mu\text{m}$	0.78 $\mu\text{m}$	1.00 $\mu\text{m}$	
3	2.86	2.99	
10	9.91	10.03	

Table II—Apparent Widths of Clear and Opaque Lines as Measured in Transmission and Reflection Illumination with Filar and Image Shearing Eyepiece Microscopes; "Bright Chrome" Target.

TRANSMISSION ILLUMINATION			
WIDTH OF OPAQUE LINE			
Nominal	Filar	Shear	
1 $\mu\text{m}$	0.61 $\mu\text{m}$	0.98 $\mu\text{m}$	
3	2.62	2.92	
10	9.50	9.91	
WIDTH OF CLEAR SPACE			
Nominal	Filar	Shear	
1 $\mu\text{m}$	1.21 $\mu\text{m}$	0.98 $\mu\text{m}$	
3	3.30	3.00	
10	10.30	10.08	

REFLECTION ILLUMINATION			
WIDTH OF OPAQUE LINE			
Nominal	Filar	Shear	
1 $\mu\text{m}$	0.79 $\mu\text{m}$	0.74 $\mu\text{m}$	
3	2.78	2.71	
10	9.56	9.68	
WIDTH OF CLEAR SPACE			
Nominal	Filar	Shear	
1 $\mu\text{m}$	1.07 $\mu\text{m}$	1.24 $\mu\text{m}$	
3	3.18	3.27	
10	10.25	10.37	

Prior to calibration, the mechanical movement of each visual eyepiece was checked quantitatively for linearity and repeatability. Contributions to the imprecision of measurements coming from this source, it was concluded, would be small compared to uncertainties in locating line edges. Similarly, effects of cosine errors (arising when the axis of measurement is not perpendicular to the measured line) were computed. Conscious alignment of the target line (perpendicular to the direction of reticle travel, sheared image travel or TV scan sweep) easily reduced misalignments to less than  $2.5^\circ$ , corresponding to errors less than  $0.01 \mu\text{m}$  in  $10 \mu\text{m}$ .

The mean widths of nominally 1, 3, and  $10 \mu\text{m}$ -wide opaque lines and clear spaces as measured in transmission (substage) and reflection (surface) illumination appear in Table I for a black-chrome NBS target and in Table II for a bright-chrome NBS target.

Each entry in Tables I and II is the arithmetic mean of 100 measurements taken in groups of ten on ten occasions. The computed average standard deviations of these means ( $\sigma_M$ ) are  $0.014 \mu\text{m}$  for the filar-eyepiece measurements and  $0.009 \mu\text{m}$  for the image-shearing eyepiece measurements.

#### Linewidth Measurement Results

The results in Tables I and II show some general trends between the apparent sizes of lines measured with the two different types of micrometer eyepieces. For example, in the case of a clear line on an opaque background viewed in transmitted bright-field light:

$$w_f > w_s \quad (1)$$

and for the same clear line viewed in reflected bright-field light:

$$w_f < w_s \quad (2)$$

where  $w_f$  is the width measured by filar, and  $w_s$  is the width measured by shear.

The existence of such trends for some combinations of three viewing variables, namely, eyepiece (filar or shear), illumination (transmission or reflection), and object polarity (clear or opaque lines), leads to the development of a phenomenological model to account for this behavior.

In an article describing the NBS photomask program, published before an NBS target with both clear and opaque lines became available, the following argument was given<sup>2</sup>: Figure 2a may be considered to represent an opaque line illuminated in reflection or a transparent line illuminated in transmission; its 'width' at a high intensity level on the image profile is *less* than its 'width' at a low intensity level. Figure 2b may be considered to represent an opaque line illuminated in transmission or a transparent line illuminated in reflection; its 'width' at a high intensity level is *greater* than its 'width' at a low intensity level. Given that a shearing eyepiece locates an edge high on this type of image profile (e.g. near the 50 percent intensity), and that a filar eyepiece locates that edge low on this profile (e.g. near the 10 percent intensity), the figure is consistent with relationships (1) and (2) given above.

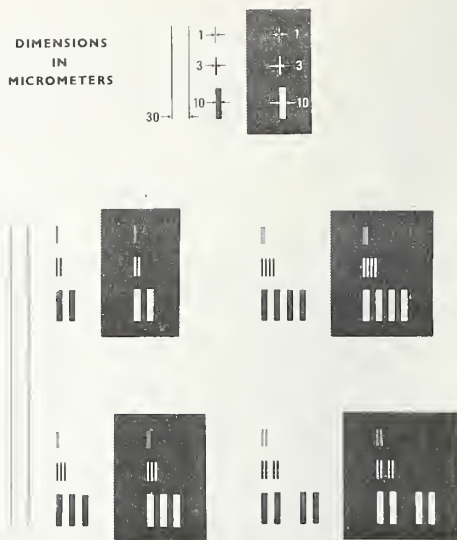


Fig. 2—Basic pattern of the NBS prototype photomask line-width-measurement target.

Table III—Relationships of Apparent Linewidths under Various Viewing Conditions. (W—Apparent Width; F—Filar; S—Image Shearing; T—Transmission; R—Reflection; C—Clear Space; O—Opaque Line).

		Clear Line	Opaque Line
2a	Transmission	$w_F > w_S$	$w_F < w_S$
	Reflection	$w_F < w_S$	$w_F > w_S^*$
		Filar	Shearing
2b	Clear Line	$w_T > w_R$	$w_T < w_R$
	Opaque Line	$w_T < w_R$	$w_T > w_R$
		Transmission	Reflection
2c	Filar	$w_C > w_O$	$w_C < w_O$
	Shear	$w_C < w_O$	$w_C > w_O^*$

The phenomenological model of Fig. 2 implies, however, a number of other relationships between apparent widths. For clear-space and opaque-line objects of equal widths, Table III gives twelve relationships of apparent image widths for the different combinations of viewing variables.

Comparison of Tables I and II with Table III shows that all but two of the twelve relationships in Table III are present in the experimental results of Tables I and II; the two odd relationships (asterisked in Table III) both involve the image-shearing eyepiece/opaque line combination. The cause of these deviations from expected behavior is not known.

The most consistent relationships are presented in Table IV where differences between filar and image-

shearing results are shown in clear and opaque lines viewed in transmitted light (the usual means of photomask inspection). These systematic differences occur even though both measuring eyepieces were calibrated with the same line scale and the same line spacing. Further, these differences are significantly greater than their uncertainty; the standard deviation of the differences of these mean line widths is  $0.05 \mu\text{m}^*$ .

The differences in Table IV are also equal within measurement uncertainties with results obtained early in the program on a non-NBS target.<sup>3</sup> For example, measurements made with filar eyepiece, image-shearing eyepiece and TV microscope systems on the same clear space on a bright chrome target yielded apparent widths of  $2.25 \mu\text{m}$  (filar),  $1.95$  (shear) and  $2.55 \mu\text{m}$  (TV); the difference between the filar and shear values is  $0.3 \mu\text{m}$  compared to the average value in Table IV of  $0.24 \mu\text{m}$ .

### Measurement Statistics

The many individual linewidths given in Tables I and II were measured repeatedly to: (1) obtain stable, representative mean values; and (2) gauge the scatter likely encountered by others doing similar measurements. The repetitions were done on an "occasion," usually the morning of one day, to establish a stable mean  $\bar{x}_i$  for that day:

$$\bar{x}_i = \frac{1}{n} \sum_{j=1}^n x_{ij} \quad (3)$$

where  $n$  = number of measurements on one occasion

$j$  = individual measurement

$i$  = occasion

and then repeated over a number of occasions, usually mornings of following days, to establish an over-all-occasions mean  $\bar{\bar{x}}$ :

$$\bar{\bar{x}} = \frac{1}{k} \sum_{i=1}^k \bar{x}_i \quad (4)$$

where  $k$  = number of occasions

Measurements were repeated often ( $n = 10$ ,  $k = 10$ ) in order to obtain reasonable approximations of the limiting means on  $k$  individual occasions  $\mu_i$ :

$$\mu_i = \lim_{n \rightarrow \infty} \bar{x}_i \quad (5)$$

and the one limiting mean of all occasions:

$$\mu = \lim_{k \rightarrow \infty} \bar{\bar{x}} \quad (6)$$

The repeated measurements were characterized by scatter among the individual measurements on individual days and among the means on different days. Used to describe the behavior was an overall standard deviation having two components<sup>6,7</sup>:

$\sigma_w$ : a "within occasion" standard deviation which statistically relates  $x_{ij}$ , a single measurement on one occasion, to  $\mu_i$ , the limiting mean of that one occasion; and

$\sigma_b$ : a "between occasion" standard deviation which statistically relates  $\mu_i$ , the limiting mean of one occasion, to  $\mu$ , the limiting mean of all occasions.

While both  $\sigma_w$  and  $\sigma_b$  are population standard devi-

Table IV—Differences between Apparent Widths of Lines on a "Black-Chrome" Target as Measured in Transmitted Light with Filar and Image Shearing Eyepieces Calibrated with Line Spacings.

Clear Spaces		
Filar	Shear	Difference
1.12 $\mu\text{m}$	0.86 $\mu\text{m}$	+ 0.26 $\mu\text{m}$
3.17	2.91	+ 0.26
10.16	9.96	+ 0.20
Opaque Lines		
Filar	Shear	Difference
0.91 $\mu\text{m}$	1.19 $\mu\text{m}$	- 0.28 $\mu\text{m}$
2.90	3.14	- 0.24
9.77	10.03	- 0.26

ations related to limiting means, good estimates ( $\sigma_w$  and  $\sigma_b$ ) can be achieved by computations where  $n$  and  $k$  are large but finite. In that case,  $x_{ij} \approx \mu_i$  and  $\bar{\bar{x}} \approx \mu$ ; then  $\sigma_w$  and  $\sigma_b$  can be computed from:

$$\hat{\sigma}_w^2 = \frac{1}{k} \sum_{i=1}^k \sigma_{w_i}^2 = \sum_{i=1}^k \sum_{j=1}^n \frac{(x_{ij} - \bar{x}_i)^2}{k(n-1)} \quad (7)$$

$$\hat{\sigma}_b^2 = \sum_{i=1}^k \frac{(x_i - \bar{\bar{x}})^2}{(k-1)} - \frac{\hat{\sigma}_w}{n} \quad (8)$$

Combination of the "within occasion" variance ( $\sigma_w^2$ ) and the "between occasion" variance ( $\sigma_b^2$ ) produced one which relates  $\bar{\bar{x}}$ , the computed mean of numerous occasions, to  $\mu$ , the limiting mean of all occasions:

$$\sigma_M^2 = \frac{\sigma_w^2 + \frac{\sigma_b^2}{n}}{k} \quad (9)$$

They may also be combined to give the variance which relates  $x_{ij}$ , a single measurement on one occasion to  $\mu$ :

$$\sigma_s^2 = \sigma_b^2 + \sigma_w^2 \quad (10)$$

For purposes of comparison and clarity, Table V lists the different variances ( $\sigma^2$ ), their relationships to each other, and the variables and means which they relate.

Given for inspection in Table VI are the computed standard deviations (in  $\mu\text{m}$ ) associated with the individual mean linewidths given in Tables I and II for clear lines viewed in transmitted light. Similar results were obtained for reflected light measurements on clear lines as well as for both types of illumination on opaque lines. The relative independence of each type of  $\sigma$  from effects of nominal linewidths, illumination type, and object polarity allows the characterization of these  $\sigma$ 's by the rms values ( $\sigma$ ) given in Table VII.

These average  $\sigma$ 's apply to the filar and image-shearing measurements made on the black-chrome NBS prototype target. For these conditions, the relative precision of the image-shearing eyepiece data was about twice as good.

\*Derived by combining the  $\sigma_M$  for the filar and image-shearing entries of Table VII.

**Table V—Variances ( $\sigma^2$ ) Useful for Describing Data which Exhibits "Within Group" and "Between Group" Scatter.**

TYPE OF VARIANCE	RELATED VARIANCES	VARIABLE AND MEAN WHICH $\sigma^2$ RELATE	DESCRIPTION
$\sigma_w^2$		$x_{ij} \rightarrow \mu_i$	Relates single measurement on one occasion to limiting mean for that one occasion
$\sigma_B^2$		$\mu_i \rightarrow \mu$	Relates limiting mean of one occasion to limiting mean of all occasions
$\sigma_s^2$	$= \sigma_B^2 + \sigma_w^2$	$x_{ij} \rightarrow \mu$	Relates single measurement on one occasion to limiting mean of all occasions
$\sigma_i^2$	$= \sigma_w^2/n$	$\bar{x}_i \rightarrow \mu_i$	Relates sample mean of measurements on one occasion to limiting mean for that one occasion
$\sigma_m^2$	$= \sigma_B^2 + \sigma_i^2$	$\bar{x}_i \rightarrow \mu$	Relates sample mean of measurements on one occasion to limiting mean of all occasions
$\sigma_M^2$	$= \sigma_m^2/k$	$\bar{x} \rightarrow \mu$	Relates sample mean of numerous occasions to limiting mean of all occasions

as that of the filar data. Both types of data exhibit large day-to-day variations ( $\sigma_B$ ) which demonstrates that any evaluation of the "precision of an instrument" requires not only a careful definition of the meaning and scope of the term, but an extended evaluation/data taking period to take these effects into account.

Table VII also provides quantitative answers to questions related to the purposes given at the beginning of this section: (1) on how well the mean values of Tables I and II are known. Using  $\sigma_M$  in Table VII to determine the three-standard-deviation limit ( $3\sigma_M$ ), one could say that the mean of an "infinite" number of measurements on each line would be no further than  $0.042 \mu\text{m}$  away from the filar values given and no further than  $0.027 \mu\text{m}$  away from the shear values given; and (2) on how much scatter is inherent in the data (and supposedly in the data of other people doing similar measurements).  $\sigma_s$  in Table VII shows that the likely range,  $R$ , of single measurements taken on ten different occasions ( $R = 3.077 \bar{\sigma}_s$ ) would be  $0.186 \mu\text{m}$  for the filar data and  $0.105 \mu\text{m}$  for the shear data, whereas the ranges on one day would be the smaller  $0.135 \mu\text{m}$  and  $0.063 \mu\text{m}$  for the filar and shear, respectively.

The general statistical character of these results is similar to that obtained from the earlier application of the same ten by ten repetition scheme to another photomask-like standard of bright-chrome on glass, one sold commercially. On that target, measurements were done with a vernier filar eyepiece, a monocular image-shearing eyepiece, and a commercial automatic TV system. The computed  $\sigma$ 's are shown in Table VIII.

**Summary of Findings**

Some of the more important effects observed during this study were:

(1) For optical microscopes calibrated with line-spacings, the apparent widths of photomask lines depend systematically on the specific combination of measuring device, illumination type and object polarity used in the measurements. Both visual and automatic types of measuring devices are susceptible to these effects.

**Table VI—Computer Deviations ( $\sigma$ ) for Repeated Measurements with Filar and Image-Shearing Eyepieces of 1, 3, and 10  $\mu\text{m}$ -Wide Lines in Transmitted Light.**

Filar Eyepiece				
W	$\sigma_W$	$\sigma_B$	$\sigma_M$	$\sigma_S$
1 $\mu\text{m}$	0.047	0.028	0.010	0.055
3	0.044	0.052	0.017	0.068
10	0.044	0.045	0.015	0.063
Image-Shearing Eyepiece				
W	$\sigma_W$	$\sigma_B$	$\sigma_M$	$\sigma_S$
1 $\mu\text{m}$	0.021	0.024	0.008	0.030
3	0.020	0.025	0.008	0.032
10	0.022	0.035	0.011	0.041

**Table VII—Mean Deviations ( $\sigma$ ) Averaged Over Lines of Three Widths for Both Illuminations and Both Object Polarities for the "Black-Chrome" Target.**

	$\bar{\sigma}_W$	$\bar{\sigma}_B$	$\bar{\sigma}_M$	$\bar{\sigma}_S$
FILAR	0.045	0.043	0.014	0.062
SHEAR	0.021	0.028	0.009	0.035

**Table VIII—Computed Deviations ( $\sigma$ ) for Repeated Measurements with Filar, Image-Shearing, and TV Microscope Systems on a Commercial, Bright Chrome Linewidth Standard.**

MEASURING DEVICE	$\sigma_W$	$\sigma_B$	$\sigma_M$	$\sigma_S$
FILAR	0.078	0.082	0.027	0.113
SHEAR	0.015	0.034	0.011	0.037
TV	0.010	0.028	0.009	0.030

(2) The sign of the difference in the apparent widths of the same line as measured with different eyepieces (for measuring devices in general) may change predictably as the polarity of the object (clear space/opaque line) or the illumination (transmission/reflection) changes.

- (3) The magnitude of the differences in the apparent widths of the same line as measured with different eyepieces may be relatively independent of the nominal linewidth over the range 1 to 10  $\mu\text{m}$ .
- (4) The presence of even fairly large systematic differences of the incremental or "offset" type may be masked by scatter in data, due probably to changes in focus settings or criteria, light levels, lenses, etc.
- (5) Total variations (that is, scatter) in linewidth measurement results may have significant day-to-day as well as reading-to-reading components.

#### Conclusion

These results and others drawn from measurements on photomask-like targets over ranges of linewidths, measuring-device types, and operating conditions, form the basis for some major conclusions, either deductive or inferential:

- (1) Proper calibration of devices for the measurement of photomask linewidths requires linewidth standards rather than line spacing standards. The results show that calibration of the overall magnification of a microscope with line spacings cannot remove from measurements (i.e., cannot "calibrate out") the effects of image edge shifts in image formation and location.
- (2) Any realistic assessment of the precision of either the measurement results, the measurement process, or the measuring instrument must include the effect of long-term or "day-to-day" variations. Computing the rms deviation of a few measurements taken at one sitting does not give a realistic estimate of variations likely to be encountered over either similar or longer periods.

While this report deals with precision, or the closeness together, of results, it does not deal with the accuracy, or closeness to the "truth," of those results. Still under development at this time are the prerequisites for a determination of accuracy in photomask linewidth measurements: accepted conceptual definitions of what to measure, established procedures of how to measure it, and recognized physical standards against which to compare results. Work at NBS on the development of calibrated linewidth standards is underway with a limited issue of prototype targets scheduled for industry evaluation during 1977.

#### References

1. "Semiconductor Measurement Technology: Optical and Dimensional Measurement Problems with Photomasking in Microelectronics" J. M. Jerke, NBS Special Publication 400-20, available from U.S. Government Printing Office, Washington D.C. 20402, CD Catalogue No. C13.10:400-20.
2. D. Swyt, "NBS Program in Photomask Linewidth Measurements," *Solid State Technology*, April 1976.
3. "Semiconductor Measurement Technology: Accurate Linewidth Measurements on Integrated Circuit Photomasks," J.M. Jerke, D. Nyssonen, F. W. Rosberry, F. E. Scire, R. E. Swing, D. A. Swyt, R. D. Young, NBS Special Publication 400-43, available from U.S. Government Printing Office, Washington, D.C. 20402.
4. "Semiconductor Measurement Technology: Progress Report, April/June 1976," W. Murray Bullis, ed., NBS Special Publication 400-19, available from U.S. Government Printing Office, Washington, D.C. 20402, CD Catalogue No. C13.10:400-19.
5. K. E. Gilliland, H. D. Cook, K. D. Mielenz, and R. B. Stephens, "Use of a Laser for Length Measurements by Fringe Counting," *Metrologia* vol. 2, pp. 95-98 (1966).
6. Eisenhart, C., "Realistic Evaluation of Precision and Accuracy of Instrument Calibration Systems," *J. Res. National Bureau of Standards (U.S.)*, vol. 67C, pp. 21-47, (1963).
7. Mandel, J., "Repeatability and Reproducibility," *Materials Research and Standards*, vol. 11, no. 8, 8-15, 52 (August 1971).

**COMPARISON OF LINEWIDTH MEASUREMENTS  
ON AN SEM/INTERFEROMETER SYSTEM AND  
AN OPTICAL LINEWIDTH-MEASURING MICROSCOPE\***

John M. Jerke, Arie W. Hartman, Diana Nyssonen,  
Richard E. Swing, and Russell D. Young  
Institute for Basic Standards  
National Bureau of Standards  
Washington, D. C. 20234

and

William J. Keery  
Institute for Applied Technology  
National Bureau of Standards  
Washington, D. C. 20234

Abstract

In the current linewidth-measurement program at the National Bureau of Standards, the primary measurement of micrometer-wide lines on black-chromium artifacts is made with an interferometer located in a scanning electron microscope (SEM). The data output consists of a line-image profile from the electron detector and a fringe pattern from the interferometer. A correlation between edge location and fringe location is made for both line edges to give the linewidth in units of the wavelength of a He-Ne laser. A model has been developed to describe the interaction of the electrons with the material line and thereby relate a threshold value on the SEM image profile to a selected point on the material line. An optical linewidth-measuring microscope is used to transfer the primary measurements to secondary measurement artifacts these artifacts will be used to transfer the linewidth measurements to the integrated-circuit industry. Linewidth measurements from the SEM/interferometer system and the optical linewidth-measuring microscope are compared, and the level of measurement uncertainty for each system is discussed.

Introduction

In the current linewidth-measurement program<sup>1,2</sup> at the National Bureau of Standards (NBS), the basic goals include making primary linewidth calibration of 1 to 10-micrometer ( $\mu\text{m}$ ) wide lines on artifacts similar to integrated-circuit (IC) photomasks and providing the IC industry with calibrated measurement artifacts and measurement procedures for optical microscopes. The calibration of artifacts and instruments is essentially a refined form of measurement. In particular, calibration is often a comparison procedure in which an unknown, or test item, is compared with a known, or standard, and the value of the test item is determined from the accepted value of the standard.

For length calibration, several calibrations are successively linked in order to relate the generally unaccessible defined unit of length<sup>3</sup> (wavelength of radiation from krypton 86) to an accessible artifact for the user. The hierarchy of the linewidth calibration is shown in Figure 1. The first stage relates the physical standard for the defined unit of length to the width of a material line on a photomask-like artifact. The primary measurement system includes a polarization interferometer located in a scanning electron microscope (SEM). The wavelength of the interferometer laser is monitored by comparison with the radiation wavelength from a stabilized laser which, in turn, is compared with the krypton radiation. This system is considered a primary measurement system and is too time consuming and costly for the routine calibration of user artifacts. Therefore, at the second stage of the linewidth calibration, a secondary measurement system relates the linewidths calibrated by the SEM/interferometer on the first artifact to linewidths on the user artifact. The secondary measurement system is an optical linewidth-measuring microscope with modifications for optimal performance. The third stage of the calibration process relates the linewidths calibrated by the optical linewidth-measuring microscope to the readout of a linewidth-measurement instrument, such as an optical microscope, used in the industry. The user, in turn, makes measurements of unknown photomask linewidths with this calibrated instrument.

\*This work was conducted as part of the Semiconductor Technology Program at the National Bureau of Standards and was supported by the Defense Advanced Research Projects Agency under Order 2397 and by the NBS. Contribution of the National Bureau of Standards, not subject to copyright.

SEM/INTERFEROMETER SYSTEM

A schematic of the SEM/interferometer system is shown in Figure 2. This system consists of a double-pass polarization interferometer located in an SEM. In an overly simple view of the measurement process, a very small beam of electrons, normally a few hundred angstroms ( $\text{\AA}$ ) in diameter, is focussed at normal incidence on the line sample and remains relatively stationary as the sample is moved. The interferometer records the motion of the sample from one line edge to the other, and the location of the line edges is determined by the change in the electron-scattering coefficient<sup>4</sup>.

In this system, the SEM is used as a very fine fiducial mark or cross hair for locating the line edges. Since conventional SEM's are not designed to operate in this mode, a number of compromises have been made in the operation of the SEM. These compromises include: (1) replacing the normally used stage with a specially designed stage assembly consisting of two substages for moving the linewidth sample; (2) operating the electron beam in a line-sweep mode with approximately  $1\text{-}\mu\text{m}$  sweep length on the sample; and (3) operating the SEM at 10 keV to reduce contamination buildup on the sample even though higher operating voltages give a smaller effective electron-beam diameter.

One substage uses two piezoelectric drivers with orthogonal motions to position the linewidth sample over a  $10\text{-mm}$  by  $10\text{-mm}$  area in the SEM field of view. The other substage is a mechanical flexure-pivot stage which moves the line from one edge to the other; this stage has a maximum travel of about  $60\ \mu\text{m}$  and a smoothness of better than  $0.001\ \mu\text{m}$  over a few micrometers. A photograph of a flexure-pivot stage is shown in Figure 3. This stage uses a stack of piezoelectric elements to drive the stage at one point and, by means of flexure-pivot lever arms, the original movement is magnified about 20X.

Because the electron beam can not be held stationary during scanning in this SEM, the beam is operated in a line-sweep mode as shown schematically in Figure 4. In this mode, the beam averages the imperfections in the line, such as edge raggedness, over the sweep length of approximately  $1\ \mu\text{m}$ . This sweep length is comparable to the effective length of the scanning slit in the optical linewidth-measuring microscope.

The spot size of the electron beam affects the ultimate precision and accuracy of the linewidth measurements. Beam diameters on the order of  $200\ \text{\AA}$  are theoretically achievable with the present SEM operating at 20 keV. However, in order to reduce the contamination buildup on the sample, it is necessary to operate the SEM around 10 keV which produces a larger beam-spot diameter. Contamination is also reduced by the use of a nitrogen cold trap. Most of the contamination occurs during focussing, repeated scanning, or waiting time; therefore, by moving to a new area of the line just before making a measurement, minimal contamination results.

A sample plot of the output from the two data channels of the SEM/interferometer is shown in Figure 5. The SEM and interferometer data are shown with respect to the same linear time base, and the interval between successive data points is 1 ms. The SEM output signal is used to determine the line-edge locations so that the linewidth, or the separation of the line edges, can be related to a number of whole fringes plus fringe fractions from the interferometer output signal. Therefore, the electron interaction with the material line must be modeled in order to specify accurately the true line-edge locations from the SEM signal or edge trace.

An illustration of the line edge which is assumed in the model is shown schematically in Figure 6(a). The line edge is a linear ramp rising at an angle  $\phi$  from the glass substrate to the top of the chromium-oxide layer on a black-chromium artifact. The incident electron beam is assumed to have a Gaussian distribution of electrons. For the model, it is necessary to specify a value of  $\phi$ , the diameter of the electron beam, the thickness of the chromium/chromium-oxide layer, and the secondary-electron emission coefficients of the glass substrate, chromium, and chromium oxide. A line-edge trace calculated from this model is compared with an experimental SEM trace in Figure 6(b). The model fits the data well in the region of the edge. In the region past the edge on the chromium-oxide side, the SEM output does not fall off as rapidly as the model predicts. This may be evidence of either electrical charging of the sample or "bloom"<sup>5</sup>.

In order to get a match between optical and SEM measurements, the line-edge location is defined as the point on the line slope corresponding to a 25-percent intensity transmittance. Figure 7 shows the correspondence between the line-edge locations on the model and the line-edge locations on the SEM image profile. The midpoint of the sloped portion of the SEM image profile corresponds to the start of the edge slope in the model. A correction term  $\Delta w$  is added, or subtracted, from the midpoint location (depending on whether the line is clear or opaque) so that the edge is located at the physical thickness of the line corresponding to the 25-percent intensity transmittance. For a black-chromium artifact with  $\phi = 55^\circ$ , the correction term is  $\pm 0.023\ \mu\text{m}$  for one edge or  $\pm 0.046\ \mu\text{m}$  for a linewidth measurement.

Optical Linewidth-Measuring Microscope

The basic approach to developing the secondary measurement system is the idea of an image-scanning optical microscope for which the line-image profiles agree well with theoretical, or calculated, profiles. Theoretical and experimental results<sup>6</sup> show the following requirements for this optical microscope: (1) a scanning slit capable of examining detail smaller than the diameter of the Airy disc of the imaging

optics<sup>7</sup>; (2) a ratio of condenser numerical aperture (N.A.) to objective numerical aperture that provides sufficient coherence so that the analytic expression for the transmittance threshold corresponding to line-edge locations in coherent illumination can be used; (3) monochromatic illumination in order to avoid chromatic aberrations associated with white light; (4) viewing the sample only on the optical axis in order to avoid off-axis aberrations; and (5) ability to control focus setting in sub-micrometer steps.

The optical linewidth-measuring microscope based on these considerations is shown in Figure 8. The major differences between this system and commercially available measurement systems with image-scanning optical microscopes include: (1) an effective scanning slit measuring  $0.13 \mu\text{m}$  by  $1.3 \mu\text{m}$ ; (2) a 150-W tungsten-halogen lamp with a filter for green light (560 nm) and a hot mirror for reducing the heat transferred to the optics; (3) a mechanical stage driven at typical speeds of  $0.5 \mu\text{m/s}$  or less by a combination of a stepping motor and function generator<sup>8</sup>; and (4) a piezoelectric focus mechanism that is adjustable to better than  $0.1 \mu\text{m}$ . An x-y recorder is used primarily for monitoring the accuracy of focus. Best focus corresponds to a maximum intensity overshoot at the edge in the image profile. (For example, see Figure 9.) The positional readout of the stage is given by a linear-voltage transducer (LVTD) gage. A microprocessor records data from the LVTD gage and the photometer. Standard operating conditions for linewidth measurements include a 0.60 N.A. condenser and 0.90 N.A. objective.

The choice of line-edge location for the image profiles generated by the optical linewidth-measuring microscope is based on the theory of partially coherent imaging<sup>9</sup>. The 25-percent intensity transmittance appears to be the best threshold for edge location. This threshold cannot be consistently distinguished in a visual-measurement system, but can be repeatedly located on the image profiles of the optical linewidth-measuring microscope. For an artifact with a finite transmittance in the opaque area, the 25-percent threshold must be corrected. The corrected threshold  $T_c$  is given by

$$T_c = 0.25 (1 + \sqrt{T_0})^2$$

where  $T_0$  is the relative transmittance of the opaque area or background. For example, with  $T_0 = 0.04$ , the corrected threshold is 36 percent. The resulting change in the edge location for a line imaged with a 0.90 N.A. objective is  $0.04 \mu\text{m}$ ; thus, the uncorrected threshold gives a linewidth error of  $0.08 \mu\text{m}$  in this case.

Figure 9 shows calculated and experimental line-image profiles of a nominally  $10\text{-}\mu\text{m}$  wide clear line for an optical microscope. The experimental profile is from the optical linewidth-measuring microscope. The calculated profile is computed for a linewidth corresponding to the width of the experimental profile at the corrected threshold. For the calculated profile, the background transmittance is assumed to be zero, whereas for the experimental profile, the background transmittance is approximately 2.5 percent. Therefore, differences between the calculated and experimental curves in the low-transmittance region are attributed, in part, to the difference in background transmittance.

Figure 10 shows calculated and experimental line-image profiles of a  $1\text{-}\mu\text{m}$  wide line for an optical microscope. There is better agreement between these profiles than between the corresponding profiles in Figure 9 because the calculated profile in Figure 10 takes into account the background transmittance of the black chromium. The remaining differences between the calculated and experimental profiles appears to be related to the physical profile of the line as compared to the ideal edge assumed in the calculated case. Although raggedness along the line edge is barely visible in SEM photomicrographs, some variations in line-edge profiles for different scan areas of the line have been detected.

#### Comparison of Linewidth Measurements

Table 1 shows linewidth measurements made with the SEM/interferometer and the optical linewidth-measuring microscope for clear and opaque lines on a black-chromium artifact. These linewidth measurements are the mean values for multiple measurements. The linewidth measurements from the SEM/interferometer have been corrected for  $2(\Delta w)$ . (See Figure 7.) Based on other experimental data, the  $3\sigma$  standard deviation associated with repeated measurements on a single occasion is  $0.016 \mu\text{m}$  for the SEM/interferometer and  $0.025 \mu\text{m}$  for the optical microscope.

There is essentially no difference in the mean values for the opaque lines as measured on the SEM/interferometer and optical microscope. For the clear lines, however, the differences are  $0.13 \mu\text{m}$  for the nominally  $1\text{-}\mu\text{m}$  wide line and  $0.34 \mu\text{m}$  for the nominally  $3\text{-}\mu\text{m}$  wide line. Part of these differences is probably due to the measurement uncertainties associated with each measurement system. For the optical microscope, the measurement uncertainty is estimated to be  $\pm 0.10 \mu\text{m}$ . For the SEM/interferometer, the uncertainty is not so well characterized, but is estimated to be smaller than  $\pm 0.10 \mu\text{m}$ . The SEM/interferometer system has the potential for a significantly smaller uncertainty than the optical microscope as a result of the better resolution of the SEM. The relatively large difference of  $0.34 \mu\text{m}$  appears to be an anomaly which is currently under investigation.

For both the SEM/interferometer and the optical microscope, the uncertainty is dependent upon the quality of the measurement artifact; in particular, the physical profile of the line edge. Variations in edge profiles for different lines are apparent in both measurement systems. In addition, there are differences in the left and right-edge profiles of a line. For the optical microscope, the calculated profiles assume an ideal edge with a vertical slope. Thus, differences in the calculated profile for this ideal edge and the experimental profiles for lines which have edge raggedness can be expected. Although the method of

averaging over a 1- $\mu$ m length of the line with the stage in motion gives a good repeatability of linewidth measurements with the SEM/interferometer, this method introduces some degradation in the steepness of the edge profile as compared with edge profiles seen in the SEM without the stage in motion. Another source of degradation of the edge profile is the contamination buildup during repeated scanning of a line. An idea of the edge quality is apparent from Figure 11 which shows SEM photomicrographs of a black-chromium artifact. Contamination from repeated scanning of a nominally 3- $\mu$ m wide clear line is visible in Figure 11(a); whereas, a nominally 1- $\mu$ m clear line located nearby has not been scanned and shows no contamination. Figure 11(b) shows one end of a nominally 1- $\mu$ m wide clear line. Some edge raggedness is visible even though the line appears to have a relatively steep slope.

Considering that the measurements in Table 1 are only preliminary values for the SEM/interferometer, the agreement between them and the corresponding measurements for the optical microscope is good. Efforts are presently underway to redesign the sample stage in the SEM/interferometer and thereby reduce mechanical vibration as well as improve reliability of the system operation. An improved data-acquisition system under development should also reduce errors in the data. An effort is underway to obtain more information on the line-edge profiles by cutting artifacts normal to the line and inspecting the resulting cross section in the SEM.

#### Summary

Primary and a secondary measurement systems have been developed for the accurate linewidth calibration of micrometer-wide line on photomask-like artifacts. Theoretical models for the imaging of a line in an optical linewidth-measuring microscope (secondary system) and the profile resulting from the interaction of electrons with a material line in an SEM/interferometer system (primary system) have been developed. Differences between calculated and experimental line-edge profiles for each measurement system are small. Comparison of linewidth measurements on the same line with both systems shows good agreement. Differences are attributable to measurement uncertainties which are related, in large part, to the variation in edge quality of the artifacts. Present efforts are underway to reduce measurement uncertainties in both systems and to characterize more accurately the line-edge profiles.

#### Acknowledgments

The authors wish to acknowledge support received from Fred E. Scire and E. Clayton Teague, Mechanics Division, NBS, for the development and fabrication of the flexure-pivot stage and from Donald B. Novotny, Electronic Technology Division, NBS, for continued interfacing between the microelectronics industry and this NBS program.

#### References

1. Swyt, D. A., NBS Program in Photomask Linewidth Measurements, *Solid State Technol.* **19**, No. 4, pp. 55-61 (April 1976).
2. Jerke, J. M., Hartman, A. W., Nyssonen, D., Rosberry, F. W., Swing, R. E., Swyt, D. A., and Young, R. D., Accurate Linewidth Measurements at the National Bureau of Standards, *Paper presented at the Kodak Microelectronics Seminar INTERFACE '76*, Monterey, Ca., Oct. 3-5, 1976.
3. *The International System of Units (SI)*, Page, C. H., and Vigoureux, P., eds, Nat. Bur. Stand. (U.S.), Spec. Publ. 330, 1972 Edition, 45 pages (April 1972).
4. Oatley, C. W., *The Scanning Electron Microscope. Part I - The Instrument*, pp. 156-161 (Cambridge University Press, London, 1972).
5. Young, R. D., Surface Microtopography, *Phys. Today* **25**, No. 11, 42-49 (Nov. 1971).
6. Nyssonen, D., Linewidth Measurement with an Optical Microscope: The Effect of Operating Conditions on the Image Profile, to be published in *Applied Optics*, Aug. 1977.
7. Born, M., and Wolf, E., *Principles of Optics*, Fifth edition, pp. 395-398 (Pergamon Press, Inc., Elmsford, N.Y., 1975).
8. Layer, H. P., High-Resolution Stepping Motor Drive, *Rev. Sci. Instrum.* **47**, No. 4, 480-483 (April 1976).
9. Beran, M. J., and Parrent, G. B., Jr., *Theory of Partial Coherence* (Prentice-Hall, Inc., Englewood Cliffs, N.J., 1964).

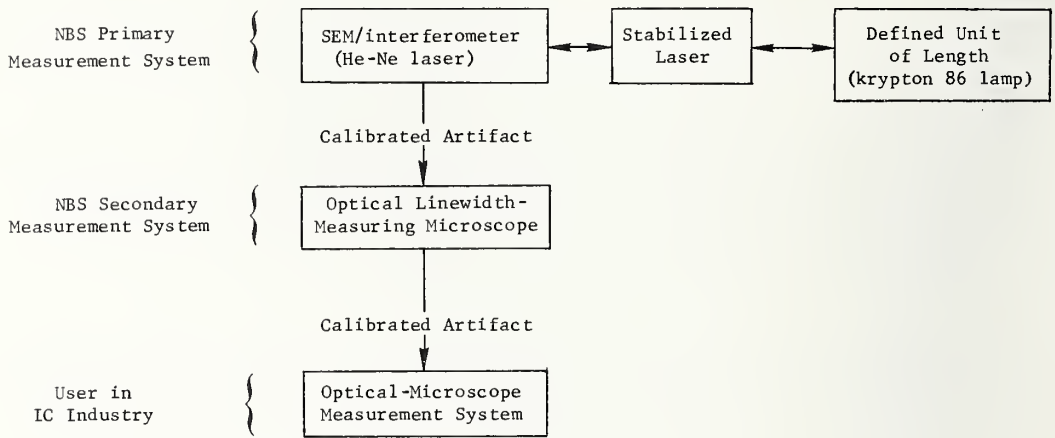


Fig. 1. Hierarchy of NBS linewidth calibrations.

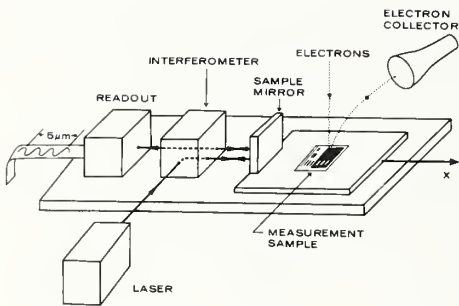


Fig. 2. Schematic of the SEM/interferometer system.

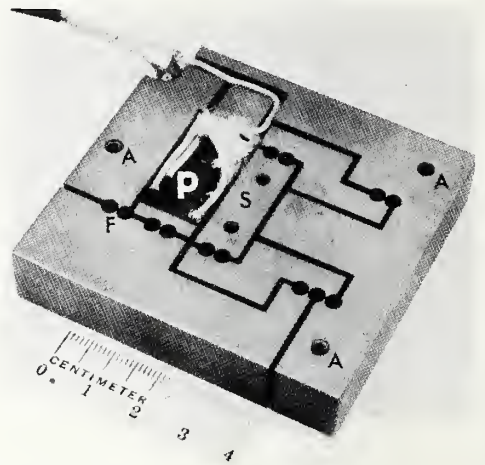


Fig. 3. Photograph of a scanning stage which uses a flexure-pivot system; stage is fixed at points A, while other stage sections move; F - flexure pivot, P - stack of piezoelectric elements, and S - sample-mounting area.

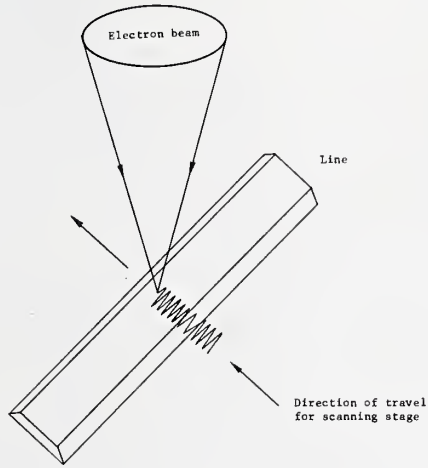


Fig. 4. Schematic of the effective path for the scanning electron beam when the linear motion of the scanning stage is combined with the line sweep of the SEM.

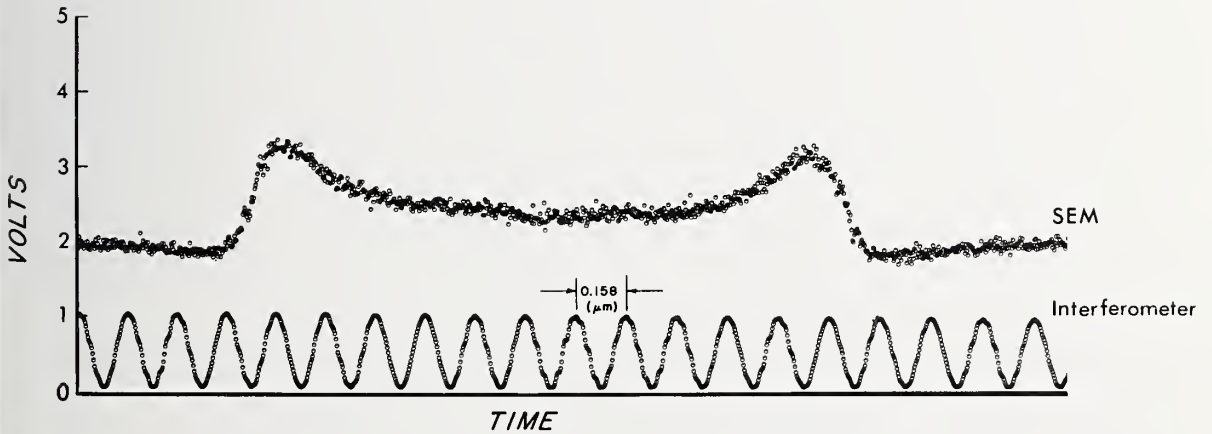
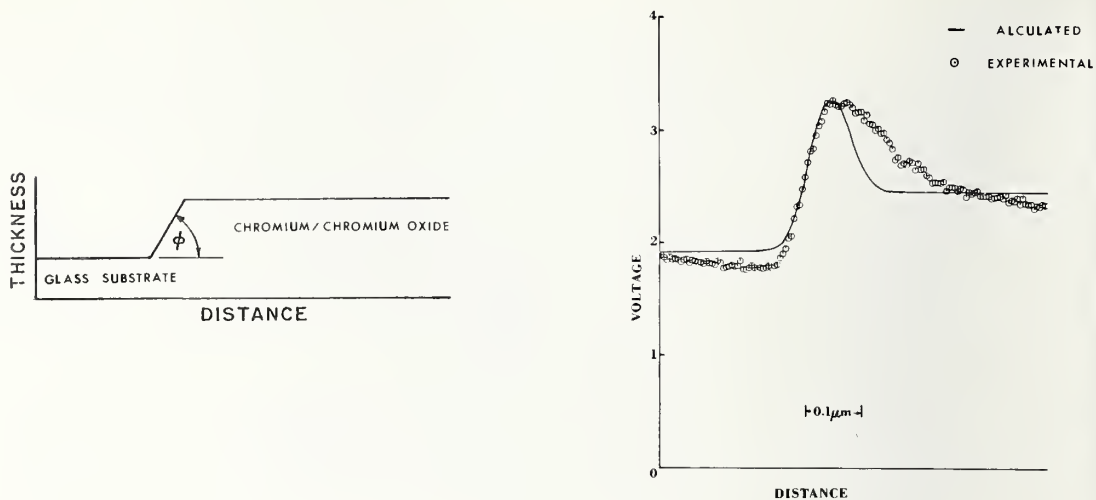


Fig. 5. Direct output of the SEM and interferometer data channels for a nominally 2- $\mu$ m wide opaque line.



(a) Line-edge profile for the model ;  $\phi$  is the angle of the line-edge slope.

(b) Comparison of an experimental SEM line-edge trace with the calculated trace; for the calculated trace, the electron-beam diameter is  $700 \text{ \AA}$ , the chromium/chromium-oxide thickness is  $1100 \text{ \AA}$ ,  $\phi$  is  $55^\circ$ , and the secondary-electron emission coefficients for the glass substrate, chromium, and chromium oxide are 1.0, 1.026, and 1.265, respectively.

Fig. 6. Line-edge profile for the model and a comparison of an experimental SEM line-edge trace with the calculated trace based on the model.

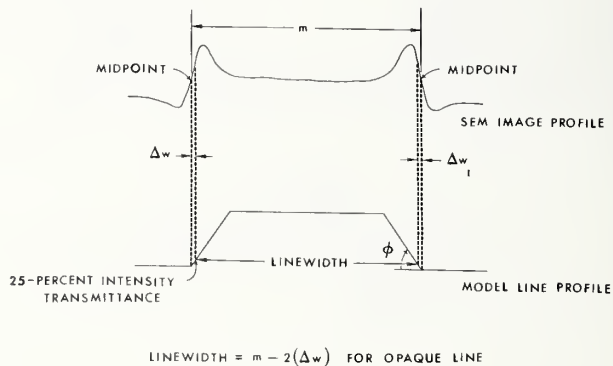


Fig. 7. Relationship between the SEM image profile and the model of an opaque line; the points defined as edge locations of the line correspond to a 25-percent intensity transmittance (50-percent amplitude transmittance).

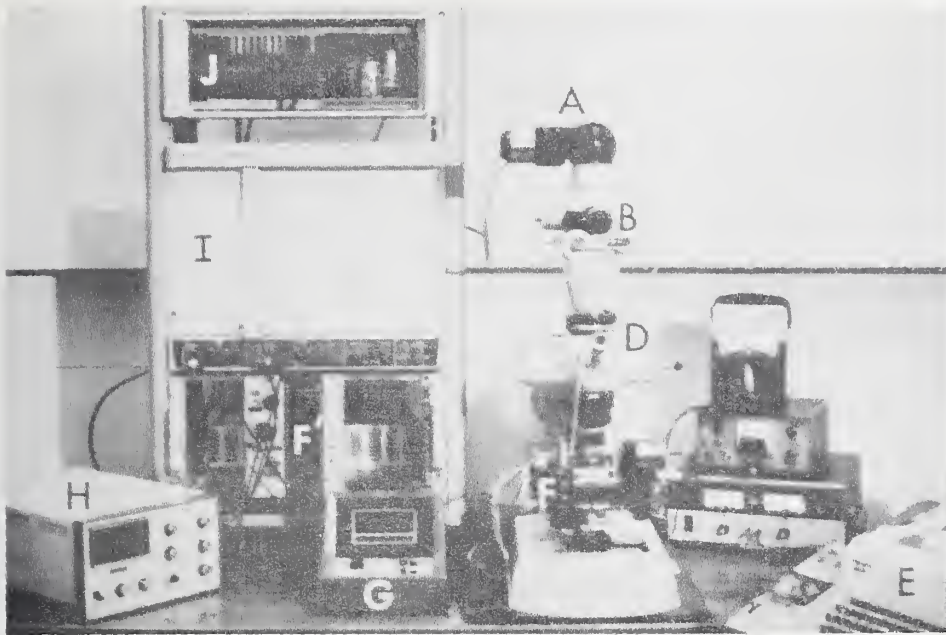


Fig. 8. Photograph of the optical linewidth-measuring microscope; A - photomultiplier tube, B - viewing eyepiece, C - scanning slit, D - optical microscope, E - teletype, F - scanning stage, F' - scanning-stage controls, G - linear voltage transducer gage, H - photometer, I - x-y recorder, and J - microprocessor.

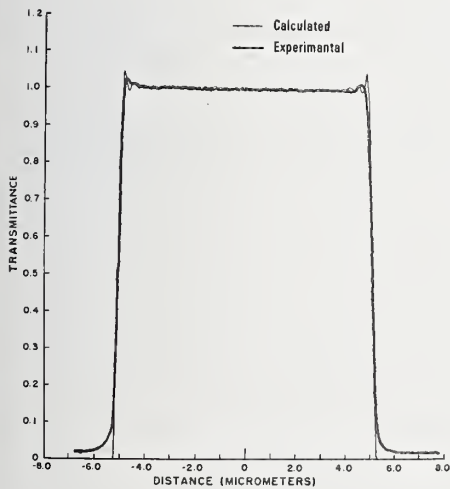


Fig. 9. Comparison of calculated and experimental image profiles of a nominally 10-  $\mu$ m wide clear line; 0.90 N.A. objective, 0.60 N.A. condenser, and 560 nm wavelength.

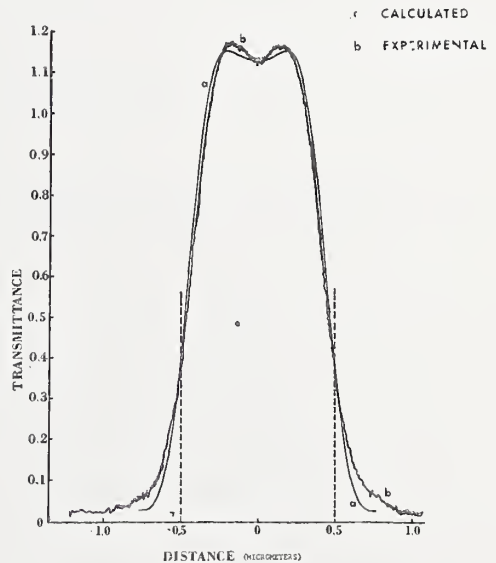


Fig. 10. Comparison of calculated and experimental image profiles of a 1.0-  $\mu$ m wide clear line; 0.90 N.A. objective, 0.60 N.A. condenser, and 560 nm wavelength. The dashed lines indicate line-edge locations based on a 33.5-percent transmittance threshold for the experimental profile.



(a) Nominally 1 and 3- $\mu\text{m}$  wide clear lines showing contamination buildup on 3- $\mu\text{m}$  wide line; 2,000X.



(b) One end of a nominally 1- $\mu\text{m}$  wide clear line; 60,000X.

Fig. 11. SEM photomicrographs of a black-chromium artifact.

Table 1. Average linewidth measurements from the optical linewidth-measuring microscope and the SEM/interferometer for a black-chromium artifact.

Nominal Linewidth	Measured Linewidths, $\mu\text{m}$		
	Optical Microscope <sup>a</sup>	SEM/Interferometer <sup>b</sup>	Difference
1 $\mu\text{m}$ Opaque	0.77	0.77	0
1 $\mu\text{m}$ Clear	0.94	1.07	0.13
3 $\mu\text{m}$ Opaque	2.90	2.91	0.01
3 $\mu\text{m}$ Clear	3.12	3.46	0.34

<sup>a</sup> $3\sigma$  standard deviation is 0.025  $\mu\text{m}$

<sup>b</sup> $3\sigma$  standard deviation is 0.016  $\mu\text{m}$

U.S. DEPT. OF COMM. BIBLIOGRAPHIC DATA SHEET		1. PUBLICATION OR REPORT NO. SP 400-43	2. Gov't. Accession No.	3. Recipient's Accession No.
4. TITLE AND SUBTITLE <i>Semiconductor Measurement Technology: Accurate Linewidth Measurements on Integrated-Circuit Photomasks</i>			5. Publication Date February 1980	6. Performing Organization Code
7. AUTHOR(S) John M. Jerke, Editor			8. Performing Organ. Report No.	
9. PERFORMING ORGANIZATION NAME AND ADDRESS NATIONAL BUREAU OF STANDARDS DEPARTMENT OF COMMERCE WASHINGTON, DC 20234			10. Project/Task/Work Unit No.	11. Contract/Grant No.
12. SPONSORING ORGANIZATION NAME AND COMPLETE ADDRESS (Street, City, State, ZIP) The Defense Advanced Research Projects Agency 1400 Wilson Boulevard Arlington, VA 22209			NBS Washington, DC 20234	13. Type of Report & Period Covered Final
15. SUPPLEMENTARY NOTES Library of Congress Catalog Card Number: 79-600191			14. Sponsoring Agency Code	
<input type="checkbox"/> Document describes a computer program; SF-185, FIPS Software Summary, is attached.				
16. ABSTRACT (A 200-word or less factual summary of most significant information. If document includes a significant bibliography or literature survey, mention it here.) The progress of the NBS program to develop improved theory for accurate linewidth measurements with optical microscopes, to develop primary linewidth calibration of 1- to 10- $\mu\text{m}$ wide lines on integrated-circuit (IC) photomasks, and to provide calibrated measurement artifacts and measurement procedures to the IC industry is discussed. This report covers the initial period from September 1974 through December 1976.  Using coherence theory, line-image profiles are calculated for real optical-microscope systems. The effects of defocus, spherical aberration, and finite transmission of opaque mask areas on the line-image profiles and the location of the line edges are discussed.  A primary linewidth-calibration system, consisting of an interferometer located in a scanning electron microscope (SEM), has been fabricated and used to make measurements of nominally 1-, 2-, and 3- $\mu\text{m}$ wide opaque and clear lines on antireflective chromium artifacts. A secondary linewidth calibration system, which is a modified photometric optical microscope, has been fabricated and provides line-image profiles that compare very well with optical theory. A comparison of measurements on opaque lines between the SEM/interferometer and the photometric optical microscope shows differences of only 0.05 $\mu\text{m}$ .  (CONTINUED ON SEPARATE SHEET)				
7. KEY WORDS (six to twelve entries; alphabetical order; capitalize only the first letter of the first key word unless a proper name; separated by semicolons) Filar eyepiece; image-shearing eyepiece; integrated circuits; linewidth measurements; microelectronics; micrometrology; optical microscope; photomask; photoelectric microscope; scanning electron microscope; semiconductor technology.				
8. AVAILABILITY <input type="checkbox"/> For Official Distribution. Do Not Release to NTIS <input checked="" type="checkbox"/> Order From Sup. of Doc., U.S. Government Printing Office, Washington, DC 20402, Stock No. 003-003-02151-2 <input checked="" type="checkbox"/> Order From National Technical Information Service (NTIS), Springfield, VA. 22161		19. SECURITY CLASS (THIS REPORT) UNCLASSIFIED		21. NO. OF PRINTED PAGES 166
		20. SECURITY CLASS (THIS PAGE) UNCLASSIFIED		22. Price \$5.00

Abstract (continued)

Linewidth measurements on optical microscopes equipped with filar and image-shearing eyepieces are presented. A preliminary effort shows that differences between linewidth measurements with these two eyepieces are significantly reduced when a linewidth artifact measured on the photometric optical microscope is used to calibrate the eyepieces.

Collaborative tests between NBS and the IC industry to evaluate procedures for accurate linewidth measurements with calibrated artifacts are discussed. Some of the methods for transferring NBS-measured values to the industry are summarized. The plans for the continuing micrometrology program include accurate linewidth measurements on opaque wafers with reflected light and on see-through masks with transmitted light and submicrometer linewidth calibration.

Announcement of Semiconductor Measurement Technology  
List of Publications 72 - 1962-1979

Chief  
Electron Devices Division  
National Bureau of Standards  
Bldg. 225, Room A305  
Washington, DC 20234

Dear Sir:

Please send a copy of your latest "Semiconductor Measurement Technology,  
List of Publications 72."

Name \_\_\_\_\_

Company \_\_\_\_\_

Address \_\_\_\_\_

City \_\_\_\_\_ State \_\_\_\_\_ Zip Code \_\_\_\_\_



# NBS TECHNICAL PUBLICATIONS

## PERIODICALS

**JOURNAL OF RESEARCH**—The Journal of Research of the National Bureau of Standards reports NBS research and development in those disciplines of the physical and engineering sciences in which the Bureau is active. These include physics, chemistry, engineering, mathematics, and computer sciences. Papers cover a broad range of subjects, with major emphasis on measurement methodology and the basic technology underlying standardization. Also included from time to time are survey articles on topics closely related to the Bureau's technical and scientific programs. As a special service to subscribers each issue contains complete citations to all recent Bureau publications in both NBS and non-NBS media. Issued six times a year. Annual subscription: domestic \$17; foreign \$21.25. Single copy, \$3 domestic; \$3.75 foreign.

NOTE: The Journal was formerly published in two sections: Section A "Physics and Chemistry" and Section B "Mathematical Sciences."

**DIMENSIONS/NBS**—This monthly magazine is published to inform scientists, engineers, business and industry leaders, teachers, students, and consumers of the latest advances in science and technology, with primary emphasis on work at NBS. The magazine highlights and reviews such issues as energy research, fire protection, building technology, metric conversion, pollution abatement, health and safety, and consumer product performance. In addition, it reports the results of Bureau programs in measurement standards and techniques, properties of matter and materials, engineering standards and services, instrumentation, and automatic data processing. Annual subscription: domestic \$11; foreign \$13.75.

## NONPERIODICALS

**Monographs**—Major contributions to the technical literature on various subjects related to the Bureau's scientific and technical activities.

**Handbooks**—Recommended codes of engineering and industrial practice (including safety codes) developed in cooperation with interested industries, professional organizations, and regulatory bodies.

**Special Publications**—Include proceedings of conferences sponsored by NBS, NBS annual reports, and other special publications appropriate to this grouping such as wall charts, pocket cards, and bibliographies.

**Applied Mathematics Series**—Mathematical tables, manuals, and studies of special interest to physicists, engineers, chemists, biologists, mathematicians, computer programmers, and others engaged in scientific and technical work.

**National Standard Reference Data Series**—Provides quantitative data on the physical and chemical properties of materials, compiled from the world's literature and critically evaluated. Developed under a worldwide program coordinated by NBS under the authority of the National Standard Data Act (Public Law 90-396).

## BIBLIOGRAPHIC SUBSCRIPTION SERVICES

The following current-awareness and literature-survey bibliographies are issued periodically by the Bureau:

**Cryogenic Data Center Current Awareness Service.** A literature survey issued biweekly. Annual subscription: domestic \$25; foreign \$30.

**Liquefied Natural Gas.** A literature survey issued quarterly. Annual subscription: \$20.

NOTE: The principal publication outlet for the foregoing data is the Journal of Physical and Chemical Reference Data (JPCRD) published quarterly for NBS by the American Chemical Society (ACS) and the American Institute of Physics (AIP). Subscriptions, reprints, and supplements available from ACS, 1155 Sixteenth St., NW, Washington, DC 20056.

**Building Science Series**—Disseminates technical information developed at the Bureau on building materials, components, systems, and whole structures. The series presents research results, test methods, and performance criteria related to the structural and environmental functions and the durability and safety characteristics of building elements and systems.

**Technical Notes**—Studies or reports which are complete in themselves but restrictive in their treatment of a subject. Analogous to monographs but not so comprehensive in scope or definitive in treatment of the subject area. Often serve as a vehicle for final reports of work performed at NBS under the sponsorship of other government agencies.

**Voluntary Product Standards**—Developed under procedures published by the Department of Commerce in Part 10, Title 15, of the Code of Federal Regulations. The standards establish nationally recognized requirements for products, and provide all concerned interests with a basis for common understanding of the characteristics of the products. NBS administers this program as a supplement to the activities of the private sector standardizing organizations.

**Consumer Information Series**—Practical information, based on NBS research and experience, covering areas of interest to the consumer. Easily understandable language and illustrations provide useful background knowledge for shopping in today's technological marketplace.

*Order the above NBS publications from: Superintendent of Documents, Government Printing Office, Washington, DC 20402.*

*Order the following NBS publications—FIPS and NBSIR's—from the National Technical Information Services, Springfield, VA 22161.*

**Federal Information Processing Standards Publications (FIPS PUB)**—Publications in this series collectively constitute the Federal Information Processing Standards Register. The Register serves as the official source of information in the Federal Government regarding standards issued by NBS pursuant to the Federal Property and Administrative Services Act of 1949 as amended, Public Law 89-306 (79 Stat. 1127), and as implemented by Executive Order 11717 (38 FR 12315, dated May 11, 1973) and Part 6 of Title 15 CFR (Code of Federal Regulations).

**NBS Interagency Reports (NBSIR)**—A special series of interim or final reports on work performed by NBS for outside sponsors (both government and non-government). In general, initial distribution is handled by the sponsor; public distribution is by the National Technical Information Services, Springfield, VA 22161, in paper copy or microfiche form.

**Superconducting Devices and Materials.** A literature survey issued quarterly. Annual subscription: \$30. Please send subscription orders and remittances for the preceding bibliographic services to the National Bureau of Standards, Cryogenic Data Center (736) Boulder, CO 80303.

**U.S. DEPARTMENT OF COMMERCE**  
**National Bureau of Standards**

Washington, D.C. 20234

OFFICIAL BUSINESS

Penalty for Private Use, \$300

POSTAGE AND FEES PAID  
U.S. DEPARTMENT OF COMMERCE  
COM-215



SPECIAL FOURTH-CLASS RATE  
BOOK

---